

การวิเคราะห์ผลกระทบจากออฟเซตประสานเวลาที่มีต่อระบบเชื่อมโยงขาขึ้นของการเข้าถึงหลาย
ทางแบบเอ็มไอเอ็มไอ-โอเอฟดีเอ็มเอ

นายโอมอร์ อับเดล ราซาค ซารีฟ

วิทยานิพนธ์นี้เป็นส่วนหนึ่งของการศึกษาตามหลักสูตรปริญญาวิศวกรรมศาสตรดุษฎีบัณฑิต

สาขาวิชาวิศวกรรมไฟฟ้า ภาควิชาวิศวกรรมไฟฟ้า

คณะวิศวกรรมศาสตร์ จุฬาลงกรณ์มหาวิทยาลัย

ปีการศึกษา 2554

ลิขสิทธิ์ของจุฬาลงกรณ์มหาวิทยาลัย
บทคัดย่อและแฟ้มข้อมูลฉบับเต็มของวิทยานิพนธ์ตั้งแต่ปีการศึกษา 2554 ที่ให้บริการในคลังปัญญาจุฬาฯ (CUIR)

เป็นแฟ้มข้อมูลของนิสิตเจ้าของวิทยานิพนธ์ที่ส่งผ่านทางบัณฑิตวิทยาลัย

The abstract and full text of theses from the academic year 2011 in Chulalongkorn University Intellectual Repository (CUIR)

are the thesis authors' files submitted through the Graduate School.

ANALYSIS OF SYNCHRONIZATION OFFSETS EFFECT ON UPLINK MIMO-OFDMA
SYSTEMS

MR.OMER ABDEL RAZAG SHARIF ABUBAKER

A Dissertation Submitted in Partial Fulfillment of the Requirements
for the Degree of Doctor of Philosophy Program in Electrical Engineering

Department of Electrical Engineering

Faculty of Engineering

Chulalongkorn University

Academic Year 2011

Copyright of Chulalongkorn University

Thesis Title ANALYSIS OF SYNCHRONIZATION OFFSETS EFFECT ON
UPLINK MIMO-OFDMA SYSTEMS
By MR. OMER ABDEL RAZAG SHARIF ABUBAKER
Field of Study ELECTRICAL ENGINEERING
Thesis Advisor ASSOCIATE PROFESSOR WATIT BENJAPOLAKUL, D.Eng.

Accepted by the Faculty of Engineering, Chulalongkorn University in Partial
Fulfillment of the Requirements for the Doctoral Degree

.....Dean of the Faculty of Engineering
(Associate Professor Boonsom Lerdhirunwong, Dr.Ing.)

THESIS COMMITTEE

..... Chairman
(Associate Professor Lunchakorn Wuttisittikulkij, Ph.D.)

..... Thesis Advisor
(Associate Professor Watit Benjapolakul, D.Eng.)

..... Examiner
(Assistant Professor Widhyakorn Asdornwised, Ph.D.)

..... Examiner
(Assistant Professor Chaiyachet Saivichit, Ph.D.)

..... External Examiner
(Chaiyaporn Khemapatapan, Ph.D.)

โอเมอร์ อับเดล ราซาค ซารีฟ: การวิเคราะห์ผลกระทบจากออฟเซตประสานเวลาที่มีต่อระบบ
 เชื่อมโยงขาขึ้นของการเข้าถึงหลายทางแบบเอ็มไอเอ็มโอ-โอเอฟดีเอ็มเอ. (ANALYSIS OF
 SYNCHRONIZATION OFFSETS EFFECT ON UPLINK MIMO-OFDMA SYSTEMS) อ.ที่
 ปรึกษาวิทยานิพนธ์หลัก: รศ. ดร.วาทีต เบญจพลกุล 161 หน้า.

ออฟเซตประสานเวลาเช่น ออฟเซตทางเวลาออฟเซตทางความถี่ของคลื่นพาห์และออฟเซต
 ทางความถี่ในการซัดตัวอย่างของสัญญาณนาฬิกา จะส่งผลกระทบต่อคุณสมบัติการตั้งฉากในระบบ
 เชื่อมโยงขาขึ้นในช่องสัญญาณเฟดดิ้งของการเข้าถึงหลายทางแบบเอ็มไอเอ็มโอ-โอเอฟดีเอ็มเอซึ่งทำ
 ให้ระบบดังกล่าวมีข้อจำกัดด้านการแทรกสอดของสัญญาณ เพื่อจัดการกับข้อบกพร่องนี้ วิทยานิพนธ์
 นี้นำเสนอการประเมินสมรรถนะการทำงานซึ่งอนุพัทธ์มาจากการเสื่อมถอยของตัววัดด้านกำลังส่ง
 อัตราส่วนของค่าเฉลี่ยกำลังสัญญาณต่อกำลังสัญญาณแทรกสอดและกำลังสัญญาณรบกวน(SINR)
 หรือการวัดอัตราความผิดพลาดเช่น อัตราความผิดพลาดบิต (BER) และ อัตราความผิดพลาด
 สัญลักษณ์ (SER)

งานวิจัยนี้พิจารณาผลกระทบของออฟเซตประสานเวลาที่มีต่อสมรรถนะของระบบเชื่อมโยง
 ขาขึ้นของการเข้าถึงหลายทางแบบเอ็มไอเอ็มโอ-โอเอฟดีเอ็มเอ ผ่านช่องสัญญาณเฟดดิ้งพหุวิถีใน
 รูปแบบอัตราส่วนของค่าเฉลี่ยกำลังสัญญาณต่อกำลังสัญญาณแทรกสอดและกำลังสัญญาณรบกวน
 (SINR) ที่ขาออกของการแปลงฟูเรียร์สังยุค(DFT)ของวงจรถ้าตามเนื้อหาในวินโดว์ของการแปลงฟู
 เรียร์สังยุค(DFT)นอกจากนี้งานวิจัยนี้ยังได้พิจารณาค่าที่แท้จริงของออฟเซตทางเวลาและประเมิน
 สมรรถนะอัตราส่วนของกำลังสัญญาณต่อกำลังสัญญาณแทรกสอดและกำลังสัญญาณรบกวน
 (SINR) ในแบบแผนการจัดสรรคลื่นพาห์ย่อยใดๆและคุณสมบัติของระบบเอ็มไอเอ็มโอตลอดจน
 เงื่อนไขความแตกต่างของไซคลิกพรีฟิก โดยไม่ต้องอาศัยสมมุติฐานเกี่ยวกับคุณสมบัติทางสถิติของ
 การแทรกสอดใดๆ งานวิจัยนี้อนุพัทธ์สมการคณิตศาสตร์สำหรับคำนวณหาอัตราความผิดพลาด
 บิต(BER) อัตราความผิดพลาดสัญญาณลักษณ์(SER) ในขณะที่มีออฟเซตประสานเวลาอยู่ด้วย ผลที่ได้รับ
 ในงานวิจัยนี้สามารถนำไปใช้กำหนดความต้องการด้านความเที่ยงตรงของอัลกอริทึมประมาณค่า
 ออฟเซต เมื่อทราบค่าความเสื่อมถอยเองสมรรถนะการทำงานของระบบที่ยอมรับได้

ภาควิชา วิศวกรรมไฟฟ้า ลายมือชื่อนิสิต

สาขาวิชา วิศวกรรมไฟฟ้า ลายมือชื่อ อ.ที่ปรึกษาวิทยานิพนธ์หลัก

ปีการศึกษา 2554 ลายมือชื่อ อ.ที่ปรึกษาวิทยานิพนธ์ร่วม

5271855521: MAJOR ELECTRICAL ENGINEERING

KEYWORDS: MIMO-OFDMA Uplink Systems/ Synchronization Offsets/ Time Offset Boundaries/ Average SINR /B(S)ER

OMER ABDEL RAZAG SHARIF ABUBAKER: ANALYSIS OF SYNCHRONIZATION OFFSETS EFFECT ON UPLINK MIMO-OFDMA SYSTEMS. ADVISOR: ASSOCIATE PROFESSOR WATIT BENJAPOLAKUL, D.Eng., 161 pp.

Synchronization offsets such as time (TO), carrier frequency (CFO), and sampling clock frequency (SCFO) offsets, destroy user's signal orthogonality in Multiple-Input Multiple-Output Orthogonal Frequency Division Multiple Access (MIMO-OFDMA) fading channel uplink systems, resulting in an interference-limited system. To cope with these impairments, performance evaluations, which can be derived as degradation in metrics of power loss such as Signal-to-Interference (plus Noise) Ratio (SI(N)R) or as an error rate measurement such as Bit Error Rate/Symbol Error Rate (BER/SER), have been proposed.

This research investigates the impact of synchronization offsets on the performance of the uplink MIMO-OFDMA systems over multipath fading channel in terms of instantaneous/average SINR at the DFT output of the receiver based on the contents of the DFT window. In addition, the boundaries of the TO are precisely determined. However, the SINR performance evaluation is carried out for arbitrary Subcarrier Allocation Schemes (SASs), and MIMO systems properties as well as various CP conditions, where there is no prior assumption on the interferences' statistical properties. A general expression for BER/SER is derived based on the analyzed SINR in presence of synchronization offsets. The results obtained in this work, determine the requirements on the accuracy of offsets estimation algorithms when an acceptable amount of performance degradation is given.

Department: Electrical Engineering Student's Signature:

Field of Study: Electrical Engineering Advisor's Signature:

Academic Year: 2011 Co-advisor's Signature:

ACKNOWLEDGEMENTS

In the name of Allah (The God), Most Gracious, Most Merciful

My deepest gratitude goes to my supervisor Assoc. Prof. Watit Benjapolakul, D. Eng., who provides guidance, encouragement and support. His never-ending enthusiasm for new and interesting ideas and his complete dedication to his work have been, and will always be, an example and inspiration for me. I would like to express my sincere thanks to the Islamic Development Bank (IDB) Jeddah, Saudi Arabia for their financial support.

Moreover, I would like to thank my thesis committee members for their cogent comments. I also want to express my appreciation to all faculty members in the Communication Division, for their invaluable teaching, and collaborations. In particular, I would like to thank Asst. Prof. Chaodit Aswakul who recommends and facilitates accessing to the Cluster Computing System at the Group in Light-wave and High-speed Communications at Chulalongkorn University, under the project grant support by TRIDI, Thailand; and the SP2-GE12 project grant of Department of Electrical Engineering, Chulalongkorn University.

I must reserve the most special thanks for my faithful friends and colleagues in Faculty of Engineering, Chulalongkorn University for their friendship, and assistance. In particular, I would like to thank Mr. Suwatchai Tangpaopong, who provides the needed support to efficiently use the Cluster Computing System as its administrator.

Finally I would like to thank my personnel support network. My parent, especially my mother, who is sacrificing, providing much support, understanding and flexibility throughout my life, I thank you from the bottom of my heart. My wife, who has providing support, encouragement, confidence, and understanding, I would also like to thanks her parents, brothers and other relatives for their true love on us. I am grateful to my brothers (Mohammed and Marwan), and uncles who have consistently give me the needed encouragements, true valuable advices and unlimited support which always helped me take the right step in life.

CONTENTS

	PAGE
ABSTRACT IN THAI	iv
ABSTRACT IN ENGLISH	v
ACKNOWLEDGEMENTS	vi
CONTENTS	vii
LIST OF TABLES	xii
LIST OF FIGURES	xiii
LIST OF ABBREVIATIONS	xx
CHAPTER I INTRODUCTION	1
1.1 Introduction	1
1.2 Motivations and Rationales	3
1.3 Objectives	6
1.4 Scope	7
1.5 Methodology	8
1.6 Thesis Overview	9
CHAPTER II BACKGROUND ON PERFORMANCE EVALUATIONS OF OFDMA/MIMO-OFDMA SYSTEMS IN PRESENCE OF SYNCHRONIZATION OFFSETS	10
2.1 Introduction	10
2.2 The Impact of the Synchronization Offsets	13
2.3 Performance Evaluation and Optimization of OFDMA/MIMO-OFDMA Uplink Systems in Presence of Synchronization Offsets	15
CHAPTER III PROPOSED ANALYSIS OF INSTANTANEOUS AND AVERAGE SIGNAL-TO-INTERFERENCE PLUS NOISE RATIO (SINR) FOR UPLINK MIMO- OFDMA FADING CHANNEL SYSTEMS IN THE PRESENCE OF SYNCHRONIZATION OFFSETS	22
3.1. Introduction	22
3.2. System, Signals and Channel Model for Uplink MIMO-OFDMA Systems	22

	PAGE
3.3. Average SINR Analysis for Uplink MIMO-OFDMA Fading Channel Systems In The Presence of Time Offsets	26
3.3.1 Single-User Single-Antenna Structure and Time Offset	26
i. The TO Towards the CP (i.e. $\mu_{u,n}^{p,q} < 0$)	28
ii. The TO Away from the CP (i.e. $\mu_{u,n}^{p,q} > 0$)	30
3.3.2 Analysis of the Boundaries of the TO	32
3.3.3 Instantaneous and Average Interferences Power and SINR with TO	33
3.3.4 Special Case of Insufficient and Absent CP	36
3.4. Average SINR Analysis for Uplink MIMO-OFDMA Fading Channel Systems In The Presence of Time and Carrier Frequency Offsets	38
3.4.1 Single-User Single-Antenna Structure and Coexistence of Time and Carrier Frequency Offsets	38
i. The TO Towards The CP (i.e. $\mu_{u,n}^{p,q} < 0$) and CFO (i.e. $\epsilon_u^q > 0$)..	40
ii. The TO Away from The CP (i.e. $\mu_{u,n}^{p,q} > 0$) and CFO (i.e., $\epsilon_u^q > 0$)	40
3.4.2 Instantaneous and Average Interferences Power and SINR with TO and CFO	41
3.5. Average SINR Analysis for Uplink MIMO-OFDMA Fading Channel Systems In The Presence of Carrier Frequency and Sampling Clock Frequency Offsets	43
3.5.1 Single-User Single-Antenna Structure and Coexistence of Carrier Frequency (CFO) and Sampling Clock Frequency (SCFO) Offsets	43
i. Negative Sampling Clock Frequency Offset (SCFO) (i.e., $0 < -\xi_{u,n}^q \leq 0.5$)	45
ii. Positive Sampling Clock Frequency Offset (SCFO) (i.e., $0 < \xi_{u,n}^q \leq 0.5$)	46
3.5.2 Instantaneous and Average Interferences Power and SINR with	47

	PAGE
CFO and SCFO in MIMO-OFDMA Uplink Systems	
CHAPTER IV PROPOSED ANALYSIS OF AVERAGE ERROR RATES FOR UPLINK MIMO-OFDMA FADING CHANNEL SYSTEMS IN THE PRESENCE OF SYNCHRONIZATION OFFSETS	50
4.1. Introduction	50
4.2. General Asynchronous SINR Statistics	50
4.3. A Lower Bound on $\mathbf{M}_{x_{CP}}^{\Delta}(i,y)$	51
4.4. Average Error Rate Analysis	51
4.4.1. Average Symbol Error Rate (SER)	52
4.4.2. Average Bit Error Rate (BER)	53
CHAPTER V RESULTS AND DISCUSSIONS	55
5.1. Introduction	55
5.2. Simulation Environment	55
5.3. System Performance in Presence of TO	57
5.3.1. The Instantaneous Interference Components and SINR of $\phi Y_{u,n}^{p,q}(i=c_{u,g})$	57
5.3.2. Instantaneous/Average Interferences and SINR for MIMO-OFDMA Uplink Systems	64
A. The Instantaneous/Average CAs-SI Analysis	64
B. The Instantaneous/Average MUI Analysis	67
C. The Instantaneous/Average SINR Analysis	74
5.4. System Performance in Presence of TO and CFO	90
5.4.1 The Instantaneous Interference Components and SINR of $\phi^{\varepsilon} Y_{u,n}^{p,q}(i=c_{u,g})$	90
5.4.2 The Instantaneous Interferences and SINR for MIMO-OFDMA Uplink Systems	91
A. Instantaneous/Average CAs-SI Analysis in Presence of TO and CFO	91

	PAGE
B. The Instantaneous/Average MUI Analysis in Presence of TO and CFO	92
C. Instantaneous/Average SINR Analysis in Presence of TO and CFO	104
5.5. System Performance in Presence of CFO and SCFO	113
5.5.1 The Instantaneous Interference Components and SINR of $\epsilon, \xi Y_{u,n}^{p,q} (i = c_{u,g})$	113
5.5.2 The Instantaneous Interference and SINR for MIMO-OFDMA Uplink Systems	118
A. Instantaneous CAs-SI in Presence of CFO and SCFO	118
B. Instantaneous MUI in Presence of CFO and SCFO	118
C. Instantaneous SINR in Presence of CFO and SCFO	119
CHAPTER VI CONCLUSIONS AND RECOMMENDATIONS	127
6.1. Introduction	127
6.2. Research Overview and Conclusions	127
6.3. Recommendation for Future Work	128
LIST OF REFERENCES	130
APPENDICES	146
APPENDIX A	147
APPENDIX B	150
APPENDIX C	153
APPENDIX D	159
BIOGRAPHY	161

LIST OF TABLES

TABLE	PAGE
5.1 System Parameters	55
5.2 Tapped Delay Line Parameters for Wireless Environment	56
5.3 The Average CAs-SI for Different CP Conditions at $c_{1,0}$ by BSAS, ISAS and GSAS	67
5.4 The Average MUI for Different CP Conditions at $c_{1,0}$ by BSAS, ISAS and GSAS for P=1	72
5.5 The Average {SCP, InCP, ACP} SINR for Synchronous and Asynchronous Desired User at $c_{1,0}$ by BSAS, ISAS and GSAS when P=1 and $N(\phi_U)=1$	77
5.6 The Average MUI for Different CP Conditions at $c_{1,0}$ by BSAS, ISAS and GSAS for P=1	93
5.7 The Instantaneous {SCP, InCP, ACP} SINR with $N(\phi_U)=1$ and $\epsilon_{u,n}^a = +0.1$ at $c_{1,0}$ by BSAS	105
5.8 The Average {SCP, InCP, ACP} SINR for Asynchronous Desired User at $c_{1,0}$ by BSAS, ISAS and GSAS when P=1	105
5.9 The Instantaneous asynchronous CAs-SI with CFO and SCFO for different SAS and P=2	119

LIST OF FIGURES

FIGURE		PAGE
3.1	Discrete-Time Model of the Baseband Uplink MIMO-OFDMA systems	23
3.2	General OFDMA Symbol Structure in Multipath fading Channels and Synchronous DFT Window along the Channel Paths	26
3.3	The Asynchronous DFT Window During the TO's Ranges towards the CP	30
3.4	The Asynchronous DFT Window During the TO's Ranges Away From the CP	32
3.5	Illustration of Sampling the Received OFDMA symbol by the l^{th} Channel Path In presence of Negative SCFO	45
3.6	Illustration of Sampling the Received OFDMA symbol by the l^{th} Channel Path In presence of Positive SCFO	47
5.1	Instantaneous powers of SCP signal components in $\phi Y_{u,n}^{p,q}(i=c_{u,g})$: (a) The DS. (b) The ICI. (c) The ISI. (d) Slices of DS, ISI, and ICI at $c_{1,0} = 0$ allocated by BSAS	58
5.2	Instantaneous powers of SCP signal components in $\phi Y_{u,n}^{p,q}(i=c_{u,g})$: (a) The DS, (b) The ICI, (c) The ISI, and (d) Slices of DS, ICI, and ISI at $c_{1,0} = 0$ allocated by ISAS	58
5.3	Instantaneous powers of SCP signal components in $\phi Y_{u,n}^{p,q}(i=c_{u,g})$: (a) The DS, (b) The ICI, (c) The ISI, and (d) Slices of DS, ICI, and ISI at $c_{1,0} = 21$ allocated by GSAS	59
5.4	Instantaneous powers of InCP signal components in $\phi Y_{u,n}^{p,q}(i=c_{u,g})$: (a) The DS, (b) The ICI, (c) The ISI, and (d) Slices of DS, ICI, and ISI at $c_{1,0} = 0$ allocated by BSAS	59
5.5	Instantaneous powers of InCP signal components in $\phi Y_{u,n}^{p,q}(i=c_{u,g})$: (a) The DS, (b) The ICI, (c) The ISI, and (d) Slices of DS, ICI, and ISI	60

FIGURE	PAGE
at $c_{1,0} = 0$ allocated by ISAS	
5.6 Instantaneous powers of InCP signal components in $\phi Y_{u,n}^{p,q} (i = c_{u,g})$: (a) The DS, (b) The ICI, (c) The ISI, and (d) Slices of DS, ICI, and ISI at $c_{1,0} = 21$ allocated by GSAS	60
5.7 Instantaneous powers of ACP signal components in $\phi Y_{u,n}^{p,q} (i = c_{u,g})$: (a) The DS, (b) The ICI, (c) The ISI, and (d) Slices of DS, ICI, and ISI at $c_{1,0} = 0$ allocated by BSAS	61
5.8 Instantaneous powers of ACP signal components in $\phi Y_{u,n}^{p,q} (i = c_{u,g})$: (a) The DS, (b) The ICI, (c) The ISI, and (d) Slices of DS, ICI, and ISI at $c_{1,0} = 0$ allocated by ISAS	61
5.9 Instantaneous powers of ACP signal components in $\phi Y_{u,n}^{p,q} (i = c_{u,g})$: (a) The DS, (b) The ICI, (c) The ISI, and (d) Slices of DS, ICI, and ISI at $c_{1,0} = 21$ allocated by GSAS	62
5.10 Instantaneous xCP SINR from $\phi Y_{u,n}^{p,q} (i = c_{u,g})$: (a) SCP SINR, (b) InCP SINR, (c) ACP SINR, and (d) Slices of instantaneous xCP SINR at $c_{1,0}$ $= 0$ allocated by BSAS	62
5.11 Instantaneous xCP SINR from $\phi Y_{u,n}^{p,q} (i = c_{u,g})$: (a) SCP SINR, (b) InCP SINR, (c) ACP SINR, and (d) Slices of instantaneous xCP SINR at $c_{1,0}$ $= 0$ allocated by ISAS	63
5.12 Instantaneous xCP SINR from $\phi Y_{u,n}^{p,q} (i = c_{u,g})$: (a) SCP SINR, (b) InCP SINR, (c) ACP SINR, and (d) Slices of instantaneous xCP SINR at $c_{1,0}$ $= 21$ allocated by GSAS	63
5.13 Instantaneous powers of the CAs-SI versus the number of transmit antennas with: (a) SCP, (b) InCP, and (c) ACP for different desired user's TO $\zeta_{1,n}^{p,q} = -64, -32, 0, 23$ and 75 at $c_{1,0} = 0$ allocated by BSAS ...	65
5.14 Instantaneous powers of the CAs-SI versus the number of transmit antennas with: (a) SCP, (b) InCP, and (c) ACP for different desired user's TO $\zeta_{1,n}^{p,q} = -64, -32, 0, 23$ and 75 at $c_{1,0} = 0$ allocated by ISAS	65

FIGURE	PAGE
5.15 Instantaneous Powers of the CAs-SI Versus the Number of Transmit Antennas with: (a) SCP, (b) InCP, and (c) ACP for Different Desired User's TO $\zeta_{1,n}^{p,q} = -64, -32, 0, 23$ and 75 at $c_{1,0} = 21$ allocated by GSAS.....	66
5.16 Average CAs-SI Versus the Number of Transmit Antennas, $P=1, 2, 4,$ and 8 with SCP, InCP and ACP Scenarios at: (a) $c_{1,0} = 0$ Allocated by BSAS, (b) $c_{1,0} = 0$ Allocated by ISAS, (c) $c_{1,0} = 21$ Allocated by GSAS...	66
5.17 Instantaneous {SCP, InCP, ACP} MUI for $N(\phi_U) = 1, 5, 10,$ and 15 at: (a) $c_{1,0} = 0$ allocated by BSAS, (b) $c_{1,0} = 0$ allocated by ISAS, and (c) $c_{1,0} = 21$ allocated by GSAS for $P=1$	68
5.18 Instantaneous {SCP, InCP, ACP} MUI for $\zeta_{u,n}^{p,q} = -128, -64, 37,$ and 146 at: (a) $c_{1,0} = 0$ allocated by BSAS, (b) $c_{1,0} = 0$ allocated by ISAS, and (c) $c_{1,0} = 21$ allocated by GSAS for $P=1$	69
5.19 Instantaneous {SCP, InCP, ACP} MUI For $P=1, 2, 4,$ And 8 Antennas At: (A) $c_{1,0} = 0$ Allocated By BSAS, (B) $c_{1,0} = 0$ Allocated By ISAS, And (C) $c_{1,0} = 21$ Allocated By GSAS For $N(\phi_U) = 15$	70
5.20 Effects of Number of Asynchronous Users $N(\phi_U)$ and Number of Transmit Antennas, P on the Average {SCP, InCP, and ACP} MUI at: (a) $c_{1,0} = 0$ allocated by BSAS, (b) $c_{1,0} = 0$ allocated by ISAS, (c) $c_{1,0} = 21$ allocated by GSAS	71
5.21 Comparison between the average MUI in (3.38) for single-transmit antenna and (Park et al., 2010 eq. 16, 17 and 18) with SCP at: (a) $c_{1,0} = 0$ allocated by BSAS, (b) $c_{1,0} = 0$ allocated by ISAS, (c) $c_{1,0} = 21$ allocated by GSAS	75
5.22 Instantaneous {SCP, InCP, ACP} SINR for $N(\phi_U) = 1, 5, 10,$ and 15 at: (a) $c_{1,0} = 0$ allocated by BSAS, (b) $c_{1,0} = 0$ allocated by ISAS, and (c) $c_{1,0} = 21$ allocated by GSAS for $P=1$ and Synchronous desired user $\zeta_{k=1,n}^{t,q} = 0$	79

FIGURE	PAGE
5.23 Instantaneous {SCP, InCP, ACP} SINR for $\zeta_{u,n}^{p,q} = -128, -64, 37,$ and 146 at: (a) $c_{1,0} = 0$ allocated by BSAS, (b) $c_{1,0} = 0$ allocated by ISAS, and (c) $c_{1,0} = 21$ allocated by GSAS for $P=1$ and Synchronous desired user $\zeta_{k=1,n}^{t,q} = 0$	80
5.24 Instantaneous {SCP, InCP, ACP} SINR for $\zeta_{u,n}^{p,q} = -128, -64, 37,$ and 146 at: (a) $c_{1,0} = 0$ allocated by BSAS, (b) $c_{1,0} = 0$ allocated by ISAS, and (c) $c_{1,0} = 21$ allocated by GSAS for $P=1$ and Asynchronous desired user $\zeta_{k=1,n}^{t,q} = -64$	81
5.25 Instantaneous {SCP, InCP, ACP} SINR for $P=1, 2, 4,$ and 8 at: (a) $c_{1,0} = 0$ allocated by BSAS, (b) $c_{1,0} = 0$ allocated by ISAS, and (c) $c_{1,0} = 21$ allocated by GSAS for $N(\phi_U) = 15$ and Synchronous desired user $\zeta_{k=1,n}^{t,q} = 0$	82
5.26 Instantaneous {SCP, InCP, ACP} SINR for $P= \{1, 2, 4, 8\}$ and $\zeta_{u,n}^{p,q} = \{-129, -64, 37, 146\}$ at: (a) $c_{1,0} = 0$ allocated by BSAS, (b) $c_{1,0} = 0$ allocated by ISAS, and (c) $c_{1,0} = 21$ allocated by GSAS for $N(\phi_U) = 1$ and Synchronous desired user $\zeta_{k=1,n}^{t,q} = 0$	83
5.27 Instantaneous {SCP, InCP, ACP} SINR for $\zeta_{k=1,n}^{t,q} = -64, -32, 0, 23$ at: (a) $c_{1,0} = 0$ allocated by BSAS, (b) $c_{1,0} = 0$ allocated by ISAS, and (c) $c_{1,0} = 21$ allocated by GSAS for $N(\phi_U) = 15$ and $P=1$	84
5.28 Effects of Number of Asynchronous Users $N(\phi_U)$ and Number of Transmit Antennas, P on the Average {SCP, InCP, and ACP} SINR at: (a) $c_{1,0} = 0$ allocated by BSAS, (b) $c_{1,0} = 0$ allocated by ISAS, (c) $c_{1,0} = 21$ allocated by GSAS for Asynchronous Desired User	85
5.29 Effects of Number of Asynchronous Users $N(\phi_U)$ and Number of Transmit Antennas, P on the Average {SCP, InCP, and ACP} SINR at: (a) $c_{1,0} = 0$ allocated by BSAS, (b) $c_{1,0} = 0$ allocated by ISAS, (c) $c_{1,0} = 21$ allocated by GSAS for Synchronous Desired User	86
5.30 Comparison between the Average SCP SINR in (3.34) for single-	87

FIGURE	PAGE
transmit antenna and (Park et al., 2010 eq. (13)) with Synchronous and Asynchronous Desired User Signal at: (a) $c_{1,0}=0$ allocated by BSAS, (b) $c_{1,0}=0$ allocated by ISAS, (c) $c_{1,0}=21$ allocated by GSAS ...	
5.31 Effects of Number of Asynchronous Users $N(\phi_U)$ on the Average {SCP, InCP, and ACP} BER for QPSK, 16-QAM, and 64-QAM at: (a) $c_{1,0}=0$ Allocated by BSAS, (b) $c_{1,0}=0$ Allocated by ISAS, (c) $c_{1,0}=21$ Allocated by GSAS for $P=1$, and Asynchronous Desired User	88
5.32 Effects of average SINR on the Average {SCP, InCP, and ACP} BER for QPSK, 16-QAM, and 64-QAM at: (a) $c_{1,0}=0$ Allocated by BSAS, (b) $c_{1,0}=0$ Allocated by ISAS, (c) $c_{1,0}=21$ Allocated by GSAS for Asynchronous Desired User	89
5.33 Instantaneous Powers of SCP Signal Components $\ln \phi_{u,n}^{\phi,\varepsilon} Y_{u,n}^{p,q} (i=c_{u,g})$ At: (A) $c_{1,0}=0$ Allocated By BSAS, (B) $c_{1,0}=0$ Allocated By ISAS, (C) $c_{1,0}=21$ Allocated By GSAS	94
5.34 Instantaneous Powers Of InCP Signal Components $\ln \phi_{u,n}^{\phi,\varepsilon} Y_{u,n}^{p,q} (i=c_{u,g})$ At: (A) $c_{1,0}=0$ Allocated By Bsas, (B) $c_{1,0}=0$ Allocated By Isas, (C) $c_{1,0}=21$ Allocated By GSAS	95
5.35 Instantaneous Powers of ACP Signal Components $\ln \phi_{u,n}^{\phi,\varepsilon} Y_{u,n}^{p,q} (i=c_{u,g})$ At: (A) $c_{1,0}=0$ Allocated By BSAS, (B) $c_{1,0}=0$ Allocated By ISAS, (C) $c_{1,0}=21$ Allocated By GSAS	96
5.36 Instantaneous {SCP, InCP, and ACP} SINR from $\phi_{u,n}^{\phi,\varepsilon} Y_{u,n}^{p,q} (i=c_{u,g})$ at: (a) $c_{1,0}=0$ allocated by BSAS, (b) $c_{1,0}=0$ allocated by ISAS, (c) $c_{1,0}=21$ allocated by GSAS	97
5.37 Instantaneous Power of The CAs-SI Versus the Number of Transmit Antennas With: (a) SCP at $c_{1,0}=0$ Allocated by BSAS, (b) InCP at $c_{1,0}=0$ Allocated by BSAS, (c) ACP at $c_{1,0}=0$ Allocated by BSAS (d) SCP at $c_{1,0}=0$ Allocated by ISAS, (e) InCP at $c_{1,0}=0$ Allocated by ISAS, (f) ACP at $c_{1,0}=0$ Allocated by ISAS, (g) SCP at $c_{1,0}=21$ allocated by	98

FIGURE	PAGE
GSAS, (h) InCP at $c_{1,0}=21$ Allocated by GSAS, (i) ACP at $c_{1,0}=0$ Allocated by GSAS for Desired User's TO $\zeta_{u,n}^{p,q}=0$, and 146	
5.38 Average {SCP, InCP, and ACP} CAs-SI Versus the Number of Transmit-Antennas in Presence of TO and CFO at: (a) $c_{1,0}=0$ Allocated by BSAS, (b) $c_{1,0}=0$ Allocated by BSAS, (c) $c_{1,0}=36$ Allocated by BSAS	99
5.39 Instantaneous {SCP, InCP, ACP} MUI for various $N(\epsilon U)$ and $\zeta_{u,n}^{p,q}=0$ at: (a) $c_{1,0}=0$ allocated by BSAS, (b) $c_{1,0}=0$ allocated by ISAS, and (c) $c_{1,0}=21$ allocated by GSAS for $P=1$	100
5.40 Instantaneous {SCP, InCP, ACP} MUI for various $N(\epsilon U)$ and $\zeta_{u,n}^{p,q}=-37$ at: (a) $c_{1,0}=0$ allocated by BSAS, (b) $c_{1,0}=0$ allocated by ISAS, and (c) $c_{1,0}=21$ allocated by GSAS for $P=1$	101
5.41 Instantaneous {SCP, InCP, ACP} MUI for $P=1, 2, 4,$ and 8 antennas at: (a) $c_{1,0}=0$ allocated by BSAS, (b) $c_{1,0}=0$ allocated by ISAS, and (c) $c_{1,0}=21$ allocated by GSAS for $N(\phi U)=15$	102
5.42 Effects of Number of Asynchronous Users $N(\phi, \epsilon U)$ and Number of Transmit Antennas, P on the Average {SCP, InCP, and ACP} MUI in Presence of TO and CFO at: (a) $c_{1,0}=0$ Allocated by BSAS, (b) $c_{1,0}=0$ Allocated by ISAS, (c) $c_{1,0}=36$ Allocated by GSAS	103
5.43 Instantaneous {SCP, InCP, ACP} SINR for Various $N(\phi, \epsilon U)$ and $\zeta_{u,n}^{p,q}=0$ at: (a) $c_{1,0}=0$ Allocated by BSAS, (b) $c_{1,0}=0$ Allocated by ISAS, and (c) $c_{1,0}=21$ Allocated by GSAS for $P=1$	106
5.44 Instantaneous {SCP, InCP, ACP} SINR for various $N(\phi, \epsilon U)$ and $\zeta_{u,n}^{p,q}=37$ at: (a) $c_{1,0}=0$ allocated by BSAS, (b) $c_{1,0}=0$ allocated by ISAS, and (c) $c_{1,0}=21$ allocated by GSAS for $P=1$	107
5.45 Instantaneous {SCP, InCP, ACP} SINR for $P=1, 2, 4,$ and 8 antennas at: (a) $c_{1,0}=0$ allocated by BSAS, (b) $c_{1,0}=0$ allocated by ISAS, and (c) $c_{1,0}=21$ allocated by GSAS for $\zeta_{u,n}^{p,q}=0$ and $N(\phi, \epsilon U)=15$	108

FIGURE	PAGE
5.46 Instantaneous {SCP, InCP, ACP} SINR for P=1, 2, 4, and 8 antennas at: (a) $c_{1,0}=0$ allocated by BSAS, (b) $c_{1,0}=0$ allocated by ISAS, and (c) $c_{1,0}=21$ allocated by GSAS for $\zeta_{u,n}^{p,q} = 37$ and $N(\phi, \varepsilon, U) = 15$	109
5.47 Effects of Number of Asynchronous Users $N(\phi, \varepsilon, U)$ and Number of Transmit Antennas, P on the Average {SCP, InCP, and ACP} SINR in Presence of TO and CFO at: (a) $c_{1,0}=0$ Allocated by BSAS, (b) $c_{1,0}=0$ Allocated by ISAS, (c) $c_{1,0}=36$ Allocated by GSAS	110
5.48 Effects of Number of Asynchronous Users $N(\phi, \varepsilon, U)$ on the Average {SCP, InCP, and ACP} BER for QPSK, 16-QAM, and 64-QAM at: (a) $c_{1,0}=0$ Allocated by BSAS, (b) $c_{1,0}=0$ Allocated by ISAS, (c) $c_{1,0}=21$ Allocated by GSAS for P=1, and Asynchronous Desired User	111
5.49 Effects of average SINR on the Average {SCP, InCP, and ACP} BER for QPSK, 16-QAM, and 64-QAM in Presence of TO and CFO at: (a) $c_{1,0}=0$ Allocated by BSAS, (b) $c_{1,0}=0$ Allocated by ISAS, (c) $c_{1,0}=21$ Allocated by GSAS for Asynchronous Desired User	112
5.50 Instantaneous Powers of the DS in $\varepsilon, \xi Y_{u,n}^{p,q} (i=c_{u,g})$ at: (a) $c_{1,0}=0$ allocated by BSAS, (b) $c_{1,0}=0$ allocated by ISAS, (c) $c_{1,0}=21$ allocated by GSAS	114
5.51 Instantaneous Powers of the ICI in $\varepsilon, \xi Y_{u,n}^{p,q} (i=c_{u,g})$ at: (a) $c_{1,0}=0$ allocated by BSAS, (b) $c_{1,0}=0$ allocated by ISAS, (c) $c_{1,0}=21$ allocated by GSAS	115
5.52 Instantaneous Powers of the ISI in $\varepsilon, \xi Y_{u,n}^{p,q} (i=c_{u,g})$ at: (a) $c_{1,0}=0$ allocated by BSAS, (b) $c_{1,0}=0$ allocated by ISAS, (c) $c_{1,0}=21$ allocated by GSAS	116
5.53 Instantaneous SINR from $\varepsilon, \xi Y_{u,n}^{p,q} (i=c_{u,g})$ at: (a) $c_{1,0}=0$ allocated by BSAS, (b) $c_{1,0}=0$ allocated by ISAS, (c) $c_{1,0}=21$ allocated by GSAS.	117
5.54 Instantaneous Power of the CAs-SI versus the Number of Transmit Antennas at: (a) $c_{1,0}=0$ Allocated by BSAS, (b) $c_{1,0}=0$ Allocated by	119

FIGURE	PAGE
ISAS, (c) $c_{1,0}=0$ Allocated by GSAS for $\epsilon_{1,n}^a \in [-0.5, -0.1, 0, 0.1, 0.5]$ and $\xi_{1,n}^a = -0.5, 0$ and 0.5	
5.55 Instantaneous MUI for $N(\epsilon, \xi, U) \neq \emptyset$, $\xi_{u,n}^a = \{-0.5, 0, 0.5\}$ and $\epsilon_{u,n}^a \in [-0.5, 0.5]$ at: (a) $c_{1,0}=0$ Allocated by BSAS, (b) $c_{1,0}=0$ Allocated by ISAS, and (c) $c_{1,0}=21$ Allocated by GSAS for $P=1$	121
5.56 Effects of Number of Asynchronous Users $N(\epsilon, \xi, U)$ on the instantaneous MUI at: (a) $c_{1,0}=0$ Allocated by BSAS, (b) $c_{1,0}=0$ Allocated by ISAS, (c) $c_{1,0}=21$ Allocated by GSAS for $\epsilon_{u,n}^a = \{-0.5, -0.05, 0.05, 0.5\}$, $\xi_{u,n}^a = \{-0.5, 0, 0, 0.5\}$ and P	122
5.57 Effects of Number of Transmit-Antennas on the Instantaneous Asynchronous MUI at: (a) $c_{1,0}=0$ Allocated by BSAS, (b) $c_{1,0}=0$ Allocated by ISAS, (c) $c_{1,0}=21$ Allocated by GSAS for $N(\epsilon, \xi, U)=1$, $\epsilon_{u,n}^a \in [-0.5, 0.5]$, and $\xi_{u,n}^a = \{-0.5, 0, 0, 0.5\}$	123
5.58 Instantaneous SINR for $N(\epsilon, \xi, U) \neq \emptyset$, $\xi_{u,n}^a = \{-0.5, 0, 0.5\}$ and $\epsilon_{u,n}^a \in [-0.5, 0.5]$ at: (a) $c_{1,0}=0$ Allocated by BSAS, (b) $c_{1,0}=0$ Allocated by ISAS, and (c) $c_{1,0}=21$ Allocated by GSAS for $P=1$	124
5.59 Effects of Number of Asynchronous Users $N(\epsilon, \xi, U)$ on the Instantaneous SINR at: (a) $c_{1,0}=0$ Allocated by BSAS, (b) $c_{1,0}=0$ Allocated by ISAS, (c) $c_{1,0}=21$ Allocated by GSAS for $\epsilon_{u,n}^a = \{-0.5, -0.05, 0.05, 0.5\}$, $\xi_{u,n}^a = \{-0.5, 0, 0, 0.5\}$ and $P=1$	125
5.60 Effects of Number of Transmit-Antennas on the Instantaneous Asynchronous SINR at: (a) $c_{1,0}=0$ Allocated by BSAS, (b) $c_{1,0}=0$ Allocated by ISAS, (c) $c_{1,0}=21$ Allocated by GSAS for $N(\epsilon, \xi, U)=1$, $\epsilon_{u,n}^a \in [-0.5, 0.5]$, and $\xi_{u,n}^a = \{-0.5, 0, 0, 0.5\}$	126

LIST OF ABBREVIATIONS

A. LIST OF SYMBOLS

B_{TO}^- and B_{TO}^+	The Boundaries of The Time Offset Towards (Negative) and Away (Positive) from The Cyclic Prefix Respectively
c_u , and $c_{u,g}$	Indices of the u^{th} user subcarriers, and index of the g^{th} subcarrier of the u^{th} user Respectively
$E[\]$	Statistical Expectation
$f_{\text{SINR}_{k,\text{XCP}}^{q,\Delta}}(i)$ (), and	Probability Density Function (pdf), and Cumulative Distribution
$F_{\text{SINR}_{k,\text{XCP}}^{q,\Delta}}(i)$ ()	Function (CDF) for Asynchronous SINR
g or m	Subcarrier Index
$G_u^{\text{syn.}}$, and $G_u^{\text{asyn.}}$	Synchronous and Asynchronous Antennas Group Respectively
$H_{u,n}^{p,q}(i)$, and $\alpha_{u,n,i}^{p,q}$	Channel frequency Response on the i^{th} Subcarrier of the u^{th} user's Channel During the n^{th} OFDMA Symbol, and Channel Complex Fading Gain
L and l	Number of Channel Paths (Taps), and index of the channel path Respectively
N_c , N_u , and N_{cp}	Total number of Subcarriers, Number of allocated subcarriers to the u^{th} user, and Number of Cyclic Prefix Samples Respectively
$N(x)$	The number of x
P and Q	Number of Receive and Transmit Antennas Respectively
P_{DS} , P_{DS-SI} , P_{CAs-SI} , P_{MUI} , and P_w	Power Of The Desired Signal, Desired Signal-Self Interference, Co-Antennas-Self Interference, Multi-User Interference and Noise Respectively
$P_{s,\text{XCP}}^{\Delta}$, and $P_{b,\text{XCP}}^{\Delta}$	Average symbol and Bit Error Rate Respectively
$\Pr(x)$	Probability of x
$r_n^q(t)$	The n^{th} Received Signal by the q^{th} Antenna
$\text{SINR}_{k,\text{XCP}}^{q,\Delta}(i)$	Asynchronous Signal-to-Interference-Plus-Noise Ratio with Different Cyclic Prefix Condition at the i^{th} Subcarrier

sgl	Signal Components in $\phi, \epsilon, \xi Y_{u,n}^{p,q}(i)$
T_s, T_c, T_{cp} , and T	Sampling Interval, Data symbol Interval, Cyclic Prefix interval, and OFDMA symbol Interval Respectively
U, u, k and $\phi, \epsilon, \xi U \subset \{1, \dots, U\}$	Number of Active Users, Index of Any User, Index of the Desired User, and Group of Asynchronous Users Respectively
$w_n^q(t), w_n^q(zT_s)$ and $w_n^q(i)$	Additive White Gaussian Noise, Sampled Additive White Gaussian Noise, and DFT of the Sampled Additive White Gaussian Noise at the i^{th} Subcarrier Respectively
$X_{u,n}^p$, and $S_{u,n}^p$	N_u -length, and N_c -length data symbol transmitted on the p^{th} antenna at the n^{th} symbol Respectively
z	An Integer Sample Index
$\delta(\cdot)$	Dirac-delta function
$\epsilon_{u,n}^q, \mu_{u,n}^{p,q} = \zeta_{u,n}^{p,q} T_s$ and $\xi_{u,n}^q$	Carrier Frequency Offset, Time Offset and Sampling Clock Frequency Offset Respectively
$\sigma_x^2, \sigma_h^2(l)$ and σ_w^2	Variance of $X_{u,n}^p(g)$, Power Delay Profile of The Channel at the l^{th} Path, and Variance of the AWGN Respectively
τ_{\max}	Maximum Possible Delay
$\Phi = \{a, b, c, d, e, f, g\}$	Ranges of the Time Offset
$\Delta \in \{\phi, \epsilon, \xi\}$	Synchronization offset(s) such as TO, CFO, and SCFO
$(x)^*$	Complex Conjugate of x

B. LIST OF ABBREVIATIONS

2D	Two(bi)-Dimensional
3G	The Third Generation
3GPP	The 3 rd Generation Partnership Project
4G	The Fourth Generation
ACP	Absent Cyclic Prefix
ADC	Analog-to-Digital Converter
AWGN	Additive White Gaussian Noise

B3G	Beyond The Third Generation
B4G	Beyond The Fourth Generation
BER	Bit Error Rate
BS	Base Station
BSAS	Block Subcarrier Allocation Scheme
CAs-SI	co-transmit antennas-Self Interference
CDF	Cumulative Distribution Function
CFO	Carrier Frequency Offset
CHF	Characteristic Function
CIR	Carrier to Interference Ratio
CP	Cyclic Prefix
CSI	Channel State Information
DAB	Digital Audio Broadcasting
DAC	Digital-to-Analog Converter
DFT	Discrete Fourier Transform
DS	Desired Signal
DS-SI	Desired Signal-Self Interference
DVB	Digital Video Broadcasting
FDMA	Frequency Division Multiple Accesses
GA	Gaussian Approximation
GI	Guard Interval
GSAS	Generalized Subcarrier Allocation Scheme
HIPERLAN	High Performance Radio Local Area Network
i.i.d	Independently And Identically Distributed
IBI	Inter-Block Interference
ICI	Inter-Carrier Interference
IDFT	Inverse Discrete Fourier Transform
IEEE	Institute of Electrical and Electronics Engineers
InCP	Insufficient Cyclic Prefix

ISAS	Interleaved Subcarrier Allocation Scheme
ISI	Inter-Symbol Interference
iSI	intra-Symbol Interference
ITU-R	International Telecommunications Union- Radio communication
LO	Local Oscillator
MAI	Multiple Access Interference
MBWA	Mobile Broad Wireless Access
MC-CDMA	Multicarrier-Carrier Division Multiple Access
MCDS-CDMA	Multi-Carrier Direct Sequence CDMA
MIMO	Multiple-Input Multiple-Output
M-OFDM	Multiuser-OFDM
MPSK	Multi-Phase Shift Keying
MT-CDMA	Multi-Tone CDMA
MUI	Multi-User Interference
NDF	Normalized Doppler Frequency
OFDM	Orthogonal Frequency Division Multiplexing
OFDMA	Orthogonal Frequency Division Multiple Access
pdf	Probability Density Function
PIC	Parallel Interference Canceller
ppm	part per million
QAM	Quadrature Amplitude Modulation
QoS	Quality of Service
QPSK	Quadrature Phase Shift Keying
S(I)NR	Signal-to-(Interference) plus Noise Ratio
SAS	Subcarrier Allocation Scheme
SCFO	Sampling Clock Frequency Offset
SCP	Sufficient Cyclic Prefix
SDMA	space division multiple access
SEP	symbol error probability

SER	Symbol Error Rate
SISO	Single-Input Single-Output
SSD	Signal Space Decomposition
TDL	Tapped Delay Line
TDVB	Terrestrial Digital Video Broadcasting
TO	Time Offset
UMTS	Universal Mobile Telecommunication System
VoIP	Voice Over Internet Protocol
w.r.t	With Respect To
WiMAX	Worldwide Interoperability for Microwave Access
WLAN	Wireless Local Area Networks
WPAN	Wireless Personal Area Network
WSSUS	Wide Sense Stationary, Uncorrelated Scattering

CHAPTER I

INTRODUCTION

1.1 Introduction

The demands for new and higher data rates wireless communication services such as multimedia streaming, video surveillance, Voice over Internet Protocol (VoIP), video conferencing, interactive gaming, and mobile TV, are rapidly growing, where new radio frequency bands are very scarce if available at all; beside the power limitations of the terminal stations. Thus, future wireless communication systems must provide higher bandwidth efficiencies that can achieve higher user capacities and faster data rate with low complexity by introducing advanced features to existing cellular and other wireless communication systems standards (Juntti et al., 2005). Concurrently, initiating the research and development towards the introduction of future wireless communication systems, including fourth generation (4G) cellular systems and beyond the fourth generation (B4G); where the vision of the next generation wireless systems is not only to support high speed data transmission and cover the need for new communication services but also to enable the integration of existing technologies in a unified platform (Fazel, and Kaizer, 2008).

The main technical and theoretical challenges in future wireless systems concepts creation are: bandwidth efficiency challenge ($2\text{--}10\text{b/s/Hz}$), and frequency selectivity challenge due to the large bandwidth ($\gg 100\text{ MHz}$). The bandwidth efficiency challenge requires novel solutions in both the network and physical layers. The latter could include powerful coding and modulation methods, transmission adaptation techniques, and antenna configurations (Juntti et al., 2005).

Multiple-Input Multiple-Output (MIMO), sometimes called a “volume-to-volume” wireless link, communications based on multiple transmit and receive antennae is a very promising technique to increase bandwidth efficiency, and is seen as a potential key solution for fading channels with rich enough scattering (Juntti et al., 2005 and references therein). The advantages of the MIMO can be used to increase both the

network's quality of service (QoS) and the operator's revenue significantly (Wang et al., 2008), which leads to propose the MIMO concept in the third generation (3G), beyond the third generation (B3G) and the fourth generation (4G) (Foschini and Gans, 1998).

On the other hand, Orthogonal Frequency Division Multiplexing (OFDM), being a multicarrier modulation technique, can effectively handle frequency-selective fading channels without complex equalization structures as well as the enhancement of noise at the receiver by dividing the given bandwidth into narrow sub-channels to make them (almost) frequency-flat. The demodulation and modulation processes have very low complexity when the Discrete Fourier Transform (DFT) and its inverse (IDFT) are used. The OFDM is widely used in both wireless and wired applications. In the wireless arena, OFDM has been standardized for Digital Audio Broadcasting (DAB), Digital Video Broadcasting (DVB), and Wireless Local Area Networks (WLAN) such as IEEE 802.11a/g (Ibars, and Bar-Ness, 2001) and IEEE 802.16a fixed wireless broadband access systems.

However, wireless communications share the transmission media, namely the wireless channel, and generally involve multiple users, hence the need for a multiple-access technique. There are different multiple access schemes based on OFDM modulation such as: Multiuser-OFDM (M-OFDM) also referred as Orthogonal Frequency Division Multiple Access (OFDMA); and Multicarrier-Carrier Division Multiple Access (MC-CDMA) (Ibars, and Bar-Ness, 2001 and references therein).

Multiuser-OFDM (M-OFDM) or OFDMA, is one of the promising candidates for efficiently sharing the wireless communication channel, which combines OFDM with frequency division multiple accesses (FDMA), by allowing multiple users to transmit information simultaneously by allocating exclusive subcarriers to each user.

The Multi-Carrier Code Division Multiple Access (MC-CDMA), which combines OFDM and CDMA with proposed techniques such as Multi-Carrier Direct Sequence CDMA (MCDS-CDMA), and Multi-Tone CDMA (MT-CDMA); permits multiple users to access the wireless channel simultaneously by modulating and spreading their input

data signals across the frequency domain using different spreading sequences (Hara and Prasad, 1997; Phasouliotis and So, 2009, and references therein).

The combination of multiple smart antennas at both transmitter and receiver (MIMO), which allows substantial increase in peak data rates, significantly higher spectrum efficiency especially in low-interference environments, and increased system capacity (number of users) without increasing the transmission bandwidth or the total transmitted power of the system, with the multi-carrier transmission techniques such as MC-CDMA and OFDMA are promising techniques for the future broadband mobile communication systems due to dealing with the multipath propagation at a low complexity, high spectral efficiency and ability to deal with frequency selective fading as well as narrowband interference (Zhou et al., 2005 ; Horlin et al., 2006; Yu et al., 2008 and reference therein).

Although MC-CDMA has garnered significant attention in China and Europe (Zhang et al., 2005) due to the success of CDMA in the existing third generation (3G) networks, a performance analysis and comparison between the two candidates i.e. MC-CDMA and OFDMA draw a great attention in the research pool. In most of these performance analyses of MIMO-MC-DMA and MIMO-OFDMA, such as (Lindner et al., 1998; Ibars and Bar-Ness, 2001; Lo et al., 2007; Phasouliotis and So, 2009), the later scheme outperforms the MIMO-MC-CDMA due to the increase of the Multiuser Interference (MUI), which is proportional to the system load. Furthermore, there was no MIMO-MC-CDMA receiver that could match the performance of MIMO-OFDMA ones. This is also a part of the reason why MIMO MC-CDMA has drawn less attention than OFDMA recently (Phasouliotis and So, 2009 and references therein).

1.2 Motivations and Rationales

Along with its attractive features, the drawbacks associated with OFDM are directly inherited by MIMO-OFDMA such as synchronization offsets between the transmitter and the receiver, channel estimation and the nonlinearities of the transmitter high power amplifiers (Barbarossa et al., 2002), which degrade crucially the performance of the candidate system (i.e. MIMO-OFDMA).

However, the synchronization is the process of acquiring the transmitted signal by the receiver through detecting the existence of the transmitted signal and determining approximately the timing of the transmission (Bliss and Parker, 2010) as well as the frequency offsets in the system, to establish a wireless communication link. Therefore, time synchronization is the process of elimination/mitigation of the time offset (TO) by finding the best possible time instant for the start of the received OFDM symbol. Although the OFDM is well known for its ability to combat Inter-Symbol Interference (ISI) introduced by multipath fading channel, incorrect positioning of the DFT window within an OFDM symbol reintroduces ISI during data demodulation at the receiver. The ISI causes delayed versions of received symbols to overlap and interfere with each other, which is causing serious performance degradation (Speth et al., 1999) through perturbing orthogonality of the received subcarriers (Zhangyong et al., 2003).

In addition, frequency synchronization deals with finding an estimate of the carrier frequency offset (CFO). Estimation of the CFO in OFDM-based systems is critical since in its presence, a demodulated signal of one subcarrier is distributed into other subcarriers (loss of subcarrier orthogonality) as interference, which is called Inter-Carrier Interference (ICI) and causes performance degradation (Moose, 1994; Pollet et al., 1995; Engels, 2002; Zhangyong et al., 2003). Accurate frequency synchronization is thus essential for reliable reception of the transmitted data.

Furthermore, in converting the received waveform back into digital signal, the Analog-to-Digital Converter (ADC) samples at time instants that are coincided with the time instant of the Digital-to-Analog Converter (DAC) at the transmitter, where the difference between these clocks of the two converters is called the sampling clock frequency offset (SCFO). Then the purpose of sampling clock frequency synchronization is to align the receiver sampling clock frequency to that of the transmitter, where the receiver sample interval is usually differ from that of the transmitter (Baoguo et al., 2000). Hence in the received signal, it will either miss a sample or gain a sample over a period of time. However, the sampling clock frequency offset (SCFO) includes the clock phase offset, of which its effect is similar to symbol time offset, as well as the clock frequency

offset (Yang et al., 2001). Hence, in this research only the clock frequency offset is treated. The SCFO can be deleterious to the OFDM-based system, by introducing ISI due to a drift in the symbol timing window because of the accumulation of offset (Yuanxin et al., 2008), and then the SCFO can further worsen the symbol synchronization problem. Furthermore, the SCFO introduces Inter-Carrier Interference ICI (Wen-Long and Chen, 2008) due to violate of the subcarriers orthogonality. In addition, the increment or decrement of the samples of the desired OFDM symbol in the DFT window due to negative or positive SCFO respectively, would cause a shift in the estimated channel impulse response.

Generally, MIMO-OFDMA system requires synchronization in the time, frequency (Zhou et al., 2005 and references therein) and sampling clock frequency (Baoguo et al., 2000). Moreover, in uplink MIMO-OFDMA systems, coherent signal detection at the base station (BS) requires the channel state information (CSI) of all uplink channels between the BS and mobile users. To obtain the CSI, channel estimators are designed at the BS receiver using pilot symbols. Due to the time-varying nature of multipath fading channels, the CSI has to be updated continuously and promptly (Wang et al., 2008).

Moreover, synchronization offsets and channel estimation are unfortunately a more difficult task in uplink scenario (Van de Beek et al., 1999; Morelli, 2004), due to the number of unknowns (Sezginer and Bianchi, 2008). In particular, parameter estimation based on the direct maximization of the log-likelihood function is impractical where it involves a bi-dimensional (2D) numerical search in the uplink OFDMA system.

The estimation complexity of the TO, CFO, SCFO and the channel impulses in OFDMA is inherited when MIMO technique is integrated, and became more complex especially when all new users enter simultaneously the system and regardless of the subcarriers assignment scheme is enabled.

However, the synchronization offsets in the OFDM-based systems, can be addressed in two different ways: the first focuses on mitigation/estimation of individual and joint asynchronous TO, CFO, and SCFO through suboptimal algorithms such as (Van de Beek et al., 1999; Morelli and Mengali, 2000; Baoguo et al., 2000; Barbarossa et

al., 2002; Cao et al., 2003; Morelli, 2004; Pun et al., 2006; Saemi et al., 2007; Sezginer and Bianchi, 2008; Xu et al., 2008) for OFDMA uplink systems. The other way involves performance evaluation such as (Pollet et al., 1995; Wei and Schlegel, 1995; Nishookar and Prasad, 1996; Speth et al., 1999; Tomba, 1998; Armstrong, 1999; Sathananthan and Tellambura, 2001; El-Tanany et al., 2001; Athaudage, 2002; Wang et al., 2003; Park et al., 2003; Lee et al., 2004; Rugini and Banelli, 2005; Zhou et al., 2006a; Zhou et al., 2006b; Mostofi and Cox, 2006; Wei and Lindner, 2007; Wen-Long and Chen, 2008; Raghunath and Chockalingam, 2009; Park et al., 2010) in OFDM/OFDMA uplink systems. Recently Voltz et al. (2006), Liu et al. (2008), Koivisto and Koivunen (2009), Kotsch and Fettweis (2010) and Kotsch et al. (2010) conducted a performance evaluation for MIMO-OFDM(A) systems. It is worthy to note that the performance evaluation, generally, can be calculated in two ways: firstly, it may be approximately derived as degradation in metrics of power loss such as Signal-to-(Interference) plus Noise Ratio (S(I)NR) and Carrier to Interference Ratio (CIR). Lastly, the Bit Error Rate/Symbol Error Rate (BER/SER) could be approximated using the central limit theory.

In this thesis, a performance evaluation in terms of the SINR at the DFT output of the receiver and BER/SER are conducted for MIMO-OFDMA uplink systems over multipath fading channel in presence of synchronization offsets. The analytical results provides a useful reference or test bed in designing suitable synchronization algorithms as well as performance evaluation for the MIMO-OFDMA uplink system applications

1.3 Objectives

The main objective of this research is to analyze comprehensively and characterize quantitatively the impacts of the individual and joint synchronization offsets on MIMO-OFDMA uplink systems performance.

This main objective includes the following sub-objectives:

1. Develop a comprehensive mathematical model represents the effect of the individual and joint synchronization offsets on the received signal at any receiving antenna in MIMO-OFDMA fading channels uplink systems. The

effects of these impairments can be represented in terms of additional amplitude reduction, and phase shift encounter the desired signal, as well as the interference such as the Multiple User Interference (MUI) i.e., Multiple Access Interference (MAI), according to the incurred ICI and ISI components at the DFT output at any subcarrier.

2. Determine the exact asymmetric boundaries of the TO, which are essential to define fully its distribution.
3. Develop exact expressions for the average Signal-to-Interference plus Noise Ratio (SINR), and the Bit Error Rate/Symbol Error Rate (BER/SER) as system performance measurements in presence of individual and joint synchronization offsets where no prior assumptions of the statistical properties of the incurred interferences.

1.4 Scope

The scope of this research includes:

- a. **System and Communication Link:** The system under consideration is the convention MIMO-OFDMA uplink system with U users and one Base Station (BS). The BS and each user are equipped with Q and P antennas respectively. The system using the Discrete Fourier transforms (DFT) and its inverse (IDFT) modules with N_c subcarriers are used. A cyclic prefix (CP) with N_{cp} samples is added to combat the ISI. Moreover, relaxing the CP condition in insufficient CP (InCP) and absent CP (ACP) on the synchronization offsets is also investigated.
- b. **Transmission Channels and Noise:** The slowly time varying multipath fading channel is modeled as a Wide Sense Stationary, Uncorrelated Scattering (WSSUS) channel. The received signal is affected only by the Additive White zero-mean Gaussian Noise (AWGN).

- c. **Synchronization Offsets Parameters:** The investigated synchronization offsets include only the time offset (TO), sampling clock frequency offset (SCFO), and carrier frequency offset (CFO).
- d. **Subcarrier Allocation Scheme:** The general subcarrier allocation schemes (SASs) such as Block SAS, Interleaved SAS and Generalized SAS are exploited.
- e. **Performance Measurement:** The instantaneous and average SINR at the DFT output as well as the BER/SER based on the SINR are nominated to reflect the impact of synchronization offsets on the performance of the system.

1.5 Methodology

To achieve the preceding objectives, the considered methodology can be briefly highlighted in the following:

1. Consider a general SISO/MIMO-OFDMA uplink systems model that compatible with the proposed systems in synchronization offset estimation algorithms such as (Van de Beek et al., 1999; Morelli, 2004; Pun et al., 2006; Saemi et al., 2007; Sezginer and Bianchi, 2008; Wang and Xin, 2008; Jiang et al., 2008a; Jiang et al., 2008b).
2. The contents of the DFT window are exploited to develop expressions for the desired signal and the associated interferences due to the synchronization offset(s) in single-user with single-transmit antenna system. This model is then generalized to MIMO-OFDMA system.
3. The boundaries of the TO be determined under the following assumption: the time index of the DFT window is coinciding to the transmission time of the dominant OFDMA samples occupied the processing window by all channel paths. Hence, the maximum TOs that conserve the n^{th} DFT window belonging to the n^{th} OFDMA symbol rather than its neighbors, are considered the TO's boundaries.

4. The instantaneous and average SINR at the DFT output in presence of synchronization offsets are derived using the power of the desired signal and the associate interferences, as well as the distribution of the synchronization offsets, where no prior assumption on the statistical properties of the interferences.
5. The BER and SER of asynchronous system are derived using the correspondence SINR by utilizing the expressions by Cho and Yoon (2002) and Simon et al. (1995; eq. (10.32)) respectively.
6. The analysis of the impact of the synchronization offsets and the system performance include the following issues as well:
 - I. Insufficient (InCP) and absent (ACP) cyclic prefix,
 - II. Different Subcarrier-Assignment Schemes.

1.6 Thesis Overview

This thesis is organized as follows. In Chapter 2, some researches that investigate the degradation in metrics of power loss in OFDM-based system are reviewed, where the rational of the conducted research can be grasped. In Chapter 3, system, signal, and channel model for uplink MIMO-OFDMA systems are presented. Moreover, the impacts of the synchronization offsets are explored for the desired signal and interference components. Hence, the corresponding instantaneous and average SINR is evaluated. In Chapter 4, the expressions for BER/SER are derived exploiting the corresponding SINR. In Chapter 5, the analytical results are simulated and compared with the competing analysis, where the simulation environments take a scenario similar to ITU-R M.1225, 3GPP TR 25.814, and 3GPP TR 29.913 recommendations. The presented results studied the influence of the CP condition and the subcarrier allocation schemes on the system performance. Finally, Chapter 6 concludes the thesis and suggests future works.

CHAPTER II

BACKGROUND ON PERFORMANCE EVALUATIONS OF OFDMA/MIMO-OFDMA SYSTEMS IN PRESENCE OF SYNCHRONIZATION OFFSETS

2.1 Introduction

Wireless systems are challenged to meet higher data rate requirements for the increasing and demanding applications. Considering the frequency spectrum as being limited and valuable resource, wireless devices are faced with the necessity to utilize the available opportunities of the spectrum and coexist with other legacy or otherwise future systems.

Studies to increase the wireless system throughput have been concerned with improving signal detection algorithms and reducing the impact of various practical impairments to wireless signals. Time, sampling clock frequency and carrier frequency offsets, radio channel propagation effects, and baseband modulator gain and phase imbalances are examples of signal degradation sources those need to be estimated and equalized. Hence determining/minimizing the effects of these impairments increase the system performance such as the *effective* Signal-to-Noise Ratio (SNR) at the receiver, and allow the system to support higher modulation orders and consequently higher data rates. This approach can be considered as maximizing the system spectral efficiency for a given allocated spectrum or bandwidth (Mahmoud, 2009).

However, Fazel and Kaizer (2008) have outlined the horizons of the next generation and beyond by declaring that the exploiting of all forms of diversity (time, frequency, and spatial) in future wireless systems, such as beyond the third generation (B3G), and the fourth generation (4G), will ensure the highest performance in terms of capacity and spectral efficiency.

Orthogonal Frequency Division Multiplexing (OFDM) is one of the most widely used technologies in current communication systems, and has been proposed for multi-user systems such as the Universal Mobile Telecommunication System (UMTS), the Wireless Local Area Network (WLAN) (Tourtier et al., 1993; Schmidl, 1997). One of the main

reasons for choosing OFDM as a multi-carrier modulation method is its robustness and high spectral efficiency especially for high data rate systems. OFDM divides the allocated spectrum into sub-bands that are modulated with orthogonal subcarriers over frequency selective channels; the subcarrier bandwidth becomes smaller than the channel coherence bandwidth. This effect allows the system to use single-tap channel equalizers, instead of the complex equalizers that are usually needed for high bandwidth single carrier signals. Another result of this subcarrier division is that every symbol is modulated over a longer time duration which reduces the Inter-Symbol Interference/Inter-Block Interference (ISI/IBI) effects caused by multipath propagation. Other advantages of OFDM include its scalability and easy implementation using Discrete Fourier Transform (DFT) methods (Mahmoud, 2009 and references therein).

Orthogonal Frequency Division Multiple Access (OFDMA), which is the multi-user version of OFDM (M-OFDM), divides the total signal bandwidth into multiple orthogonal subcarrier groups, with each group being allocated to one user through different subcarrier allocation schemes (SASs), thus each user's signal can be separated easily in the frequency domain. OFDMA has been selected as the physical-layer technology for a number of wireless applications, such as Digital Audio Broadcasting (DAB), Terrestrial Digital Video Broadcasting (TDVB), and also has been adopted by IEEE 802.11a standard in the 5 GHz band, IEEE 802.11g standard in the 2- 4 GHz band, IEEE 802.16d/e WiMAX, and HIPERLAN/2 for high-data-rate wireless packet transmissions (Cao et al., 2004 and references therein). Also, the OFDM-based physical layer is being considered by several standardization groups such as the IEEE 802.15.3 Wireless Personal Area Network (WPAN) and the IEEE 802.20 Mobile Broad Wireless Access (MBWA) groups. Furthermore, OFDMA has been adopted by wireless communication standards as the multiple access technology, which has the advantages of scalability, multi-user gains, and more; compared to the traditional access technologies (Gao et al., 2009), which is emerging as a promising technology for next generation wireless communication systems.

On the other hand, Multiple-Input Multiple-Output (MIMO) transmission techniques seem to be the ultimate way of fulfilling the high data and superior performance requirements of the future generations of wireless and cellular communication systems. The MIMO system, which uses multiple antenna elements to simultaneously transmit and receive signals, proportionally boosts the transmission rate by a factor equal to the number of transmit antenna elements and the signal quality by a factor equal to the number of receive antenna elements. The multiple wireless channels between the transmitter and the receiver are denoted the MIMO channel, since all data are transmitted both in the same frequency band and at the same time, this technique utilizes spectrum very efficiently (Fazel and Kaizer, 2008 and references therein). In addition, if a broadband wireless connection is desired, the data rate must be increased further, which at some point will lead to a frequency selective channel. There are two ways to go, either pre- or post-equalization of the channel is employed or the channel is divided into many narrowband flat fading sub-channels, a technique utilized by OFDM, and transmits data on these sub-channels without the need for channel equalization. Hence, it is possible to convert a frequency selective channel to many flat fading channels using OFDM and apply the developed flat fading MIMO signaling techniques to each of these sub-channels (subcarriers).

Moreover, MIMO technique allows substantial increase in peak data rates, significantly higher spectrum efficiency especially in low-interference environments, and increased system capacity (i.e. number of users) without increasing the transmission bandwidth or the total transmitted power of the system. With the multi-carrier transmission techniques such as Multi-Carrier Code Division Multiple Access (MC-CDMA) and OFDM, MIMO is a promising technique for the future broadband mobile communication systems due to dealing with the multipath propagation at a low complexity and high spectral efficiency and ability to deal with frequency selective fading and narrowband interference, respectively (Zhou et al., 2005; Horlin et al., 2006; Yu et al., 2008 and reference therein). Thus, the combination of OFDMA and MIMO

techniques i.e. MIMO-OFDMA, has become a strong candidate for the next generation wireless networks (Wang et al., 2008; Stuber et al., 2004).

2.2 The Impact of the Synchronization Offsets

Along with its attractive features, the well known drawbacks associated with OFDM are directly inherited by all the OFDM-based systems such as OFDMA systems, MIMO-OFDM(A) systems, and cooperating space division multiple access (SDMA) systems (i.e., Network MIMO-OFDM systems). These drawbacks are: synchronization offsets between the transmitter and the receiver, channel estimation and nonlinearities of the transmitter high power amplifiers (Barbarossa et al., 2002), which degrade crucially the performance of the candidate systems.

The synchronization is the process of acquiring the transmitted signal by the receiver through detecting the existence of the transmitted signal and determining approximately the timing of the transmission (Bliss and Parker, 2009) as well as the frequency offsets in the system, to establish a wireless communication link. In OFDM-based systems, three different effects of synchronization offsets can be identified: Time (TO), Carrier Frequency (CFO), and Sampling Clock Frequency (SCFO) Offsets. Therefore, frequency synchronization deals with finding an estimate of the CFO, which is due to the difference between the Local Oscillator (LO) in the receiver and the transmitter, Doppler shift due to user mobility, and carrier frequency compensation offset (Zhang and Tellambura, 2007). The CFO estimation in OFDM-based systems is critical since in its presence, a demodulated signal of one subcarrier is distributed into other subcarriers (loss of subcarrier orthogonality) as interference, which is called inter-carrier interference (ICI) and causes performance degradation (Moose, 1994; Pollet et al., 1995; Engels, 2002; Zhangyong et al., 2003).

Time synchronization is the process of elimination/mitigation of the TO, which is due to path delay differences between different users, and imperfect time synchronization (RaghuNath and Chockalingam, 2009), by finding the best possible time instant for the start of the received OFDM symbol. Although the OFDM is well known for its ability to

combat inter-symbol interference/inter-block interference (ISI/IBI) introduced by multipath fading channel, incorrect positioning of the discrete Fourier transform (DFT) window within an OFDM symbol reintroduces ISI/IBI during data demodulation at the receiver. This ISI/IBI is causing serious performance degradation (Speth et al., 1999) through perturbing orthogonality of the received subcarriers (Zhangyong et al., 2003).

Moreover, the purpose of sampling clock frequency synchronization is to align the receiver sampling clock frequency to that of the transmitter, where the optimum sampling time in the Digital-to-Analog Converter (DAC) at the transmitter is usually differ from the actual sampling time in the Analog-to-Digital Converter (ADC) at the receiver (Baoguo et al., 2000; Wang et al, 2003). The SCFO can be deleterious to the OFDM-based systems, by introducing ISI due to a drift in the symbol timing window because of the accumulation of offset (Yuanxin et al., 2008), and then the SCFO can further worsen the symbol synchronization problem. Furthermore, the SCFO introduces ICI (Wen-Long and Chen, 2008) due to violate of the subcarriers orthogonality. However, the caused increment or decrement in the number of samples of the desired OFDM symbol in the DFT window due to SCFO would cause a shift in the estimated channel impulse response.

In addition to the ISI/IBI and ICI, inaccurate synchronization offsets estimation introduces Multi-User Interference (MUI) in multiuser-OFDM uplink systems (i.e., OFDMA uplink systems), which degrades as well the overall system's performance (Sezginer and Bianchi, 2008).

Furthermore, coherent detection which constitutes the best demodulation principle implies an accurate estimation of the unknown synchronization offsets as well as channel coefficients. The synchronization offsets estimations in OFDMA/MIMO-OFDMA uplink systems are much more difficult than that in downlink (Sezginer and Bianchi, 2008). In uplink transmission, the correction of the TO of one user's offsets, as example, would misalign the other users (Morelli, 2004), whereas different users introduce different CFO, and SCFO which make their estimation at the base station is a multi-variable estimation problem (Jiang et al., 2008b; Wang and Xin, 2008).

2.3 Performance Evaluation and Optimization of OFDMA/MIMO-OFDMA Uplink Systems In Presence of Synchronization Offsets

The compensation of the synchronization offsets of OFDMA/MIMO-OFDMA uplink systems can be addressed in two different ways: the first focus on mitigation/estimation of synchronization offsets; and the second involves performance evaluation.

However, to cope with ISI from frequency-selective fading channel, as well as possible TO from all uplink users (Park et al., 2010), the last N_{cp} input samples in each input symbol of length N_c , which is known as the Guard Interval (GI) or the Cyclic Prefix (CP), are repeated at the beginning of the symbol. This makes the input sequence periodic and clears the channel memory at the end of each input symbol making the successive OFDMA symbols independent (Lashkarian and Kiaei, 2000). To obtain this benefit, unfortunately, a long timing duration is required, resulting in some reduction in data throughput (Park et al., 2010).

Furthermore, to alleviate the misalignment of the other users encounters the TO compensation of one user, a downlink synchronization scheme was proposed. In this approach an uplink user first estimates the starting point of the downlink frame by means of a specially designed preamble or embedded redundancy (such as a CP), and then adjusts the uplink transmission accordingly, which provides only a rough synchronization for the uplink transmission, and therefore does not guarantee precisely synchronized reception (Park et al., 2010).

The effects of synchronization offsets in OFDM-based systems are, generally, calculated in two ways. Firstly, it may be approximately derived as degradation in Signal-to-Noise Ratio/Signal-to-Interference Ratio/Signal-to-Interference plus Noise Ratio (SNR/SIR/SINR) or the statistical average of the Carrier-to-Interference Ratio (CIR) or the average ICI power, all of which are known as metrics of power loss. Secondly, the Bit Error Rate/Symbol Error Rate (BER/SER) could be approximated by assuming the ICI to be Gaussian base on central limit theory. Alternatively, computer simulations may be used to obtain the performance degradation caused by the ICI (Zhou et al., 2007). It is also both interesting and useful to know the precise correlation between the BER or SER

and these impairments (Santhanam and Tellambura, 2001). Moreover, CFO and clock offset are usually combined as frequency offset, while sampling timing offset is identified as time offset (Wang et al., 2003).

These performance measurements i.e., metrics of power loss and BER/SER, can be reviewed in several papers that have studied the effect of asynchronous OFDM-based systems such as (Pollet et al., 1995; Wei and Schlegel, 1995; Nishookar and Prasad, 1996; Speth et al., 1999; Tomba, 1998; Armstrong, 1999; Santhanam and Tellambura, 2001; El-Tanany et al., 2001; Athaudage, 2002; Wang et al., 2003; Park et al., 2003; Lee et al., 2004; Rugini and Banelli, 2005; Zhou et al., 2006a; Zhou et al., 2006b; Mostofi and Cox, 2006; Wen-Long and Chen, 2008; Raghunath and Chockalingam, 2009; Park et al., 2010).

An approximate analysis of the SNR degradation and BER of single-user OFDM with CFO on additive white Gaussian Noise (AWGN) channels was introduced in (Pollet et al., 1995), which is followed by Speth et al. (1999) who have provided an approximated formula with limited applications for the interference caused by TO. Zhou et al. (2006a) achieved the closed-form expressions of the CIR and ICI power in AWGN channels. Although these analyses have the merit of mathematical simplicity, it is valuable to characterize the performance through the precise relation between the average error probability and the CFO (Zhou et al., 2007). Furthermore, Santhanam and Tellambura (2001) derived the exact SER performance using the Characteristic Function (CHF) of the ICI and the well-known Beaulieu series with CFO on AWGN channels; by making a Gaussian approximation of the ICI, while Zhou et al. (2006b) extended the result to Multi-Phase Shift Keying (MPSK) OFDM systems using the Signal Space Decomposition (SSD). The CIR of OFDM systems with CFO in multipath fading channel was analyzed by Lee et al. (2004).

Exploiting the Gaussian Approximation (GA) of the ICI to determine the average error probability, Rugini and Banelli (2005) presented the BER performance of Quadrature Amplitude Modulation (QAM) and it was expressed as a sum of an infinite series according to the generalized hyper-geometric functions in frequency-selective Rayleigh

and Ricean fading channel with CFO. The GA approach, however, has three main weaknesses. At first, the analytical results using GA of the ICI are identical to both cases that the fixed phase shift is compensated and uncompensated, whereas BER performance will be further degraded for the case of the fixed phase shift not being compensated compared with those of it being compensated. Although it is, secondly, acceptable for the case that both the normalized CFO and the SNR are small, the theoretical analysis of the GA method mismatches the simulation results for other cases. Finally, it appears difficult to evaluate the SER performance such as QPSK and 16-QAM that the conditional SER expression exists the form of $Q^2(\cdot)$, where $Q(\cdot)$ is Q-function (Zhou et al., 2007). However, Zhou et al. (2007) present a performance analysis when the CFO impairs OFDM systems in frequency selective Rayleigh fading channels by applying the CHF of the ICI and the well-known Beaulieu series to evaluate the effects of CFO on SER and BER performance. Note that the analyses in (Pollet et al., 1995; Santhanam and Tellambura, 2001; Lee et al., 2004; Rugini and Banelli, 2005; Zhou et al., 2006a; Zhou et al., 2006b) were conducted without considering the TO.

Mostofi and Cox (2006) have provided a mathematical analysis of the effect of the TO, when the CFO was assumed to be zero, on the performance of an OFDM receiver in a frequency-selective fading environment, and have formulated exact expressions for the power of interference terms and the resulting average SIR, including the impact of ICI and ISI. Furthermore, the analysis was extended to the subsample level. The derived formulas reflected the nonsymmetrical effect of TO on the performance of an OFDM system due to the presence of the CP.

Furthermore, in (Wang et al., 2003) the reception process of OFDM signal with frequency and time offsets was presented, and a closed-form analytical result on the SER with residual synchronization offsets, which are the difference between the estimated and the correct offsets, was derived, when these residuals was proven to be Gaussian distributed.

In the uplink OFDMA systems, however, Wei and Schlegel (1995), El-Tanany et al. (2001), Park et al. (2003), Raghunath and Chockalingam (2009), Zhang and Lindner

(2007), Wen-Long and Chen (2008) and Raghunath and Chockalingam (2009) derived analytical expressions for the system performance such as SIR at the receiver, where most of the BER evaluations in uplink OFDMA are based on simulations such as (Fantacci et al., 2004; Huang and Letaief, 2005; Manohar et al., 2007; Raghunath and Chockalingam, 2010).

Wei and Schlegel (1995) noted that the synchronization requirements for OFDMA systems are tighter than those for single-user systems, where Tonello et al. (2000) consider the joint effects of the TO and CFO in static multipath channels. El-Tanany et al. (2001) presented a performance analysis with CFO, SCFO, and TO. However, their analysis for the TO was based on a restrictive assumption, that the TO is small enough not to cause ISI. With this assumption, the TO results only in a phase rotation. The MUI arising from TO over frequency-selective fading channels is ignored.

Park et al. (2003) expressed the symbol TO between users, when zero CFO was assumed, as the symbol TO with respect to the desired user, and derived an explicit expression of the SNR after analyzing the MUI using the frequency-domain channel transfer function. The SNR expression was a function of the maximum value of the symbol TO in static multipath channels where the TO was uniformly distributed in two regions limited by $[0, N_{cp})$ and $[N_{cp}, N_c + N_{cp})$ respectively. Although this approach simplifies the analysis, it cannot explicitly present the mechanism relating ISI and ICI to MUI. Therefore, these studies do not present how well the analytical results match simulations (Park et al., 2010). Moreover, in (El-Tanany et al., 2001; Park et al., 2003), only analytical results are provided without verification.

Park et al. (2010) have generalized prior work in analyzing MUI in (van de Beek et al., 1999; Morelli, 2004; Park et al., 2003) where the single asynchronous user was studied, and in (Wei and Schlegel, 1995; El-Tanany et al., 2001) where the MUI-free range of asynchronous time offset is assumed. The MUI analysis in (Park et al., 2010) was carried out by dividing the extended range of relative TO into five regions edged by $\left[-(N_c + N_{cp})/2, (N_c + N_{cp})/2\right]$, and by using the Gaussian approximation.

In (Zhang and Lindner, 2007) the effects of CFO on OFDMA systems at downlink and uplink scenarios were investigated. Zhang and Lindner (2007) have stated that the SINR loss due to CFO can be exactly given for AWGN channels, where only an approximate SINR can be obtained in frequency selective fading channels since the average SINR will depend on the values of CFOs as well as the channel characteristics.

Moreover, in (Wen-Long and Chin, 2008) a theoretical SINR is formulated to characterize the losses due to joint synchronization offsets in time-variant multipath fading channels, where the symbol time offsets were confined within three ranges bounded by $(-N_{cp})$ and $(N_c - 1)$. Wen-Long and Chin (2008) concluded that the Normalized Doppler Frequency (NDF) and CFO have similar impacts on the SIR which its values remain the same when $NDF = \sqrt{2}$ CFO. Moreover, Raghunath and Chockalingam (2009) analytically characterized the degradation in the SIR due to large CFO and TO in uplink OFDMA, and presented a Parallel Interference Canceller (PIC) receiver that effectively cancelled the interferences caused by CFO and TO to handle their effect in uplink OFDMA, which in turn can reduce user terminal cost and complexity.

Recently, Park et al. (2010) investigated the effect of asynchronous MUI on the performance of the OFDMA uplink systems in frequency selective Rayleigh fading channel environments using the GA where also the un-coded average symbol error probability (SEP) was obtained with various modulation schemes. In addition, Raghunath and Chockalingam (2010) have extended their research and derived an analytical BER expression that quantify the degradation in BER due to the combined effect of both CFO and TO in uplink OFDMA on Rician fading channels in different cases such as perfect synchronization for the desired user while the other users have non-zero CFO and TO, and when all the users (including the desired user) have non-zero CFO and TO.

Unfortunately, the interference modeling in MIMO environment involves a large number of random variables, and extra interference sources, therefore the extension of these methods i.e. (Wei and Schlegel, 1995; El-Tanany et al., 2001; Park et al., 2003;

Zhang and Lindner, 2007; Wen-Long and Chen, 2008; Raghunath and Chockalingam, 2009; Park et al., 2010), which is not straightforward, should be achieved. Then, a recognizable attention is drawn to evaluate the performance of the asynchronous MIMO system, and some performance studies are available in the open literature such as Voltz et al. (2006), Liu et al. (2008), Koivisto and Koivunen (2009), Kotzsch and Fettweis (2010), and Kotzsch et al. (2010).

Voltz et al. (2006) investigated the performance of a frequency domain re-sampler for MIMO-OFDM systems which has developed for a proposed IEEE 802.11n Task Group in terms of the loss in SNR. Moreover, available frequency domain correction technique was proposed and compared to a competing technique passed upon available digital delay filter (Farrow Filter). Moreover, Liu et al. (2008) proposed a spatial diversity algorithm of sampling clock offset estimation in MIMO-OFDM systems. In addition, a lower complexity sampling clock recovery design was presented.

Koivisto and Koivunen (2009) have studied the impact of frequency and time offsets on cooperative multi-user MIMO-OFDM down-link systems. An expression for the SINR seen at the receiver showing especially how frequency offsets rotate the equivalent channel, thereby causing pre-coding imperfections was also derived (Koivisto and Koivunen, 2009). However, Kovisto and Koivunen (2009) concluded that in cooperative MIMO-OFDM systems, transmission timing imperfections and different propagation delays cause larger time offsets than typically faced in MIMO-OFDM systems.

Kotzsch and Fettweis (2010) have considered fully asynchronous spatially multiplexed transmission with different symbol TO and CFO on each transmitter-receiver link which appears in distributed MIMO systems with multiple users and BSs. A factorized system model for signal transmission in frequency domain where the different effects of the ICI and ISI/IBI are separated and analyzed in terms of SINR degradation was derived (Kotzsch and Fettweis, 2010). Recently, Kotzsch et al. (2010) have presented an analysis of the impact of the ISI in CP limited cooperating space division multiple access (SDMA) systems, which are often referred to as network MIMO systems, where cooperating base stations apply joint signal processing to the receive signals of

several users. Moreover, an investigation of the combined effect of ISI and path loss in a simple symmetric user configuration scenario as well as in a scenario with arbitrary user positioning was carried out based on the derived expression for the post equalization SINR for transmissions with arbitrary symbol timings (Kotzsch et al., 2010).

Moreover, in the considered cooperating SDMA uplink systems (network MIMO) by Kotzsch et al. (2010), both the active users and the cooperating BSs were equipped with a single antenna, which is the same structure of (Kotzsch and Fettweis, 2010), where in (Kovisto and Koivunen, 2009) only the downlink scenario was studied.

However, the maximum allowable TO towards and away from the cyclic prefix, which is known as **the boundaries of the TO**, to the best of our knowledge, is not analyzed in the reviewed literature, although these boundaries were mentioned explicitly such as in (Park et al., 2003; Wen-Long and Chen, 2008; Park et al., 2010); and implicitly such as in (Van de Beek et al., 1999; Morelli, 2004), where the asymmetric (Mostofi and Cox, 2006) boundaries of the TO towards and away from the CP of the OFDM symbol are crucial for defining the distribution of the TO in both estimation algorithms and performance evaluations techniques, and need to be analyzed.

CHAPTER III

PROPOSED ANALYSIS OF INSTANTANEOUS AND AVERAGE SIGNAL-TO-INTERFERENCE PLUS NOISE RATIO (SINR) FOR UPLINK MIMO-OFDMA FADING CHANNEL SYSTEMS IN THE PRESENCE OF SYNCHRONIZATION OFFSETS

3.1. Introduction

In this chapter, a precise interferences analysis of MIMO-OFDMA uplink system in presence of synchronization offsets such as time, carrier frequency and sampling clock frequency offsets with arbitrary subcarrier assignment scheme in multipath Rayleigh fading channel of arbitrary power-delay profiles as well as various CP scenarios is achieved.

The considered system and signals are initially presented, where the correspondence model of the fading channel is described. The impact of the synchronization offsets are analyzed for single-user single-transmit-antennas structure at first, and then generalized for multi-user MIMO systems. It is worthy to mention that the contents of the DFT window are exploited to derive the expressions for the desired signal and the associated interferences in presence of synchronization offsets. Hence, the instantaneous and average SINR can be readily evaluated.

3.2. System, Signals and Channel Model for Uplink MIMO-OFDMA Systems

An uplink OFDMA system with single base station (BS) and U active users is considered as in Figure 3.1. The BS and each user are equipped with Q and P antennas, respectively. N_c -subcarriers, which are sequentially indexed with $\{m\}; m \in [0, N_c - 1]$, are shared by all users; and N_u subcarriers are assigned exclusively, with the index $c_u = \{c_{u,g}\}; u \in [1, U], g \in [0, N_u - 1]$ ¹, to the u^{th} user through dynamic Subcarrier-Assignment Scheme (SAS).

¹ Throughout this thesis, the first subscript (i.e., u) is the user index; while the second (i.e., n) is the symbol index. Furthermore, the single superscript (i.e., p or q) is the index of transmit or receive antenna, while superscript with two arguments (i.e., p, q) is the index of transmit-receive pair antennas. Generally the index within the symbol block is denoted by the arguments (m, g , and i) of the variable such as $x_{u,n}^e(g)$.

It is worthy to note that the SAS (i.e., subcarrier allocation scheme) is used to decide which carrier frequency (subcarrier) will be used for each parallel subset of original binary sequence representing the information source. In other words, each information service requiring access to the wireless medium is assigned a number of subcarriers. Generally, there are three major SASs, namely the Block SAS (BSAS), the Interleaved SAS (ISAS) and the Generalized SAS (GSAS) (Hara and Prasad, 1997). In BSAS, contiguous subcarriers are assigned to each user, where in ISAS; adjacent subcarriers are assigned to different users. Furthermore, in GSAS each user can select the best available subcarriers with the largest channel gains (IEEE 802.16a Standard).

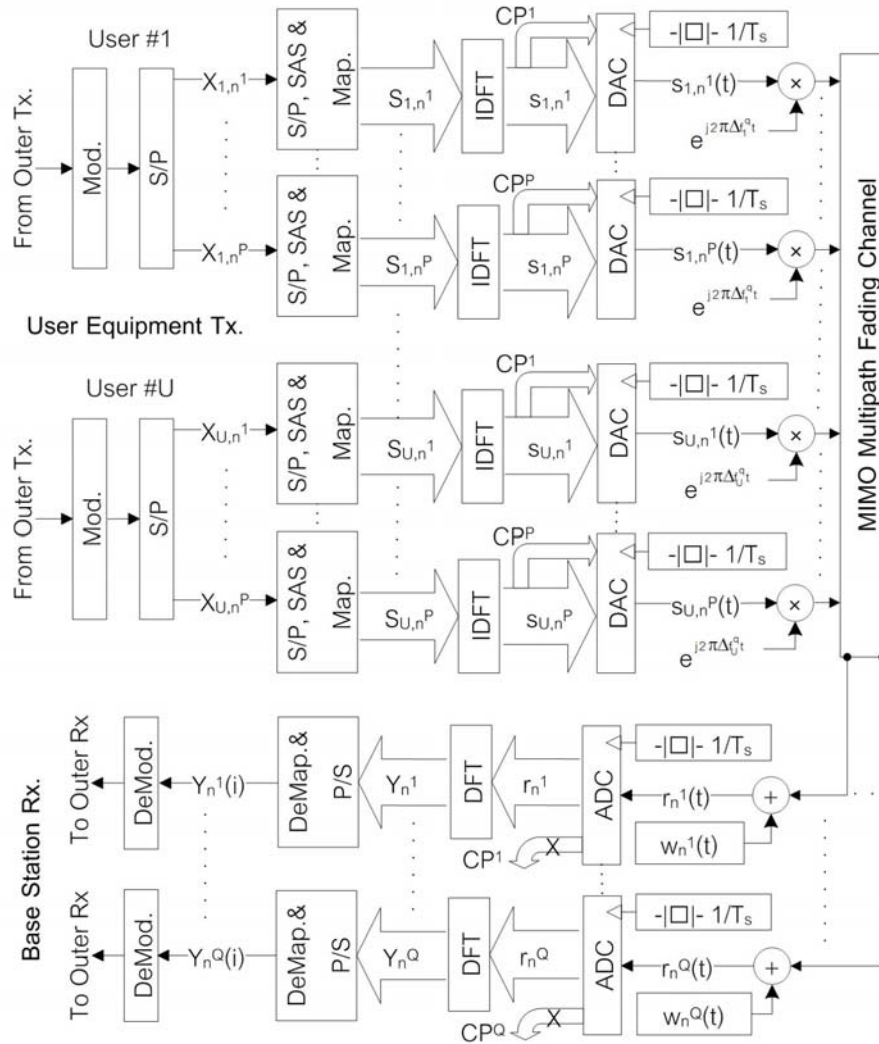


Figure 3.1 Discrete-Time Model of the Baseband Uplink MIMO-OFDMA systems

At the u^{th} user's transmitter, the N_u -length data symbol transmitted on the p^{th} antenna at the n^{th} symbol $X_{u,n}^p = \{X_{u,n}^p(g)\}$ where elements of $X_{u,n}^p$ are assumed to be independently and identically distributed (i.i.d) with zero-mean and variance $E[X_{u,n}^p(g)(X_{u,n}^p(g))^*] = \sigma_x^2$, where $E[\]$ and $(\)^*$ are the statistical expectation and the complex conjugate value, respectively (Zhang and Tellambura, 2007; Zeng and Minny, 2007 and reference therein). $X_{u,n}^p$ is mapped into an N_c -length data symbol $S_{u,n}^p = \{S_{u,n}^p(m)\}$ by:

$$S_{u,n}^p(m) = \begin{cases} X_{u,n}^p(g) & , m = c_{u,g} \\ 0 & , \text{otherwise} \end{cases} \quad m \in [0, N_c - 1] \quad (3.1)$$

Then, $S_{u,n}^p$ is processed by an inverse discrete Fourier transform (IDFT) unit. Before transmission, a cyclic prefix (CP) of length $T_{cp} = N_{cp} T_s$, where N_{cp} is the CP discrete-time samples and T_s is sampling interval, is appended to the IDFT output to combat the ISI due to the dispersive nature of the transmission channel (Cao et al., 2003; Saemi et al., 2007). Thus the n^{th} time-domain signal transmitted on the p^{th} antenna is given by:

$$\begin{aligned} x_{u,n}^p(t) &= \frac{1}{\sqrt{N_c}} \sum_{m=0}^{N_c-1} S_{u,n}^p(m) e^{j2\pi m(t-T_{cp}-nT)/T_c} \\ &= \frac{1}{\sqrt{N_c}} \sum_{g=0}^{N_u-1} X_{u,n}^p(g) e^{j2\pi c_{u,g}(t-T_{cp}-nT)/T_c} \quad ; nT \leq t < (n+1)T, -\infty < n < \infty \end{aligned} \quad (3.2)$$

where $T = (T_c + T_{cp})$ is the duration of one OFDMA symbol, $T_c = N_c T_s$ and $f = 1/T_c$ is the subcarrier frequency spacing.

The signals are transmitted through slowly time-varying multipath fading channel i.e., fading coefficients are assumed to be constant during one OFDMA symbol with unity expected power (Huang et al., 2010; Yang et al., 2001). The channel between the u^{th} user's p^{th} transmit antenna and the BS's q^{th} receive antenna is characterized by a tapped delay line (TDL) with L being the channel order as (Van de Beek et al., 1999; Fuchs, 1999):

$$h_{u,n}^{p,q}(t, \tau) = \sum_{l=0}^{L-1} \alpha_{u,n,l}^{p,q}(t) \delta(\tau - \tau_l^{p,q}) \quad (3.3)$$

where $\alpha_{u,n,l}^{p,q}(t)$ represents the complex fading gain, $\delta(\cdot)$ is the Dirac-delta function and $\tau_l^{p,q} = lT_s$ is the integer value time propagation delay of the l^{th} path, where the maximum possible delay is $\tau_{\max} = (L-1)T_s \leq T_{\text{cp}}$ i.e., sufficient CP (SCP). The correlation relationship between the paths can be expressed by the wide sense stationary uncorrelated scattering (WSSUS) model as (Park et al., 2010): $E\left[\alpha_{k,n,l_1}^{p,q}(t_1) \left(\alpha_{k,n,l_2}^{p,q}(t_2)\right)^*\right] = \delta(l_1 - l_2) \sigma_h^2(l; t_1 - t_2)$, where $\sigma_h^2(l; t)$ is the autocorrelation of the l^{th} path at time t . When $t_1 = t_2$, the autocorrelation function yields the power delay profile of the channel $\sigma_h^2(l; 0) = \sigma_h^2(l)$.

At the uplink receiver side, the signal of one OFDMA symbol is the superposition of signal from all U active users, thus with synchronized system, the received signal at the q^{th} antenna is given by:

$$r_n^q(t) = \sum_{u=1}^U \sum_{p=1}^P \sum_{l=0}^{L-1} \alpha_{u,n,l}^{p,q}(t) x_{u,n}^p(t - lT_s) + w_n^q(t) \quad (3.4)$$

where $w_n^q(t)$ is zero-mean additive white Gaussian Noise (AWGN) with variance σ_w^2 . For demodulation, $r_n^q(t)$ is sampled at $zT_s \equiv (z + N_{\text{cp}})T_s + nT$; $z \in [0, N_c - 1]$ instants, where z is an integer sample index, to remove the CP. If the DFT's search window starts at sample index z , vector $r_n^q(z)$ consisting of N_c consecutive samples is defined as (Figure 3.2): $r_n^q(z) = [r_n^q(z), r_n^q(z+1), \dots, r_n^q(z+N_c-1)]$ and its synchronized DFT output at the i^{th} subcarrier at the BS's q^{th} antenna during the n^{th} OFDMA symbol is given by:

$$Y_n^q(i) = \sum_{u=1}^U \sum_{p=1}^P H_{u,n}^{p,q}(i) S_{u,n}^p(i) + W_n^q(i); i \in [0, N_c - 1] \quad (3.5)$$

where $H_{u,n}^{p,q}(i)$ denote the channel frequency response on the i^{th} subcarrier of the u^{th} user's channel during the n^{th} OFDMA symbol, i.e.,

$$H_{u,n}^{p,q}(i) = \sum_{l=0}^{L-1} \alpha_{u,n,l}^{p,q}(zT_s) e^{-j2\pi i l T_s / T_c}; i \in [0, N_c - 1] \quad (3.6)$$

and $w_n^q(i)$ is the DFT of $w_n^q(zT_s)$.

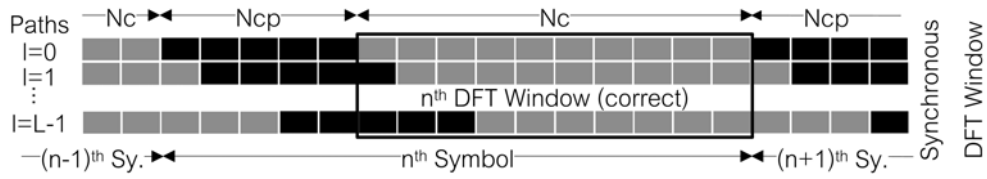


Figure 3.2 General OFDMA Symbol Structure in Multipath fading Channels and Synchronous DFT Window along the Channel Paths

3.3. Average SINR Analysis for Uplink MIMO-OFDMA Fading Channel Systems In The Presence of Time Offset

3.3.1 Single-User Single-Antenna Structure and Time Offset

For the purpose of derivation, only one user u with single-transmit antenna p is firstly analyzed in presence of the TO, where the used notations are kept for smooth analysis generalization to multi-user multiple-antenna structure in subsection 3.3.3.

Considering that each subcarrier is assigned exclusively to one user, linearity of the DFT, and superposition technique; the DFT output for the u^{th} user's p^{th} transmit antenna in the absence of noise can be written from (3.2 and 3.5) as:

$$Y_{u,n}^{p,q}(c_{u,g}) = H_{u,n}^{p,q}(c_{u,g}) X_{u,n}^p(g); g \in [0, N_u - 1] \quad (3.7)$$

Let $\mu_{u,n}^{p,q} = \zeta_{u,n}^{p,q} T_s$ denote the TO encountered over the link between the u^{th} user's p^{th} transmit antenna and the BS's q^{th} receive antenna during the n^{th} OFDMA symbol, which is due to path delay differences between different users, and imperfect time synchronization (Raghunath and Chockalingam, 2009). Moreover, $\mu_{u,n}^{p,q}$ can be decomposed into an integer and fractional parts with respect to T_s (Morelli, 2004). Without loss of generality, only the integer part of the TO is considered in this research, when the fractional, of which its effect is only a phase shift in the received signal (Engels, 2002), is indistinguishable from the phase of the channel impulse response and can be incorporated into its samples $h_{u,n}^{p,q}(t)$ (Morelli, 2004).

From (3.1-3.7), the presence of the TO $\{\zeta_{u,n}^{p,q}\}; \forall p,u$ changes the signal model of (3.7) to:

$$\phi_{u,n}^{p,q}(i) = \frac{1}{\sqrt{N_c}} \sum_{z=0}^{N_c-1} \sum_{l=0}^{L-1} \alpha_{u,n,l}^{p,q}(zT_s) x_{u,n}^p(zT_s - \zeta_{u,n}^{p,q} T_s - lT_s) e^{j2\pi z/N_c}; i \in [0, N_c - 1]^2 \quad (3.8)$$

Considering that the TO in the n^{th} DFT window can occur towards or away from the CP to include samples from either the previous (i.e., the $(n-1)^{\text{th}}$) or the next (i.e., the $(n+1)^{\text{th}}$) OFDMA symbol, respectively, we can define:

$$\frac{1}{N_c} \sum_{z=\phi_{1,sgl}}^{\phi_{2,sgl}} e^{j2\pi z(c_{u,g}-1)/N_c} = \begin{cases} \frac{(\phi_{2,sgl} - \phi_{1,sgl} + 1)}{N_c} & ; c_{u,g} = i \\ \frac{\sin\left(\pi\left(\frac{c_{u,g}-1}{N_c}\right)(\phi_{2,sgl} - \phi_{1,sgl} + 1)\right)}{N_c \sin\left(\pi\left(\frac{c_{u,g}-1}{N_c}\right)\right)} e^{j\pi\left(\frac{c_{u,g}-1}{N_c}\right)(\phi_{1,sgl} + \phi_{2,sgl})/N_c} & ; \text{elsewhere} \end{cases} \quad (3.9)$$

as the interference coefficient between the $c_{u,g}^{\text{th}}$ and i^{th} subcarriers for each signal components: desired signal (DS), ICI, and ISI i.e., $sgl \in \{\text{DS}, \text{ICI}, \text{ISI}\}$. Then, and with the aid of (3.1-3.9), $\phi_{u,n}^{p,q}(i)$ can be rewritten as:

$$\begin{aligned} \phi_{u,n}^{p,q}(i) = & \underbrace{e^{j2\pi\zeta_{u,n}^{p,q}/N_c} x_{u,n}^p(g|_{c_{u,g}=i}) \sum_I \alpha_{u,n,l}^{p,q}(zT_s) e^{-j2\pi l/N_c} \frac{(\phi_{2,DS} - \phi_{1,DS} + 1)}{N_c}}_{\phi_{DS}^{p,q}(i)} \\ & + \sum_{g=0, c_{u,g} \neq i}^{N_c-1} x_{u,n}^p(g) e^{j2\pi c_{u,g}^{p,q}/N_c} \sum_I \alpha_{u,n,l}^{p,q}(zT_s) e^{-j2\pi c_{u,g}/N_c} \frac{1}{N_c} \sum_{z=\phi_{1,ICI}}^{\phi_{2,ICI}} e^{j2\pi z(c_{u,g}-1)/N_c} \\ & + \underbrace{\sum_{g=0}^{N_c-1} x_{u,n\mp 1}^p(g) e^{j2\pi c_{u,g}(\frac{c_{u,n}^{p,q} \pm N_{cp}}{\text{mod} N_c})/N_c} \sum_I \alpha_{u,n\mp 1,l}^{p,q}(zT_s) e^{-j2\pi l/N_c} \frac{1}{N_c} \sum_{z=\phi_{1,ISI}}^{\phi_{2,ISI}} e^{j2\pi z(c_{u,g}-1)/N_c}}_{\phi_{DS-SI}^{p,q}(i)} \end{aligned} \quad (3.10)$$

where the first term on the right-hand side represents the DS i.e. $\phi_{DS}^{p,q}(i)$, which is linearly phase shifted by $j2\pi\zeta_{u,n}^{p,q}/N_c$. The second and the last terms are the ICI and ISI; respectively i.e. $\phi_{DS-SI}^{p,q}(i)$ represent the self-interference (SI) associated with the DS i.e. DS-SI.

² Throughout this thesis, the left superscript such as ϕ , ε and ξ is the asynchronous signal with the TO, CFO, and SCFO respectively. The left subscript such as DS, DS-SI, CAs-SI and MUI is the type of the signal at the DFT output.

The impact of the different signal components of $\phi Y_{u,n}^{p,q}(i)$, especially the ISI, can be investigated comprehensively through proposing a wide range of the TO to the limits that the n^{th} DFT window contains only one sample from the n^{th} OFDMA symbol in any channel path.

To meet the limits of the TO's wide range, seven ranges $\Phi = \{a,b,c,d,e,f,g\}$ are figured, where the main system parameters such as: τ_{max} , L , N_c , and N_{cp} are used to define each range $\phi \in \Phi$. An investigation of contents of the $\phi Y_{u,n}^{p,q}(i)$'s DFT window and an evaluation of the sgl are carried out for each TO's range ϕ in the following.

i. The TO Towards The CP (i.e. $\mu_{u,n}^{p,q} < 0$)

In this scenario, the n^{th} DFT window is formed by samples from the current and the previous OFDMA symbols, according to the value of the TO, which is explored in the following ranges (Figure 3.3):

$$\text{a. } 0 \leq -\mu_{u,n}^{p,q} \leq (T_{\text{cp}} - \tau_{\text{max}}) \equiv 0 \leq -\zeta_{u,n}^{p,q} \leq (N_{\text{cp}} - L + 1)$$

During this interval, all the N_c demodulated samples for any l^{th} path contain only the transmitted data symbols. Moreover, the erroneous n^{th} DFT window captures $(1 - \zeta_{u,n}^{p,q})$ samples from its own CP, and $(N_c + \zeta_{u,n}^{p,q} - 1)$ samples from the desired symbol in each l^{th} path. Then the corresponding $(\phi_{1,\text{sgl}}, \phi_{2,\text{sgl}}) = (a_{1,\text{sgl}}, a_{2,\text{sgl}}); \forall \text{sgl} \in \{\text{DS, ICI, ISI}\}$ to different signal components is given by:

$$(a_{1,\text{DS}}, a_{2,\text{DS}}) = (0, N_c - 1); l \in [0, L - 1] \quad (3.11)$$

$$(a_{1,\{\text{ICI, ISI}\}}, a_{2,\{\text{ICI, ISI}\}}) = 0; l \in [0, L - 1] \quad (3.12)$$

It is worth to note from (3.11-3.12) that the received signal is immune to ICI as well as ISI due to orthogonality conservation because of the CP, then (3.10) can be given by:

$$Y_{u,n}^{p,q}(i) = e^{j2\pi\zeta_{u,n}^{p,q}i/N_c} H_{u,n}^{p,q}(i) X_{u,n}^p(g|_{c_{u,g}=i}) \quad (3.13)$$

$$\text{b. } (T_{\text{cp}} - \tau_{\text{max}}) < -\mu_{u,n}^{p,q} \leq T_{\text{cp}} \equiv (N_{\text{cp}} - L + 1) < -\zeta_{u,n}^{p,q} \leq N_{\text{cp}}$$

In this scenario, two groups of paths can be recognized in the n^{th} DFT window: the first $(N_{\text{cp}} + \zeta_{u,n}^{p,q} + 1); i \in [0, (N_{\text{cp}} + \zeta_{u,n}^{p,q})]$ paths have the same structure as that of range (a). The following $(L - N_{\text{cp}} - \zeta_{u,n}^{p,q} - 1); i \in [(N_{\text{cp}} + \zeta_{u,n}^{p,q} + 1), L - 1]$ paths include $(L - \zeta_{u,n}^{p,q} - N_{\text{cp}})$ samples from the previous OFDMA symbol to compensate the lost samples from the current symbol, generating what is called self interference (i.e. ISI as well as ICI) by the previous symbol contents. Then the corresponding $(\phi_{1,\text{sgl}}, \phi_{2,\text{sgl}}) = (b_{1,\text{sgl}}, b_{2,\text{sgl}}); \forall \text{sgl}$ to different signal components is given by:

$$(b_{1,\text{DS}}, b_{2,\text{DS}}) = \begin{cases} (0, N_c - 1) & ; i \in [0, (N_{\text{cp}} + \zeta_{u,n}^{p,q})] \\ (L - N_{\text{cp}} - \zeta_{u,n}^{p,q}, N_c - 1); & i \in [(N_{\text{cp}} + \zeta_{u,n}^{p,q} + 1), L - 1] \end{cases} \quad (3.14)$$

$$(b_{1,\text{ICI}}, b_{2,\text{ICI}}) = (L - N_{\text{cp}} - \zeta_{u,n}^{p,q}, N_c - 1); i \in [(N_{\text{cp}} + \zeta_{u,n}^{p,q} + 1), L - 1] \quad (3.15)$$

$$(b_{1,\text{ISI}}, b_{2,\text{ISI}}) = (0, L - N_{\text{cp}} - \zeta_{u,n}^{p,q} - 1); i \in [(N_{\text{cp}} + \zeta_{u,n}^{p,q} + 1), L - 1] \quad (3.16)$$

$$\text{c. } T_{\text{cp}} < -\mu_{u,n}^{p,q} \leq (T - \tau_{\text{max}} - T_s) \equiv N_{\text{cp}} < -\zeta_{u,n}^{p,q} \leq (N_c + N_{\text{cp}} - L)$$

During this TO interval, the received OFDMA symbols by all paths include the last $(L - \zeta_{u,n}^{p,q} - N_{\text{cp}}); i \in [0, L - 1]$ samples from the previous OFDMA symbol and $(N_c - L + \zeta_{u,n}^{p,q} + N_{\text{cp}})$ samples from the current symbol to form the DFT window. Then the corresponding $(\phi_{1,\text{sgl}}, \phi_{2,\text{sgl}}) = (c_{1,\text{sgl}}, c_{2,\text{sgl}}); \forall \text{sgl}$ to different signal components is given by:

$$(c_{1,\{\text{DS,ICI}\}}, c_{2,\{\text{DS,ICI}\}}) = (L - N_{\text{cp}} - \zeta_{u,n}^{p,q}, N_c - 1); i \in [0, L - 1] \quad (3.17)$$

$$(c_{1,\text{ISI}}, c_{2,\text{ISI}}) = (0, L - N_{\text{cp}} - \zeta_{u,n}^{p,q} - 1); i \in [0, L - 1] \quad (3.18)$$

$$\text{d. } (T - \tau_{\text{max}} - T_s) < -\mu_{u,n}^{p,q} \leq (T - T_s) \equiv (N_c + N_{\text{cp}} - L) < -\zeta_{u,n}^{p,q} \leq (N_c + N_{\text{cp}} - 1)$$

Throughout this TO interval, the received OFDMA symbols by the first $(N_c + N_{\text{cp}} + \zeta_{u,n}^{p,q}); i \in [0, (N_c + N_{\text{cp}} + \zeta_{u,n}^{p,q} - 1)]$ paths follow the same scenario in range (c).

In the following $(L - N_c - N_{cp} - \zeta_{u,n}^{p,q}); i \in [(N_c + N_{cp} + \zeta_{u,n}^{p,q}), L - 1]$ paths, the N_c samples in the n^{th} DFT window are from the previous OFDMA symbol. Then the corresponding $(\phi_{1,sgl}, \phi_{2,sgl}) = (d_{1,sgl}, d_{2,sgl})$; $\forall sgl$ to different signal components is given by:

$$(d_{1,\{BS,ICI\}}, d_{2,\{BS,ICI\}}) = (l - N_{cp} - \zeta_{u,n}^{p,q}, N_c - 1); l \in [0, (N_c + N_{cp} + \zeta_{u,n}^{p,q} - 1)] \quad (3.19)$$

$$(d_{1,ISI}, d_{2,ISI}) = \begin{cases} (0, l - N_{cp} - \zeta_{u,n}^{p,q} - 1); l \in [0, (N_c + N_{cp} + \zeta_{u,n}^{p,q} - 1)] \\ (0, N_c - 1) & ; l \in [(N_c + N_{cp} + \zeta_{u,n}^{p,q}), L - 1] \end{cases} \quad (3.20)$$

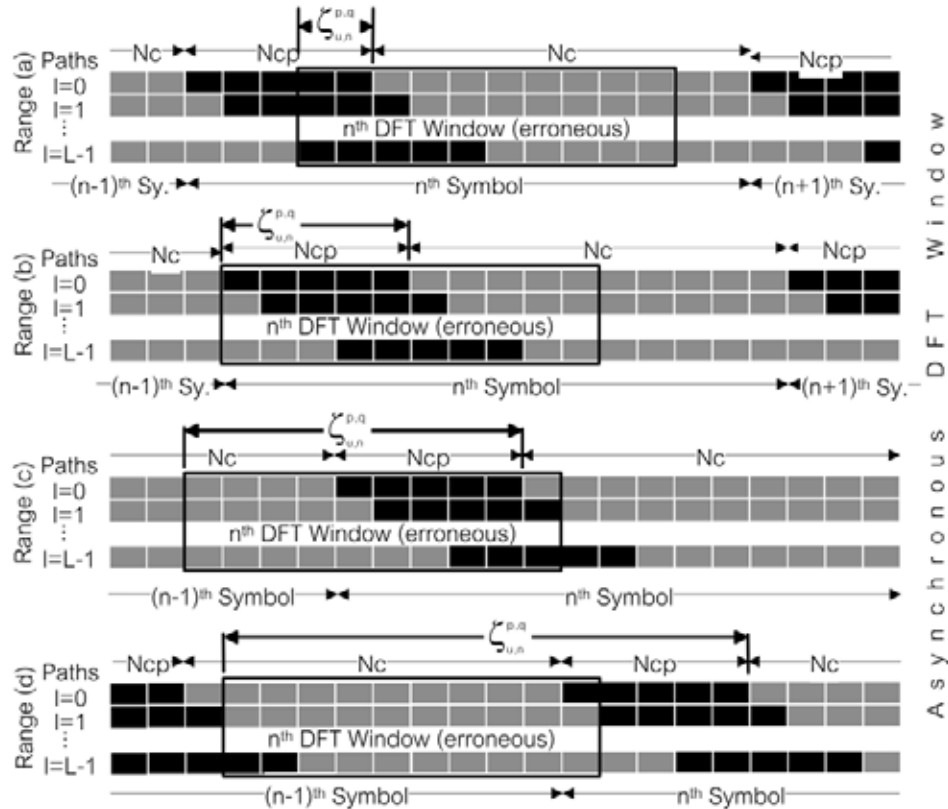


Figure 3.3 The Asynchronous DFT Window During the TO's Ranges towards the CP

ii. The TO Away from the CP (i.e. $\mu_{u,n}^{p,q} > 0$)

In this scenario, the n^{th} DFT window is formed by samples from the current and the next OFDMA symbols according to the value of the TO, which is explored through the following ranges (Figure 3.4):

$$e. 0 < \mu_{u,n}^{p,q} \leq \tau_{\max} \equiv 0 < \zeta_{u,n}^{p,q} \leq (L-1)$$

Throughout this range, the first $\zeta_{u,n}^{p,q}; i \in [0, (\zeta_{u,n}^{p,q} - 1)]$ paths include $(\zeta_{u,n}^{p,q} - 1)$ samples from the CP of the next OFDMA symbol, which are appended to $(N_c - \zeta_{u,n}^{p,q} + 1)$ samples from the current symbol to form the DFT window. The N_c captured samples of the following $(L - \zeta_{u,n}^{p,q}); i \in [\zeta_{u,n}^{p,q}, L-1]$ paths are from the current OFDMA symbol. Then the corresponding $(\phi_{1,sgl}, \phi_{2,sgl}) = (e_{1,sgl}, e_{2,sgl}); \forall sgl$ to different signal components is given by:

$$(e_{1,DS}, e_{2,DS}) = \begin{cases} (0, N_c - \zeta_{u,n}^{p,q} + i - 1); i \in [0, (\zeta_{u,n}^{p,q} - 1)] \\ (0, N_c - 1) & ; i \in [\zeta_{u,n}^{p,q}, L-1] \end{cases} \quad (3.21)$$

$$(e_{1,ICI}, e_{2,ICI}) = (0, N_c - \zeta_{u,n}^{p,q} + i - 1); i \in [0, (\zeta_{u,n}^{p,q} - 1)] \quad (3.22)$$

$$(e_{1,ISI}, e_{2,ISI}) = (N_c - \zeta_{u,n}^{p,q} + i, N_c - 1); i \in [0, (\zeta_{u,n}^{p,q} - 1)] \quad (3.23)$$

$$f. \tau_{\max} < \mu_{u,n}^{p,q} \leq (T_c - T_s) \equiv (L-1) < \zeta_{u,n}^{p,q} \leq (N_c - 1)$$

Within this interval, all paths include $(\zeta_{u,n}^{p,q} - 1); i \in [0, L-1]$ samples from the next OFDMA symbol, which are suffixed to $(N_c - \zeta_{u,n}^{p,q} + 1)$ samples from the desired symbol to form the n^{th} DFT window, and then the corresponding $(\phi_{1,sgl}, \phi_{2,sgl}) = (f_{1,sgl}, f_{2,sgl}); \forall sgl$ to different signal components is given by:

$$(f_{1,\{DS,ICI\}}, f_{2,\{DS,ICI\}}) = (0, N_c - \zeta_{u,n}^{p,q} + i - 1); i \in [0, L-1] \quad (3.24)$$

$$(f_{1,ISI}, f_{2,ISI}) = (N_c - \zeta_{u,n}^{p,q} + i, N_c - 1); i \in [0, L-1] \quad (3.25)$$

$$g. (T_c - T_s) < \mu_{u,n}^{p,q} < (T_c + \tau_{\max}) \equiv (N_c - 1) < \zeta_{u,n}^{p,q} < (N_c + L - 1)$$

In this duration of TO, only the last $(L - \zeta_{u,n}^{p,q} + N_c - 1); i \in [(\zeta_{u,n}^{p,q} - N_c + 1), L-1]$ paths contain $(N_c - \zeta_{u,n}^{p,q} + 1)$ samples from the current OFDMA symbol similar to range (f), whereas the first $(\zeta_{u,n}^{p,q} - N_c + 1); i \in [0, (\zeta_{u,n}^{p,q} - N_c)]$ paths include only samples from

the next symbol. Then the corresponding $(\phi_{1,sgl}, \phi_{2,sgl}) = (g_{1,sgl}, g_{2,sgl})$; $\forall sgl$ to different signal components is given by:

$$(g_{1,\{ps,ici\}}, g_{2,\{ps,ici\}}) = (0, N_c - \zeta_{u,n}^{p,q} + l - 1); l \in [(\zeta_{u,n}^{p,q} - N_c + 1), L - 1] \quad (3.26)$$

$$(g_{1,\{sl\}}, g_{2,\{sl\}}) = \begin{cases} (0, N_c - 1) & ; l \in [0, (\zeta_{u,n}^{p,q} - N_c)] \\ (N_c - \zeta_{u,n}^{p,q} + l, N_c - 1) & ; l \in [(\zeta_{u,n}^{p,q} - N_c + 1), L - 1] \end{cases} \quad (3.27)$$

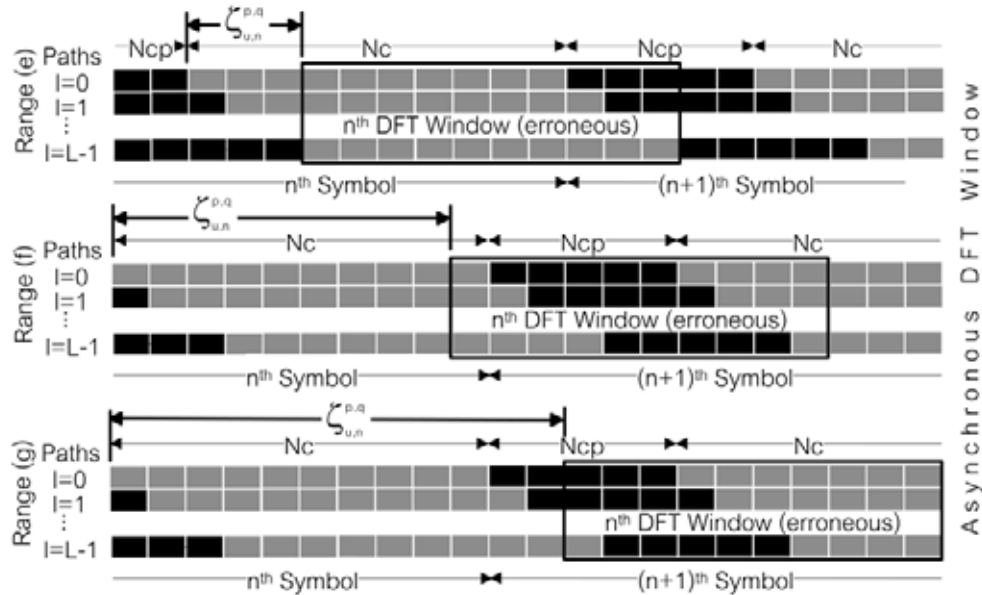


Figure 3.4 The Asynchronous DFT Window During the TO's Ranges Away From the CP

3.3.2 Analysis of the Boundaries of the TO

To determine the boundaries of the TO, the following assumption is considered: the time index of the DFT window is coincided to the transmission time of the dominant OFDMA samples that are occupied in the processing window by all channel paths. Hence, the maximum TOs that conserve the n^{th} DFT window belonging to the n^{th} OFDMA symbol rather than its neighbors are the TO's boundaries. This can be interpreted as:

$$\max_{\zeta_{u,n}^{p,q}} \arg \left[\sum_l N(n^{\text{th}} \text{ Symbol}) \geq \sum_l N((n \mp 1)^{\text{th}} \text{ Symbol}) \right] \quad (3.28)$$

where $N(x^{\text{th}} \text{symbol})$ represents the number of samples belong to the x^{th} symbol. The solutions of the inequality in (3.28) can be found within ranges (c) and (f), which can be precisely determined by the statistical median of each range, respectively. Consequently, the boundaries of the TO can be given by:

$$B_{\text{TO}}^- = \begin{cases} -(N_c + 2N_{\text{cp}} - L)/2 & ; \text{if } (N_c - L)_{\text{mod}2} = 0 \\ -(N_c + 2N_{\text{cp}} - L - 1)/2 & ; \text{if } (N_c - L)_{\text{mod}2} \neq 0 \end{cases} \quad (3.29)$$

$$B_{\text{TO}}^+ = \begin{cases} (N_c + L - 2)/2 & ; \text{if } (N_c - L)_{\text{mod}2} = 0 \\ (N_c + L - 1)/2 & ; \text{if } (N_c - L)_{\text{mod}2} \neq 0 \end{cases} \quad (3.30)$$

where B_{TO}^- and B_{TO}^+ are the boundaries of the TO towards and away from the CP, respectively.

It can be concluded from (3.29) and (3.30) that the effective ranges of the TO that were discussed in the previous section are $\phi \in \Phi = \{a, b, c, e, f\}$ where ranges (c) and (f) can be redefined as:

$$\text{c. } T_{\text{cp}} < -\mu_{u,n}^{p,q} \leq B_{\text{TO}}^- T_s \equiv N_{\text{cp}} < -\zeta_{u,n}^{p,q} \leq B_{\text{TO}}^- \quad (3.31)$$

$$\text{f. } (\tau_{\text{max}} - T_s) < \mu_{u,n}^{p,q} \leq B_{\text{TO}}^+ T_s \equiv (L-1) < \zeta_{u,n}^{p,q} \leq B_{\text{TO}}^+ \quad (3.32)$$

Note that ranges (d) and (g) became ineffective because their ranges are beyond the TO boundaries.

3.3.3 Instantaneous and Average Interferences Power and SINR with TO

Consider that among the U active users in the MIMO-OFDMA uplink systems, $\phi U \subset \{1, \dots, U\}$ users belong to effective TO's range ϕ , where $N(\phi U)$ represent the number of asynchronous users in ϕU . The u^{th} user is considered as asynchronous user (i.e., $u \in \phi U$), when at least one of its belonging transmit antennas experience TO w.r.t a certain BS's receive antenna, where the TO is transmitter-receiver pair specific. Generally, any of the P antennas of the u^{th} user can be a member of either synchronous

$G_u^{\text{syn.}}$ or asynchronous $G_u^{\text{asyn.}}$ antennas group, where $G_u^{\text{syn.}} \cup G_u^{\text{asyn.}} = \{1, \dots, P\} \forall u$ and $G_u^{\text{syn.}} \cap G_u^{\text{asyn.}} = \emptyset$. Since the k^{th} user's t^{th} transmit antenna is the antenna of interest, $\phi Y_n^q(i = c_{k,g})$ can be simply rewritten from (3.5 and 3.10) with the AWGN as:

$$\phi Y_n^q(i) = \underbrace{\phi Y_{k,n}^{\text{DS},q}(i) + \phi Y_{k,n}^{\text{DS-SI},q}(i)}_{\text{DS and DS-SI}} + \underbrace{\sum_{p=1, p \neq t}^P \phi Y_{k,n}^{p,q}(i)}_{\text{CAs-SI}} + \underbrace{\sum_{u \in \Phi, u \neq k} \sum_{p \in G_u^{\text{asyn.}}} \phi Y_{u,n}^{p,q}(i)}_{\text{MUI}} + W_n^q(i) \quad (3.33)$$

where the first and the second terms in the right-hand side represent the DS and DS-SI, respectively as derived in (3.10). The third term represents the interferences caused by the co-transmit antennas of the k^{th} user (CAs-SI) as an additional SI component in the MIMO-OFDMA uplink systems (comparable to the OFDMA uplink systems), where all user's transmit antennas exploit the same allocated subcarriers. The last term in (3.33) represents the MUI which is the interferences incurred by all other asynchronous users except the desired one.

The average SINR at the output of the DFT on the i^{th} subcarrier at the BS's q^{th} receive antenna of the desired k^{th} user with SCP, $\phi \text{SINR}_{k,SCP}^q(i)$ is defined as the ratio of the average power of the DS to the average interference power which contains the powers of the DA-SI, CAs-SI, and MUI, plus the average noise power as:

$$\text{SINR}_{k,SCP}^q(i) = \frac{P_{\text{DS}}}{P_{\text{DS-SI}} + P_{\text{CAs-SI}} + P_{\text{MUI}} + P_w} \quad (3.34)$$

where $P_w = \sigma_w^2$. The average desired and interference signal powers can be obtained by averaging them with respect to $\zeta_{u,n}^{p,q}$ as well as $c_{u,g}$ and i .

Since all the available subcarriers are allocated to the users in the MIMO-OFDMA uplink systems which implies that at most one subcarrier from each set c_u ; $\forall u$ may interfere with the i^{th} subcarrier, then the averaging over $c_{u,g}$ and i is not required (Park et

³ Throughout this thesis, the second argument in the superscript of the asynchronous SINR such as $\Delta \in \{\phi, \epsilon, \xi\}$ represents the incurred synchronization offset(s), where the second argument of the subscript such as $xCP \in \{\text{SCP}, \text{InCP}, \text{ACP}\}$ represents the condition of the CP.

al., 2010 ; Ashore, 2010). Then, from (3.10, 3.33 and 3.34) the following expressions can be obtained:

$$P_{DS} = E \left[\left| \phi_{DS-SI} Y_{k,n}^{t,q}(i) \right|^2 \right] = \sigma_x^2 \sum_I \sigma_h^2(l) E \left[\left| (\phi_{2,DS} - \phi_{1,DS} + 1) \right|^2 \right] \quad (3.35)$$

$$\begin{aligned} P_{DS-SI} &= E \left[\left| \phi_{DS-SI} Y_{k,n}^{t,q}(i) \right|^2 \right] \\ &= \sigma_x^2 \sum_{g=0, c_{k,g} \neq i}^{N_k-1} \sum_I \sigma_h^2(l) E \left[\left| \sum_{z=\phi_{1,ICI}}^{\phi_{2,ICI}} \frac{e^{j2\pi z(c_{k,g}-i)/N_c}}{N_c} \right|^2 \right] + \sigma_x^2 \sum_{g=0}^{N_k-1} \sum_I \sigma_h^2(l) E \left[\left| \sum_{z=\phi_{1,ISI}}^{\phi_{2,ISI}} \frac{e^{j2\pi z(c_{k,g}-i)/N_c}}{N_c} \right|^2 \right] \end{aligned} \quad (3.36)$$

$$\begin{aligned} P_{CAS-SI} &= \sum_{p=1, p \neq t}^P E \left[\left| \phi_{CAS-SI} Y_{k,n}^{p,q}(i) \right|^2 \right] \\ &= \sum_{p=1, p \neq t}^P \left(\sigma_x^2 \sum_{g=0}^{N_k-1} \sum_I \sigma_h^2(l) E \left[\left| \sum_{z=\phi_{1,ICI}}^{\phi_{2,ICI}} \frac{e^{j2\pi z(c_{k,g}-i)/N_c}}{N_c} \right|^2 \right] + \sigma_x^2 \sum_{g=0}^{N_k-1} \sum_I \sigma_h^2(l) E \left[\left| \sum_{z=\phi_{1,ISI}}^{\phi_{2,ISI}} \frac{e^{j2\pi z(c_{k,g}-i)/N_c}}{N_c} \right|^2 \right] \right) \end{aligned} \quad (3.37)$$

$$\begin{aligned} P_{MUI} &= \sum_{u \in \Phi_{U,u \neq k}^{asyn.}} \sum_{p \in C_{u,n}^{asyn.}} E \left[\left| \phi_{MUI} Y_{u,n}^{p,q}(i) \right|^2 \right] = \sum_{u \in \Phi_{U,u \neq k}^{asyn.}} \sum_{p \in C_{u,n}^{asyn.}} \left(\sigma_x^2 \sum_{g=0}^{N_k-1} \sum_I \sigma_h^2(l) E \left[\left| \sum_{z=\phi_{1,ICI}}^{\phi_{2,ICI}} \frac{e^{j2\pi z(c_{u,g}-i)/N_c}}{N_c} \right|^2 \right] \right. \\ &\quad \left. + \sigma_x^2 \sum_{g=0}^{N_k-1} \sum_I \sigma_h^2(l) E \left[\left| \sum_{z=\phi_{1,ISI}}^{\phi_{2,ISI}} \frac{e^{j2\pi z(c_{u,g}-i)/N_c}}{N_c} \right|^2 \right] \right) \end{aligned} \quad (3.38)$$

where the data signal and the channel are assumed to be independent. It is worthy to note that substituting the instantaneous power of the interference coefficient such as:

$$\left| (\phi_{2,DS} - \phi_{1,DS} + 1) \right|^2, \left| \sum_{z=\phi_{1,ICI}}^{\phi_{2,ICI}} \frac{e^{j2\pi z(c_{k,g}-i)/N_c}}{N_c} \right|^2, \text{ and } \left| \sum_{z=\phi_{1,ISI}}^{\phi_{2,ISI}} \frac{e^{j2\pi z(c_{k,g}-i)/N_c}}{N_c} \right|^2 \text{ at any TO's value for the DS,}$$

ICI and ISI respectively, in (3.35-3.38) producing the instantaneous SINR in (3.34).

However, the TO is assumed to be i.i.d uniform discrete random variable $\zeta_{u,n}^{p,q}$ (Jung and Zoltowski, 2004; Park et al., 2010; Kotzsch et al., 2010; and Kotzsch and Fettweis, 2010), therefore for any function $g(\zeta_{u,n}^{p,q})$, $E \left[g(\zeta_{u,n}^{p,q}) \right] = \sum_{\zeta_{u,n}^{p,q} = B_{TO}^-}^{B_{TO}^+} g(\zeta_{u,n}^{p,q}) \Pr(\zeta_{u,n}^{p,q} = \zeta_{u,n}^{p,q})$ (Papoulis, 1965) where $\Pr(\cdot)$ is the probability, thus:

$$E \left[\left| \frac{(\phi_{2,DS} - \phi_{1,DS} + 1)}{N_c} \right|^2 \right] = \sum_{\zeta_{u,n}^{p,q} = B_{TO}^-}^{B_{TO}^+} \frac{(\phi_{2,DS} - \phi_{1,DS} + 1)^2}{N_c^2 (B_{TO}^+ - B_{TO}^-)} \quad (3.39)$$

$$E \left[\left| \sum_{z=\phi_{1,\{ICI,ISI\}}}^{\phi_{2,\{ICI,ISI\}}} \frac{e^{j2\pi z(c_{u,g}-i)/N_c}}{N_c} \right|^2 \right] = \sum_{\zeta_{u,n}^{p,q} = B_{TO}^-}^{B_{TO}^+} \frac{\sin^2 \left(\pi \left(\frac{c_{u,g}-i}{N_c} \right) (\phi_{2,\{ICI,ISI\}} - \phi_{1,\{ICI,ISI\}} + 1) \right)}{N_c^2 (B_{TO}^+ - B_{TO}^-) \sin^2 \left(\pi \left(\frac{c_{u,g}-i}{N_c} \right) \right)} \quad (3.40)$$

where $\Pr(\zeta_{u,n}^{p,q} = \zeta_{u,n}^{p,q}) = \frac{1}{(B_{TO}^+ - B_{TO}^-)}$. A detailed derivation of (3.39-3.40) is carried out in

Appendix A.

However, from (3.34-3.40), it is worthy to have the following remarks: In order to evaluate the average SINR, the power delay profile of the channel i.e., $\{\sigma_h^2(l)\}$ is needed. Generally, an evaluation procedure, model or tabulation of the $\{\sigma_h^2(l)\}$ is provided by the recommendations of the wireless applications such as Recommendation ITU-R M.1225, 3GPP TR 25.814, and 3GPP TR 29.913 which are adopted in running the simulation environment. In addition, the difference between the allocated subcarriers i.e., $(c_{u,g} - i)$ plays a vital role in evaluating the interference coefficient (and the SINR), which is closely related to the applied SAS, however, the analytical results are illustrated based on different SASs.

3.3.4 Special Case of Insufficient and Absent CP

In this section, the expressions for signal and interference terms at the DFT output of the BS's q^{th} receive antenna are redefined for insufficient CP (InCP) where $\tau_{\max} = (L-1)T_s > T_{cp} \equiv (L-1) > N_{cp}$ as well as absent CP (ACP) where $T_{cp} = T_s N_{cp} = 0$ during the following TO's ranges:

$$\text{A. } 0 \leq -\mu_{u,n}^{p,q} \leq T_{cp} \equiv 0 \leq -\zeta_{u,n}^{p,q} \leq N_{cp}$$

During this interval and with insufficient CP, the DS, ICI and ISI components are equivalent to the corresponding expressions in range (b) i.e. equations (3.14-3.16). However, with absent CP, only $\zeta_{u,n}^{p,q} = 0$ is defined in this range and the signal components are corresponding to those in range (b) when $N_{cp} = 0$ is substituted.

$$\text{B. } T_{cp} < -\mu_{u,n}^{p,q} \leq B_{TO}^- T_s \equiv N_{cp} < -\zeta_{u,n}^{p,q} \leq B_{TO}^-$$

Throughout this interval and with both insufficient and absent CP, the DS, ICI and ISI components are equivalent to the corresponding expressions in effective range (c) i.e. equations (3.17-3.18).

$$\text{C. } 0 < \mu_{u,n}^{p,q} \leq T_{cp} \equiv 0 < \zeta_{u,n}^{p,q} \leq N_{cp}$$

Along this interval, and with InCP, the first $\zeta_{u,n}^{p,q}; l \in [0, \zeta_{u,n}^{p,q} - 1]$ paths include $(\zeta_{u,n}^{p,q} - l)$ samples from the next OFDMA symbol, which are appended to $(N_c - \zeta_{u,n}^{p,q} + l)$ samples from the desired OFDMA symbol. The next path $l = \zeta_{u,n}^{p,q}$ includes all the N_c - samples from the desired OFDMA symbol, where the following $(L - \zeta_{u,n}^{p,q} - 1); l \in [\zeta_{u,n}^{p,q} + 1, L - 1]$ paths contain $(l - \zeta_{u,n}^{p,q})$ samples from the previous OFDMA symbol and $(N_c - l + \zeta_{u,n}^{p,q})$ samples from the desired OFDMA symbol to form the DFT window. Then the corresponding $(\phi_{1,sgl}, \phi_{2,sgl}) = (c_{1,sgl}, c_{2,sgl})$ to different signal components is given by:

$$(C_{1,DS}, C_{2,DS}) = \begin{cases} (0, N_c - \zeta_{u,n}^{p,q} + l - 1); l \in [0, \zeta_{u,n}^{p,q} - 1] \\ (0, N_c - 1) & ; l = \zeta_{u,n}^{p,q} \\ (l - \zeta_{u,n}^{p,q}, N_c - 1); l \in [\zeta_{u,n}^{p,q} + 1, L - 1] \end{cases} \quad (3.41)$$

$$(C_{1,ICI}, C_{2,ICI}) = \begin{cases} (0, N_c - \zeta_{u,n}^{p,q} + l - 1); l \in [0, \zeta_{u,n}^{p,q} - 1] \\ (l - \zeta_{u,n}^{p,q}, N_c - 1); l \in [\zeta_{u,n}^{p,q} + 1, L - 1] \end{cases} \quad (3.42)$$

$$(C_{1,ISI}, C_{2,ISI}) = \begin{cases} (N_c - \zeta_{u,n}^{p,q} + l, N_c - 1); l \in [0, \zeta_{u,n}^{p,q} - 1] \\ (0, l - \zeta_{u,n}^{p,q} - 1); l \in [\zeta_{u,n}^{p,q} + 1, L - 1] \end{cases} \quad (3.43)$$

With ACP, the signal components are corresponding to those in range (b) when $N_{cp} = 0$ is substituted.

$$\text{D. } 0 < \mu_{u,n}^{p,q} \leq \tau_{max} \equiv 0 < \zeta_{u,n}^{p,q} \leq (L - 1)$$

Within this interval and with InCP, the signal components are equivalent to the

corresponding expressions in range (e) i.e., equations (21-23). And with ACP, the signal components are equivalent to the corresponding expressions in range (C) i.e., equations (41-43).

$$E. \tau_{\max} < \mu_{u,n}^{p,q} \leq B_{TO}^+ T_s \equiv (L-1) < \zeta_{u,n}^{p,q} \leq B_{TO}^+$$

During this interval and with both insufficient CP and absence CP, the signal components are equivalent to the corresponding expressions in effective range (f) i.e. equations (3.24-3.25).

The corresponding average SINR for InCP, $\text{SINR}_{k,\text{InCP}}^{q,\phi}(i)$ and ACP, $\text{SINR}_{k,\text{ACP}}^{q,\phi}(i)$ are equivalent to expression in (3.34) and its follows when the corresponding values of $(\phi_{1,\text{sgl}}, \phi_{2,\text{sgl}})$ are substituted along any CP scenarios.

3.4. Average SINR Analysis for Uplink MIMO-OFDMA Fading Channel Systems In Presence of Time and Carrier Frequency Offsets

3.4.1 Single-User Single-Antenna Structure and Coexistence of Time and Carrier Frequency Offsets

The coexistence of the TO and CFO is analyzed firstly for single-user single-antennas system using the same method in subsection 3.3.1. However, and analogue to the TO, the CFO can be also divided into an integer and fractional parts. The integer part shifts all the subcarrier locations in the frequency domain by the amount of the integer offset (Lee et al., 2006), which results in cyclic shift of the subcarriers, and the fractional part, which is analyzed in this research, makes the OFDMA symbol lose the orthogonality between its subcarriers (Zhangyong et al., 2003). Since the antenna separation on each user's mobile terminal is generally much smaller than that on the BS, it can be reasonably assumed that the CFO between transmit antennas of the same user and a specific receive antenna on the BS is identical (Kim et al., 2010), thus let $\epsilon_{u,n}^q \equiv \delta_{u,n}^q T_c$, where $-0.5 \leq \epsilon_{u,n}^q < 0.5$ (Lee et al., 2006), be the normalized fractional CFO w.r.t. the subcarrier spacing frequency between transmit antennas of the u^{th} user and the BS's q^{th} receive antenna, which is modeled as a complex multiplicative distortion of

the received signal in the time domain i.e., $e^{j2\pi\epsilon_u^q t/T_c}$. The presence of the TO $\zeta_{u,n}^{p,q}$ and CFO ϵ_u^q change the signal model of (3.7) to:

$$\phi, \epsilon Y_{u,n}^{p,q}(i) = \frac{\mathbf{v}_n(\boldsymbol{\epsilon}_{u,n}^q)}{\sqrt{N_c}} \sum_{z=0}^{N_c-1} \sum_{l=0}^{L-1} \alpha_{u,n,l}^{p,q}(zT_s) x_{u,n}^p(zT_s - \zeta_{u,n}^{p,q} T_s - lT_s) e^{j2\pi z(\epsilon_{u,n}^q + i)/N_c}; i \in [0, N_c - 1] \quad (3.44)$$

where $\mathbf{v}_n(\boldsymbol{\epsilon}_{u,n}^q) = e^{j2\pi\epsilon_{u,n}^q(N_{cp} + n(N_c + N_{cp}))/N_c}$. Considering (3.8) and (3.44), reduction and rotation of each DFT output i.e., $\mathbf{v}_n(\boldsymbol{\epsilon}_{u,n}^q)$ and ICI are additionally introduced by the CFO to the TO detriments. In presence of TO and CFO, the interference coefficient in (3.9) can be redefined as:

$$\frac{1}{N_c} \sum_{z=\phi_{1,sgl}}^{\phi_{2,sgl}} e^{j2\pi z(\epsilon_{u,g} + \epsilon_{u,n}^q - i)/N_c} = \frac{\sin\left(\pi\left(\frac{\epsilon_{u,g} + \epsilon_{u,n}^q - i}{N_c}\right)\right) (\phi_{2,sgl} - \phi_{1,sgl} + 1)}{N_c \sin\left(\pi\left(\frac{\epsilon_{u,g} + \epsilon_{u,n}^q - i}{N_c}\right)\right)} e^{j2\pi z(\epsilon_{u,g} + \epsilon_{u,n}^q - i)(\phi_{1,sgl} + \phi_{2,sgl})/N_c} \quad (3.45)$$

Then, $\phi, \epsilon Y_{u,n}^{p,q}(i)$ and its components can be represented by:

$$\begin{aligned} \phi, \epsilon Y_{u,n}^{p,q}(i) &= \underbrace{e^{j2\pi\zeta_{u,n}^{p,q}/N_c} \mathbf{v}_n(\boldsymbol{\epsilon}_{u,n}^q) X_{u,n}^p(g|_{\epsilon_{u,g}=i}) \sum_l \alpha_{u,n,l}^{p,q}(zT_s) e^{-j2\pi l/N_c}}_{\phi, \epsilon Y_{DS}^{p,q}(i)} \frac{1}{N_c} \sum_{z=\phi_{1,DS}}^{\phi_{2,DS}} e^{j2\pi z\epsilon_{u,n}^q/N_c} \\ &+ \mathbf{v}_n(\boldsymbol{\epsilon}_{u,n}^q) \sum_{\substack{g=0, \epsilon_{u,g} \neq i \\ g=0, \epsilon_{u,g} \neq i}}^{N_u-1} X_{u,n}^p(g) e^{j2\pi\zeta_{u,g}^{p,q}/N_c} \sum_l \alpha_{u,n,l}^{p,q}(zT_s) e^{-j2\pi\zeta_{u,g}^{p,q}/N_c} \frac{1}{N_c} \sum_{z=\phi_{1,ICI}}^{\phi_{2,ICI}} e^{j2\pi z(\epsilon_{u,g} + \epsilon_{u,n}^q - i)/N_c} \\ &+ \underbrace{\mathbf{v}_n(\boldsymbol{\epsilon}_{u,n}^q) \sum_{g=0}^{N_u-1} X_{u,n}^p(g) e^{j2\pi\zeta_{u,g}^{p,q}(\frac{r_{u,n}^{p,q} \pm N_{cp}}{\zeta_{u,n}^{p,q} \pm N_{cp}})_{\text{mod } N_c}/N_c} \sum_l \alpha_{u,n,l}^{p,q}(zT_s) e^{-j2\pi\zeta_{u,g}^{p,q}/N_c}}_{\phi, \epsilon Y_{DS-SI}^{p,q}(i)} \frac{1}{N_c} \sum_{z=\phi_{1,ISI}}^{\phi_{2,ISI}} e^{j2\pi z(\epsilon_{u,g} + \epsilon_{u,n}^q - i)/N_c} \end{aligned} \quad (3.46)$$

where the first term on the right-hand side represents the desired signal (DS) i.e. $\phi, \epsilon Y_{DS}^{p,q}(i)$. The following terms are the ICI, and ISI, respectively represent the self interference (SI) associated with the asynchronous DS i.e. $\phi, \epsilon Y_{DS-SI}^{p,q}(i)$.

Considering the wide range of the TO towards and away from the CP in section 3.3.1, it is easily expected that *only* the corresponding $(\phi_{1,ICI}, \phi_{2,ICI})$ is affected by the coexistence of the TO and CFO to be coincided with the $(\phi_{1,DS}, \phi_{2,DS})$, where the

$(\phi_{1,ISI}, \phi_{2,ISI})$ is as given in subsection 3.3.1 along the different TO ranges. The corresponding $(\phi_{1,\{DS,ICI\}}, \phi_{2,\{DS,ICI\}})$ along the various TO ranges can be represented as:

i. The TO Towards The CP (i.e. $\mu_{u,n}^{p,q} < 0$) and CFO (i.e. $\epsilon_u^q > 0$)

$$(a_{1,\{DS,ICI\}}, a_{2,\{DS,ICI\}}) = (0, N_c - 1); l \in [0, L - 1] \quad (3.47)$$

$$(b_{1,\{DS,ICI\}}, b_{2,\{DS,ICI\}}) = \begin{cases} (0, N_c - 1) & ; l \in [0, (N_{cp} + \zeta_{u,n}^{p,q})] \\ (l - N_{cp} - \zeta_{u,n}^{p,q}, N_c - 1); & ; l \in [(N_{cp} + \zeta_{u,n}^{p,q} + 1), L - 1] \end{cases} \quad (3.48)$$

$$(c_{1,\{DS,ICI\}}, c_{2,\{DS,ICI\}}) = (l - N_{cp} - \zeta_{u,n}^{p,q}, N_c - 1); l \in [0, L - 1] \quad (3.49)$$

$$(d_{1,\{DS,ICI\}}, d_{2,\{DS,ICI\}}) = (l - N_{cp} - \zeta_{u,n}^{p,q}, N_c - 1); l \in [0, (N_c + N_{cp} + \zeta_{u,n}^{p,q} - 1)] \quad (3.50)$$

ii. The TO Away from The CP (i.e. $\mu_{u,n}^{p,q} > 0$) and CFO (i.e. $\epsilon_u^q > 0$)

$$(e_{1,\{DS,ICI\}}, e_{2,\{DS,ICI\}}) = \begin{cases} (0, N_c - \zeta_{u,n}^{p,q} + l - 1); & ; l \in [0, (\zeta_{u,n}^{p,q} - 1)] \\ (0, N_c - 1) & ; l \in [\zeta_{u,n}^{p,q}, L - 1] \end{cases} \quad (3.51)$$

$$(f_{1,\{DS,ICI\}}, f_{2,\{DS,ICI\}}) = (0, N_c - \zeta_{u,n}^{p,q} + l - 1); l \in [0, L - 1] \quad (3.52)$$

$$(g_{1,\{DS,ICI\}}, g_{2,\{DS,ICI\}}) = (0, N_c - \zeta_{u,n}^{p,q} + l - 1); l \in [(\zeta_{u,n}^{p,q} - N_c + 1), L - 1] \quad (3.53)$$

It is worthy to note from (3.12 and 3.47) that the received signal is immune to ISI because of the CP where the introduced ICI is due to the CFO not the TO, hence (3.46) can be given by:

$$\begin{aligned} a, \epsilon Y_{u,n}^{p,q}(i) &= e^{j2\pi c_{u,n}^{p,q}/N_c} \mathbf{v}_n(\epsilon_u^q) \frac{\sin(\pi \epsilon_u^q)}{N_c \sin(\pi \epsilon_u^q / N_c)} e^{j\pi \epsilon_u^q (N_c - 1)/N_c} H_{u,n}^{p,q}(i) X_{u,n}^p(g|_{c_{u,g}=i}) \\ &+ \mathbf{v}_n(\epsilon_u^q) \sum_{g=0, c_{u,g} \neq i}^{N_u-1} e^{j2\pi c_{u,g}^{p,q}/N_c} \frac{\sin(\pi(c_{u,g} + \epsilon_u^q - i))}{N_c \sin(\pi(c_{u,g} + \epsilon_u^q - i)/N_c)} e^{j\pi(c_{u,g} + \epsilon_u^q - i)(N_c - 1)/N_c} H_{u,n}^{p,q}(c_{u,g}) X_{u,n}^p(g) \end{aligned} \quad (3.54)$$

Consequently, $\varepsilon Y_{u,n}^{p,q}(i) = \left. \varepsilon Y_{u,n}^{p,q}(i) \right|_{\varepsilon_{u,n}^{p,q}=0}$ represents the DFT output in presence of only the CFO as in (Lee et al., 2006; Lin and Ma, 2009). However, the effective range and boundaries of the TO in subsection 3.3.2 are not affected by presence of the CFO.

3.4.2 Instantaneous and Average Interferences Power and SINR with TO and CFO

In the presence of TO and CFO, $\phi Y_n^q(i)$ in (3.33) can be rewritten as:

$$\phi \varepsilon Y_n^q(i) = \underbrace{\phi_{DS} \varepsilon Y_{k,n}^{t,q}(i) + \phi_{DS-SI} \varepsilon Y_{k,n}^{t,q}(i)}_{\text{CAS-SI}} + \underbrace{\sum_{p=1, p \neq t}^P \phi_{k,n} \varepsilon Y_{k,n}^{p,q}(i) + \sum_{u \in \overline{\Phi_{U,u \neq k}^{p \in C_u^{\text{syn}}}}} \phi_{u,n} \varepsilon Y_{u,n}^{p,q}(i) + W_n^q(i)}_{\text{MUI}} \quad (3.55)$$

And the expression of the $\text{SINR}_{k, \text{SCP}}^{q, \phi, \varepsilon}(i)$ is equivalent to (3.34). Then, and with (3.45)-(3.53), and (3.34) the following expressions can be obtained:

$$P_{DS} = E \left[\left| \phi_{DS} \varepsilon Y_{k,n}^{t,q}(i) \right|^2 \right] = \sigma_x^2 \sum_l \sigma_h^2(l) E \left[\left| \sum_{z=\phi_{1,DS}}^{\phi_{2,DS}} \frac{e^{j2\pi z \varepsilon_{k,n}^q / N_c}}{N_c} \right|^2 \right] \quad (3.56)$$

$$P_{DS-SI} = E \left[\left| \phi_{DS-SI} \varepsilon Y_{k,n}^{t,q}(i) \right|^2 \right] = \sigma_x^2 \sum_{g=0, c_{k,g} \neq i}^{N_k-1} \sum_l \sigma_h^2(l) E \left[\left| \sum_{z=\phi_{1,DSI}}^{\phi_{2,DSI}} \frac{e^{j2\pi z (c_{k,g} + \varepsilon_{k,n}^q - i) / N_c}}{N_c} \right|^2 \right] \\ + \sigma_x^2 \sum_{g=0}^{N_k-1} \sum_l \sigma_h^2(l) E \left[\left| \sum_{z=\phi_{1,JSI}}^{\phi_{2,JSI}} \frac{e^{j2\pi z (c_{k,g} + \varepsilon_{k,n}^q - i) / N_c}}{N_c} \right|^2 \right] \quad (3.57)$$

$$P_{\text{CAS-SI}} = \sum_{p=1, p \neq t}^P E \left[\left| \phi_{k,n} \varepsilon Y_{k,n}^{p,q}(i) \right|^2 \right] = \sum_{p=1, p \neq t}^P \left(\sigma_x^2 \sum_{g=0}^{N_k-1} \sum_l \sigma_h^2(l) E \left[\left| \sum_{z=\phi_{1,DCI}}^{\phi_{2,DCI}} \frac{e^{j2\pi z (c_{k,g} + \varepsilon_{k,n}^q - i) / N_c}}{N_c} \right|^2 \right] \right. \\ \left. + \sigma_x^2 \sum_{g=0}^{N_k-1} \sum_l \sigma_h^2(l) E \left[\left| \sum_{z=\phi_{1,JSI}}^{\phi_{2,JSI}} \frac{e^{j2\pi z (c_{k,g} + \varepsilon_{k,n}^q - i) / N_c}}{N_c} \right|^2 \right] \right) \quad (3.58)$$

$$\begin{aligned}
P_{\text{MUI}} = \sum_{u \in \Phi_{\varepsilon}} \sum_{U, u \neq k}^P \mathbb{E} \left[\phi_{u,n}^{p,q} (i) \right] &= \sum_{u \in \Phi_{\varepsilon}} \sum_{U, u \neq k}^P \left(\sigma_x^2 \sum_{g=0}^{N_x-1} \sum_l \sigma_h^2 (l) \mathbb{E} \left[\left| \sum_{z=\phi_{1,|C|}}^{\phi_{2,|C|}} \frac{e^{j2\pi z(c_{u,g} + \varepsilon_{u,n}^q - i)/N_c}}{N_c} \right|^2 \right] \right. \\
&\quad \left. + \sigma_x^2 \sum_{g=0}^{N_x-1} \sum_l \sigma_h^2 (l) \mathbb{E} \left[\left| \sum_{z=\phi_{1,|S|}}^{\phi_{2,|S|}} \frac{e^{j2\pi z(c_{u,g} + \varepsilon_{u,n}^q - i)/N_c}}{N_c} \right|^2 \right] \right) \quad (3.59)
\end{aligned}$$

where the data signal and the channel are assumed to be independent. Moreover, substituting the instantaneous power of the interference coefficient i.e.

$$\left| \sum_{z=\phi_{1,\text{sgl}}}^{\phi_{2,\text{sgl}}} \frac{e^{j2\pi z(c_{u,g} + \varepsilon_{u,n}^q - i)/N_c}}{N_c} \right|^2 = \left| \sin \pi \left(c_{u,g} + \varepsilon_{u,n}^q - i / N_c \right) (\phi_{2,\text{sgl}} - \phi_{1,\text{sgl}} + 1) / N_c \sin \pi \left(c_{u,g} + \varepsilon_{u,n}^q - i / N_c \right) \right|^2$$

in (3.56-3.59) and (3.34) producing the instantaneous power of the corresponding signal components and SINR respectively, at any TO and/or CFO value. Furthermore, and by carefully examining equations (3.56-3.59), it can be easily seen that evaluating the average SINR can be achieved by quantifying the average power of the interference coefficient i.e., $\mathbb{E} \left[\left| \sum_{z=\phi_{1,\text{sgl}}}^{\phi_{2,\text{sgl}}} \frac{e^{j2\pi z(c_{u,g} + \varepsilon_{u,n}^q - i)/N_c}}{N_c} \right|^2 \right]; \forall \text{sgl}$.

Considering the assumed independency in generation between the TO and the CFO, which is justified in (Park et al., 2010), the average power of the interference coefficient can be given by:

$$\mathbb{E} \left[\left| \sum_{z=\phi_{1,\text{sgl}}}^{\phi_{2,\text{sgl}}} \frac{e^{j2\pi z(c_{u,g} + \varepsilon_{u,n}^q - i)/N_c}}{N_c} \right|^2 \right] = \sum_{\zeta_{u,n}^{p,q} = B_{\text{TO}}^-}^{B_{\text{TO}}^+} \int_{-\varepsilon}^{\varepsilon} \frac{\sin^2 \left(\pi \left(\frac{c_{u,g} + \varepsilon_{u,n}^q - i}{N_c} \right) (\phi_{2,\text{sgl}} - \phi_{1,\text{sgl}} + 1) \right)}{N_c^2 \left(B_{\text{TO}}^+ - B_{\text{TO}}^- \right) (2\varepsilon) \sin^2 \left(\pi \left(\frac{c_{u,g} + \varepsilon_{u,n}^q - i}{N_c} \right) \right)} d\varepsilon_{u,n}^q \quad (3.60)$$

where the TO is assumed to be i.i.d uniform discrete random variable $\zeta_{u,n}^{p,q}$ with probability $\Pr \left(\zeta_{u,n}^{p,q} = \zeta_{u,n}^{p,q} \mid \zeta_{u,n}^{p,q} \in [B_{\text{TO}}^-, B_{\text{TO}}^+] \right) = \frac{1}{(B_{\text{TO}}^+ - B_{\text{TO}}^-)}$, and CFO is i.i.d uniform random

variable $\varepsilon_{u,n}^q$ with a probability density function $f_{\varepsilon} \left(\varepsilon_{u,n}^q \mid \varepsilon_{u,n}^q \in [-\varepsilon, \varepsilon] \right) = \frac{1}{2\varepsilon}$ (Zhang and

Tellambura, 2007). Note that the detailed derivation of (3.60) is provided in Appendix B.

3.5. Average SINR Analysis for Uplink MIMO-OFDMA Fading Channel Systems In Presence of Carrier Frequency and Sampling Clock Frequency Offsets

3.5.1 Single-User Single-Antenna Structure and Coexistence of Carrier Frequency (CFO) and Sampling Clock Frequency(SCFO) Offsets

In this subsection, the received signal $r_{u,n}^{p,q}(t)$ and the DFT output $\varepsilon, \xi Y_{u,n}^{p,q}(i) = \left(1/\sqrt{N_c}\right) \sum_{z=0}^{N_c-1} \varepsilon, \xi r_{u,n}^{p,q}(zT'_s) e^{-j2\pi z/N_c}$ are exploited to obtain the analytical expressions for the desired signal and the interferences with transmit-receive antennas pair in presence of carrier frequency (CFO) and sampling clock frequency (SCFO) offsets.

In converting the received waveform $r_{u,n}^{p,q}(t)$ back into digital signal, the Analog-to-Digital Converter (ADC) samples at time instants $zT'_s; z \in [0, N_c - 1]$, which is usually different from the sampling instant $T_{u,s}; \forall u$ at the Digital-to-Analog Converter (DAC) of the u^{th} user (Pollet et al., 1995; Liu et al., 2008) which is primarily because of the tolerances of quartz oscillators and temperature variations (Sliskovic, 2001). This offset is known as SCFO.

Let $\xi_{u,n}^q = (T'_s - T_{u,s})/T_{u,s}; \forall u$ denote the normalized SCFO, which can be split into an integer part and a fractional part. Considering the mitigation algorithms of synchronization offsets such as closed-loop synchronization offsets correction between the user transmitters and the BS receivers such as IEEE 802.16e standard, only the fractional part of the SCFO (i.e., residual SCFO) is considered and can be assumed to be $-0.5 \leq \xi_{u,n}^q \leq 0.5$ (Yang et al., 2000). For instant, if the sampling clock specification is 10 ppm (part per million) and the sampling frequency is 5 MHz, then the clock has adrift of about 500 samples per second (Yang et al., 2000).

Without loss of generality, assuming the time synchronization was successful enough to find the OFDMA symbol start within ISI/IBI-free region, two kinds of synchronization offsets remain after the acquisition mode: CFO and SCFO (Langowski, 2001; Morelli and Moretti, 2010). In presence of CFO and SCFO $r_{u,n}^{p,q}(zT'_s)$ and $\varepsilon, \xi Y_{u,n}^{p,q}(i)$ can be represented as:

$$\varepsilon_{u,n}^{\xi} \Gamma_{u,n}^{p,q}(zT_s') = \frac{1}{N_c} \sum_{g=0}^{N_c-1} X_{u,n}^p(g) H_{u,n}^{p,q}(c_{u,g}) e^{\frac{j2\pi c_{u,g}[z+N_{cp}+n(N_c+N_{cp})](1+\xi_{u,n}^q)\varepsilon_{u,n}^q}{N_c}} e^{\frac{j2\pi z c_{u,g}(1+\xi_{u,n}^q)}{N_c}} e^{\frac{j2\pi c_{u,g}[N_{cp}+n(N_c+N_{cp})]\xi_{u,n}^q}{N_c}} \quad (3.61)$$

$$\begin{aligned} \varepsilon_{u,n}^{\xi} Y_{u,n}^{p,q}(i) = & \mathbf{v}_n(\boldsymbol{\varepsilon}_{u,n}^q, \boldsymbol{\xi}_{u,n}^q) X_{u,n}^p(g_{c_{u,g}=i}) H_{u,n}^{p,q}(i) e^{\frac{j2\pi[N_{cp}+n(N_c+N_{cp})]\xi_{u,n}^q}{N_c}} \frac{1}{N_c} \sum_{z=0}^{N_c-1} e^{\frac{j2\pi z[(1+\xi_{u,n}^q)+(1+\xi_{u,n}^q)\varepsilon_{u,n}^q-i]}{N_c}} \\ & + \mathbf{v}_n(\boldsymbol{\varepsilon}_{u,n}^q, \boldsymbol{\xi}_{u,n}^q) \sum_{g=0, c_{u,g} \neq i}^{N_c-1} X_{u,n}^p(g) H_{u,n}^{p,q}(c_{u,g}) e^{\frac{j2\pi[N_{cp}+n(N_c+N_{cp})]c_{u,g}\xi_{u,n}^q}{N_c}} \frac{1}{N_c} \sum_{z=0}^{N_c-1} e^{\frac{j2\pi z[(1+\xi_{u,n}^q)c_{u,g}+(1+\xi_{u,n}^q)\varepsilon_{u,n}^q-i]}{N_c}} \end{aligned} \quad (3.62)$$

where $\mathbf{v}_n(\boldsymbol{\varepsilon}_{u,n}^q, \boldsymbol{\xi}_{u,n}^q) = e^{j2\pi[N_{cp}+n(N_c+N_{cp})](1+\xi_{u,n}^q)\varepsilon_{u,n}^q/N_c}$, and the interference coefficient in presence of CFO and SCFO can be given by:

$$\frac{1}{N_c} \sum_{z=0}^{N_c-1} e^{\frac{j2\pi z[(1+\xi_{u,n}^q)c_{u,g}+(1+\xi_{u,n}^q)\varepsilon_{u,n}^q-i]}{N_c}} = \frac{\sin\left(\pi\left[(1+\xi_{u,n}^q)c_{u,g}+(1+\xi_{u,n}^q)\varepsilon_{u,n}^q-i\right]\right)}{N_c \sin\left(\pi\left[(1+\xi_{u,n}^q)c_{u,g}+(1+\xi_{u,n}^q)\varepsilon_{u,n}^q-i\right]/N_c\right)} \times e^{j\pi\left[(1+\xi_{u,n}^q)c_{u,g}+(1+\xi_{u,n}^q)\varepsilon_{u,n}^q-i\right]} \quad (3.63)$$

It is worthy to mention that equation (3.62) is equivalent to (Nguyen-Le et al., 2009 eq. (5)) in the case of single-user MIMO systems i.e., MIMO-OFDM, which can be approximated to be equivalent to (Speth et al., 1999 eq. (37)) in the case of a single-input-single-output SISO-OFDM systems.

It is easily to observe that $\varepsilon_{u,n}^{\xi} Y_{u,n}^{p,q}(i)$ in (3.62) consists of several contributions: the first term represents the DS which is affected by the channel i.e., $H_{u,n}^{p,q}(i)$, rotated and attenuated by $\mathbf{v}_n(\boldsymbol{\varepsilon}_{u,n}^q, \boldsymbol{\xi}_{u,n}^q) e^{j2\pi[N_{cp}+n(N_c+N_{cp})]\xi_{u,n}^q/N_c}$ and $(1/N_c) \sum_{z=0}^{N_c-1} e^{j2\pi z[(1+\xi_{u,n}^q)+(1+\xi_{u,n}^q)\varepsilon_{u,n}^q-i]/N_c}$, respectively, where both latter effects depend on the incurred offsets as well as the subcarrier index i.e., i . Moreover, the second term in (3.62) denotes the ICI due to CFO and SCFO.

However, the SCFO can also induce ISI because of the accumulation of offset (Yuanxin et al., 2007). Moreover, the SCFO not only cause synchronization offset, it may also cause the duration of an OFDMA symbol at the receiver to be different from that of the transmitter (Prema and Ananthi, 2011).

Unfortunately, the induced ISI by the SCFO, specifically positive SCFO, is not explicitly presented in equation (3.62). Therefore, an exact expression for $\varepsilon, \xi Y_{u,n}^{p,q}(i)$, which includes the ISI as well as the ICI, is proposed in the following, where two scenarios of the residual SCFO can be recognized according to the value of $\xi_{u,n}^a$:

i. **Negative Sampling Clock Frequency Offset (SCFO) (i.e., $0 < -\xi_{u,n}^a \leq 0.5$)**

In this scenario, the ADC clock is faster than the DAC clock of the u^{th} user as in Figure 3.5. At regular interval, one sample is added every $\left\lfloor 1/\xi_{u,n}^a \right\rfloor$ sample, where $|x|$ is the absolute value of x , by sampling twice a particular sample (e.g. samples 3 and 7 in Figure 3.5), which implies that some samples from the desired n^{th} OFDMA symbol are lost (e.g. samples 8 and 9 in Figure 3.5), which cause ICI. Note that there is no browsing samples from the next (i.e., the $(n+1)^{\text{th}}$) OFDMA symbol to complete the window of the DFT, then only **intra-Symbol Interference (ISI)** can be recognized in the DFT window.

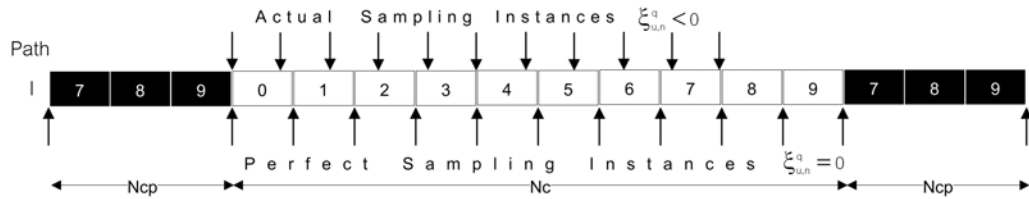


Figure 3.5 Illustration of Sampling the Received OFDMA symbol by the l^{th} Channel Path In presence of Negative SCFO

The number of ISI in each channel tap in the DFT window can be given by: $\left\lfloor \xi_{u,n}^a N_c \right\rfloor$ where $\lfloor x \rfloor$ is the nearest integer less than or equal to x (i.e., floor (x)). The indices of the ISI samples in the DFT window can be grouped in G^{ISI} as: $G^{\text{ISI}} = \left\{ z : \left\lfloor (z+1)(1+\xi_{u,n}^a) \right\rfloor = \left\lfloor (z+2)(1+\xi_{u,n}^a) \right\rfloor ; \forall z \in [0, N_c - 1] \right\}$, then $\varepsilon, \xi Y_{u,n}^{p,q}(i)$ in (3.62) can be rewritten as:

$$\begin{aligned}
\varepsilon_{u,n} \xi_{u,n}^- Y_{u,n}^{p,q}(i) &= \underbrace{\mathbf{v}_n(\boldsymbol{\varepsilon}_{u,n}^q, \boldsymbol{\xi}_{u,n}^q) X_{u,n}^p(g|_{c_{u,g}=i}) H_{u,n}^{p,q}(c_{u,g}) e^{j2\pi [N_{cp} + (N_c + N_{cp}) \xi_{u,n}^q] c_{u,g} / N_c} \sum_{z \in \mathcal{G}^{SI}} \frac{e^{j2\pi z [i \xi_{u,n}^q + (1 + \xi_{u,n}^q) c_{u,n}^q] / N_c}}{N_c}}_{\varepsilon_{DS}^+ \xi_{u,n}^{p,q}(i)} \\
&+ \underbrace{\mathbf{v}_n(\boldsymbol{\varepsilon}_{u,n}^q, \boldsymbol{\xi}_{u,n}^q) \sum_{g=0, c_{u,g} \neq i}^{N_c-1} X_{u,n}^p(g) H_{u,n}^{p,q}(c_{u,g}) e^{j2\pi [N_{cp} + (N_c + N_{cp}) \xi_{u,n}^q] c_{u,g} / N_c} \sum_{z \in \mathcal{G}^{SI}} \frac{e^{j2\pi z [(1 + \xi_{u,n}^q) c_{u,g} + (1 + \xi_{u,n}^q) c_{u,n}^q] / N_c}}{N_c}}_{ICI} \\
&+ \underbrace{\mathbf{v}_n(\boldsymbol{\varepsilon}_{u,n}^q, \boldsymbol{\xi}_{u,n}^q) \sum_{g=0}^{N_c-1} X_{u,n}^p(g) H_{u,n}^{p,q}(c_{u,g}) e^{j2\pi [N_{cp} + (N_c + N_{cp}) \xi_{u,n}^q] c_{u,g} / N_c} \sum_{z \in \mathcal{G}^{SI}} \frac{e^{j2\pi z [(1 + \xi_{u,n}^q) c_{u,g} + (1 + \xi_{u,n}^q) c_{u,n}^q - 1] / N_c}}{N_c}}_{iSI}
\end{aligned} \tag{3.64}$$

where the first and the second term on the right-hand-side of (3.64) represents the DS, and the ICI respectively. The iSI term is represented by the last term in (3.64). Note that

$\varepsilon_{DS-SI}^+ \xi_{u,n}^{p,q} = ICI + iSI$. Note the interference coefficient for the DS/ICI and iSI with negative SCFO can be given by: $(1/N_c) \sum_{z \in \mathcal{G}^{SI}} e^{j2\pi z [(1 + \xi_{u,n}^q) c_{u,g} + (1 + \xi_{u,n}^q) c_{u,n}^q] / N_c}$ and $(1/N_c) \sum_{z \in \mathcal{G}^{SI}} e^{j2\pi z [(1 + \xi_{u,n}^q) c_{u,g} + (1 + \xi_{u,n}^q) c_{u,n}^q - 1] / N_c}$ respectively.

ii. Positive Sampling Clock Frequency Offset (SCFO) (i.e., $0 < \xi_{u,n}^q \leq 0.5$)

In this scenario, the ADC clock is slower than the DAC clock of the u^{th} user as in Figure 3.6. At regular interval, one sample is missed every $1/\xi_{u,n}^q$ sample (e.g. samples 0, 2, 5, and 8 in Figure 3.6), which causes ISI due to sample the following symbol i.e., $(n+1)^{\text{th}}$ symbol, by the accumulated $\xi_{u,n}^q (N_c + N_{cp}) T_s$ per symbol (Gallardo et al., 2001) to compensate the missed samples. It is worthy to note that using the CP reduces the number of the ISI samples for $l > 0$.

The DFT window can be formed by the samples with the following indices along the channel paths: $\text{sampleindices} = \lfloor (z+1)(1 + \xi_{u,n}^q) - l \rfloor; \forall z \in [0, N_c - 1], l \in [0, L - 1]$, where the negative indices and the indices greater than $(N_c - 1)$ represent the CP samples and the ISI samples respectively. Then the total number of the ISI samples from the next OFDMA symbol, $N(\text{ISI}_l)$, which is depends on the SCFO and the channel path, can be easily obtained. In addition the location of the ISI sample can be given by:

$G_1^{ISI} \in [N_c - N(|S_1|), N_c - 1]$; $\forall l$. Therefore, the asynchronous DFT output $\varepsilon, \xi^+ Y_{u,n}^{p,q}(i)$ can be given by:

$$\begin{aligned}
\varepsilon, \xi^+ Y_{u,n}^{p,q}(i) &= \underbrace{\mathbf{v}_n(\boldsymbol{\varepsilon}_{u,n}^q, \boldsymbol{\xi}_{u,n}^q) \chi_{u,n}^p(g|_{c_{u,g}=i}) \sum_{l=0}^{L-1} \boldsymbol{\alpha}_{u,n,l}^{p,q}(zT_s') e^{-j2\pi c_{u,g}/N_c} e^{j2\pi [N_{cp} + (N_c + N_{cp})] c_{u,g} \xi_{u,n}^q / N_c} \sum_{z \in G_1^{ISI}} \frac{e^{j2\pi z [(+ \xi_{u,n}^q) c_{u,g} + (+ \xi_{u,n}^q) c_{u,n}^-]} / N_c}{N_c}}_{\varepsilon, \xi^+ Y_{DS}^{p,q}(i)} \\
&+ \underbrace{\mathbf{v}_n(\boldsymbol{\varepsilon}_{u,n}^q, \boldsymbol{\xi}_{u,n}^q) \sum_{g=0, c_{u,g} \neq i}^{N_c-1} \chi_{u,n}^p(g) \sum_{l=0}^{L-1} \boldsymbol{\alpha}_{u,n,l}^{p,q}(zT_s') e^{-j2\pi c_{u,g}/N_c} e^{j2\pi [N_{cp} + (N_c + N_{cp})] c_{u,g} \xi_{u,n}^q / N_c} \sum_{z \in G_1^{ISI}} \frac{e^{j2\pi z [(+ \xi_{u,n}^q) c_{u,g} + (+ \xi_{u,n}^q) c_{u,n}^-]} / N_c}{N_c}}_{ICI} \\
&+ \underbrace{\mathbf{v}_n(\boldsymbol{\varepsilon}_{u,n}^q, \boldsymbol{\xi}_{u,n}^q) \sum_{g=0}^{N_c-1} \chi_{u,n}^p(g) \sum_{l=0}^{L-1} \boldsymbol{\alpha}_{u,n,l}^{p,q}(zT_s') e^{-j2\pi c_{u,g}/N_c} e^{j2\pi [N_{cp} + (N_c + N_{cp})] c_{u,g} \xi_{u,n}^q / N_c} \sum_{z \in G_1^{ISI}} \frac{e^{j2\pi z [(+ \xi_{u,n}^q) c_{u,g} + (+ \xi_{u,n}^q) c_{u,n}^-]} / N_c}{N_c}}_{ISI}
\end{aligned} \tag{3.65}$$

where the first, the second and the last term on the right-hand-side of (3.65) represents the DS, the ICI and ISI respectively, with the associated phase rotation and attenuation. Moreover, the ICI and ISI figure the incurred interferences of the DS as:

$\varepsilon, \xi^- Y_{DS-ISI}^{p,q} = ICI + ISI$. From (3.65) the interference coefficient for the DS/ICI and ISI with negative SCFO is $(1/N_c) \sum_{z \in G_1^{ISI}} e^{j2\pi z [(+ \xi_{u,n}^q) c_{u,g} + (+ \xi_{u,n}^q) c_{u,n}^-]} / N_c$ and $(1/N_c) \sum_{z \in G_1^{ISI}} e^{j2\pi z [(+ \xi_{u,n}^q) c_{u,g} + (+ \xi_{u,n}^q) c_{u,n}^-]} / N_c$ respectively.

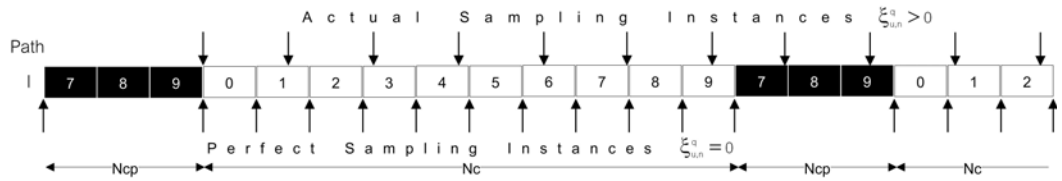


Figure 3.6 Illustration of Sampling the Received OFDMA symbol by the l^{th} Channel Path In presence of Positive SCFO

3.5.2 Instantaneous and Average Interferences Power and SINR with CFO and SCFO in MIMO-OFDMA Uplink Systems

In the presence of CFO and SCFO, $\varepsilon, \xi Y_n^q(i)$ as in (3.33) and (3.55) can be rewritten as:

$$\varepsilon_n^{\xi} Y_n^q(i) = \varepsilon_{DS}^{\xi} Y_{k,n}^{l,q}(i) + \varepsilon_{DS-SI}^{\xi} Y_{k,n}^{l,q}(i) + \underbrace{\sum_{p=1, p \neq t}^P \varepsilon_{k,n}^{\xi} Y_{k,n}^{p,q}(i)}_{\text{CAAs-SI}} + \underbrace{\sum_{u \in \emptyset^c, u \neq k} \sum_{p=1}^P \varepsilon_{u,n}^{\xi} Y_{u,n}^{p,q}(i)}_{\text{MUI}} + W_n^q(i) \quad (3.66)$$

The expression of the $\text{SINR}_{k,SCP}^{q,\varepsilon,\xi}(i)$ is equivalent to (3.34) as: $\text{SINR}_{k,SCP}^{q,\varepsilon,\xi}(i) = P_{DS} / (P_{DS-SI} + P_{CAAs-SI} + P_{MUI} + P_w)$. Then, and with (3.64)-(3.65), and (3.66) the following expressions can be obtained:

$$P_{DS} = E \left[\left| \varepsilon_{DS}^{\xi} Y_{k,n}^{l,q}(i) \right|^2 \right] = \sigma_x^2 \sum_l \sigma_h^2(l) E \left[\left| \sum_{z \notin G_1^{xSI}} e^{\frac{j2\pi z \left[i \xi_{k,n}^q + (1 + \xi_{k,n}^q) \varepsilon_{k,n}^q \right] / N_c}{N_c}} \right|^2 \right] \quad (3.67)$$

$$P_{DS-SI} = E \left[\left| \varepsilon_{DS-SI}^{\xi} Y_{k,n}^{l,q}(i) \right|^2 \right] = \sigma_x^2 \sum_{g=0, c_{k,g} \neq i}^{N_k-1} \sum_l \sigma_h^2(l) E \left[\left| \sum_{z \notin G_1^{xSI}} e^{\frac{j2\pi z \left[(1 + \xi_{k,n}^q) c_{k,g} + (1 + \xi_{k,n}^q) \varepsilon_{k,n}^q \right] / N_c}{N_c}} \right|^2 \right] \\ + \sigma_x^2 \sum_{g=0}^{N_k-1} \sum_l \sigma_h^2(l) E \left[\left| \sum_{z \in G_1^{xSI}} e^{\frac{j2\pi z \left[(1 + \xi_{k,n}^q) c_{k,g} + (1 + \xi_{k,n}^q) \varepsilon_{k,n}^q \right] / N_c}{N_c}} \right|^2 \right] \quad (3.68)$$

$$P_{CAAs-SI} = \sum_{p=1, p \neq t}^P E \left[\left| \varepsilon_{k,n}^{\xi} Y_{k,n}^{p,q}(i) \right|^2 \right] = \sum_{p=1, p \neq t}^P \left(\sigma_x^2 \sum_{g=0}^{N_k-1} \sum_l \sigma_h^2(l) E \left[\left| \sum_{z \notin G_1^{xSI}} e^{\frac{j2\pi z \left[(1 + \xi_{k,n}^q) c_{k,g} + (1 + \xi_{k,n}^q) \varepsilon_{k,n}^q \right] / N_c}{N_c}} \right|^2 \right] \right) \\ + \sigma_x^2 \sum_{g=0}^{N_k-1} \sum_l \sigma_h^2(l) E \left[\left| \sum_{z \in G_1^{xSI}} e^{\frac{j2\pi z \left[(1 + \xi_{k,n}^q) c_{k,g} + (1 + \xi_{k,n}^q) \varepsilon_{k,n}^q \right] / N_c}{N_c}} \right|^2 \right] \quad (3.69)$$

$$P_{MUI} = \sum_{u \in \emptyset^c, u \neq k} \sum_{p=1, p \neq t}^P E \left[\left| \varepsilon_{u,n}^{\xi} Y_{u,n}^{p,q}(i) \right|^2 \right] \\ = \sum_{u \in \emptyset^c, u \neq k} \sum_{p=1, p \neq t}^P \left(\sigma_x^2 \sum_{g=0}^{N_k-1} \sum_l \sigma_h^2(l) E \left[\left| \sum_{z \notin G_1^{xSI}} e^{\frac{j2\pi z \left[(1 + \xi_{k,n}^q) c_{k,g} + (1 + \xi_{k,n}^q) \varepsilon_{k,n}^q \right] / N_c}{N_c}} \right|^2 \right] \right) \\ + \sigma_x^2 \sum_{g=0}^{N_k-1} \sum_l \sigma_h^2(l) E \left[\left| \sum_{z \in G_1^{xSI}} e^{\frac{j2\pi z \left[(1 + \xi_{k,n}^q) c_{k,g} + (1 + \xi_{k,n}^q) \varepsilon_{k,n}^q \right] / N_c}{N_c}} \right|^2 \right] \quad (3.70)$$

where $x \in \{i, l\}$. Moreover, substituting the instantaneous power of the interference coefficient i.e. $\left| \left(\frac{1}{N_c} \right) \sum_{z \in G_1^{SI}} e^{j2\pi z \left[(1+\xi_{u,n}^q) c_{u,g} + (1+\xi_{u,n}^q) \varepsilon_{u,n}^q - i \right] / N_c} \right|^2$ and $\left| \left(\frac{1}{N_c} \right) \sum_{z \in G_1^{SI}} e^{j2\pi z \left[(1+\xi_{u,n}^q) c_{u,g} + (1+\xi_{u,n}^q) \varepsilon_{u,n}^q - i \right] / N_c} \right|^2$ in (3.67-3.70) producing the instantaneous power of the corresponding signal components and the corresponding SINR. Considering the assumed independency in generation between the CFO and the SCFO, which is justified in (Park et al., 2010), the average power of the interference coefficient in presence of CFO and SCFO can be given generally by:

$$\begin{aligned} & \mathbb{E} \left[\left| \left(\frac{1}{N_c} \right) \sum_{z \in G_1^{SI}} e^{j2\pi z \left[(1+\xi_{u,n}^q) c_{u,g} + (1+\xi_{u,n}^q) \varepsilon_{u,n}^q - i \right] / N_c} \right|^2 \right] \\ &= \int_{-\varepsilon}^{\varepsilon} \int_{-\xi}^{\xi} \frac{\sin^2 \left(\pi \left[(1+\xi_{u,n}^q) c_{u,g} + (1+\xi_{u,n}^q) \varepsilon_{u,n}^q - i \right] N (|S_l|) / N_c \right)}{(2\varepsilon)(2\xi) \sin^2 \left(\pi \left[(1+\xi_{u,n}^q) c_{u,g} + (1+\xi_{u,n}^q) \varepsilon_{u,n}^q - i \right] / N_c \right)} d\xi_{u,n}^q d\varepsilon_{u,n}^q \end{aligned} \quad (3.71)$$

where the CFO and SCFO is assumed to be i.i.d uniform continuous random variable $\underline{\varepsilon}_{u,n}^q$ and $\underline{\xi}_{u,n}^q$ with a probability density function $f_{\varepsilon} \left(\underline{\varepsilon}_{u,n}^q \mid \varepsilon_{u,n}^q \in [-\varepsilon, \varepsilon] \right) = \frac{1}{2\varepsilon}$ (Zhang and Tellambura, 2007) and $f_{\xi} \left(\underline{\xi}_{u,n}^q \mid \xi_{u,n}^q \in [-\xi, \xi] \right) = \frac{1}{2\xi}$. Note that the detailed derivation of (3.71) is provided in Appendix C.

CHAPTER IV

PROPOSED ANALYSIS OF AVERAGE ERROR RATES FOR UPLINK MIMO-OFDMA FADING CHANNEL SYSTEMS IN THE PRESENCE OF SYNCHRONIZATION OFFSETS

4.1. Introduction

In this Chapter, an exact distribution of the SINR is derived. Consider a linearly modulated signal of MIMO-OFDMA uplink system in Rayleigh fading channel, the symbol error rate (SER) and bit error rate (BER) of different linearly modulated signals with Gray coding is computed based on the obtained SINR at the DFT output.

4.2. General Asynchronous SINR Statistics

In this subsection, an exact expressions for the probability density function (pdf), $f_{\text{SINR}_{k,\text{xCP}}^{q,\Delta}(i)}(\text{SINR}_{k,\text{xCP}}^{q,\Delta}(i) \leq y)$, and cumulative distribution function (CDF), $F_{\text{SINR}_{k,\text{xCP}}^{q,\Delta}(i)}(\text{SINR}_{k,\text{xCP}}^{q,\Delta}(i) \leq y)$, of asynchronous SINR where $\Delta \in \{\phi, \epsilon, \xi\}$ represents the type of the incurred offset(s) is derived. The distribution of instantaneous $\text{SINR}_{k,\text{xCP}}^{q,\Delta}(i)$ is a Chi-squared distribution of degree 2 (equivalent to an exponential distribution) (Proakis, 2001; Choi, 2004; Athaudage and K. Sathananthan, 2005; Hamdi, 2010), therefore, since the denominator of $\text{SINR}_{k,\text{xCP}}^{q,\Delta}(i)$ at (3.34) is non-negative, the conditional $\text{SINR}_{k,\text{xCP}}^{q,\Delta}(i)$ can be represented as:

$$F_{\text{SINR}_{k,\text{xCP}}^{q,\Delta}(i)}(\text{SINR}_{k,\text{xCP}}^{q,\Delta}(i) \leq y | \Delta) = 1 - e^{-\frac{y}{\text{SINR}_{k,\text{xCP}}^{q,\Delta}(i)}} \quad (4.1)$$

Without loss of generality, let $\mathbf{M}_{\text{xCP}}^{\Delta}(i, y)$ define as:

$$\mathbf{M}_{\text{xCP}}^{\Delta}(i, y) = \mathbb{E} \left(e^{-\frac{y}{\text{SINR}_{k,\text{xCP}}^{q,\Delta}(i)}} \right) \quad (4.2)$$

then, the CDF of the asynchronous SINR can be given by:

$$F_{\text{SINR}_{k,\text{xCP}}^{q,\Delta}(i)}(\text{SINR}_{k,\text{xCP}}^{q,\Delta}(i) \leq y) = 1 - \mathbf{M}_{\text{xCP}}^{\Delta}(i, y) \quad (4.3)$$

For instance, the pdf of $\text{SINR}_{k,\text{xCP}}^{q,\Delta}(i)$, can be obtained when $f_{\text{SINR}_{k,\text{xCP}}^{q,\Delta}(i)}(y) = \frac{d}{dy} F_{\text{SINR}_{k,\text{xCP}}^{q,\Delta}(i)}(y)$ (Papolius, 1965, eq. (4-15)) is applied to (4.3) as follow:

$$\begin{aligned} f_{\text{SINR}_{k,\text{xCP}}^{q,\Delta}(i)}(y) &= \frac{d}{dy} F_{\text{SINR}_{k,\text{xCP}}^{q,\Delta}(i)}(y) = \frac{d}{dy} (1 - M_{\text{xCP}}^{\Delta}(i, y)) = -\frac{d}{dy} M_{\text{xCP}}^{\Delta}(i, y) \\ &= -E \left[\frac{d}{dy} e^{-\frac{y}{\text{SINR}_{k,\text{xCP}}^{q,\Delta}(i)}} \right] = E \left[\frac{1}{\text{SINR}_{k,\text{xCP}}^{q,\Delta}(i)} e^{-\frac{y}{\text{SINR}_{k,\text{xCP}}^{q,\Delta}(i)}} \right] \end{aligned} \quad (4.4)$$

4.3. A Lower Bound on $M_{\text{xCP}}^{\Delta}(i, y)$

For any arbitrary subcarrier assignment schemes, is readily obtained a lower bound on $M_{\text{xCP}}^{\Delta}(i, y)$ by noticing that the function $e^{-y/\text{SINR}_{k,\text{xCP}}^{q,\Delta}(i)}$ is *convex* $\forall \text{SINR}_{k,\text{xCP}}^{q,\Delta}(i), y > 0$, and therefore, Jensen's inequality can be applied as follow:

$$\begin{aligned} M_{\text{xCP}}^{\Delta}(i, y) &= E \left[e^{-\frac{y}{\text{SINR}_{k,\text{xCP}}^{q,\Delta}(i)}} \right] \\ &\geq e^{-\frac{y}{E[\text{SINR}_{k,\text{xCP}}^{q,\Delta}(i)]}} \end{aligned} \quad (4.5)$$

where $E[\text{SINR}_{k,\text{xCP}}^{q,\Delta}(i)]$ is the average asynchronous SINR. Without loss of generality, the lower bound of $M_{\text{xCP}}^{\Delta}(i, y) = e^{-y/E[\text{SINR}_{k,\text{xCP}}^{q,\Delta}(i)]}$ is considered as in (Proakis, 2001). As expected, upper bounds on the exact error probabilities are then achieved when this lower bound of $M_{\text{xCP}}^{\Delta}(i, y)$ is used. It is worthy to note that with the distribution of the asynchronous SINR on hand; it is straight forward to derive exact expressions for average error rates as in the following.

4.4. Average Error Rate Analysis

The obtained distribution of the SINR can be exploited to derive an exact expression for an average error rate. Generally, the average of any arbitrary function $P_x(\text{SINR}_{k,\text{xCP}}^{q,\Delta}(i) \leq y)$ can be computed using the rule of integration by parts as follows (Hamdi, 2010):

$$E\left[P_x\left(\text{SINR}_{k,\text{XCP}}^{q,\Delta}(i) \leq y\right)\right] = P_x(0) + \int_0^\infty \left(\frac{d}{dy}P_x(y)\right) \Pr\left(\text{SINR}_{k,\text{XCP}}^{q,\Delta}(i) > y\right) dy \quad (4.6)$$

Then, in the following, the average symbol and bit error rates are derived.

4.4.1. Average Symbol Error Rate (SER)

The conditional symbol error rate (SER), $P_{s,\text{XCP}}^\Delta$, of square Gray-coded M-QAM is given by Simon et al. (1995; eq. (10.32)) as:

$$P_{s,\text{XCP}}^\Delta\left(\text{SINR}_{k,\text{XCP}}^{q,\Delta}(i)\right) = 1 - \left[1 - \left(1 - \frac{1}{\sqrt{M}}\right) \text{erfc}\left(\sqrt{\text{SINR}_{k,\text{XCP}}^{q,\Delta}(i)}\right)\right]^2 \quad (4.7)$$

where $\text{erfc}(x) = \left(2/\sqrt{\pi}\right) \int_x^\infty e^{-t^2} dt$ is the complementary error function. Therefore, the average SER can be obtained from (4.6) and (4.7) as follow:

$$P_{s,\text{XCP}}^\Delta(0) = 1 - \left[1 - \left(1 - \frac{1}{\sqrt{M}}\right) \text{erfc}(\sqrt{0})\right]^2 = 1 - \left(\frac{1}{\sqrt{M}}\right)^2 = 1 - \frac{1}{M} \quad (4.8)$$

where $\text{erfc}(0) = 1$, and

$$\frac{dP_{s,\text{XCP}}^\Delta\left(\text{SINR}_{k,\text{XCP}}^{q,\Delta}(i)\right)}{d\text{SINR}_{k,\text{XCP}}^{q,\Delta}(i)} = -2 \left[1 - \left(1 - \frac{1}{\sqrt{M}}\right) \text{erfc}\left(\sqrt{\text{SINR}_{k,\text{XCP}}^{q,\Delta}(i)}\right)\right] \left(1 - \frac{1}{\sqrt{M}}\right) \frac{e^{-\text{SINR}_{k,\text{XCP}}^{q,\Delta}(i)}}{\sqrt{\pi \text{SINR}_{k,\text{XCP}}^{q,\Delta}(i)}} \quad (4.9)$$

$$\text{where } \frac{d\text{erfc}\left(\sqrt{\text{SINR}_{k,\text{XCP}}^{q,\Delta}(i)}\right)}{d\text{SINR}_{k,\text{XCP}}^{q,\Delta}(i)} = -\frac{e^{-\text{SINR}_{k,\text{XCP}}^{q,\Delta}(i)}}{\sqrt{\pi \text{SINR}_{k,\text{XCP}}^{q,\Delta}(i)}}.$$

By substituting (4.8) and (4.9) into (4.6), the average SER can be given by:

$$P_{s,\text{XCP}}^\Delta = \left(1 - \frac{1}{M}\right) - 2 \left(1 - \frac{1}{\sqrt{M}}\right) \int_0^\infty \left[1 - \left(1 - \frac{1}{\sqrt{M}}\right) \text{erfc}(\sqrt{y})\right] \frac{e^{-y}}{\sqrt{\pi y}} M_{\text{XCP}}^\Delta(i, y) dy \quad (4.10)$$

For $M_{\text{XCP}}^\Delta(i, y) = e^{-y/E\left[\text{SINR}_{k,\text{XCP}}^{q,\Delta}(i)\right]}$, $P_{s,\text{XCP}}^\Delta$ can be given by:

$$\begin{aligned}
P_{s,\text{XCP}}^\Delta &= \left(1 - \frac{1}{M}\right) - 2 \left(1 - \frac{1}{\sqrt{M}}\right) \sqrt{\frac{E[\text{SINR}_{k,\text{XCP}}^{q,\Delta}(i)]}{E[\text{SINR}_{k,\text{XCP}}^{q,\Delta}(i)] + 1}} + 2 \left(1 - \frac{1}{\sqrt{M}}\right)^2 \sqrt{\frac{E[\text{SINR}_{k,\text{XCP}}^{q,\Delta}(i)]}{E[\text{SINR}_{k,\text{XCP}}^{q,\Delta}(i)] + 1}} \\
&\quad - \frac{4}{\pi} \left(1 - \frac{1}{\sqrt{M}}\right)^2 \sqrt{\frac{E[\text{SINR}_{k,\text{XCP}}^{q,\Delta}(i)]}{E[\text{SINR}_{k,\text{XCP}}^{q,\Delta}(i)] + 1}} \tan^{-1} \left(\sqrt{\frac{E[\text{SINR}_{k,\text{XCP}}^{q,\Delta}(i)]}{E[\text{SINR}_{k,\text{XCP}}^{q,\Delta}(i)] + 1}} \right)
\end{aligned} \tag{4.11}$$

where the detailed derivation of (4.11) is presented in Appendix D.

4.4.2. Average Bit Error Rate (BER)

General expressions for bit error probabilities of generalized square M-QAM are given by Cho and Yoon (2002), which can be written in the following form:

$$P_{b,\text{XCP}}^\Delta \left(\text{SINR}_{k,\text{XCP}}^{q,\Delta}(i) \right) = \sum_{v=0}^{\sqrt{M}-2} a_v \text{erfc} \left((2v+1) \sqrt{\text{SINR}_{k,\text{XCP}}^{q,\Delta}(i)} \right) \tag{4.12}$$

where a constants a_v depend on the constellation size, such as $a_0 = 1/2$ in case of QPSK, $a_v \in \{3/8, 2/8, -1/8\}, v \in [0, 2]$ in case of 16-QAM, whereas $a_v \in \{7/24, 6/24, -1/24, 0, 1/24, 0, -1/24\}, v \in [0, 6]$ in case of 64-QAM. From (4.6) and (4.12) we have,

$$P_{b,\text{XCP}}^\Delta(0) = \sum_{v=0}^{\sqrt{M}-2} a_v \text{erfc} \left((2v+1) \sqrt{0} \right) = \sum_{v=0}^{\sqrt{M}-2} a_v = \frac{1}{2} \tag{4.13}$$

$$\frac{d}{dy} P_{b,\text{XCP}}^\Delta \left(\text{SINR}_{k,\text{XCP}}^{q,\Delta}(i) \right) = - \sum_{v=0}^{\sqrt{M}-2} a_v \frac{(2v+1) e^{-(2v+1)^2 \text{SINR}_{k,\text{XCP}}^{q,\Delta}(i)}}{\sqrt{\pi \text{SINR}_{k,\text{XCP}}^{q,\Delta}(i)}} \tag{4.14}$$

Thus,

$$P_{b,\text{XCP}}^\Delta = \frac{1}{2} - \sum_{v=0}^{\sqrt{M}-2} a_v (2v+1) \int_0^\infty \frac{e^{-(2v+1)^2 y}}{\sqrt{\pi y}} M_{\text{XCP}}^\Delta(i, y) dy \tag{4.15}$$

With $M_{\text{XCP}}^\Delta(i, y) = e^{-y/E[\text{SINR}_{k,\text{XCP}}^{q,\Delta}(i)]}$, the $P_{b,\text{XCP}}^\Delta$ can be given by:

$$P_{b,xCP}^{\Delta} = \frac{1}{2} - \sum_{v=0}^{\sqrt{M}-2} a_v (2v+1) \int_0^{\infty} \frac{1}{\sqrt{\pi y}} e^{-y \left((2v+1)^2 + \frac{1}{E[\text{SINR}_{k,xCP}^{q,\Delta}(i)]} \right)} dy$$

$$P_{b,xCP}^{\Delta} = \frac{1}{2} - \sum_{v=0}^{\sqrt{M}-2} a_v (2v+1) \sqrt{\frac{E[\text{SINR}_{k,xCP}^{q,\Delta}(i)]}{(2v+1)^2 E[\text{SINR}_{k,xCP}^{q,\Delta}(i)] + 1}} \quad (4.16)$$

where $\int_0^{\infty} \frac{e^{-\alpha y}}{\sqrt{y}} dy = \sqrt{\frac{\pi}{\alpha}}$; $\alpha > 0$ (Jeffery and Dai, 2008, eq.(15.3.1-10),, page 270).

CHAPTER V

RESULTS AND DISCUSSIONS

5.1. Introduction

In this Chapter, the analytical results are verified by simulation and comparison with the competing analysis expressions. The simulation environment takes a scenario similar to ITU-R M.1225, 3GPP TR 25.814 and 3GPP TR 29.913 recommendations into account. Note that only the analytical unit in any synchronization scenario i.e., $\varepsilon, \phi, \xi Y_{u,n}^{p,q}(i)$ is simulated to validate our assumption, where coincided results between the analytical $\varepsilon, \phi, \xi Y_{u,n}^{p,q}(i)$ and the simulated one are obtained. Moreover, the effects of utilizing the MIMO technique, CP conditions and different SASs are explored.

5.2. Simulation Environment

An MIMO-OFDMA uplink system with 10MHz bandwidth working in 2GHz band is considered. Table 5.1 shows the major system parameters. In addition, the standardized channel model in (Recommendation ITU-R M.1225, Channel B, Table 4, page 28), which complies with WSSUS modeling for frequency selective Rayleigh fading channels, is considered.

Table 5.1: System Parameters

Parameters	Value
Number of Subcarriers, N_c	256
Number of CP Samples, N_{cp} (Sufficient /Insufficient/Absent)	(64/20/0)
Sample Time Interval, T_s (ns)	100
Number of Users, U	16
User terminal (UT) power class, (dBm)	24
Thermal noise level (dBm/Hz)	-174

Table 5.2 shows the tapped-delay-line for wireless environment, where the Doppler spectrum for each tap is eliminated in order to make the simulation environment a better match with the analyzed models. Moreover, the path coefficients of all users are assumed to be statistically independent and therefore independently generated for different users, whereas perfect channel knowledge at the BS's receive antennas is assumed.

On the other hand, the N_c subcarriers are allocated by BSAS, ISAS, and GSAS. For BSAS, a set of $\left(N_c/U\right)$ contiguous subcarriers are allocated to each user as: $\left[(u-1)\left(N_c/U\right), u\left(N_c/U\right)-1 \right]$, where u is the user index i.e., $u \in [1, U]$. In addition, the subcarriers are spaced at a distance $\left(N_c/U\right)$ from each other in ISAS to be given as: $\{(u-1) + Ug\}; \forall g \in \left[0, \left(N_c/U\right)-1 \right]$, while for GSAS, a set of $\left(N_c/U\right)$ exclusive random subcarriers are allocated to each user. Furthermore, the asynchronous users' indices are generated randomly where the desired user's index is selected to be $u=1$.

Table 5.2 Tapped Delay Line Parameters for Wireless Environment

Tap	Pedestrian Channel	
	Relative delay (ns)	Average Power (dB)
1	0	0
2	200	-0.9
3	800	-4.9
4	1200	-8.0
5	2300	-7.8
6	3700	-23.9

Without loss of generality, the u^{th} user's transmit antennas are assumed to have the same synchronization offset, whereas the employed asynchronous users experienced equal offset. Moreover, only the thermal noise is considered at the BS's receiving antennas in order to confine the performance degradation to the synchronization offsets.

5.3. System Performance In Presence of TO

In this section, the analytical results are verified by simulations and validated by the competing analyzed in (Park et al., 2010). The effects of utilizing the MIMO technique, CP scenarios and different SASs are also explored.

5.3.1. The Instantaneous Interference Components and SINR of $\phi Y_{u,n}^{p,q}(i=c_{u,g})$

The instantaneous power of the signal components of $\phi Y_{u,n}^{p,q}(i=c_{u,g})$ in (3.10) are depicted in Figures 5.1-5.9 for SCP, InCP and ACP conditions where $c_u, \forall u$ are allocated by BSAS, ISAS and GSAS. In addition, the correspondence instantaneous SINR is presented in Figures 5.10-5.12.

Consider SCP condition, the DS maintains its maximum level at $\zeta_{u,n}^{p,q}=0$ throughout the effective CP duration i.e., range (a) for all the $c_{u=1}$, where both the ICI and ISI are combated as shown in Figure 5.1. The Figure shows that the associated interferences' power, especially the ISI, increases enormously as the TO increases beyond the effective CP duration, while the DS decreases accordingly.

It is worthy to note that using sufficient CP length is also reducing the potential of the interference generated by the TO towards the CP. For example, the generated interference by $\zeta_{u,n}^{p,q} = -(N_{cp} - L + 2)$ i.e., beyond the effective CP duration, is lowered by around -47dB to that generated by $\zeta_{u,n}^{p,q} = 1$ as can be seen from Figure 5.1(b and d). Relaxing the CP condition, however, shortens the immune interval to the interferences, and numerously improves the power of the generated interferences by the TO towards the CP to be more equally to the corresponding one by the TO away from the CP.

Although an ideal time synchronization offset is experienced, a minimal interferences signature is detected with InCP and ACP scenarios due to the dispersive nature of the fading channel as can be recognized in Figures 5.4-5.9 at $\zeta_{u,n}^{p,q} = 0$.

However, it is worthy to note that $\phi Y_{u,n}^{p,q}(i)$ in (3.10) is equivalent to the DFT output at subcarrier $i \in c_{u=1}$ when only the desired user experiences TO for OFDMA uplink systems, where the summation of ICI and ISI represent the DS-SI.

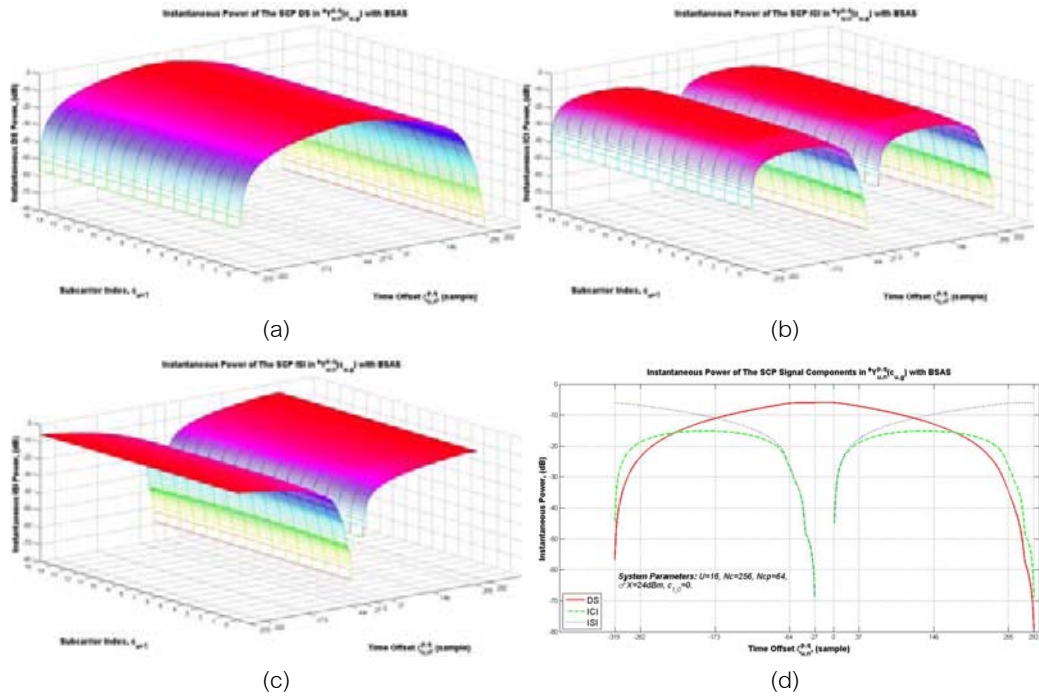


Figure 5.1 Instantaneous powers of SCP signal components in $\phi_{u,n}^{p,q} (i = c_{u,g})$: (a) The DS, (b) The ICI, (c) The ISI, (d) Slices of the DS, ISI, and ICI at $c_{1,0} = 0$ allocated by BSAS

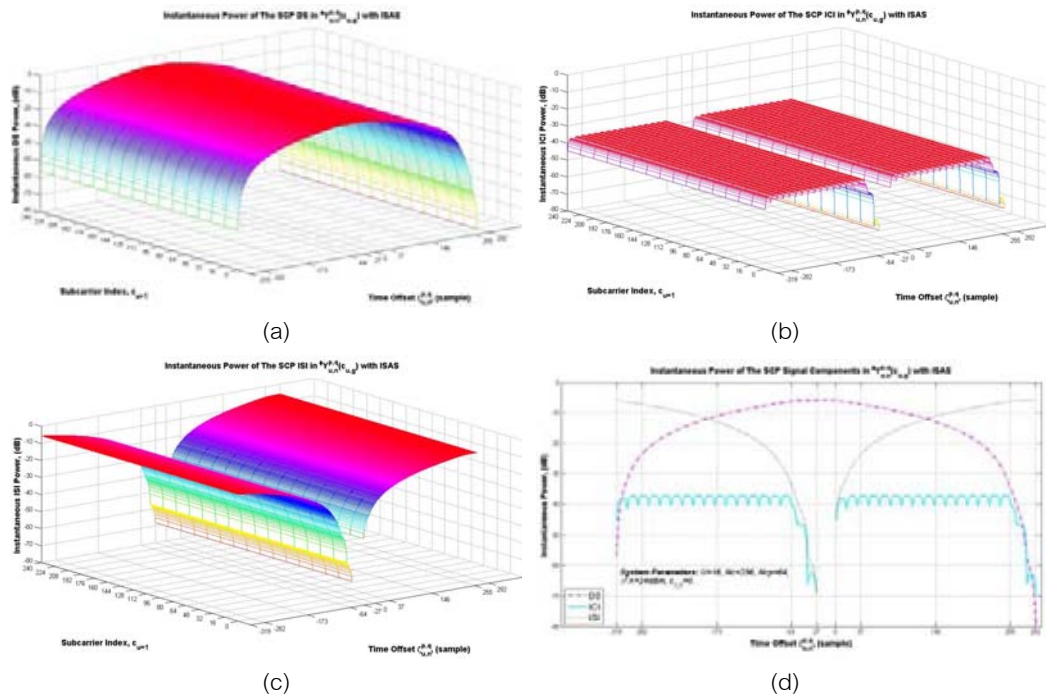


Figure 5.2 Instantaneous powers of SCP signal components in $\phi_{u,n}^{p,q} (i = c_{u,g})$: (a) The DS, (b) The ICI, (c) The ISI, and (d) Slices of the DS, ICI, and ISI at $c_{1,0} = 0$ allocated by ISAS

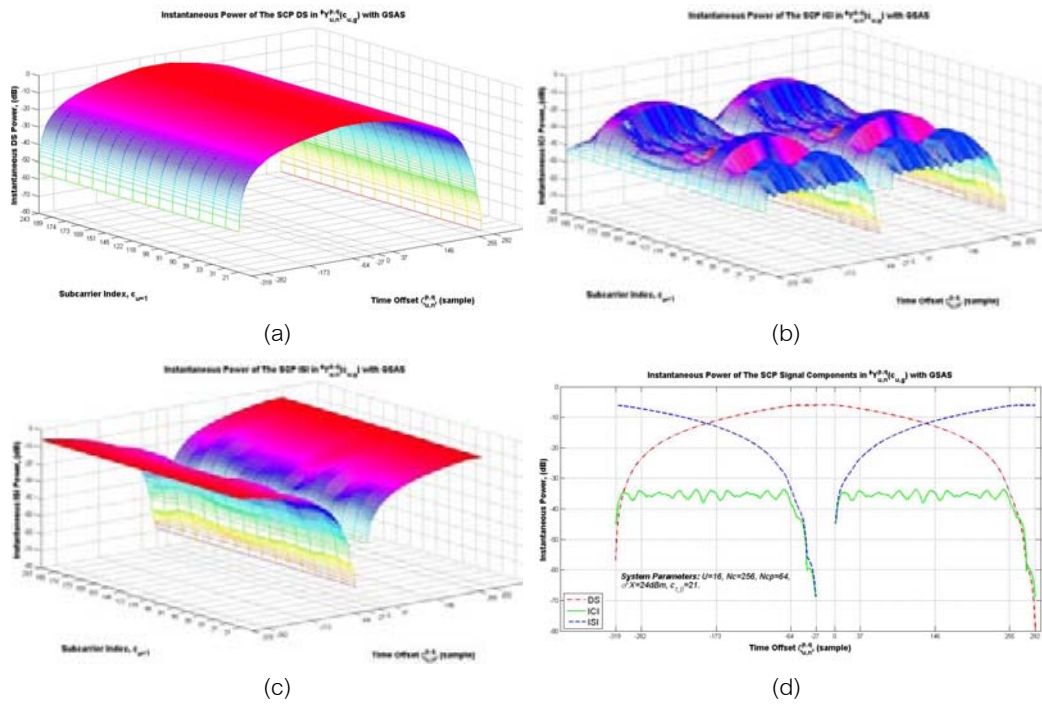


Figure 5.3 Instantaneous powers of SCP signal components in $\phi_{u,n}^{p,q}(i=c_{u,g})$: (a) The DS, (b) The ICI, (c) The ISI, and (d) Slices of the DS, ICI, and ISI at $c_{1,0} = 21$ allocated by GSAS

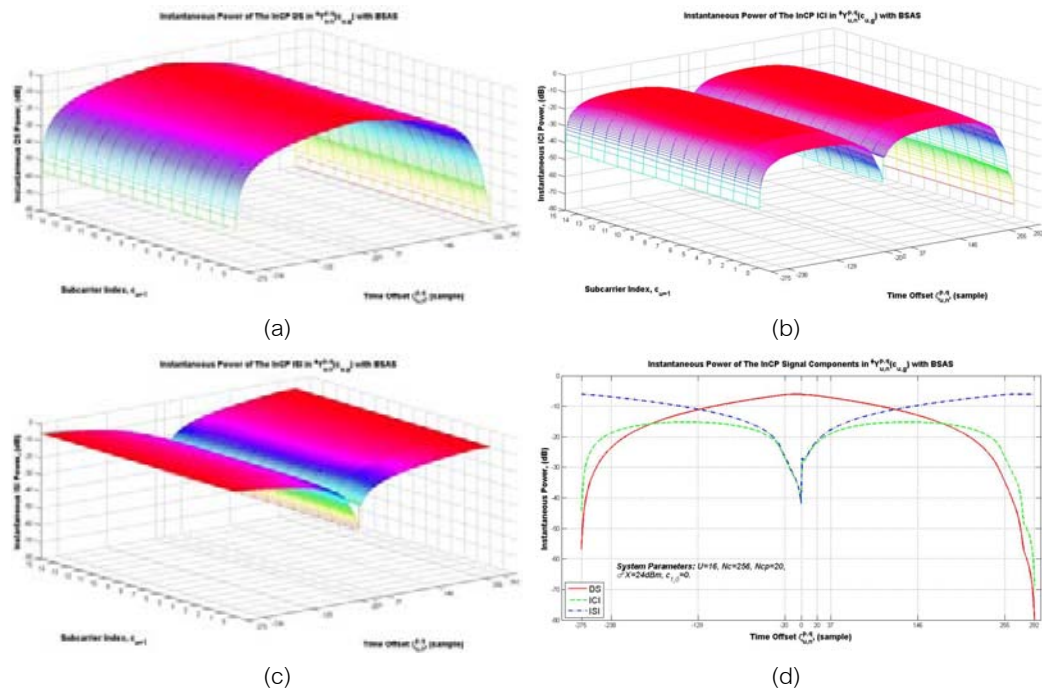


Figure 5.4 Instantaneous powers of InCP signal components in $\phi_{u,n}^{p,q}(i=c_{u,g})$: (a) The DS, (b) The ICI, (c) The ISI, and (d) Slices of the DS, ICI, and ISI at $c_{1,0} = 0$ allocated by BSAS

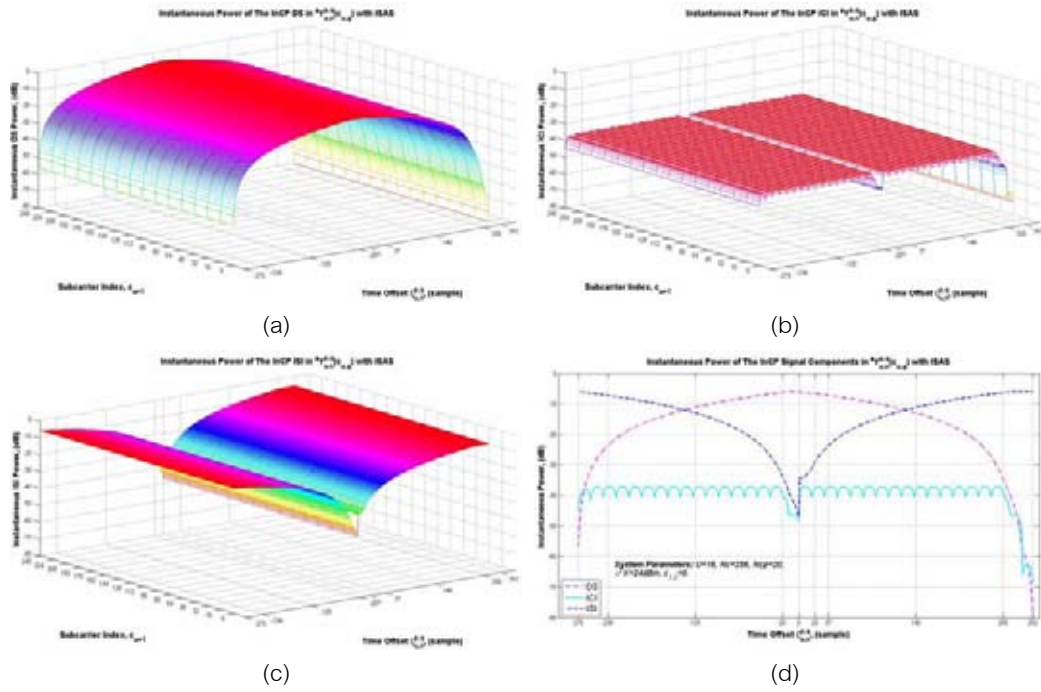


Figure 5.5 Instantaneous powers of InCP signal components in $\phi_{u,n}^{p,q} (i=c_{u,g})$: (a) The DS, (b) The ICI, (c) The ISI, and (d) Slices of the DS, ICI, and ISI at $c_{1,0} = 0$ allocated by ISAS

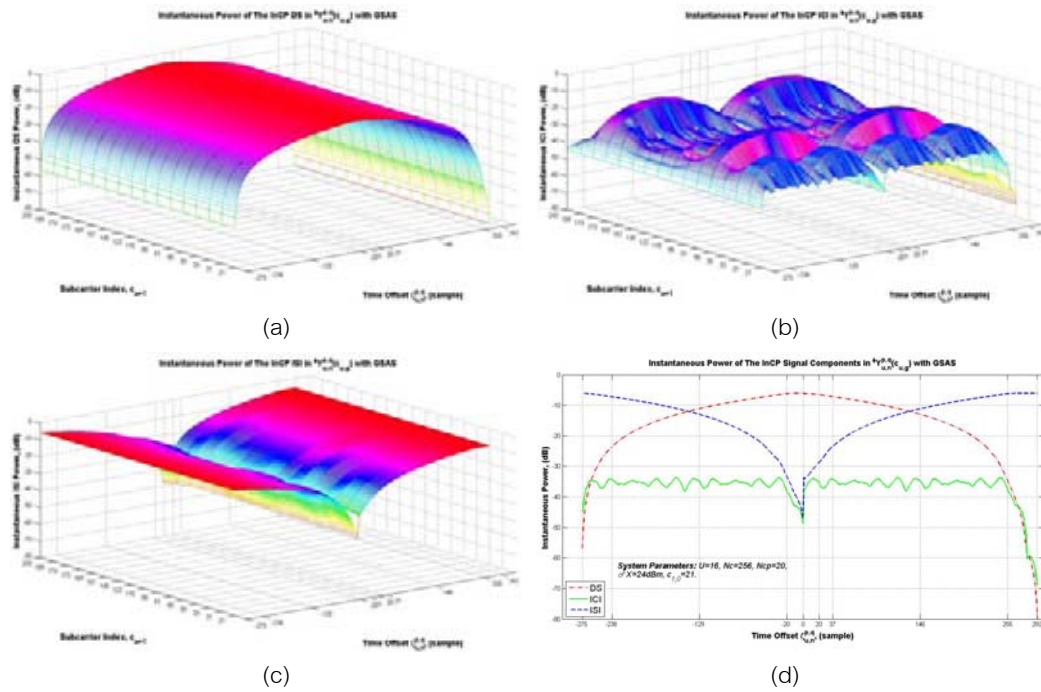


Figure 5.6 Instantaneous powers of InCP signal components in $\phi_{u,n}^{p,q} (i=c_{u,g})$: (a) The DS, (b) The ICI, (c) The ISI, and (d) Slices of the DS, ICI, and ISI at $c_{1,0} = 21$ allocated by GSAS

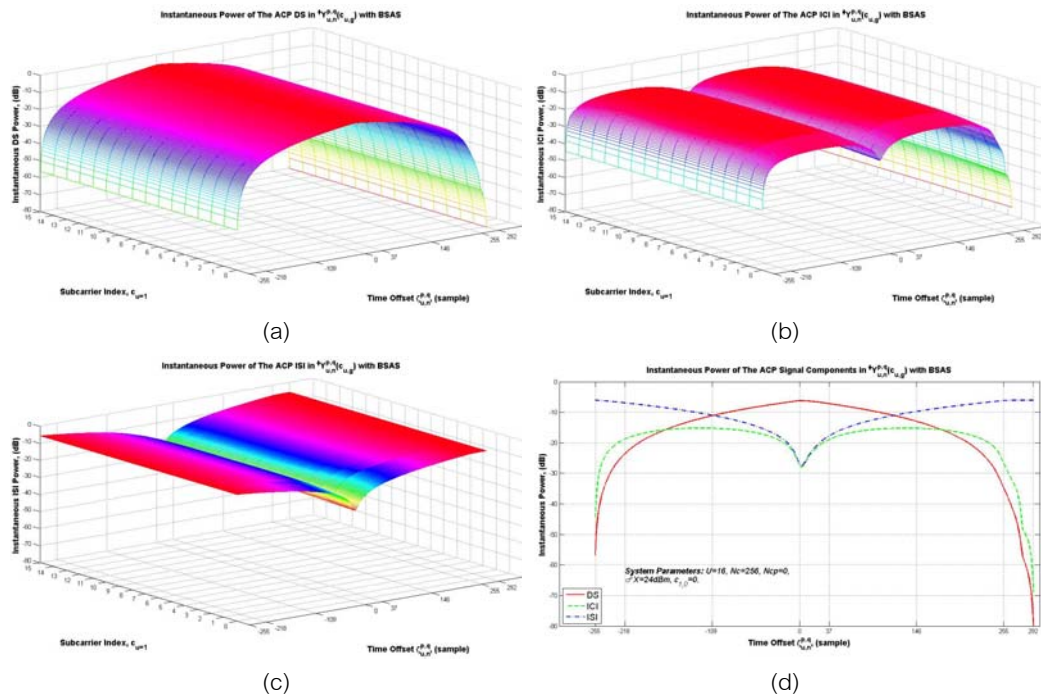


Figure 5.7 Instantaneous powers of ACP signal components in $\phi_{u,n}^{p,q} (i=c_{u,g})$: (a) The DS, (b) The ICI, (c) The ISI, and (d) Slices of the DS, ICI, and ISI at $c_{1,0} = 0$ allocated by BSAS

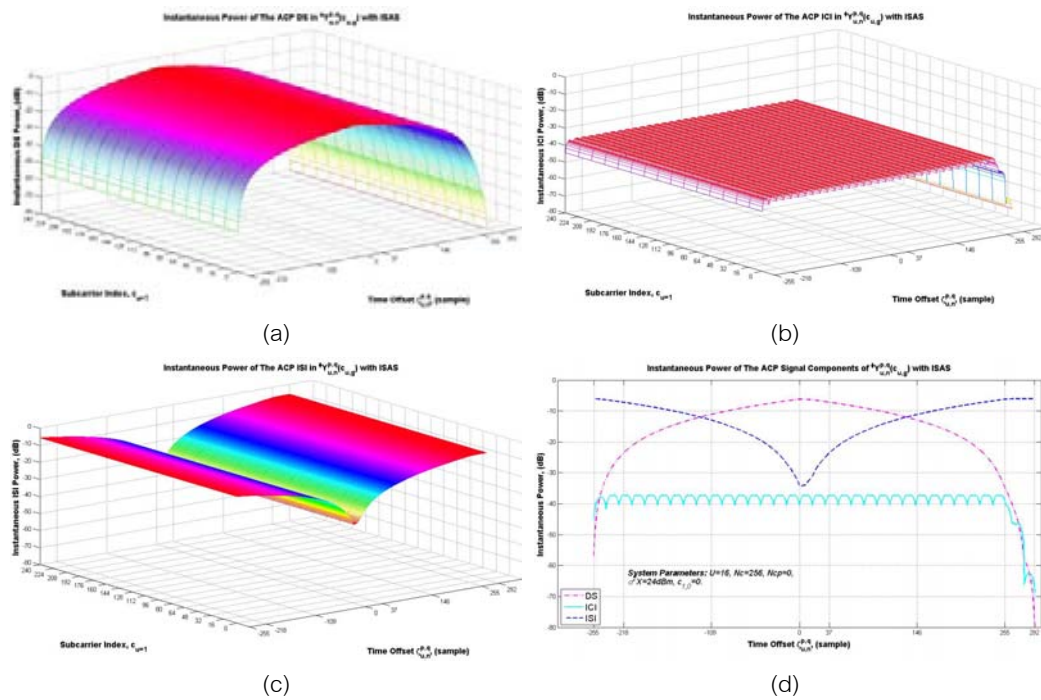


Figure 5.8 Instantaneous powers of ACP signal components in $\phi_{u,n}^{p,q} (i=c_{u,g})$: (a) The DS, (b) The ICI, (c) The ISI, and (d) Slices of the DS, ICI, and ISI at $c_{1,0} = 0$ allocated by ISAS

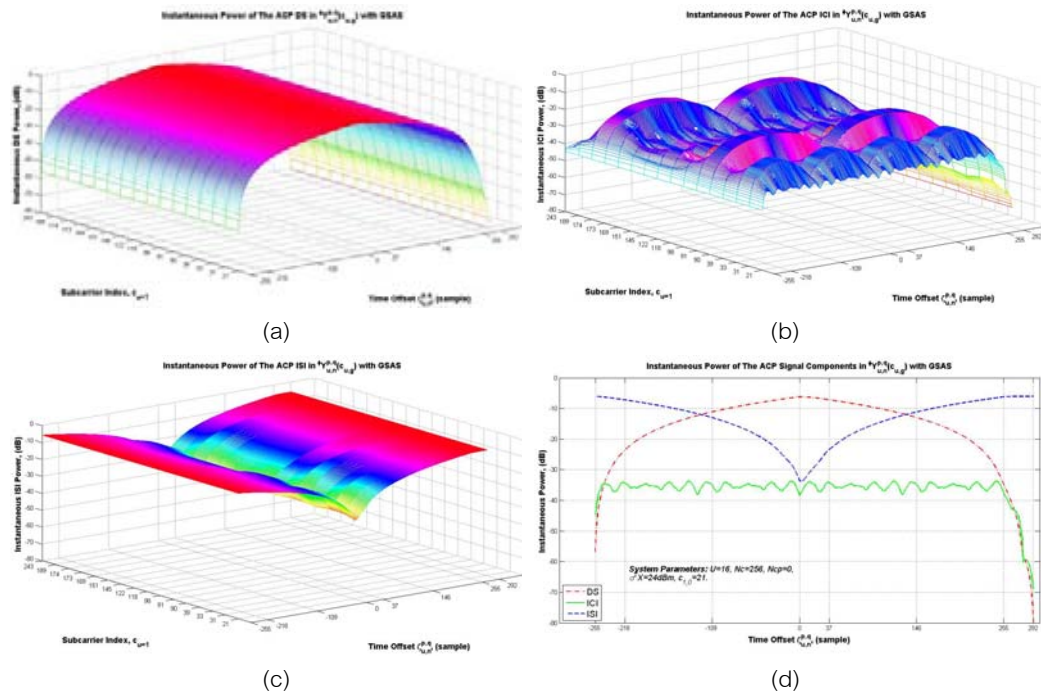


Figure 5.9 Instantaneous powers of ACP signal components in $\phi Y_{u,n}^{p,q} (i=c_{u,g})$: (a) The DS, (b) The ICI, (c) The ISI, and (d) Slices of the DS, ICI, and ISI at $c_{1,0} = 21$ allocated by GSAS

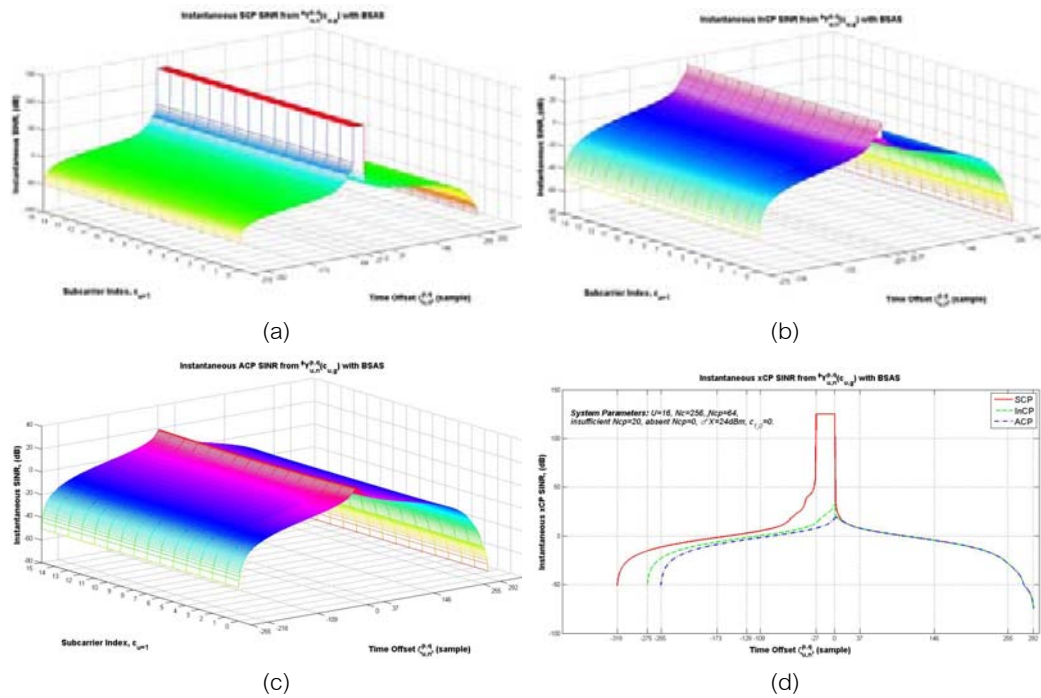


Figure 5.10 Instantaneous xCP SINR from $\phi Y_{u,n}^{p,q} (i=c_{u,g})$: (a) SCP SINR, (b) InCP SINR, (c) ACP SINR, and (d) Slices of the Instantaneous xCP SINR at $c_{1,0} = 0$ allocated by BSAS

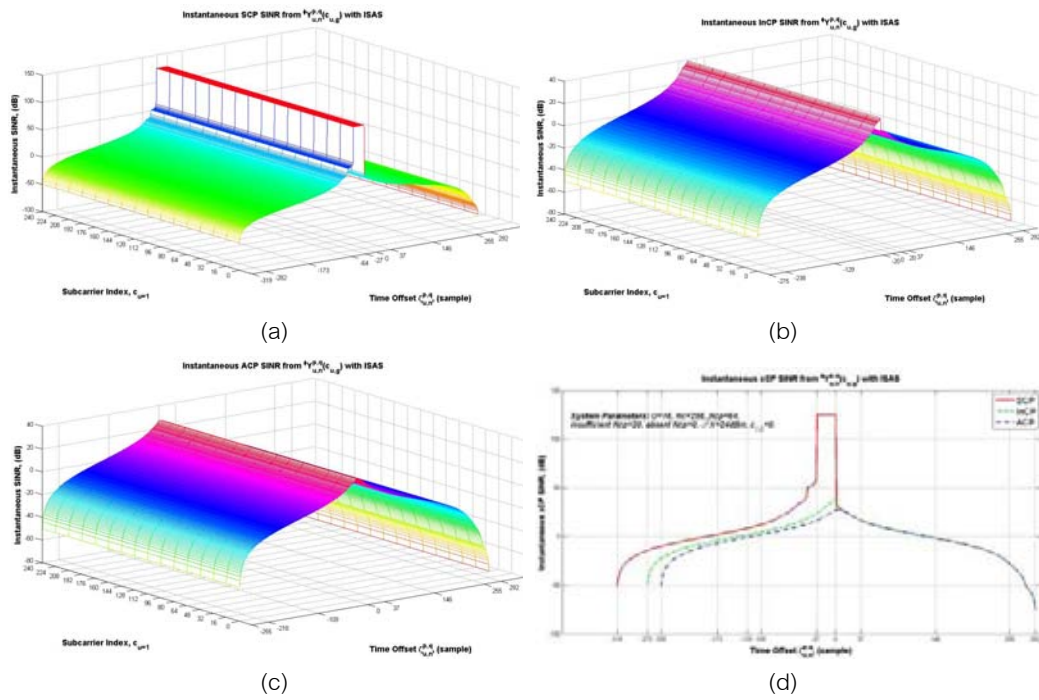


Figure 5.11 Instantaneous xCP SINR from $\phi_{u,n}^{p,q} (i = c_{u,g})$: (a) SCP SINR, (b) InCP SINR, (c) ACP SINR, and (d) Slices of the Instantaneous xCP SINR at $c_{1,0} = 0$ allocated by ISAS

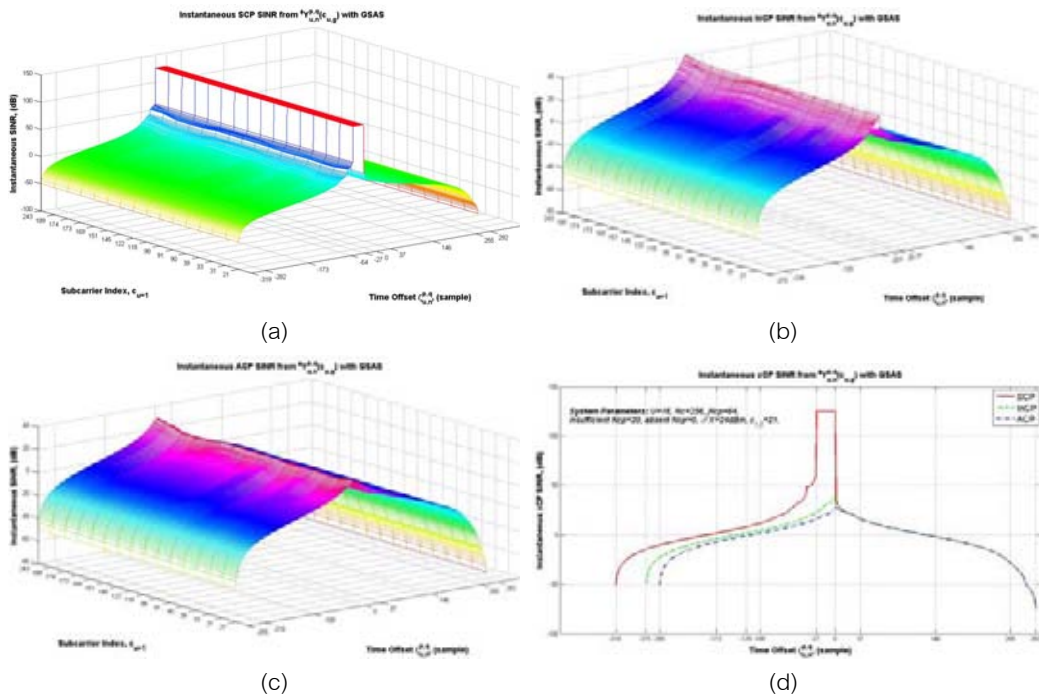


Figure 5.12 Instantaneous xCP SINR from $\phi_{u,n}^{p,q} (i = c_{u,g})$: (a) SCP SINR, (b) InCP SINR, (c) ACP SINR, and (d) Slices of the Instantaneous xCP SINR at $c_{1,0} = 21$ allocated by GSAS

Hence the corresponding instantaneous SINR, which is evaluated by (3.34), are depicted in Figures 5.10-5.12. In Figure 5.10, and with SCP, the instantaneous SINR in the ideal case of time synchronization offset shows its maximum value (i.e. 137dB), which is maintained throughout the effective CP length.

As expected, the instantaneous SINR enormously decreases as the TO increases towards and away from the CP, because of the concurrent substantial increment and decrement of the DS-SI and the DS, with the TO, respectively. Moreover, this maximum instantaneous SINR with SCP is deducted dramatically to 37.7dB and 18.3dB when the CP is eased to InCP and ACP, respectively, as in Figures 5.10-5.12.

5.3.2. Instantaneous/Average Interferences and SINR for MIMO-OFDMA Uplink Systems

In this subsection, the introduced instantaneous/average interferences and SINR at the DFT output in presence of the TO are analyzed, where the properties of the MIMO technique, the influence of the CP condition and SASs are considered.

A. The Instantaneous/Average CAs-SI Analysis

Figures 5.13-5.15 present the incurred CAs-SI in presence of desired user's TO. In MIMO context, the CAs-SI increases as the number of transmit-antennas increases. Employing 2, 4 and 8 synchronous antennas by the desired user increase the SCP CAs-SI by around -6dB, -3dB and 0.02dB respectively at $c_{k=1,0} = 0$ allocated by BSAS, ISAS and GSAS as in Figures 5.13(a)-5.15(a).

Furthermore, Figures 5.13-5.15 show that the correspondence CAs-SI is minimally reduced when the CP is shorten and/or the antennas itself experience TO. For example, the difference between the synchronized SCP (ACP) CAs-SI and the asynchronous one with $\zeta_{1,n}^{p,q} = -32$ is around -20.6dB (-10.5dB), -15.8dB (-5.7dB), and -12.0dB (-2.0dB) for 2, 4, and 8 employed antennas respectively at $c_{1,0} = 21$ allocated by GSAS, as can be recognized in Figure 5.15. Note that with ISAS, the CAs-SI maintains a constant value

along the $c_{k=1}$, where the generated CAs-SI with BSAS and GSAS is subject to the subcarrier index as well as the experienced TO

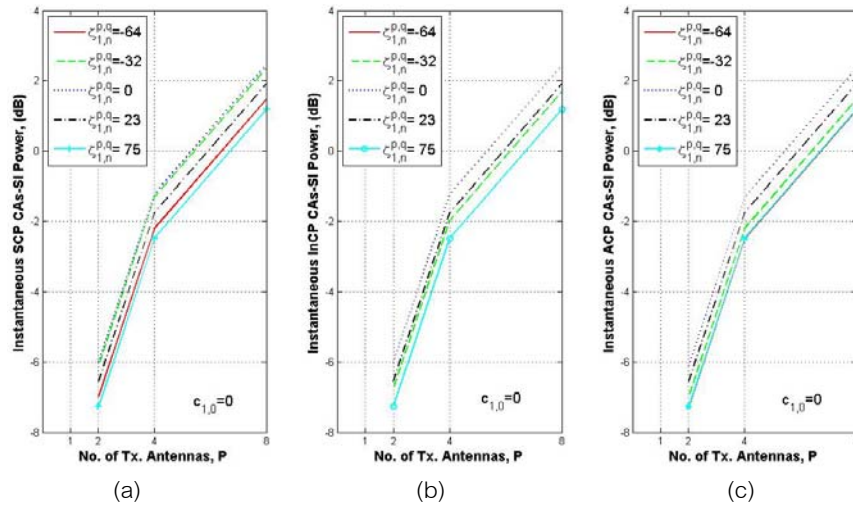


Figure 5.13 Instantaneous Powers of the CAs-SI Versus the Number of Transmit-Antennas With: (a) SCP, (b) InCP, and (c) ACP for Different Desired User's TO $\zeta_{1,n}^{p,q} = -64, -32, 0, 23$ and 75 at $c_{1,0} = 0$ Allocated by BSAS.

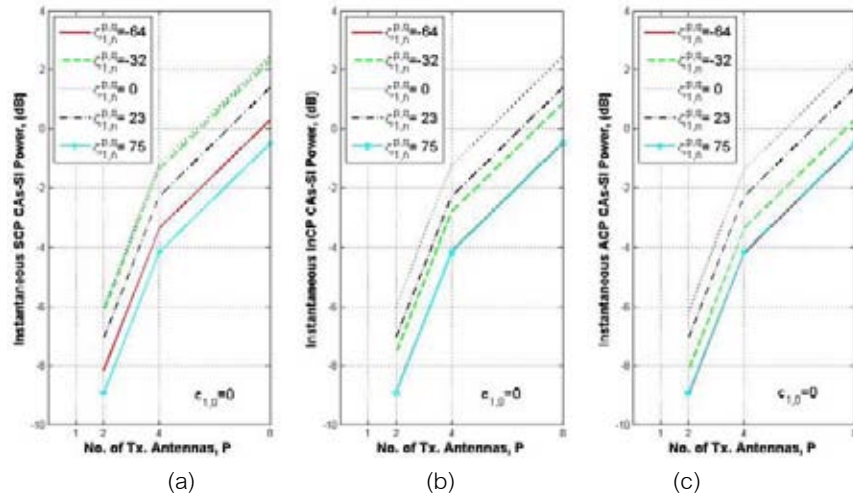


Figure 5.14 Instantaneous Powers of the CAs-SI Versus the Number of Transmit-Antennas with: (a) SCP, (b) InCP, and (c) ACP for Different Desired User's TO $\zeta_{1,n}^{p,q} = -64, -32, 0, 23$ and 75 at $c_{1,0} = 0$ Allocated by ISAS

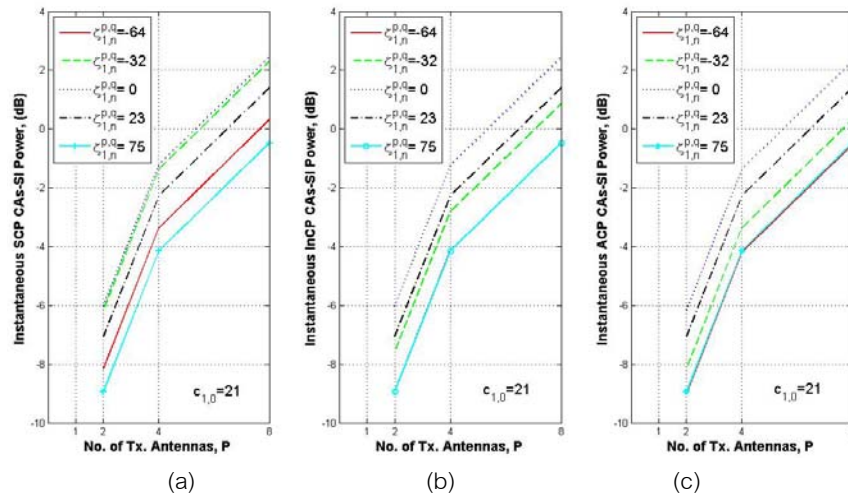


Figure 5.15 Instantaneous Powers of the CAs-SI Versus the Number of Transmit-Antennas with: (a) SCP, (b) InCP, and (c) ACP for Different Desired User's TO $\zeta_{1,n}^{p,q} = -64, -32, 0, 23$ and 75 at $c_{1,0} = 21$ Allocated by GSAS.

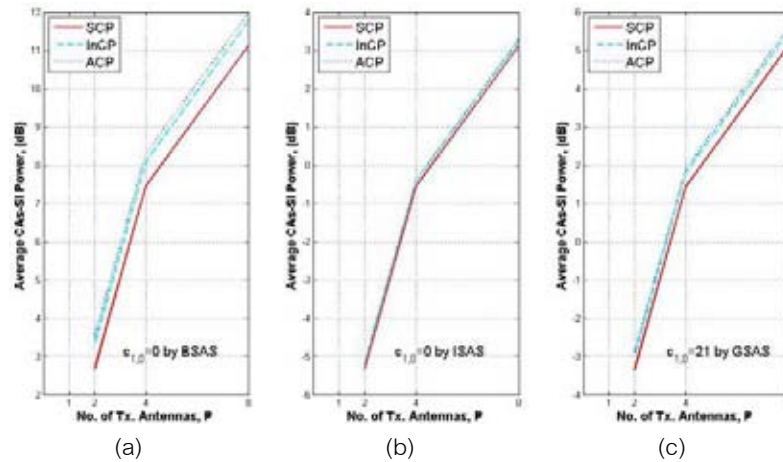


Figure 5.16 Average CAs-SI Versus The Number Of Transmit Antennas, $P=1, 2, 4,$ And 8 With SCP, InCP And ACP Scenarios At: (A) $c_{1,0} = 0$ Allocated By BSAS, (B) $c_{1,0} = 0$ Allocated By ISAS, (C) $c_{1,0} = 21$ Allocated By GSAS

Figure 5.16 explores the incurred average CAs-SI. The Figure shows that the average CAs-SI increases as the number of transmit antennas increases where eases the CP condition increases the corresponding CAs-SI. For example, the SCP (ACP) CAs-SI is being 2.67dB (3.52dB), 7.44dB (8.30dB), and 11.12dB (11.98dB) when $2, 4,$

and 8 antennas are deployed respectively at $c_{1,0} = 0$ allocated by BSAS as in Figure 5.16. Moreover, the degree of improvement on the CAs-SI due to easing the CP condition is governed by the exploited SAS. Table 5.3 shows this effect at $c_{1,0}$ allocated by BSAS, ISAS and GSAS.

From subcarrier allocation view of point, the ISAS alleviates the CAs-SI comparable to the GSAS and BSAS, where the generated CAs-SI by the later SAS is the highest one, as can be recognized from Table 5.3.

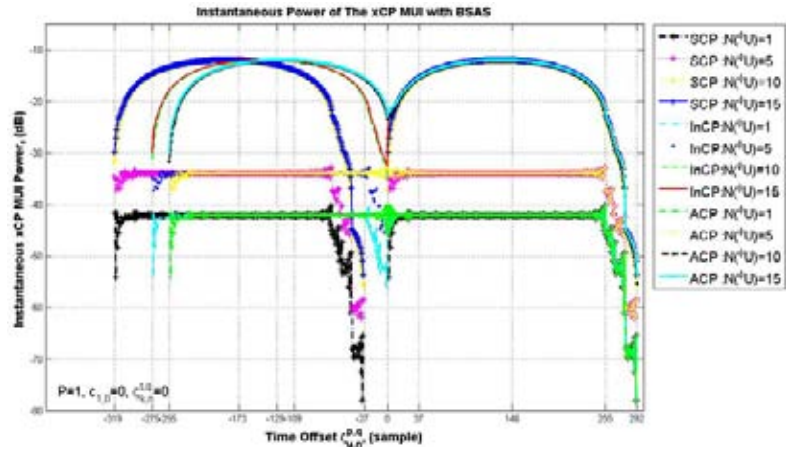
Table 5.3: The Average CAs-SI for Different CP Conditions at $c_{1,0}$ by BSAS, ISAS and GSAS

CAs-SI (dB)	P=2			P=4			P=8		
	BSAS	ISAS	GSAS	BSAS	ISAS	GSAS	BSAS	ISAS	GSAS
SCP	2.67	-5.32	-3.34	7.44	-0.55	1.43	11.12	3.13	5.11
InCP	3.32	-5.19	-2.98	8.09	-0.42	1.79	11.77	3.26	5.47
ACP	3.52	-5.17	-2.87	8.30	-0.40	1.90	11.98	3.28	5.58

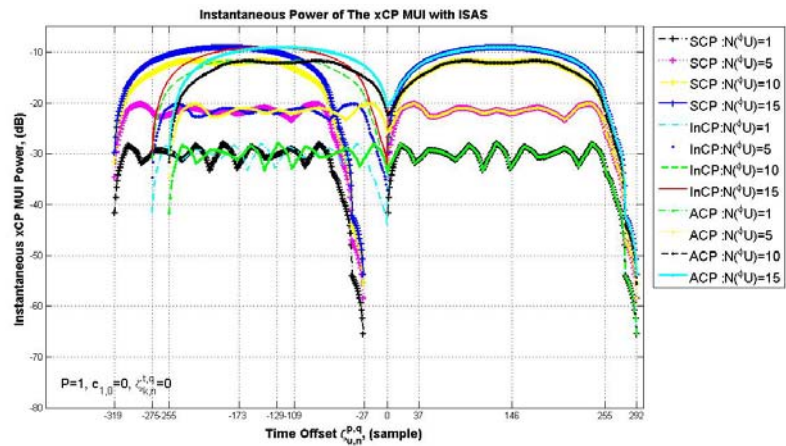
B. The Instantaneous/Average MUI Analysis

The instantaneous MUI is improved and be more susceptible to the variation of the TO when more asynchronous users are incurred as depicted in Figures 5.17-5.18. Using the SCP alleviates the MUI along the effective CP duration and reduces markedly the generated one beyond this immune duration towards the CP. For example the corresponding MUI at $\zeta_{u,n}^{p,q} = -(N_{cp} - L + 2) = -28$ is less by -41.6304dB than the coincidental one at $\zeta_{u,n}^{p,q} = 1$ at $c_{1,0} = 0/0/21$ allocated by BSAS/ISAS/GSAS respectively in Figure 5.17 for $N(\phi_U) = 1$. These immunity and reduction to the MUI is eased by shortening the CP duration even though the trend of the MUI is conserved. For example, the SCP/InCP/ACP MUI at $\zeta_{u,n}^{p,q} = -1$ is $-\infty$ dB/-42.3430dB/-42.1112dB at $c_{1,0} = 0/0/21$ allocated by BSAS/ISAS/GSAS respectively in Figure 5.17 for $N(\phi_U) = 1$.

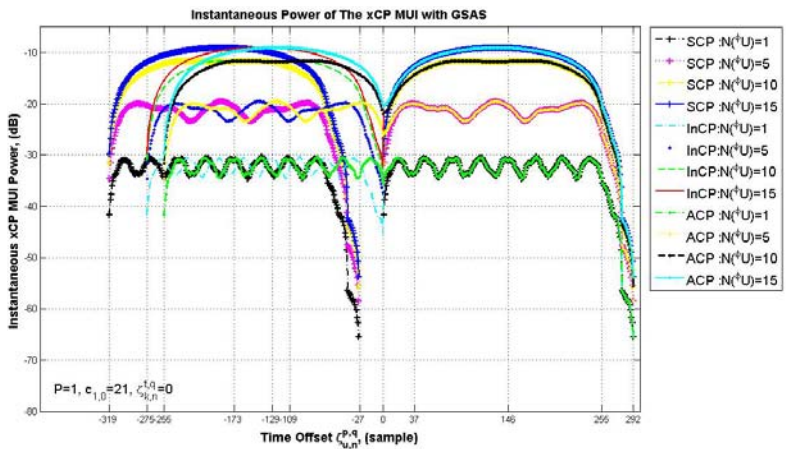
From the subcarrier allocation perspective, the BSAS performs better than the ISAS and GSAS by producing the lowest instantaneous MUI for all the CP conditions.



(a)



(b)



(c)

Figure 5.17 Instantaneous {SCP, InCP, ACP} MUI for $N^{(\phi U)}=1, 5, 10,$ and 15 at: (a) $c_{1,0}=0$ Allocated By BSAS, (b) $c_{1,0}=0$ Allocated By ISAS, and (c) $c_{1,0}=21$ Allocated By GSAS for $P=1$

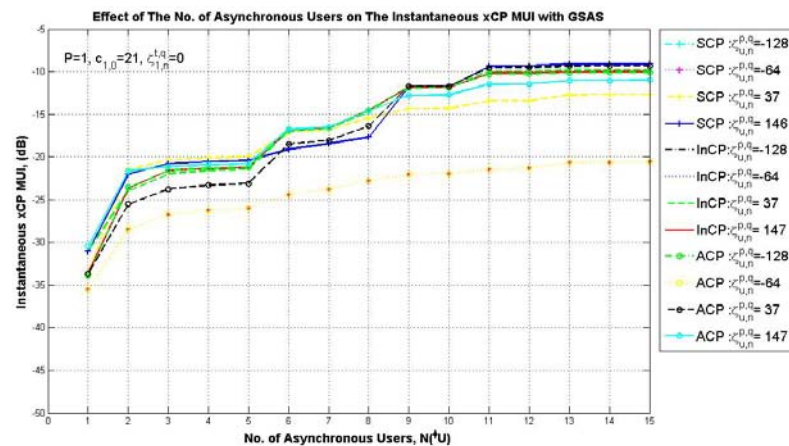
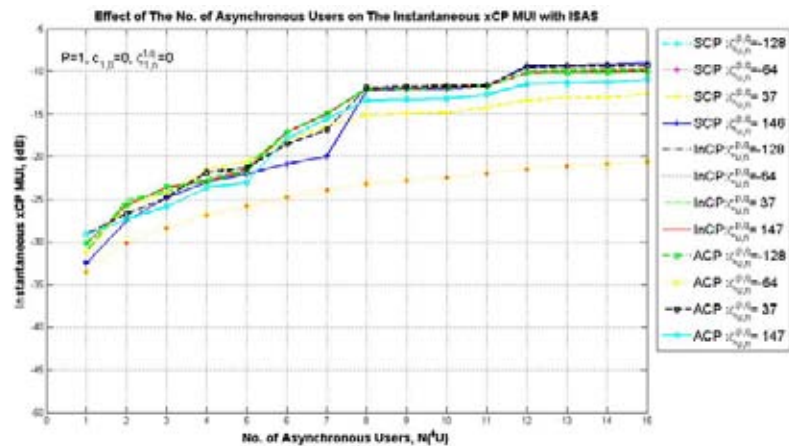
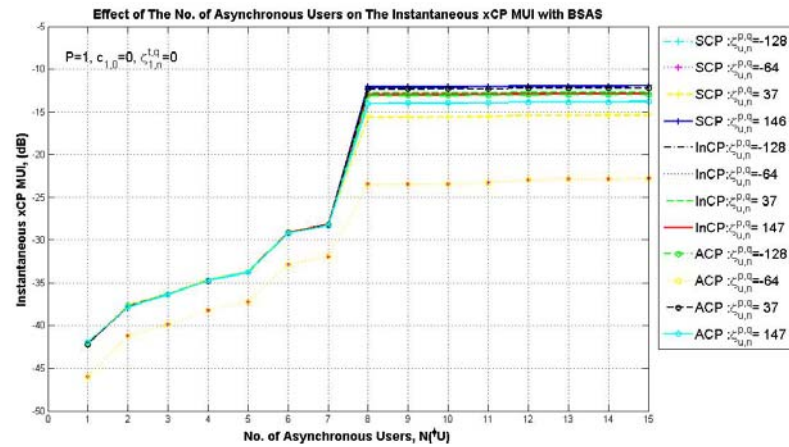
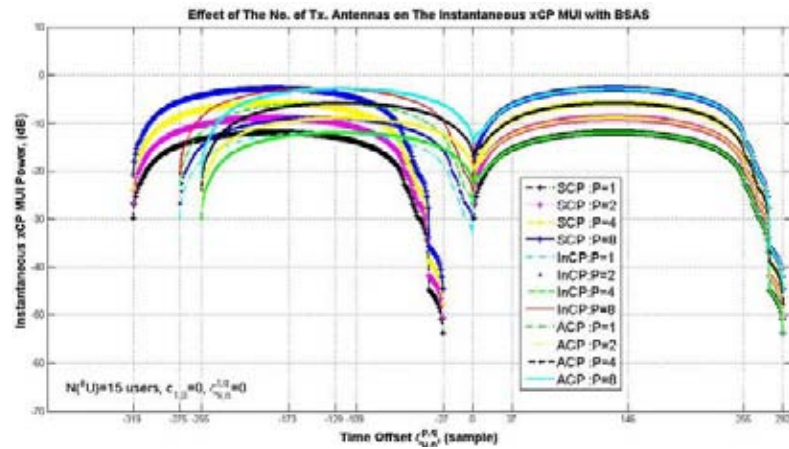
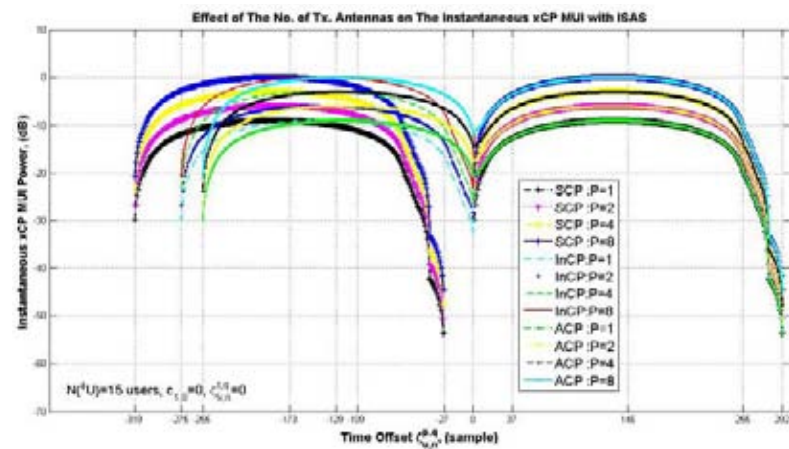


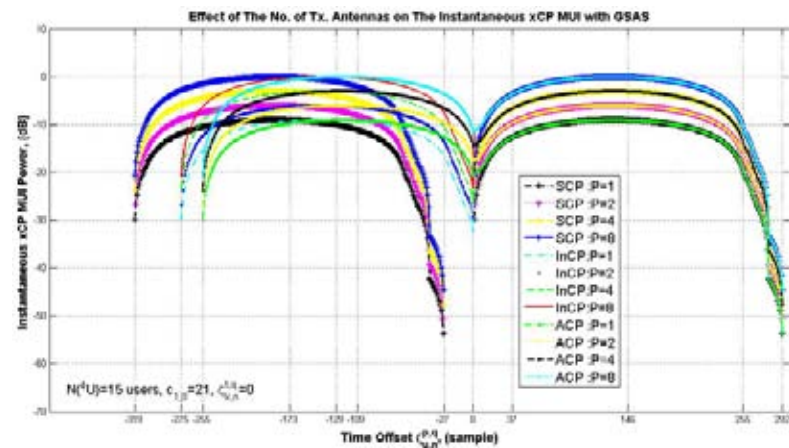
Figure 5.18 Instantaneous {SCP, InCP, ACP} MUI for $\zeta_{u,n}^{p,q} = -128, -64, 37, \text{ and } 146$ at: (a) $c_{1,0} = 0$ Allocated by BSAS, (b) $c_{1,0} = 0$ Allocated by ISAS, and (c) $c_{1,0} = 21$ Allocated by GSAS for $P=1$



(a)

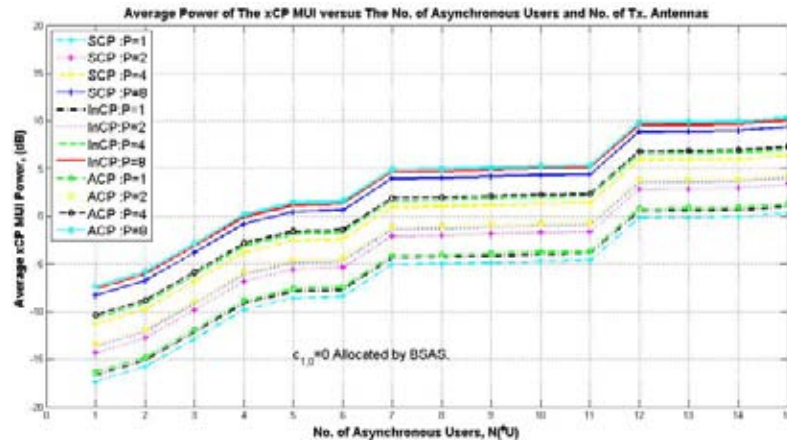


(b)

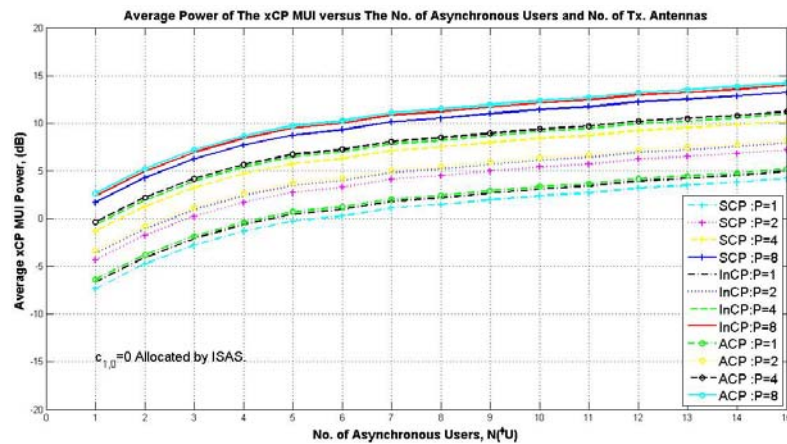


(c)

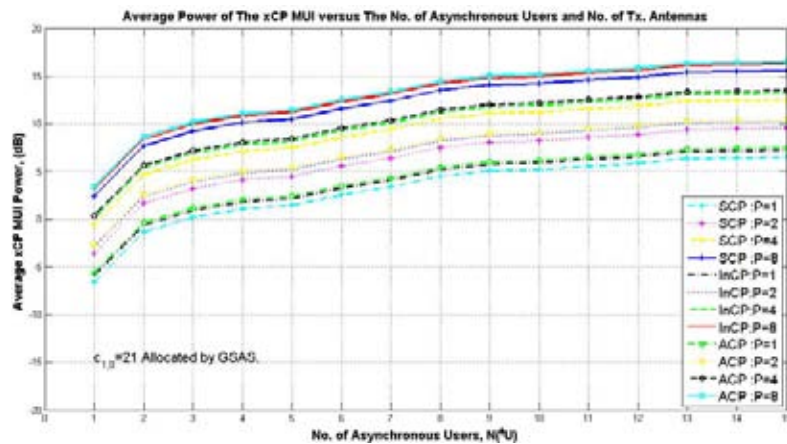
Figure 5.19 Instantaneous {SCP, InCP, ACP} MUI for $P=1, 2, 4,$ and 8 Antennas at: (a) $c_{1,0}=0$ Allocated by BSAS, (b) $c_{1,0}=0$ Allocated by ISAS, and (c) $c_{1,0}=21$ Allocated by GSAS for $N^t(\phi U)=15$



(a)



(b)



(c)

Figure 5.20 Effects of Number of Asynchronous Users N^U and Number of Transmit Antennas, P on the Average {SCP, InCP, and ACP} MUI at: (a) $c_{1,0}=0$ Allocated by BSAS, (b) $c_{1,0}=0$ Allocated by ISAS, (c) $c_{1,0}=21$ Allocated by GSAS

For example, the instantaneous SCP MUI by $N(\phi_U)=7(15)$ is around -32.0dB (-22.8 dB), -24.0 dB (-20.6 dB), and -23.8 dB (-20.6 dB) at $c_{1,0}=0, 0,$ and 21 allocated by BSAS, ISAS and GSAS respectively when $\zeta_{u,n}^{p,q}=-64$ as in Figure 5.18. Figure 5.19 presents the effect of the number of transmit antennas, P , on the instantaneous MUI.

Employing multiple transmit antennas improves the instantaneous MUI accordingly for certain $N(\phi_U)$ and $\zeta_{u,n}^{p,q}$, where the trend of the MUI is conserved. This because the employed antennas exploit the same allocated subcarriers c_u when they transmit simultaneously. For example, the instantaneous SCP MUI is around -22.8dB (-20.6dB), -19.8dB (-17.6dB), -16.8dB (-14.6dB), and -13.8dB (-11.6dB) for $P=1, 2, 4,$ and 8 respectively at $c_{1,0}=0(21)$ allocated by BSAS (GSAS), when $N(\phi_U)=15$ and $\zeta_{u,n}^{p,q}=-64$ as in Figure 5.19.

Figure 5.20 explores the influence of the number of asynchronous users and the number of transmit antennas on the average MUI through the CP conditions. As expected, the average MUI increases as the number of asynchronous users and the number of transmit antennas increase as well as ease the CP condition.

It is worthy to note that the produced average MUI when BSAS is exploited is lower than the induced one when ISAS and GSAS is utilized along the CP condition. Considering single-transmit antenna, the BSAS meets the average SCP/InCP/ACP MUI ≤ 0 dB when $N(\phi_U) \leq 14/11/11$ at $c_{1,0}$ allocated by BSAS, where the ISAS and GSAS can meet this average MUI at $c_{1,0}$ when $N(\phi_U) \leq 5/4/4$ and $N(\phi_U) \leq 2/2/2$ respectively, as show in Figure 5.20. In addition, the corresponding incurred average MUI is enhanced as the CP is shortened as in Table 5.4.

Table 5.4: The Average MUI for Different CP Conditions at $c_{1,0}$ by BSAS, ISAS and GSAS for $P=1$

MUI(dB)	$N(\phi_U)=1$			$N(\phi_U)=7$			$N(\phi_U)=15$		
	BSAS	ISAS	GSAS	BSAS	ISAS	GSAS	BSAS	ISAS	GSAS
SCP	-17.32	-7.34	-6.62	-5.07	1.11	3.39	0.33	4.21	6.51
InCP	-16.64	-6.63	-5.91	-4.38	1.82	4.11	1.01	4.92	7.23
ACP	-16.35	-6.37	-5.65	-4.10	2.08	4.36	1.30	5.18	7.48

However, Park et al., (2010) have derived a closed form of the average MUI in OFDMA uplink systems for three different asynchronous regions

$$R_{\alpha_1} = \left\{ -\left(\frac{T_c + T_{cp}}{2}\right) \leq \mu_{u,n}^{p,q} < \left(\frac{T_c + T_{cp}}{2}\right) \right\}, \quad R_{\alpha_2} = \left\{ -T_{cp} \leq \mu_{u,n}^{p,q} < T_{cp} \right\}, \quad \text{and}$$

$$R_{\alpha_3} = \left\{ 0 \leq \mu_{u,n}^{p,q} < T_{cp} \right\} \text{ as follow (Park et al., 2010, eq. 16, 17 and 18 respectively):}$$

$$E_{\mu_{u,n}^{p,q}} \left[\text{var}(\text{MUI}) \left| -\frac{(T_c + T_{cp})}{2}, \frac{(T_c + T_{cp})}{2} \right. \right] = \sum_{u \in \Phi_U} \sum_{g=0}^{N_u-1} \frac{1}{T_c \pi^2 (c_{u,g} - i)^2} \left[\sum_{l=0}^{L-1} T_c W_u(l) \right. \\ \left. + \sum_{l=0}^{L-1} \left(T_s l - \frac{(T_c + T_{cp})}{2} \right) W_u(l) \text{sinc} \left(\theta \left(T_s l - \frac{(T_c + T_{cp})}{2} \right) \right) \right. \\ \left. - \sum_{l=0}^{L-1} \left(T_s l + \frac{(T_c + T_{cp})}{2} - T_{cp} \right) W_u(l) \text{sinc} \left(\theta \left(T_s l + \frac{(T_c + T_{cp})}{2} - T_{cp} \right) \right) \right] \quad (5.1)$$

$$E_{\mu_{u,n}^{p,q}} \left[\text{var}(\text{MUI}) \left| -T_{cp}, T_{cp} \right. \right] = \sum_{u \in \Phi_U} \sum_{g=0}^{N_u-1} \frac{1}{2T_{cp} \pi^2 (c_{u,g} - i)^2} \left[\sum_{l=0}^{L-1} T_{cp} W_u(l) \right. \\ \left. - \sum_{l=0}^{L-1} T_s l W_u(l) \text{sinc}(\theta T_s l) - \sum_{l=0}^{L-1} (T_s l - T_{cp}) W_u(l) \text{sinc}(\theta (T_s l - T_{cp})) \right] \quad (5.2)$$

$$E_{\mu_{u,n}^{p,q}} \left[\text{var}(\text{MUI}) \left| 0, T_{cp} \right. \right] = \sum_{u \in \Phi_U} \sum_{g=0}^{N_u-1} \frac{1}{T_{cp} \pi^2 (c_{u,g} - i)^2} \sum_{l=0}^{L-1} T_s l W_u(l) \left[1 - \text{sinc}(\theta T_s l) \right] \quad (5.3)$$

where $\text{var}(\cdot)$ is the variance, $W_u(l) = \sigma_h^2(l)$, $\theta = 2(c_{u,g} - i)/T_c$ and $\text{sinc}(x) = \sin(\pi x)/\pi x$ (Park et al., 2010).

A comparison to these competing derivations of the average MUI by Park et al., (2010) and the average MUI in (3.38) with single-transmit antenna is presented in Figure 5.21. Although the similarity trend between (Park et al., 2010, eq. 16-18) and (3.38), the difference in the generated average MUI can be justified as:

- i. The average MUI power decreases as the asynchronous region i.e. $R_{\alpha_{\{1,2,3\}}}$, shortens (Park et al., 2010) where the asynchronous region of the average MUI in (3.38) is ${}^{-}B_{T_0} T_s \leq \mu_{u,n}^{p,q} \leq {}^{+}B_{T_0} T_s$.

- ii. Only the ISI is considered in derivation of the average MUI in (Park et al., 2010, eq. 16-18), which is referred to as ICI (Park et al., 2010, Appendix I), where both of the ICI and ISI are included in (3.38).

It is worthy to note that the average MUI in (Park et al., 2010) was only derived for SCP. $\tau_{\max} \leq T_{\text{cp}}$.

C. The Instantaneous/Average SINR Analysis

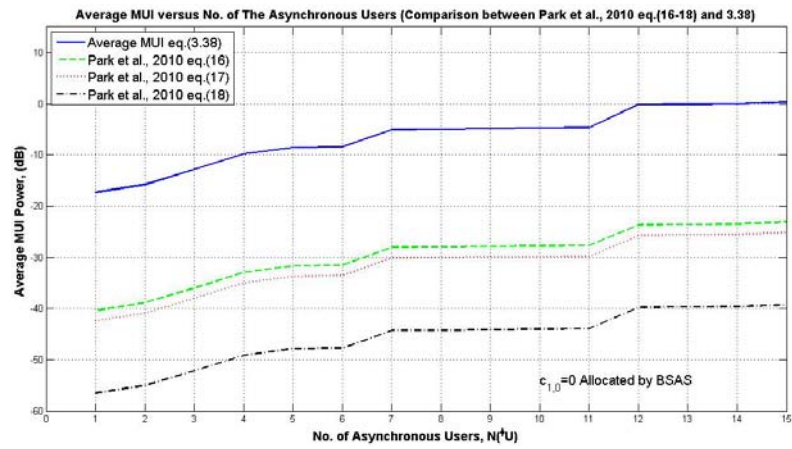
The instantaneous SINR is presented in Figures 5.22-5.27 where the influence of the number of asynchronous users, multiple transmit antennas, and the desired user's TOs are explored respectively, for various CP conditions and different SASs.

In the ideal case of the synchronization offset (i.e. $\zeta_{u,n}^{p,q} = 0; \forall p,q,u$) for a single-input system i.e. OFDMA system, the instantaneous SINR is large i.e. $\text{SINR} > 120$ dB, as in Figure 5.22. This large value is also conserved for the effective CP duration $0 < -\zeta_{u,n}^{p,q} \leq (N_{\text{cp}} - L + 1)$ i.e. case (a), where the incurred interferences are totally eliminated by the CP.

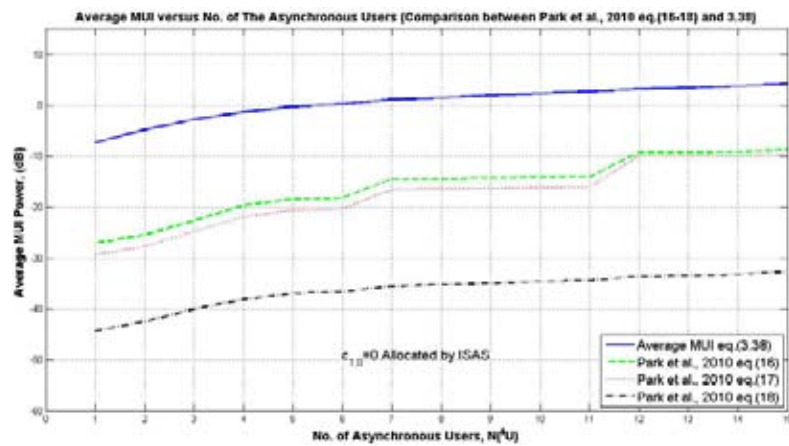
Furthermore, in presence of increased TO $\zeta_{u,n}^{p,q} \notin (0, -(N_{\text{cp}} - L + 1)]$; $\forall u \neq k$ towards and away from the CP, the instantaneous SINR degrades accordingly because of the MUI in synchronous desired user mode (i.e., $\zeta_{k=1,n}^{t,q} = 0$), as depicted in Figure 5.22.

The increasable trend of the instantaneous SINR beyond the TO boundaries i.e., ${}^+B_{\text{TO}} = 146$ and ${}^-B_{\text{TO}} = -173/-129/-109$ for SCP/InCP/ACP respectively in Figure 5.22, can be grasped by exploring the contents of the n^{th} DFT window which is dominated by the samples of the $(n \mp 1)^{\text{th}}$ OFDMA symbol for the TO towards and away from the CP, respectively, where the erroneous n^{th} DFT window is considered to be the window of the $(n \mp 1)^{\text{th}}$ OFDMA symbol instead (see Figures 3.3-3.4).

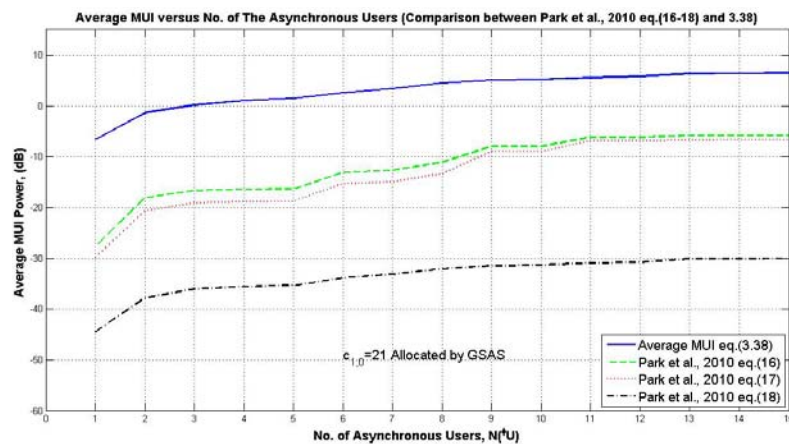
In asynchronous desired user mode i.e., $\zeta_{k=1,n}^{t,q} \notin (0, -(N_{\text{cp}} - L + 1)]$, the DS-SI and CAs-SI are combined with the MUI to further degrade the instantaneous SINR.



(a)



(b)



(c)

Figure 5.21 Comparisons between the Average MUI in (3.38) for Single-Transmit Antenna and (Park et al., 2010 eq. 16, 17 and 18) with SCP at: (a) $c_{1,0}=0$ Allocated by BSAS, (b) $c_{1,0}=0$ Allocated by ISAS, (c) $c_{1,0}=21$ Allocated by GSAS

Consider single-input system with $N(\phi_U)=1$, the instantaneous SCP SINR degrades from its large value (>120 dB) at $0 \leq -\zeta_{k=1,n}^{t,q} \leq (N_{cp} - L + 1)$ to around 18.0dB, and 8.0dB by $\zeta_{k=1,n}^{t,q} = -64$, and $\zeta_{k=1,n}^{t,q} = 23$ respectively, at $c_{1,0} = 0$ allocated by BSAS as can be recognized from Figures 5.22 and 5.24.

As expected, the instantaneous SINR is significantly degraded by incurring more asynchronous users, where the correspondence incurred MUI are increased accordingly as depicted in Figures 5.22.

However, the BSAS performs better than the ISAS and GSAS by producing the lowest instantaneous SINR particularly for SCP. For example, the instantaneous SCP (ACP) SINR ≥ 20 dB with $\zeta_{u,n}^{p,q} = -64; \forall u, u \neq k$ can be maintained by $N(\phi_U) \leq 7(0), 5(3)$, and $5(2)$ users at $c_{1,0}$ allocated by BSAS, ISAS and GSAS respectively, for synchronous desired user $\zeta_{k=1,n}^{t,q} = 0$ as in Figure 5.23.

In addition, for asynchronous desired user the ISAS performs better than the GSAS and BSAS. For example, in Figure 5.24 with $\zeta_{k=1,n}^{t,q} = -64$, the instantaneous SCP (ACP) SINR ≥ 20.0 dB (8.0dB) with $\zeta_{u,n}^{p,q} = -64$ can be maintained by $N(\phi_U) \leq 0(0), 3(5)$, and $2(3)$ users at $c_{1,0}$ allocated by BSAS, ISAS and GSAS respectively. Note that the asynchronous instantaneous SINR is substantially affected by the subcarrier index $c_{k=1}$, being less degraded for the subcarriers away from the centre of the spectrum at the desired DFT output when BSAS and GSAS is applied. The ISAS maintained the same level of performance tendency along the $c_{k=1}$ for all CP scenarios.

Employing multiple transmit antennas, obviously, degrades the instantaneous SINR, where its tendency is preserved as in Figure 5.25 due to incur the CAs-SI. For example, and with synchronous desired user $\zeta_{k=1,n}^{t,q} = 0, \zeta_{u,n}^{p,q} = -64; \forall u, u \neq k$ and $N(\phi_U)=1$, the instantaneous SCP/InCP/ACP SINR degrades from around 40.0dB/32.0dB/17.7dB with $P=1$ to 0.0dB/-0.0054dB/-0.1448dB, -4.7718dB/-4.7748dB/-4.8683dB and -8.4515dB/-8.4541dB/-8.5343dB with $P=2, 4$, and 8 respectively, at $c_{1,0} = 0$ allocated by BSAS, as in Figure 5.26.

In addition, the effect of the desired user's TO on the instantaneous SINR is depicted in Figures 5.27. The Figure shows that although the absent of the CAs-SI i.e., $P=1$, the

DS-SI degrades markedly the system performance in term of SINR, where it may integrate with MUI for further degradation. The synchronous instantaneous SCP SINR with 128dB experiences numerous degradation to around 18.0dB, 8.0dB, and 3.0dB due to desired user's TO $\zeta_{1,n}^{1,q} = -64, 37, \text{ and } -128$ respectively, for $P=1$ at $c_{1,0} = 0$, allocated by BSAS as can be grasped from Figure 5.27(a).

Figures 5.28 and 5.29 investigate the impact of the number of asynchronous users and the number of transmit antennas on the average SCP/InCP/ACP SINR for asynchronous and synchronous desired user scenarios respectively along the different SASs. Following the instantaneous SINR, the average SINR increases as the number of asynchronous users i.e., MUI, and the number of transmit antennas i.e., CAs-SI, increase, where eases the CP condition also increases the average SINR as in Figures 5.28-5.29. Table 5.5 investigates the effect of the CP conditions and the desired user condition on the average SINR at the DFT output.

Table 5.5: The Average {SCP, InCP, ACP} SINR for Synchronous and Asynchronous Desired User at $c_{1,0}$ by BSAS, ISAS and GSAS when $P=1$ and $N(U^\phi) = 1$

Average SINR (dB)	Synchronous Desired User			Asynchronous Desired User		
	BSAS	ISAS	GSAS	BSAS	ISAS	GSAS
SCP	11.3212	1.3401	0.6183	-10.0745	-2.6909	5.1507
InCP	10.6430	0.6262	-0.0891	-11.1434	-3.7345	-5.9264
ACP	10.3487	0.3676	-0.3542	-11.6317	-4.2481	-6.4334

Figures 5.28-5.29 and Table 5.5 show that the corresponding average SINR for certain setup decreases as the CP duration eases. For example, with single transmit antenna the -10.1588 dB (0.9828 dB) average SCP SINR is declined to -11.2272 dB (-10.1025 B) and to -11.7160 dB (-10.6013) when the CP is eased to InCP and ACP respectively, at $c_{1,0} = 0$ ($c_{1,0} = 21$) allocated by BSAS (GSAS) for asynchronous desired user and $N(U^\phi) = 3$ users as in Figure 5.28.

In synchronous desired mode, the BSAS performs better than the ISAS and GSAS respectively. For example, considering single-input system, it can be found that the BSAS meets an average SCP $\text{SINR} \geq -5\text{dB}$ when $N(\phi_U) \leq 11$ users, where the ISAS and GSAS meets this performance with $N(\phi_U) \leq 4$ and 2 users respectively, at $c_{1,0}$ as in Figure 5.29.

In asynchronous desired user mode, the ISAS performs better than the BSAS. Furthermore, ISAS performs the GSAS, particularly for insufficient and absent CP. For example, it can be recognized that the BSAS, ISAS and GSAS meets an average InCP (ACP) $\text{SINR} \geq -11.5\text{ dB}$ when $N(\phi_U) \leq 6(0), 9(9)$ and $5(4)$ respectively at $c_{1,0}$ for single transmit antenna as in Figure 5.28. For other number of transmit antennas, one can observe similar results.

However, Park et al., (2010) have derived the average SINR based on the Gaussian approximation for OFDMA uplink systems. In (Park et al., 2010), the average effective SINR is defined as the ratio of the average power of the desired signal P_{DS} to the average MUI power P_{MUI} plus the average noise power P_w as in (Park et al, 2010, eq. 13)

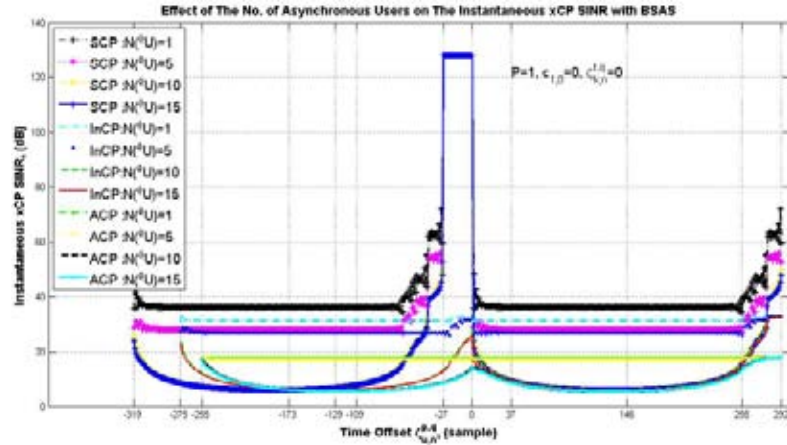
$$\text{SINR}_{\text{Park et al.,2010}} = \frac{P_{DS}}{P_{MUI} + P_w} \quad (5.4)$$

where $P_{DS} = 1$ (Park et al., 2010). The average SINR in (5.4) can be evaluated by substituting P_{MUI} in (5.1-5.3) for various asynchronous regions $R_{\alpha_{\{1,2,3\}}}$.

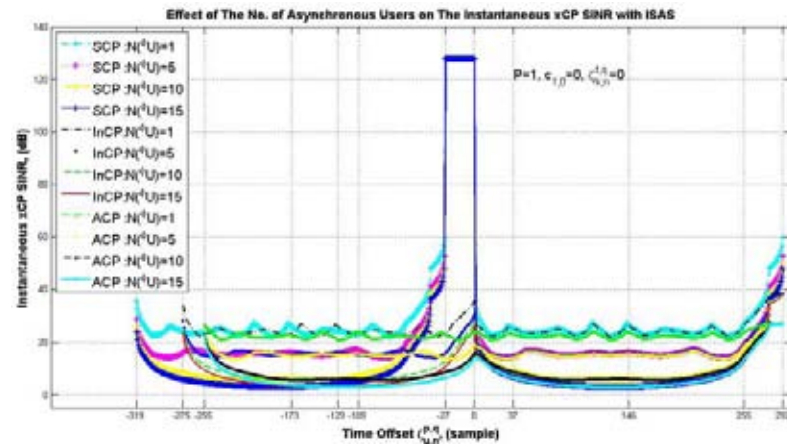
A comparison to this effective average SINR by Park et al., (2010, eq. (13)) and the average SINR in (3.34) with single-transmit antenna is presented in Figure 5.30.

It is worthy to note that the utilization of the Gaussian approximation in the frame work of (Park et al., 2010) as well as the asynchronous regions $R_{\alpha_{\{1,2,3\}}}$, considerably affect the formulated average SINR of OFDMA uplink systems. In addition, Park et al., (2010) considers only the synchronized desired signal user scenario and sufficient CP.

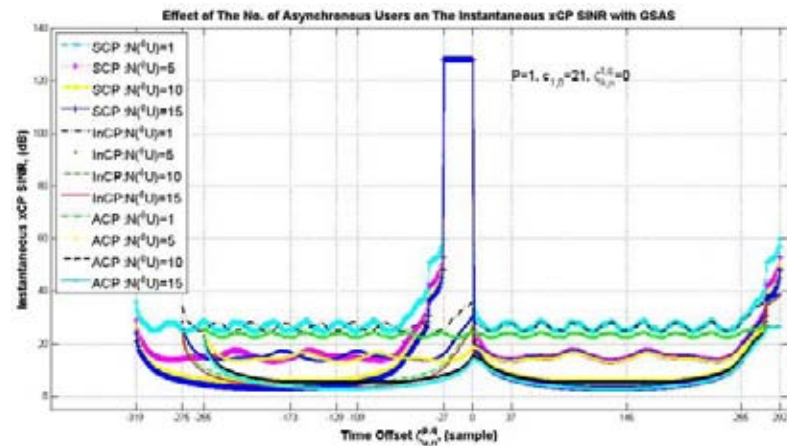
The corresponding BER for different asynchronous users and average SINR presented in Figures 5.20 and 5.28 are depicted in Figures 5.31 and 5.32, respectively.



(a)



(b)



(c)

Figure 5.22 Instantaneous {SCP, InCP, ACP} SINR for $N(\phi U) = 1, 5, 10,$ and 15 at: (a) $c_{1,0} = 0$ allocated by BSAS, (b) $c_{1,0} = 0$ allocated by ISAS, and (c) $c_{1,0} = 21$ allocated by GSAS for $P=1$ and Synchronous desired user $\zeta_{k=1,n}^{1,q} = 0$

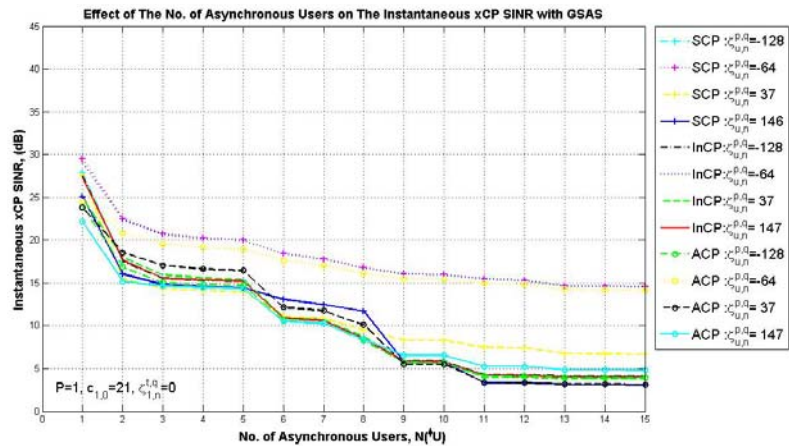
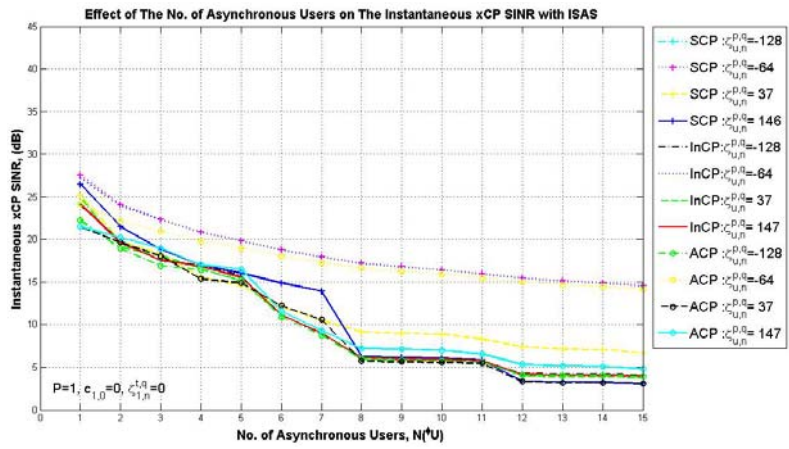
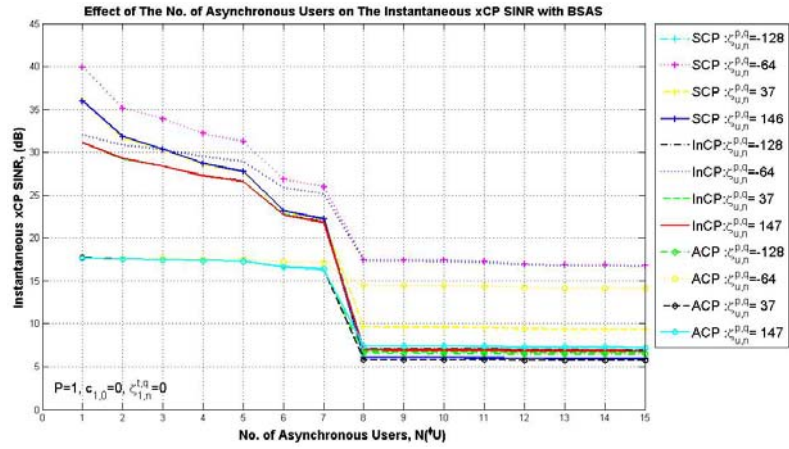
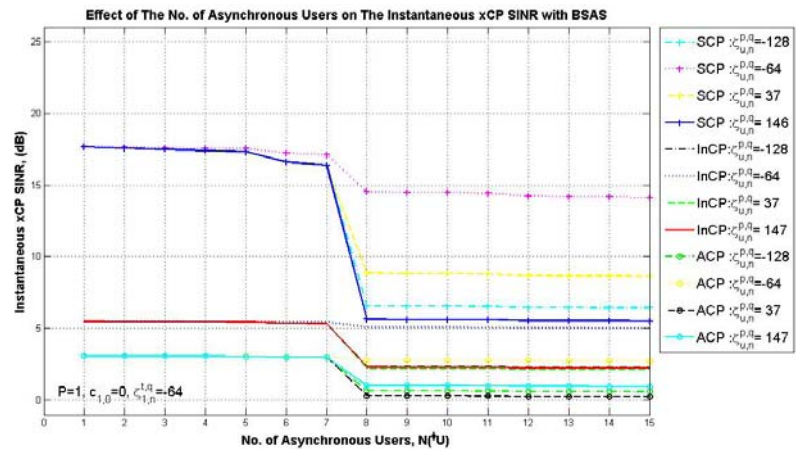
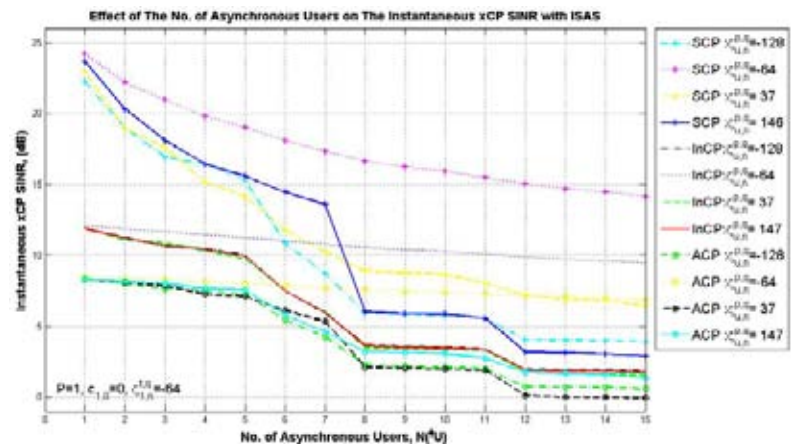


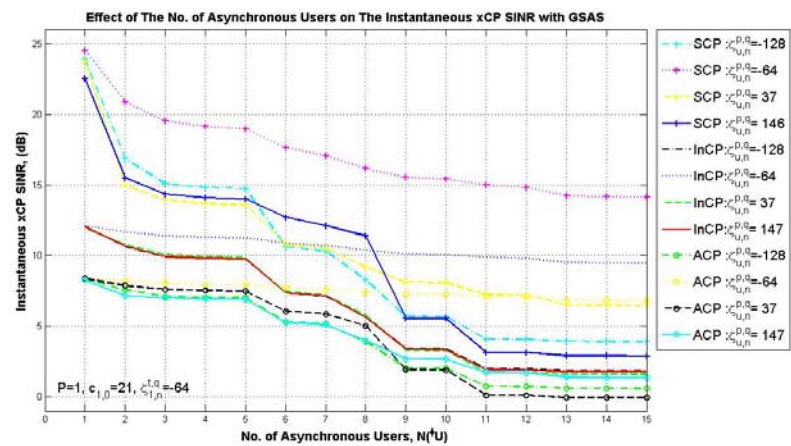
Figure 5.23 Instantaneous {SCP, InCP, ACP} SINR for $\zeta_{u,n}^{p,q} = -128, -64, 37, \text{ and } 146$ at: (a) $c_{1,0} = 0$ allocated by BSAS, (b) $c_{1,0} = 0$ allocated by ISAS, and (c) $c_{1,0} = 21$ allocated by GSAS for $P=1$ and Synchronous desired user $\zeta_{k=1,n}^{t,q} = 0$



(a)



(b)



(c)

Figure 5.24 Instantaneous {SCP, InCP, ACP} SINR for $\zeta_{u,n}^{p,q} = -128, -64, 37,$ and 146 at: (a) $c_{1,0} = 0$ Allocated by BSAS, (b) $c_{1,0} = 0$ Allocated by ISAS, and (c) $c_{1,0} = 21$ Allocated by GSAS for $P=1$ and Asynchronous desired user $\zeta_{k=1,n}^{1,q} = -64$

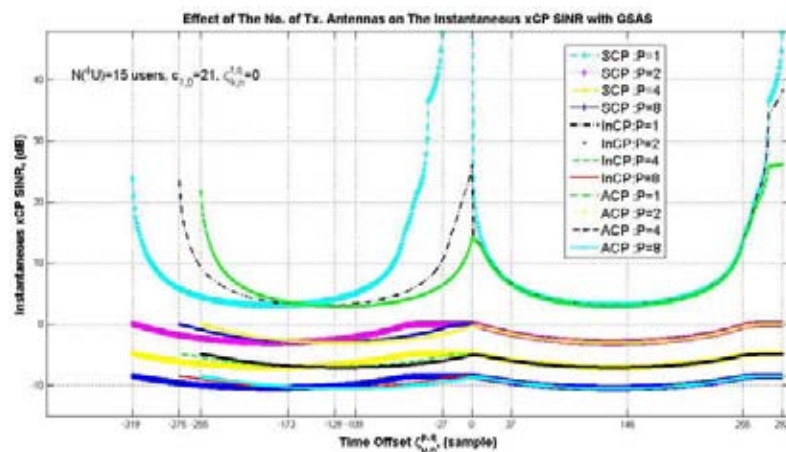
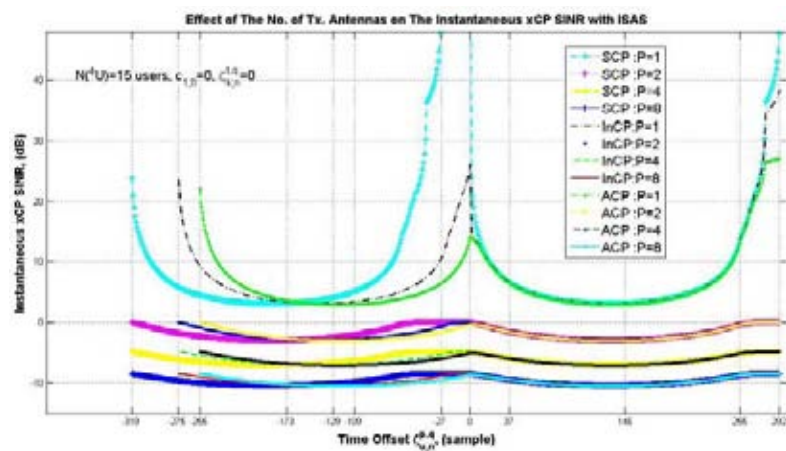
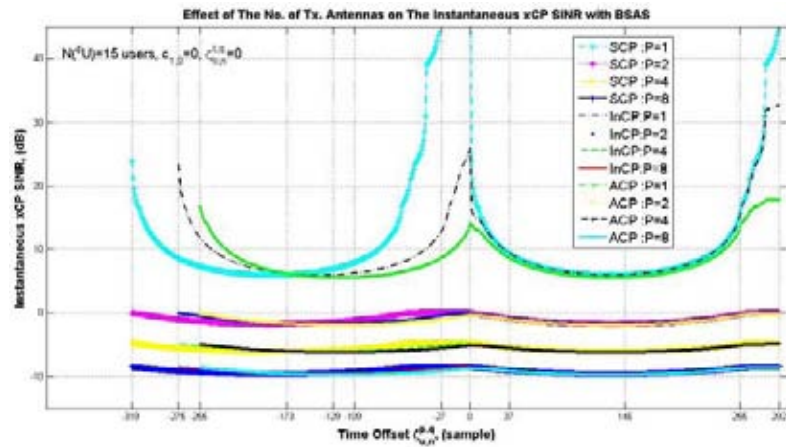
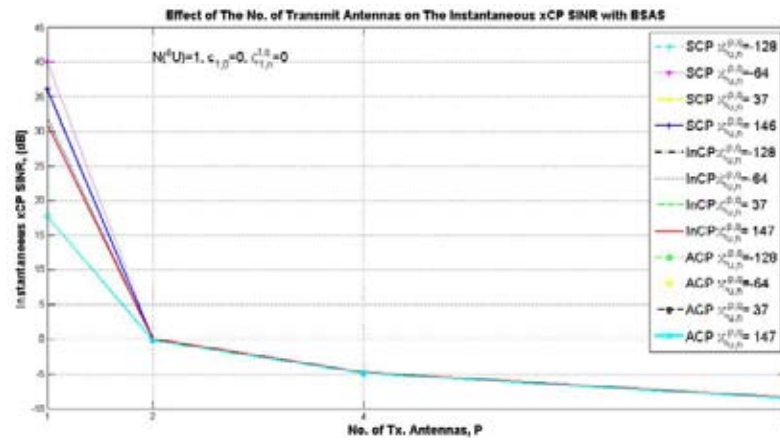
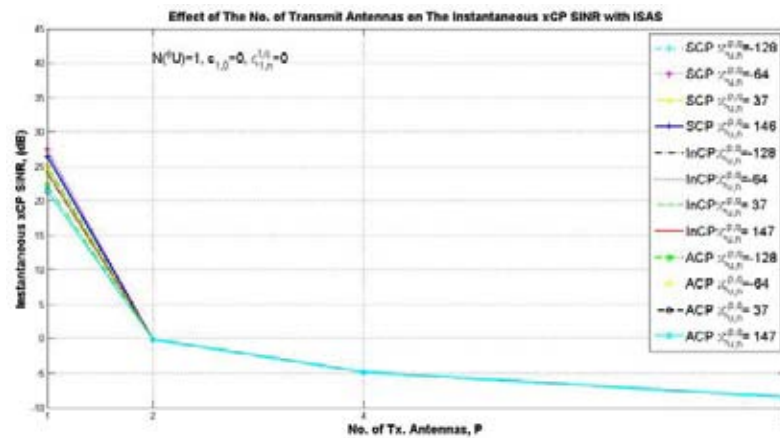


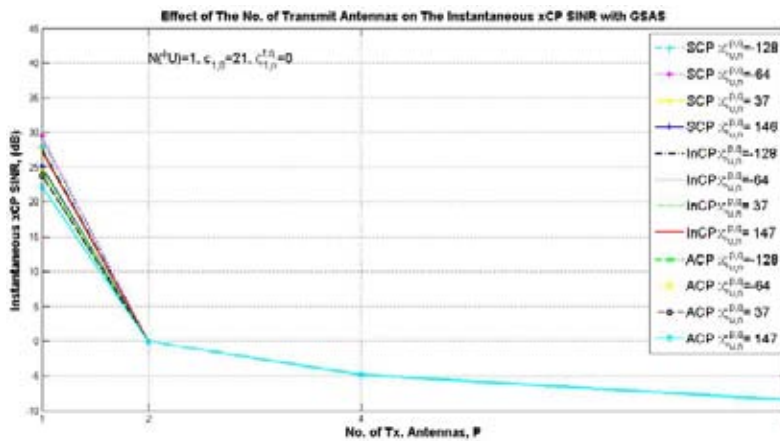
Figure 5.25 Instantaneous {SCP, InCP, ACP} SINR for $P=1, 2, 4,$ and 8 at: (a) $c_{1,0}=0$ Allocated by BSAS, (b) $c_{1,0}=0$ Allocated by ISAS, and (c) $c_{1,0}=21$ Allocated by GSAS for $N(\phi_U)=15$ and Synchronous desired user $\zeta_{k=1,n}^{1,q}=0$



(a)



(b)



(c)

Figure 5.26 Instantaneous $\{SCP, \lnCP, ACP\}$ SINR for $P = \{1, 2, 4, 8\}$ and $\zeta_{u,n}^{p,q} = \{\}$ at: (a) $c_{1,0} = 0$ Allocated by BSAS, (b) $c_{1,0} = 0$ Allocated by ISAS, and (c) $c_{1,0} = 21$ Allocated by GSAS for $N(\phi_U) = 1$ and Synchronous desired user $\zeta_{k=1,n}^{1,q} = 0$

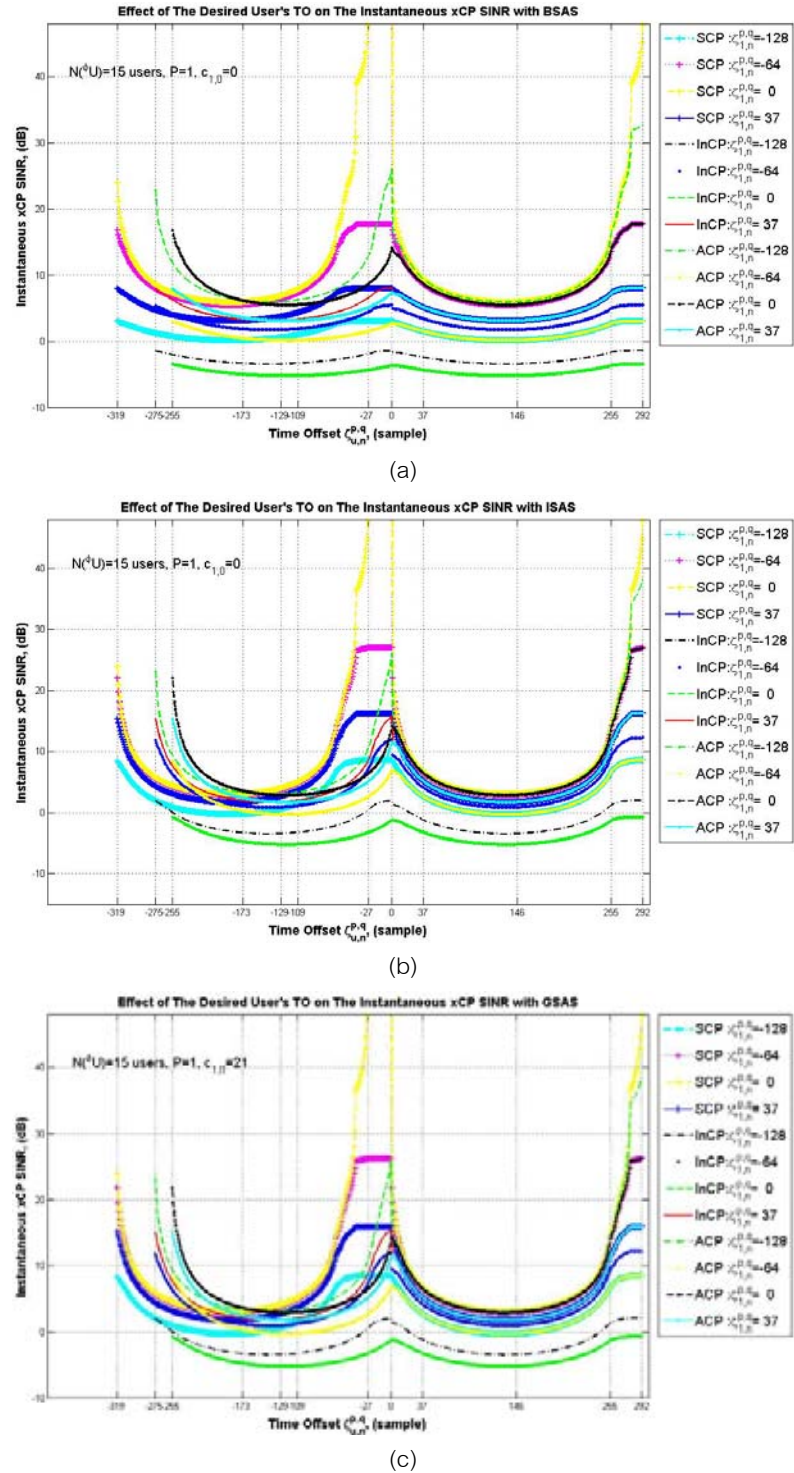
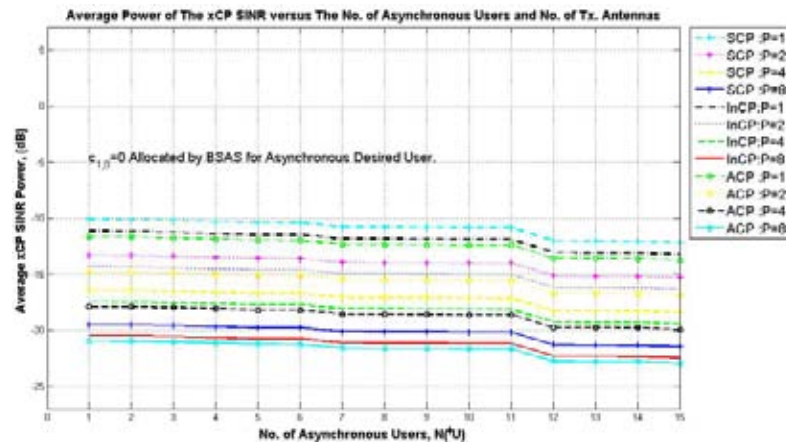
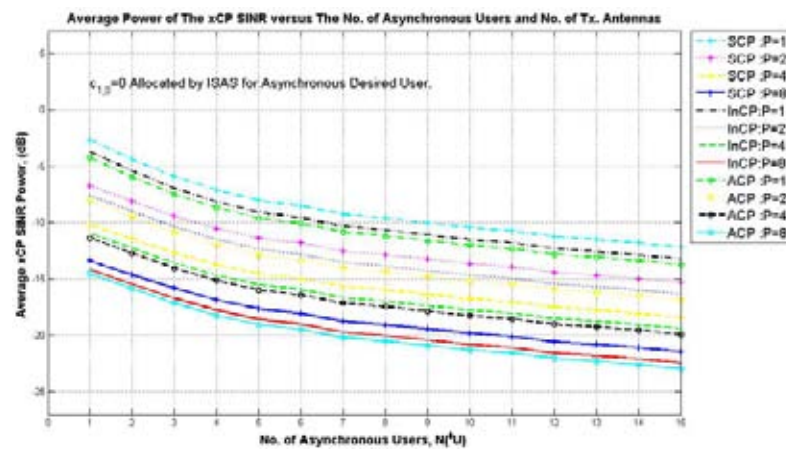


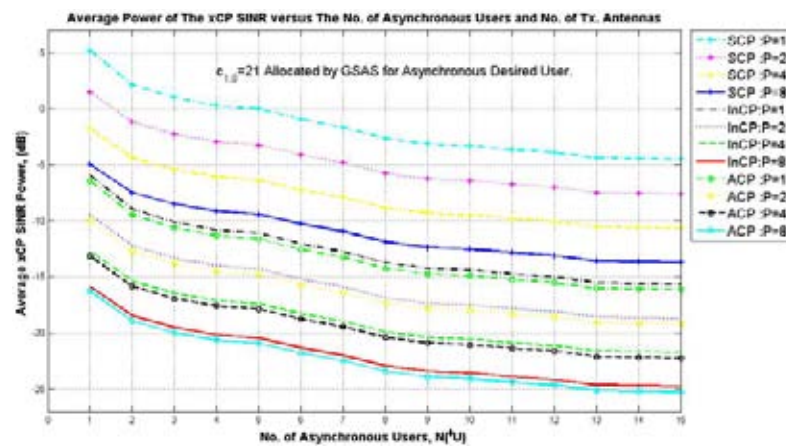
Figure 5.27 Instantaneous {SCP, InCP, ACP} SINR for $\zeta_{k=1,n}^{t,q} = -64, -32, 0, 23$ at: (a) $c_{1,0} = 0$ Allocated by BSAS, (b) $c_{1,0} = 0$ Allocated by ISAS, and (c) $c_{1,0} = 21$ Allocated by GSAS for $N(\phi U) = 15$ and $P = 1$



(a)

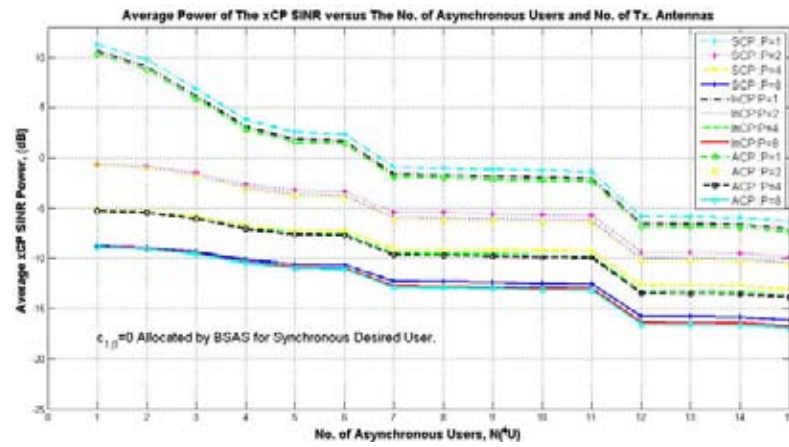


(b)

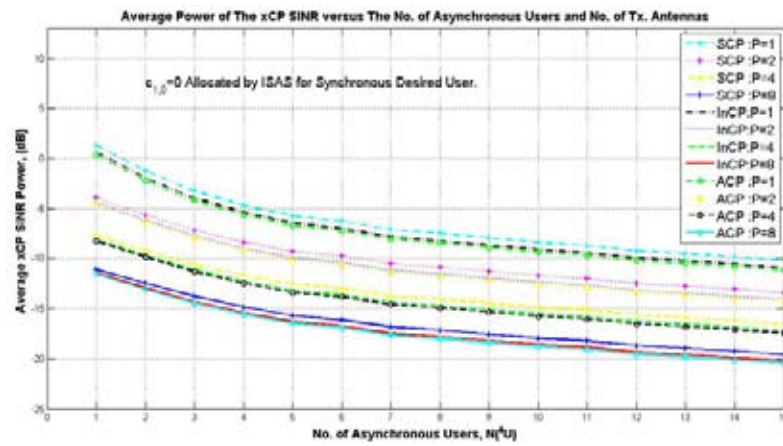


(c)

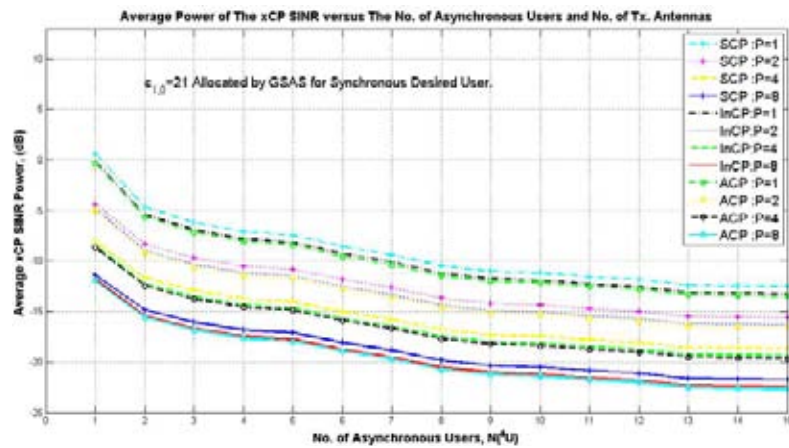
Figure 5.28 Effects of Number of Asynchronous Users $N^a(\phi_U)$ and Number of Transmit Antennas, P on the Average {SCP, InCP, and ACP} SINR at: (a) $c_{1,0}=0$ Allocated by BSAS, (b) $c_{1,0}=0$ Allocated by ISAS, (c) $c_{1,0}=21$ Allocated by GSAS for Asynchronous Desired User



(a)

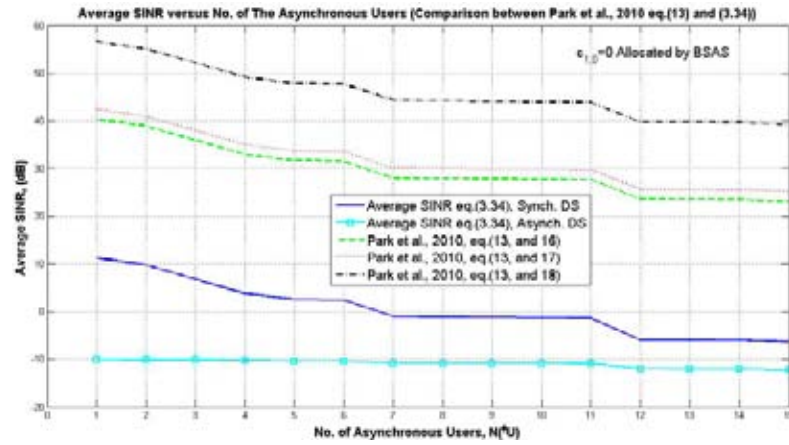


(b)

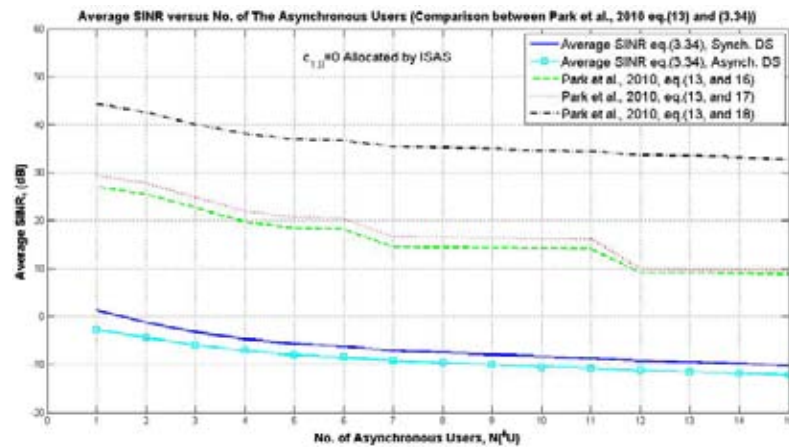


(c)

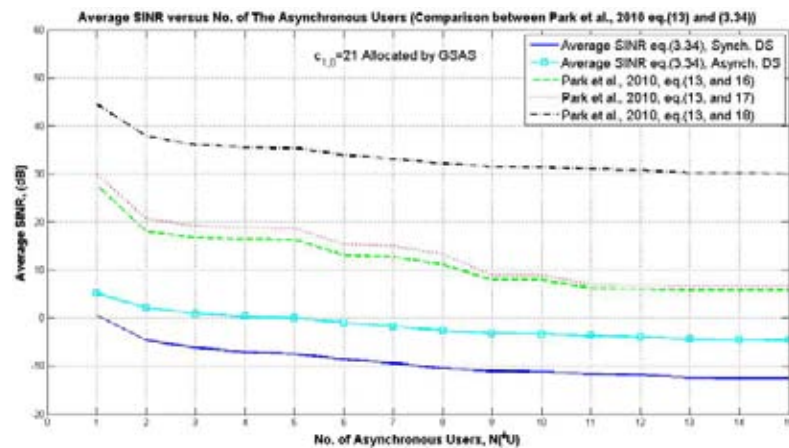
Figure 5.29 Effects of Number of Asynchronous Users $N^a(U)$ and Number of Transmit Antennas, P on the Average {SCP, InCP, and ACP} SINR at: (a) $c_{1,0}=0$ Allocated by BSAS, (b) $c_{1,0}=0$ Allocated by ISAS, (c) $c_{1,0}=21$ Allocated by GSAS for Synchronous Desired User



(a)

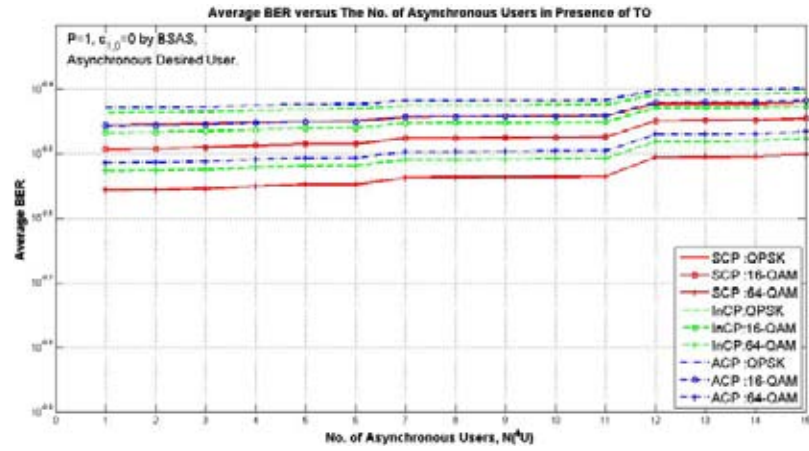


(b)

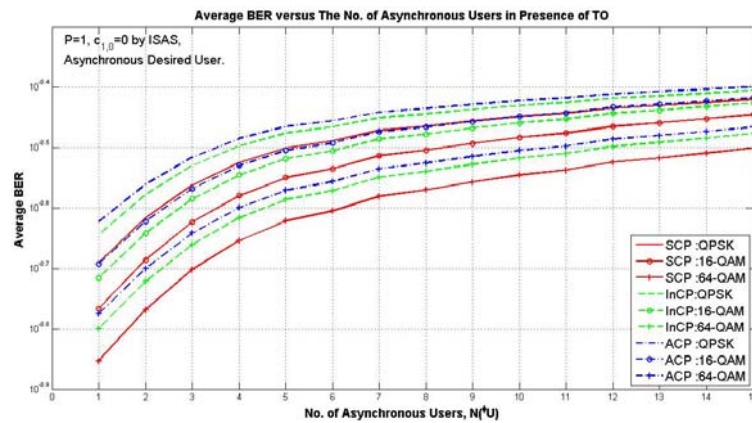


(c)

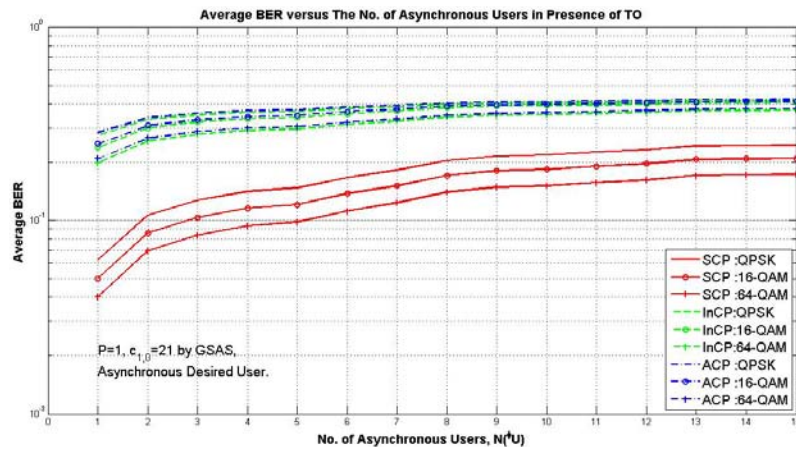
Figure 5.30 Comparison between the Average SCP SINR in (3.34) for single-transmit antenna and (Park et al., 2010 eq. (13)) with Synchronous and Asynchronous Desired User Signal at: (a) $c_{1,0}=0$ Allocated by BSAS, (b) $c_{1,0}=0$ Allocated by ISAS, (c) $c_{1,0}=21$ Allocated by GSAS



(a)

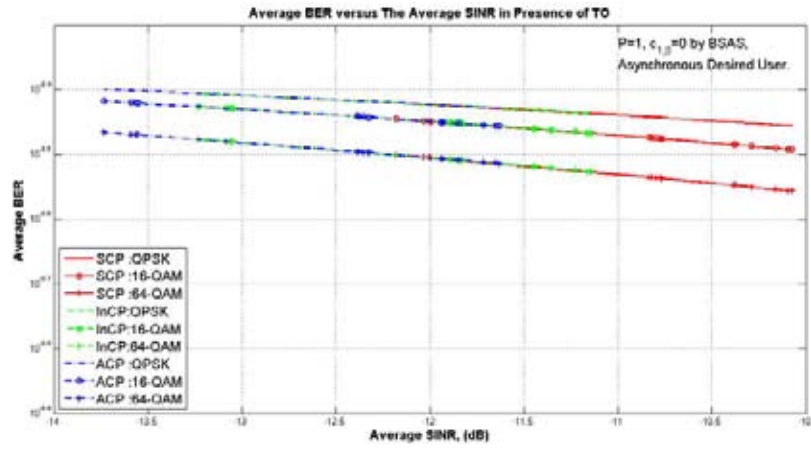


(b)

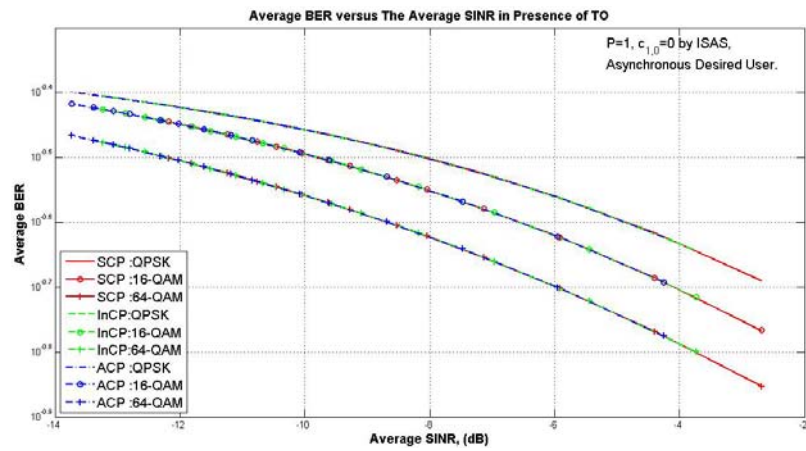


(c)

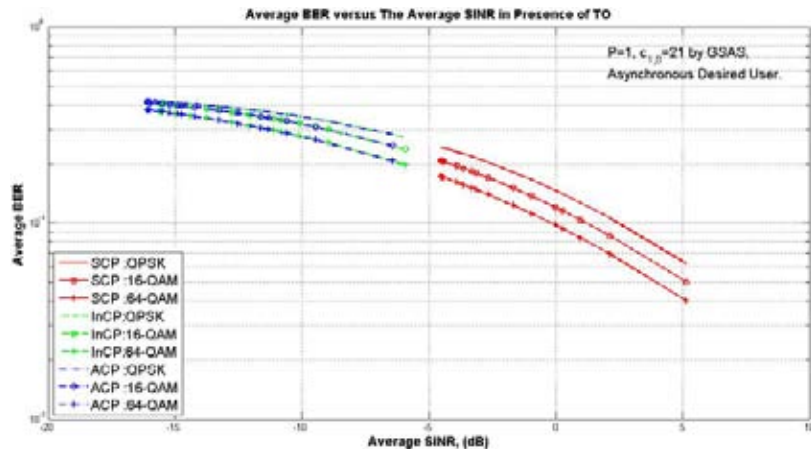
Figure 5.31 Effects of Number of Asynchronous Users $N^a(U)$ on the Average {SCP, InCP, and ACP} BER for QPSK, 16-QAM, and 64-QAM at: (a) $c_{1,0}=0$ Allocated by BSAS, (b) $c_{1,0}=0$ Allocated by ISAS, (c) $c_{1,0}=21$ Allocated by GSAS for P=1, and Asynchronous Desired User



(a)



(b)



(c)

Figure 5.32 Effects of average SINR on the Average {SCP, InCP, and ACP} BER for QPSK, 16-QAM, and 64-QAM at: (a) $c_{1,0}=0$ Allocated by BSAS, (b) $c_{1,0}=0$ Allocated by ISAS, (c) $c_{1,0}=21$ Allocated by GSAS for Asynchronous Desired User

5.4. System Performance in Presence of TO and CFO

As elaborated in Section 3.4, reduction and rotation of each DFT output and ICI are additionally introduced by the CFO to the TO detriments. In this section, the interference sources in the elementary analytical system as well as the MIMO-OFDMA uplink systems due to TO and CFO are investigated. Note that the elaborated analysis in the preceding section is considered through the achieved commentary in this section.

5.4.1 The Instantaneous Interference Components and SINR of $\phi^{\varepsilon} Y_{u,n}^{p,q} (i = c_{u,g})$

The instantaneous power of the signal components of $\phi^{\varepsilon} Y_{u,n}^{p,q} (i = c_{u=1,g})$ in (3.46) are depicted in Figures 5.33-5.35 for SCP, InCP and ACP conditions where $c_u; \forall u$ are allocated by BSAS, ISAS and GSAS. In addition, the corresponding instantaneous SINR is presented in Figure 5.36. From Figures 5.33-5.35, it is clear that the presence of the CFO, when $\zeta_{u,n}^{p,q} \neq 0$, is worsen the violated orthogonality between the subcarriers, whereas the generated interferences is considerably enhanced.

More particularly, the following remarks on the signal components of $\phi^{\varepsilon} Y_{u,n}^{p,q} (i = c_{u=1,g})$ and $\phi^{\varepsilon} Y_{u,n}^{p,q} (i = c_{u=1,g})$ can be drawn:

- i. All the signal components in $\phi^{\varepsilon} Y_{u,n}^{p,q} (i = c_{u=1,g})$ follows the trend of the coincident signal in $\phi^{\varepsilon} Y_{u,n}^{p,q} (i = c_{u=1,g})$,
- ii. Presence of the CFO reduces the power of the DS where $(1/N_c) \sum_{z=\phi_{1,DS}}^{\phi_{2,DS}} e^{j2\pi z \zeta_u^q / N_c} < (\phi_{2,DS} - \phi_{1,DS} + 1) / N_c$ as in Figures 5.33-5.35. Note that the DS is not affected by the positivity/negativity of the CFO.
- iii. The ICI is considerably enhanced by the CFO, where the utilized subcarrier allocation and the positivity/negativity of the CFO affect crucially the amount of the incurred ICI. The negative CFO adds more interference than the positive CFO as in Figures 5.33-5.35.
- iv. The ISI is minimally affected by the CFO, where the negative CFO enhances the ISI and the positive CFO reduces it, especially in a high TO value as depicted in Figures 5.33-5.35.

- v. The impact of eases the CP condition in presence of TO is conserved for the joint interference by CFO.
- vi. The signal components in ${}^{\phi,\varepsilon}Y_{u,n}^{p,q}(i=c_{u=1,g})$ are less affected by the CFO where the ISAS and GSAS are exploited. It is worthy to note that $(c_{u,g} + \varepsilon_u^q - i)/N_c \approx (c_{u,g} - i)/N_c \left| (c_{u,g} - i)/N_c \gg \varepsilon_u^q/N_c \right.$ in the interference coefficient in (3.45) which is can be easily obtained by the ISAS and GSAS.

In Figure 5.36, the instantaneous SINR from ${}^{\phi,\varepsilon}Y_{u,n}^{p,q}(i=c_{u=1,g})$ is depicted, where the performance is additionally degraded by $\varepsilon_u^q \neq 0$ in presence of the TO. The ISAS performs better than the GSAS and BSAS where the latter is more susceptible to the CFO.

5.4.2 The Instantaneous Interferences and SINR for MIMO-OFDMA Uplink Systems

In this subsection, the incurred interferences and the corresponding SINR at the DFT output are presented in coexistence of TO and CFO, where the MIMO and multiuser environment properties are investigated accordingly.

A. Instantaneous/Average CAs-SI Analysis in Presence of TO and CFO

Figures 5.37 shows the influence of the TO and CFO on the {SCP, InCP, and ACP} CAs-SI along the various SASs. The increasable trend of the instantaneous CAs-SI with the number of transmit antennas in synchronous desired user as well as the minimal reduction in the corresponding CAs-SI in presence of the TO are conserved when the CFO is concurrently incurred.

Moreover, with $\zeta_{k=1,n}^{t,q} = 0$, presence of the CFO reduced the CAs-SI slightly where coincide negative and positive CFO have similar reductive effect. For example, with $\zeta_{k=1,n}^{t,q} = 0$, the incurred CAs-SI is improved from -6.0dB with two-transmit antenna to -1.23dB and 2.45dB when four- and eight-transmit antennas are employed respectively, at $c_{1,0} = 0$ allocated by BSAS. These CAs-SI are deducted to -6.58dB (-6.14dB), -1.81dB (-1.37dB), and 1.87dB (2.31) for P=2, 4, and 8 respectively, when $\varepsilon_{1,n}^q = \pm 0.2 (\pm 0.1)$ as in

Figure 3.37(a). With $\zeta_{k=1,n}^{l,q} \neq 0$ and $\epsilon_{1,n}^q \neq 0$, the CAs-SI additionally decreases where the exploited SAS governs the response of the CAs-SI by the CFO.

More specifically, the BSAS is more affected by the CFO, where negative CFO adds more interference to the CAs-SI. The ISAS and GSAS are less affected by the CFO where also the positive CFO adds less interference to the CAs-SI as shown in Figure 5.37.

Figure 5.38 explores the incurred average CAs-SI. The Figure shows that the average CAs-SI increases as the number of transmit antennas increases in presence of TO and CFO. Moreover, eases the CP condition decreases slightly the corresponding CAs-SI. For example, the SCP (ACP) CAs-SI is being -8.1752dB (-8.5372dB), -3.4040dB (-3.7660dB), and 0.2758dB (-0.0863dB) when 2, 4, and 8 antennas are deployed respectively at $c_{1,0} = 0$ allocated by BSAS.

B. The Instantaneous/Average MUI Analysis in Presence of TO and CFO

The produced MUI by the CFO and CFO/TO asynchronous user is explored in Figures 5.39 and 5.40 respectively. Consider only CFO asynchronous users, the produced MUI is proportioned to $N(\phi, \epsilon, U)$ and $\epsilon_{u,n}^q$. For example, -46.68dB (-19.51dB) and -52.26dB (-23.3dB) of the SCP MUI can be generated by $\epsilon_{u,n}^q = -0.2$ and 0.1 respectively when $N(\phi, \epsilon, U) = 1(10)$ and $P=1$, at $c_{1,0} = 0$ allocated by BSAS as in Figure 5.39 (a).

Furthermore, shortens the CP condition, eases the ability to combat the dispersive nature of the multipath fading channels in presence of synchronized system, whereas the ISI can be recognized. Consider, $\zeta_{u,n}^{p,q} = 0$ and $\epsilon_{u,n}^q = 0$, -41.83dB (-14.70dB) and -42.05dB (-13.37dB) can be recognized for InCP and ACP MUI respectively by $N(\phi, \epsilon, U) = 1(15)$ with $P=1$, at $c_{1,0} = 0$ allocated by BSAS as in Figure 5.39 (a).

In addition, with $\zeta_{u,n}^{p,q} \neq 0$ and $\epsilon_{u,n}^q \neq 0$, the produced MUI, for certain $N(\phi, \epsilon, U)$ and $\zeta_{u,n}^{p,q} \neq 0$, increases as the CFO increases. Consider, $\zeta_{u,n}^{p,q} = 37$ and $N(\phi, \epsilon, U) = 1(15)$, the corresponding SCP MUI for $\epsilon_{u,n}^q = -0.2, -0.1, 0.1, \text{ and } 0.2$ is -41.93dB (-16.85dB),-

41.99dB (-16.42dB), -42.16dB (-13.98dB), and -42.21dB (-12.52dB) respectively with $P=1$, at $c_{1,0}=0$ allocated by BSAS as in Figure 5.40 (a).

It is worthy to note that the produced MUI by the BSAS is lower than the one by the ISAS and GSAS along the CP condition. For example, the SCP (ACP) MUI by $N(\phi, \epsilon)U=1$, is -41.93dB (-42.15dB), -31.21dB (-29.25dB), and -33.90dB (-33.56dB) at $c_{1,0}$ allocated by BSAS, ISAS and GSAS respectively for $\zeta_{u,n}^{p,q}=37$ and $P=1$, as can be grasped from Figure 5.40. A similar result can be recognized for $\zeta_{u,n}^{p,q}=37$.

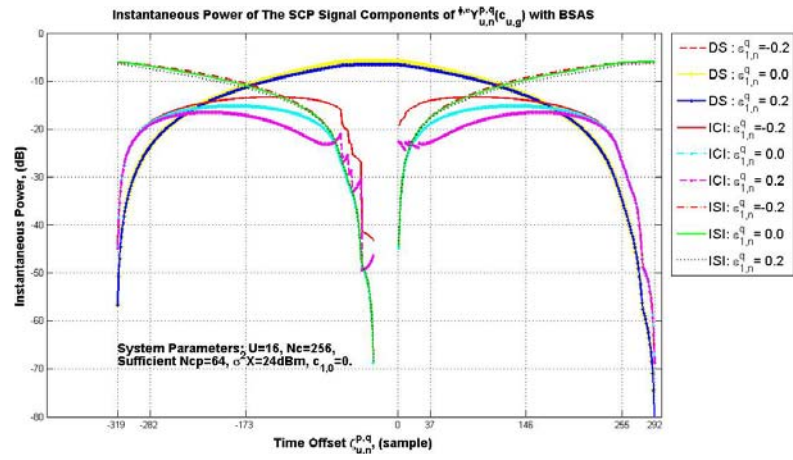
However, in MIMO technique, the MUI by $N(\epsilon)U$ improves as the number of transmit antennas increases with constant amount, where all the employed antennas have the same CFO i.e., CFO is user-based. For example, with $\zeta_{u,n}^{p,q}=0$, $\epsilon_{u,n}^q=-0.2$ and $N(\epsilon)U=15$, -19.31dB (-15.07dB), -16.30dB (-12.05dB), -13.29dB (-9.04dB) and -10.28dB (-6.03dB) of the SCP MUI is recorded for $P=1, 2, 4$, and 8 antennas respectively $c_{1,0}=0$ (21) allocated by BSAS (GSAS) as can be viewed from Figure 5.41.

Figure 5.42 explores the influence of the number of asynchronous users and the number of transmit-antennas on the average MUI through the different CP conditions. As expected, the average MUI increases as the number of asynchronous users and the number of transmit-antennas increase as well as ease the CP condition.

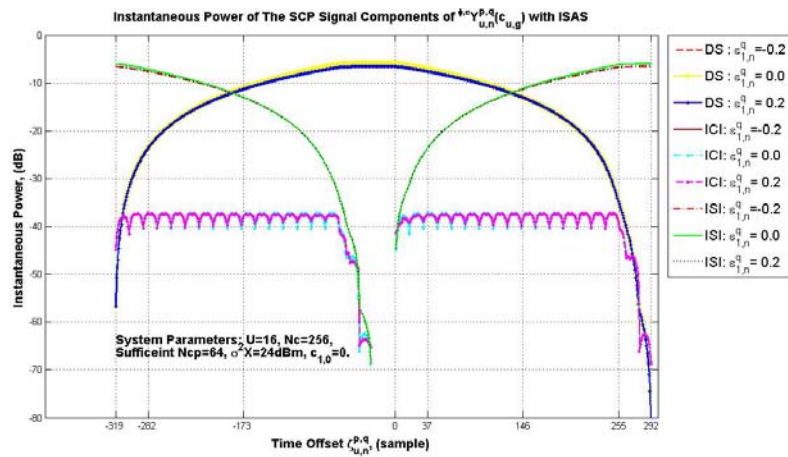
It is worthy to note that the produced average MUI when BSAS is exploited is slightly lower than the induced one when ISAS and GSAS are utilized along the CP condition. Considering single-transmit antenna, the BSAS meets the average SCP/InCP/ACP MUI ≤ 1 dB when $N(\phi)U \leq 9/9/9$ at $c_{1,0}$ allocated by BSAS, where the ISAS and GSAS can meet this average MUI at $c_{1,0}$ when $N(\phi)U \leq 8/9/9$ and $N(\phi)U \leq 8/8/9$ respectively, as show in Figure 5.42. In addition, the corresponding incurred average MUI is enhanced as the CP is shortened as in Table 5.6.

Table 5.6: The Average MUI for Different CP Conditions at $c_{1,0}$ by BSAS, ISAS and GSAS for $P=1$

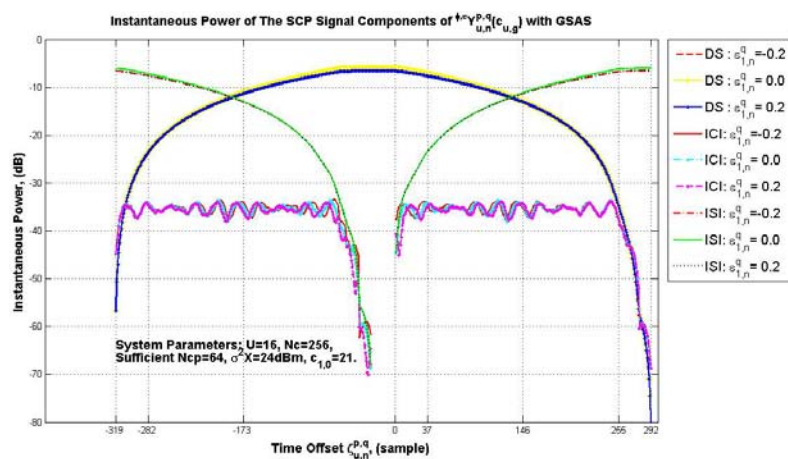
Average MUI (dB)	SCP			InCP			ACP		
	BSAS	ISAS	GSAS	BSAS	ISAS	GSAS	BSAS	ISAS	GSAS
$N(\phi)U=15$	3.214	3.231	3.453	3.046	3.063	3.28	2.832	2.848	3.058



(a)

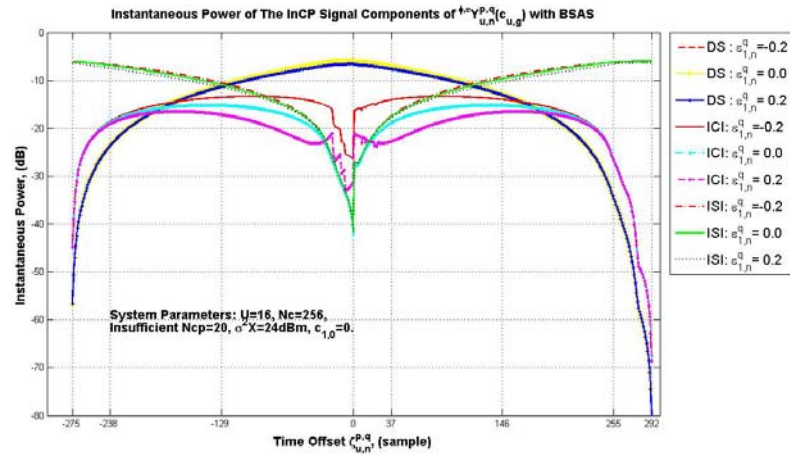


(b)

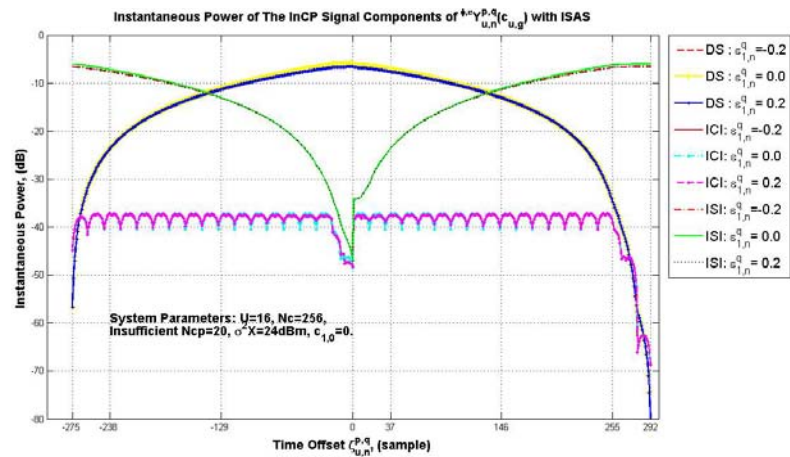


(c)

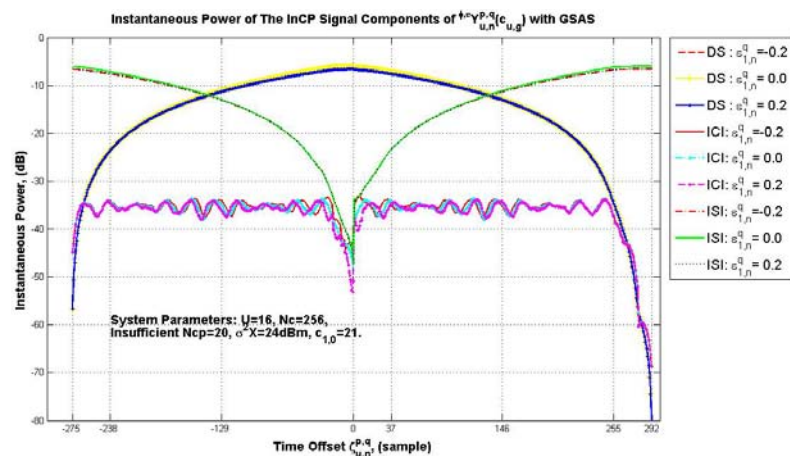
Figure 5.33 Instantaneous Powers of SCP Signal Components $\ln \phi_{u,n}^{\varepsilon} Y_{u,n}^{p,q} (i = c_{u,g})$ At: (A) $c_{1,0} = 0$ Allocated By BSAS, (B) $c_{1,0} = 0$ Allocated By ISAS, (C) $c_{1,0} = 21$ Allocated By GSAS



(a)

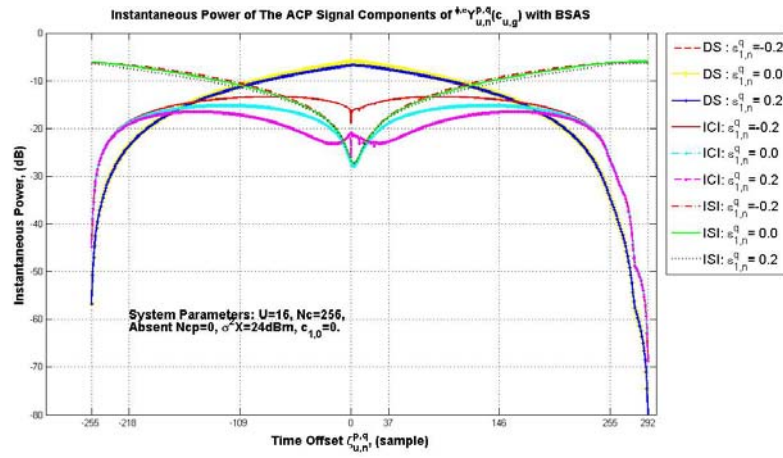


(b)

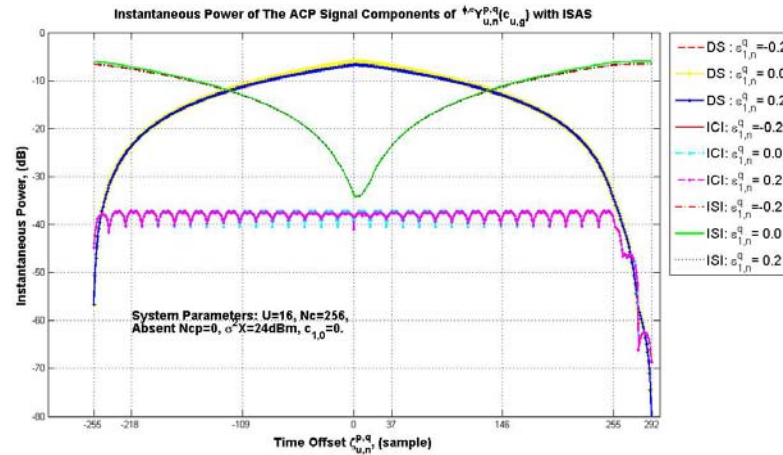


(c)

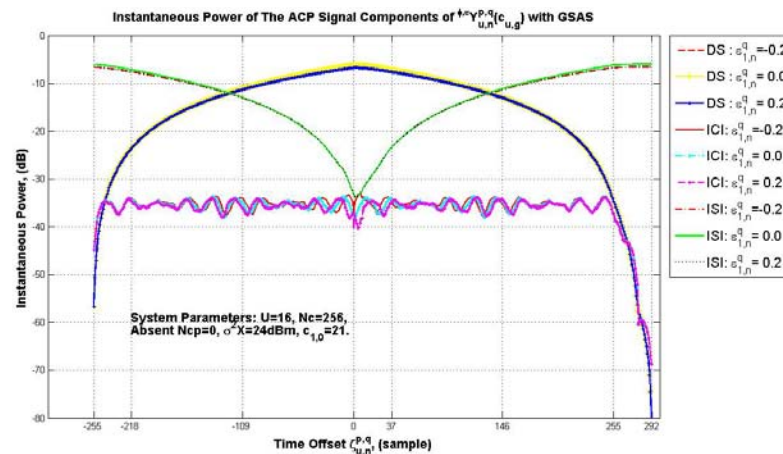
Figure 5.34 Instantaneous Powers of InCP Signal Components $\ln \phi^{\epsilon} \gamma^{p,q}(i = c_{u,g})$ At: (A) $c_{1,0} = 0$ Allocated By BSAS, (B) $c_{1,0} = 0$ Allocated By ISAS, (C) $c_{1,0} = 21$ Allocated By GSAS



(a)

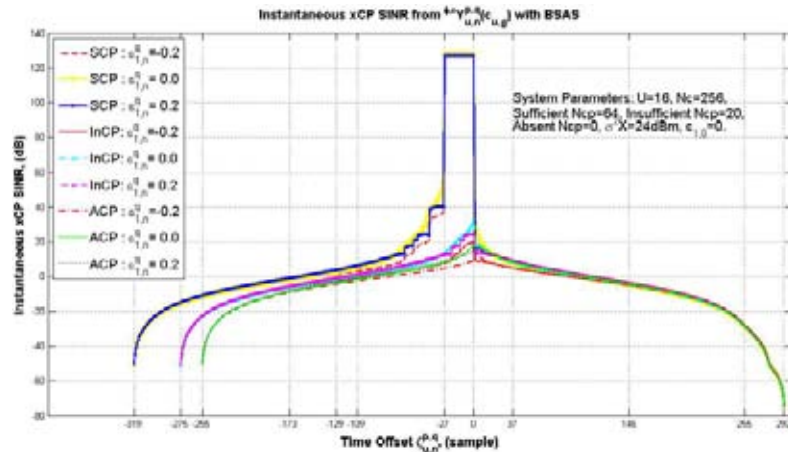


(b)

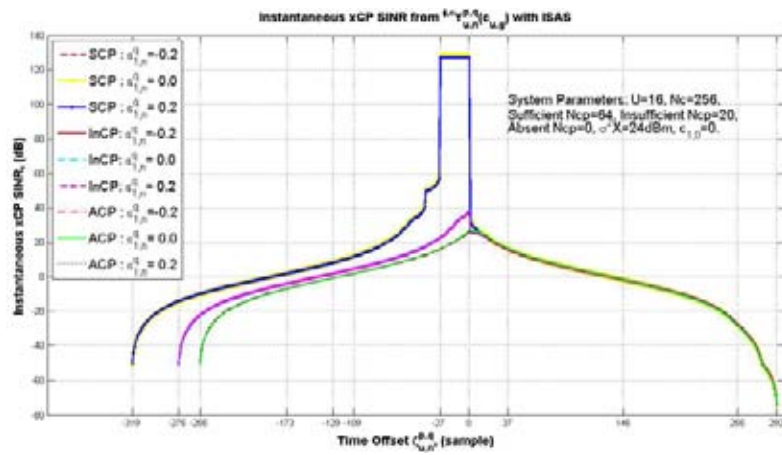


(c)

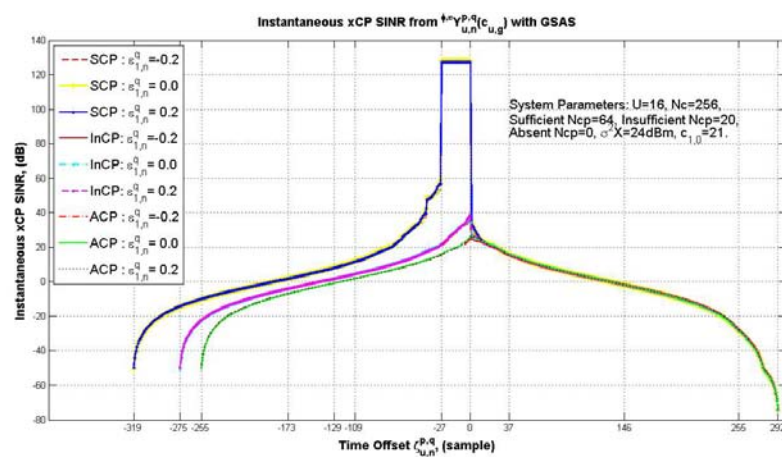
Figure 5.35 Instantaneous Powers of ACP Signal Components in $\phi, \varepsilon Y_{u,n}^{p,q} (i = c_{u,g})$ at: (a) $c_{1,0} = 0$ Allocated by BSAS, (b) $c_{1,0} = 0$ Allocated by ISAS, (c) $c_{1,0} = 21$ Allocated by GSAS



(a)



(b)



(c)

Figure 5.36 Instantaneous {SCP, InCP, and ACP} SINR from $\phi_{u,n}^{\varepsilon} Y_{u,n}^{p,q} (i=c_{u,g})$ at: (a) $c_{1,0} = 0$ Allocated by BSAS, (b) $c_{1,0} = 0$ Allocated by ISAS, (c) $c_{1,0} = 21$ Allocated by GSAS

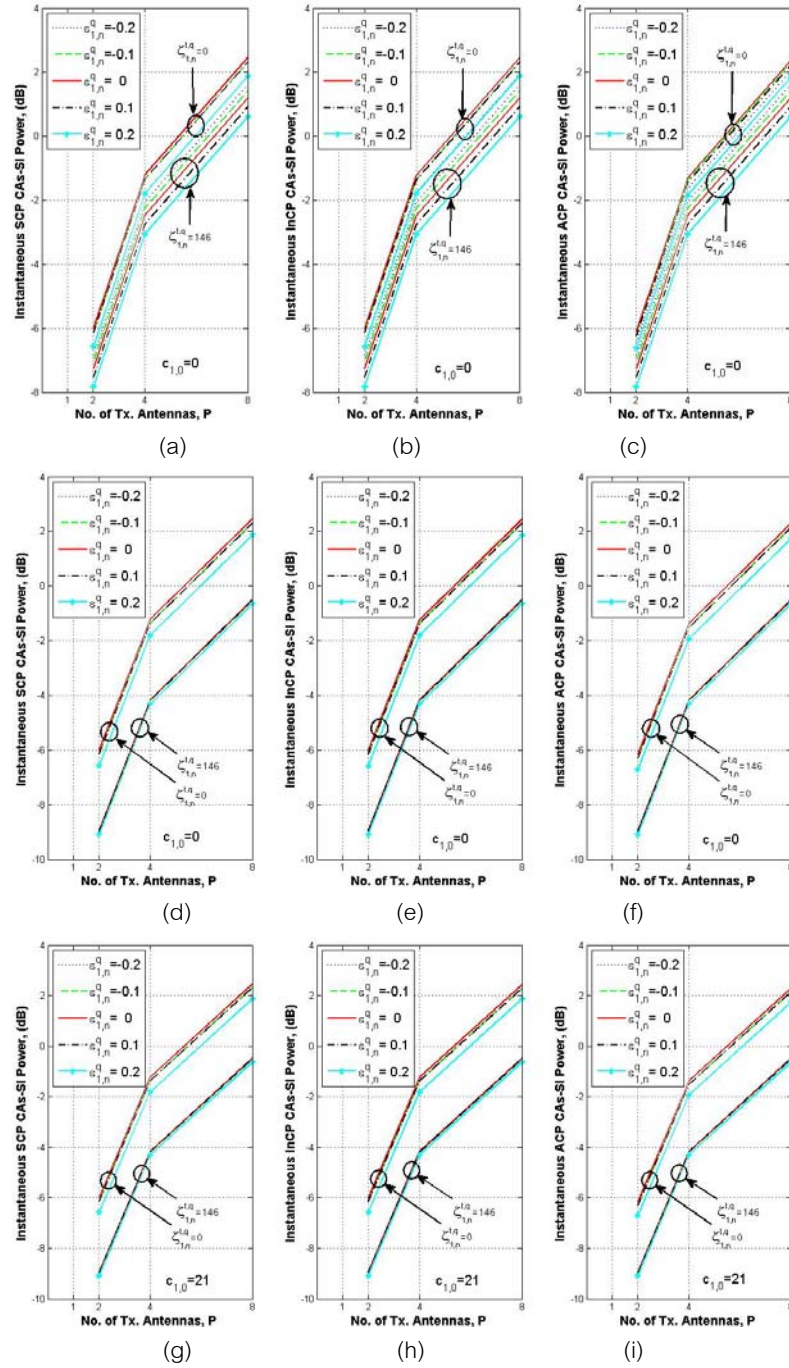
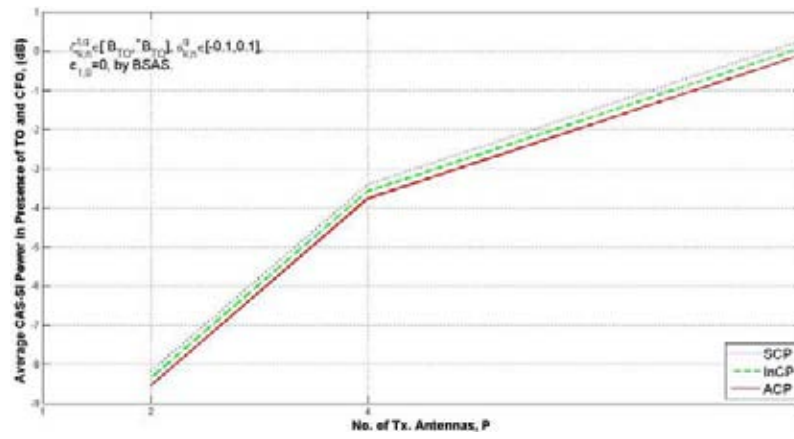
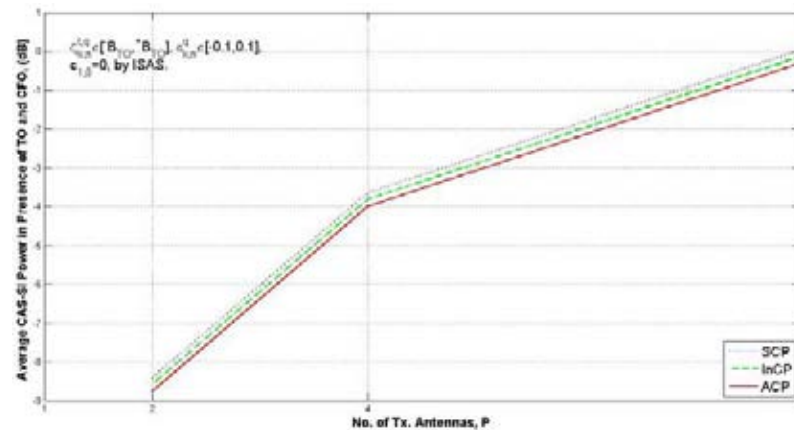


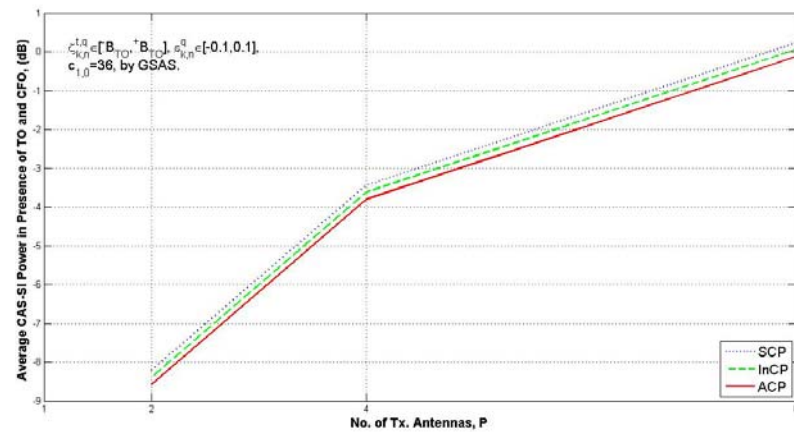
Figure 5.37 Instantaneous Power of The CAs-SI versus the Number of Transmit Antennas With: (a) SCP at $c_{1,0}=0$ Allocated by BSAS, (b) InCP at $c_{1,0}=0$ Allocated by BSAS, (c) ACP at $c_{1,0}=0$ Allocated by BSAS (d) SCP at $c_{1,0}=0$ Allocated by ISAS, (e) InCP at $c_{1,0}=0$ Allocated by ISAS, (f) ACP at $c_{1,0}=0$ Allocated by ISAS, (g) SCP at $c_{1,0}=21$ allocated by GSAS, (h) InCP at $c_{1,0}=21$ Allocated by GSAS, (i) ACP at $c_{1,0}=0$ Allocated by GSAS for Desired User's TO $\zeta_{1,n}^{p,q}=0$, and 146



(a)

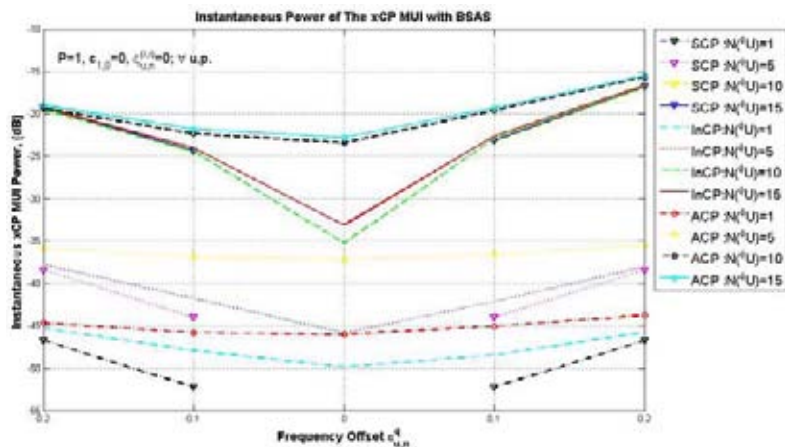


(b)

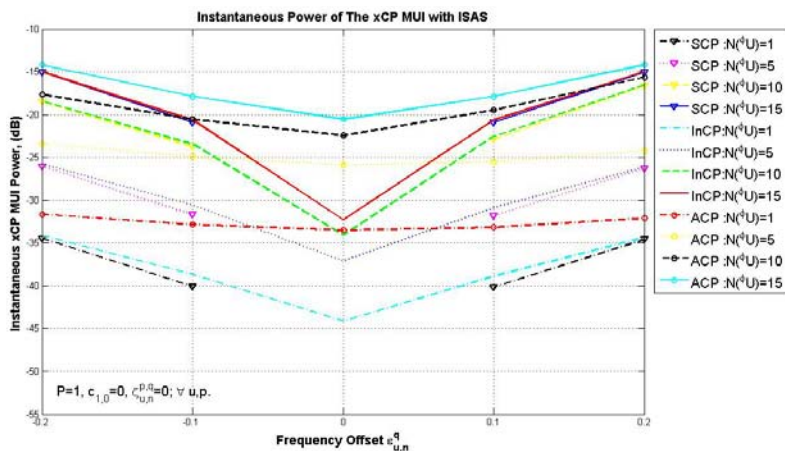


(c)

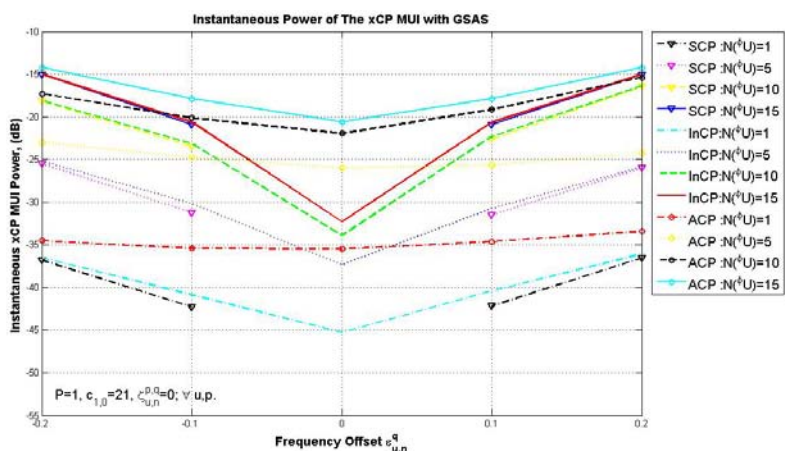
Figure 5.38 Average {SCP, InCP, and ACP} CAS-SI versus the Number of Transmit-Antennas in Presence of TO and CFO at: (a) $c_{1,0} = 0$ Allocated by BSAS, (b) $c_{1,0} = 0$ Allocated by ISAS, (c) $c_{1,0} = 36$ Allocated by BSAS



(a)

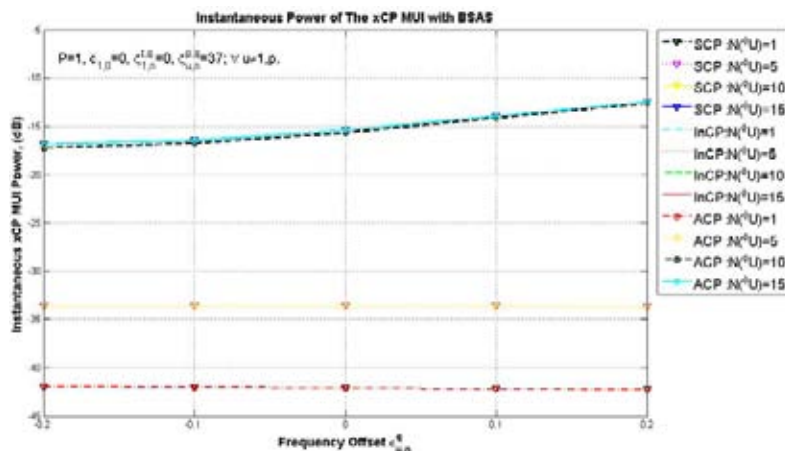


(b)

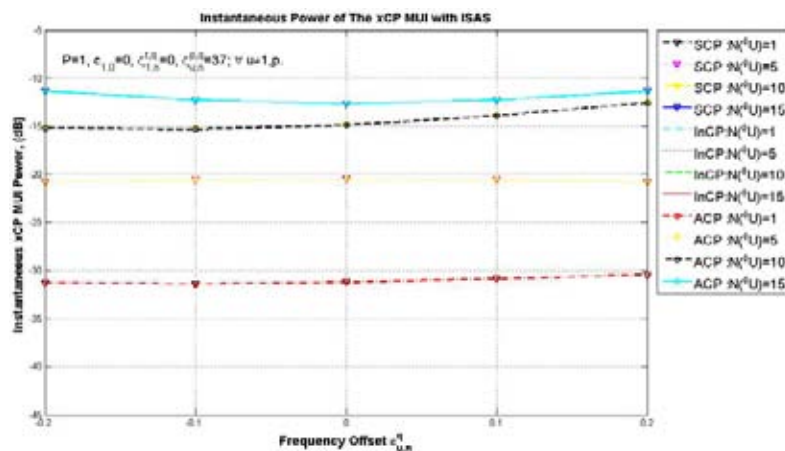


(c)

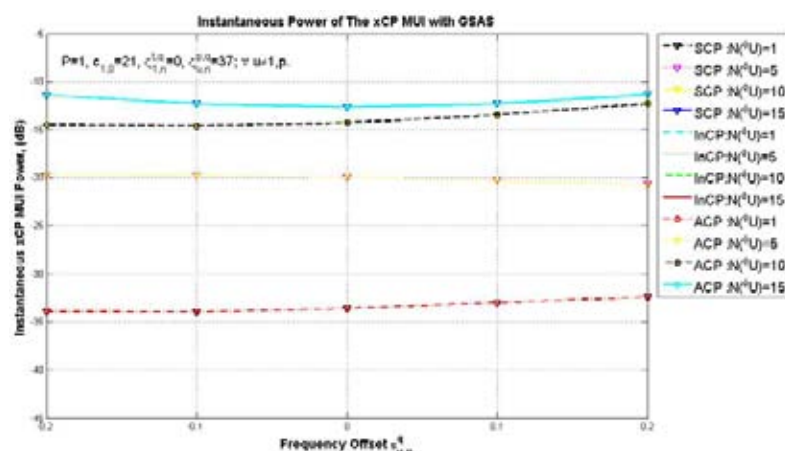
Figure 5.39 Instantaneous {SCP, InCP, ACP} MUI for Various $N^{(\phi, \epsilon, U)}$ and $\zeta_{u,n}^{p,q} = 0$ at: (a) $c_{1,0} = 0$ Allocated by BSAS, (b) $c_{1,0} = 0$ Allocated by ISAS, and (c) $c_{1,0} = 21$ Allocated by GSAS for $P=1$



(a)

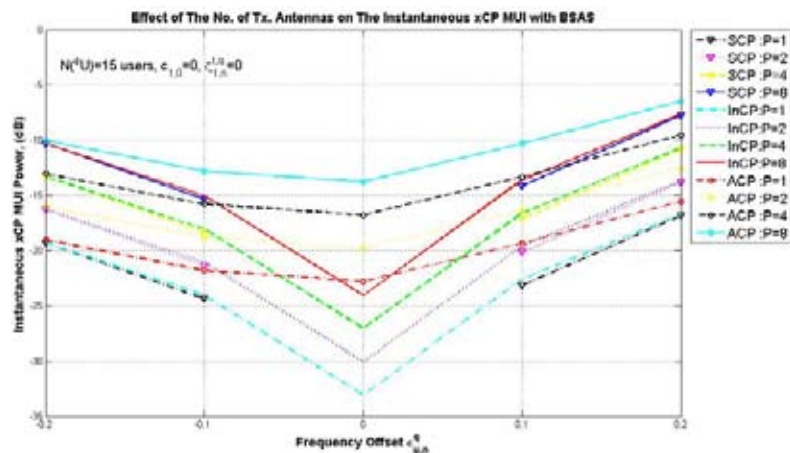


(b)

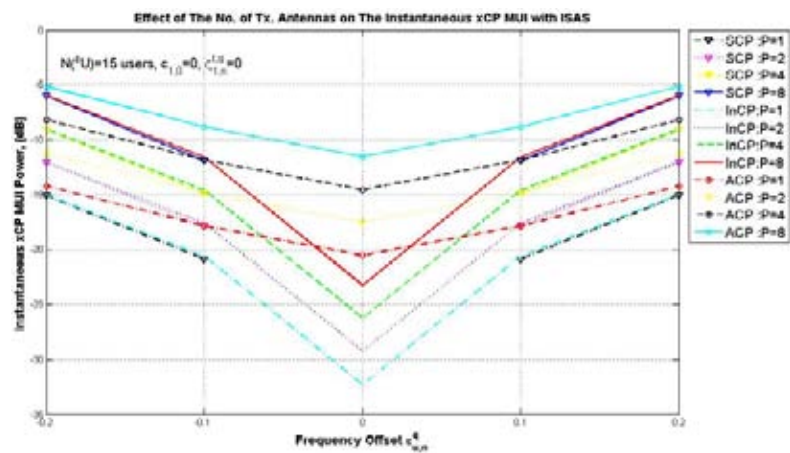


(c)

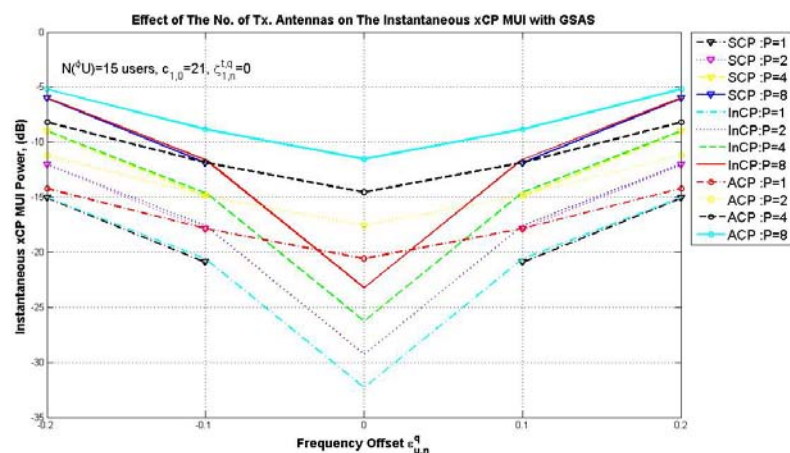
Figure 5.40 Instantaneous {SCP, InCP, ACP} MUI for Various $N^{\phi,\varepsilon}U$ and $\zeta_{u,n}^{p,q} = -37$ at: (a) $c_{1,0} = 0$ Allocated by BSAS, (b) $c_{1,0} = 0$ Allocated by ISAS, and (c) $c_{1,0} = 21$ Allocated by GSAS for $P=1$



(a)

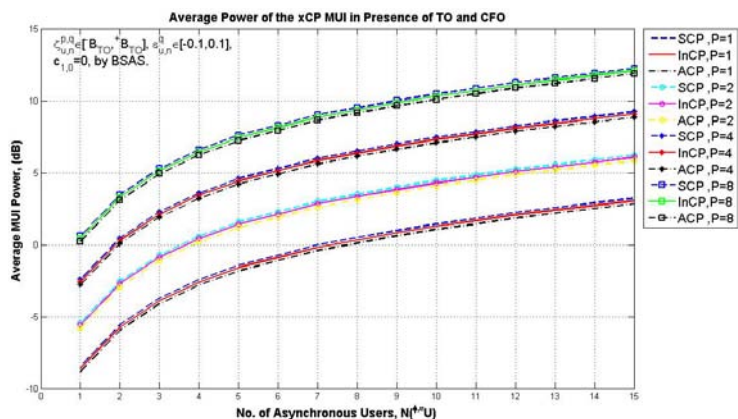


(b)

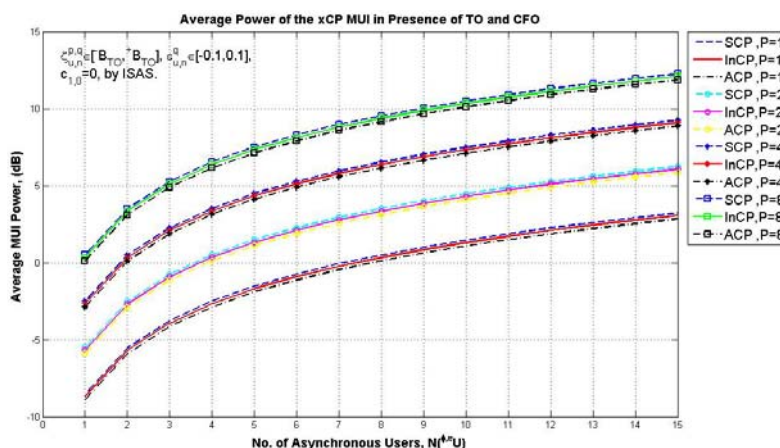


(c)

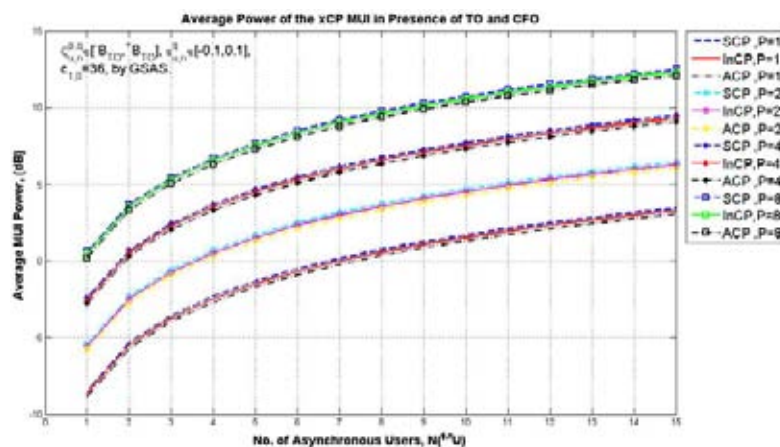
Figure 5.41 Instantaneous {SCP, InCP, ACP} MUI for P=1, 2, 4, and 8 antennas at: (a) $c_{1,0} = 0$ Allocated by BSAS, (b) $c_{1,0} = 0$ Allocated by ISAS, and (c) $c_{1,0} = 21$ Allocated by GSAS for $N(\phi,\epsilon) = 15$



(a)



(b)



(c)

Figure 5.42 Effects of Number of Asynchronous Users $N(\epsilon^U)$ and Number of Transmit Antennas, P on the Average {SCP, InCP, and ACP} MUI in Presence of TO and CFO at: (a) $c_{1,0} = 0$ Allocated by BSAS, (b) $c_{1,0} = 0$ Allocated by ISAS, (c) $c_{1,0} = 36$ Allocated by GSAS

C. Instantaneous/Average SINR Analysis in Presence of TO and CFO

The resultant instantaneous SINR at the DFT output with TO and/or CFO are depicted in Figures 5.43-5.46 for multiuser environment and MIMO context properties. Figures 5.43 and 5.44 present the impact of the number of asynchronous user in the system on the instantaneous SINR in presence of CFO and CFO/TO respectively.

In the ideal case of the synchronization offset (i.e. $\zeta_{u,n}^{p,q} = 0$ and $\epsilon_{u,n}^q = 0$) for a single-input system i.e. OFDMA system, the instantaneous SINR is large i.e. $\text{SINR} > 120$ dB, as in Figure 5.43 for SCP. The instantaneous SINR decreases as the CFO increases and/or the CP condition eases for certain number of asynchronous user.

Consider TO synchronous system with $N(\phi, \epsilon, U) = 1$, the instantaneous SCP/InCP/ACP SINR is decreased from 128dB/31.05dB/17.67dB by $\epsilon_{u,n}^q = 0$ to 46.12dB/24.78dB/14.75dB and 40.10dB/19.69dB/11.48dB by $\epsilon_{u,n}^q = -0.1$ and -0.2 respectively at $c_{1,0} = 0$ allocated by BSAS as depicted in Figure 5.43(a) for $P=1$.

Note that with $\zeta_{u,n}^{p,q} \neq 0$ and $\epsilon_{u,n}^q \neq 0$, the performance of the system is substantially degraded due to accumulation of the interferences by the TO and CFO. For example, with $\zeta_{u,n}^{p,q} = 37$ and $N(\phi, \epsilon, U) = 1$, the violated instantaneous SCP/InCP/ACP SINR is additionally decreased from 36.08dB/31.13dB/17.67dB by $\epsilon_{u,n}^q = 0$ to 35.85dB/24.80dB/14.75dB and 35.35dB/19.69dB/11.48dB by $\epsilon_{u,n}^q = -0.1$ and -0.2 respectively at $c_{1,0} = 0$ allocated by BSAS as depicted in Figure 5.44 for $P=1$.

Note that the BSAS performs better than GSAS and ISAS in alleviating the incurred interferences by the CFO for $\zeta_{u,n}^{p,q} = 0$ and $\zeta_{u,n}^{p,q} \neq 0$ respectively. For example, with $N(\phi, \epsilon, U) = 1$ and $\epsilon_{u,n}^q = +0.1$, the instantaneous SCP SINR is 46.12dB (36.02dB), 36.05dB (26.84dB) and 34.0dB (24.67dB) with $\zeta_{u,n}^{p,q} = 0$ (37) at the $c_{1,0}$ allocated by BSAS, GSAS and ISAS respectively, as can be shown in Figure 5.43(a) (5.44 (a)). However, Figures 5.45 and 5.46 present the impact of utilizing MIMO technique on the instantaneous SINR at the DFT output in presence of CFO and CFO/TO. From Figures 5.45-5.46 and Table 5.7, it can be concluded that the instantaneous SINR decreases as the number of transmit-antennas and/or the CFO increases, as well as eases the CP condition.

Table 5.7: The Instantaneous {SCP, InCP, ACP} SINR with $N(\phi, \epsilon, U) = 1$ and $\epsilon_{u,n}^q = +0.1$ at $c_{1,0}$ by BSAS

Instantaneous SINR (dB)	$\zeta_{u,n}^{p,q} = 0$ and $\zeta_{k=1,n}^{t,q} = 0$				$\zeta_{u,n}^{p,q} = 37$ and $\zeta_{k=1,n}^{t,q} = 0$			
	P=1	P=2	P=4	P=8	P=1	P=2	P=4	P=8
SCP	46.12	0.00	-4.77	-8.45	36.02	0.00	-4.77	-8.45
InCP	28.63	-0.01	-4.77	-8.46	28.67	-0.01	-4.78	-8.46
ACP	18.34	-0.13	-4.86	-8.52	18.34	-0.13	-4.86	-8.52

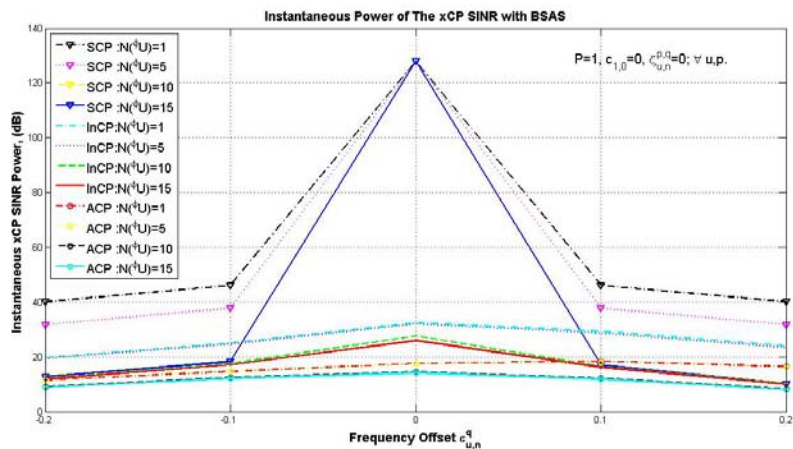
Figure 5.47 investigates the impact of the number of asynchronous users and the number of transmit antennas on the average xCP SINR for asynchronous desired user along the different SASs. Following the instantaneous SINR, the average SINR increases as the number of asynchronous users i.e., MUI, and the number of transmit antennas i.e., CAs-SI, increase, where eases the CP condition also increases the average SINR as in Figure 5.47.

Table 5.8 investigates the effect of the CP conditions as well as the performance of the subcarrier allocation schemes on the average SINR at the DFT output. From the table, it can be recognized that the ISAS performs slightly the BSAS and GSAS by producing higher average SINR for asynchronous desired user. In presence of TO and CFO, the lowest average SINR can be obtained when InCP condition is applied, along the different types of SAS.

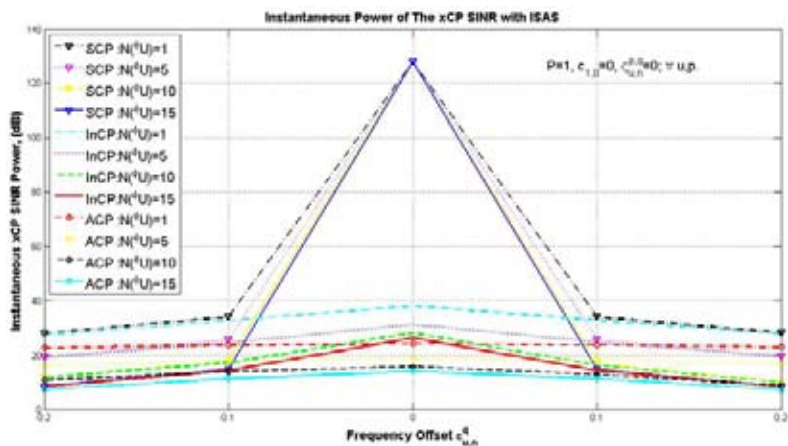
Table 5.8: The Average {SCP, InCP, ACP} SINR for Asynchronous Desired User at $c_{1,0}$ by BSAS, ISAS and GSAS when P=1

Average SINR (dB)	$N(\phi, \epsilon, U) = 7$			$N(\phi, \epsilon, U) = 15$		
	BSAS	ISAS	GSAS	BSAS	ISAS	GSAS
SCP	-20.0275	-20.0133	-20.2363	-21.3064	-21.3147	-21.5377
InCP	-20.1237	-20.1098	-20.3281	-21.4030	-21.4110	-21.6294
ACP	-20.0494	-20.0359	-20.2466	-21.3293	-21.3370	-21.5478

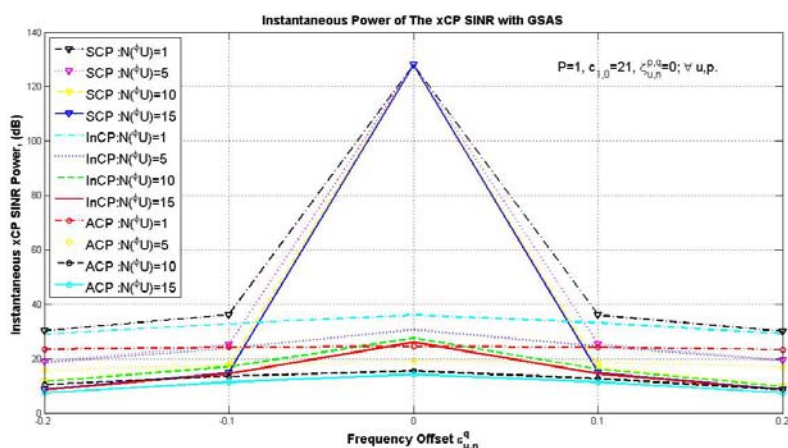
In addition, the corresponding BER of Figures 5.42 and 5.47 is shown in Figures 5.48-5.49, respectively for single-transmit antenna and asynchronous desired user. Same conclusions for the exploited SAS and CP condition can be drawn for the BER at the DFT output.



(a)

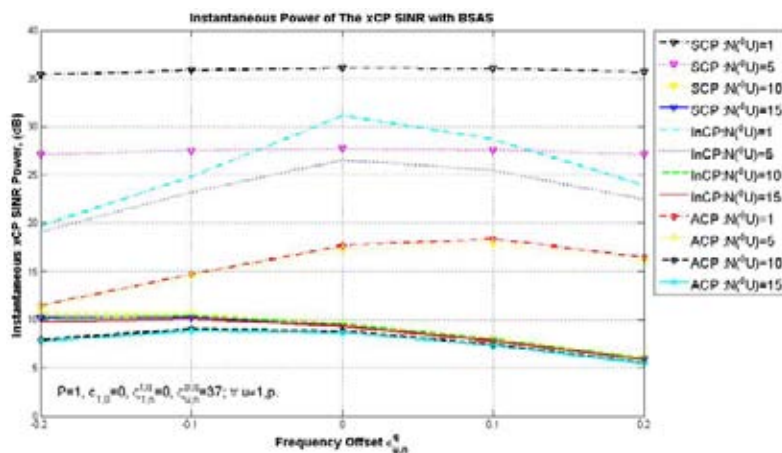


(b)

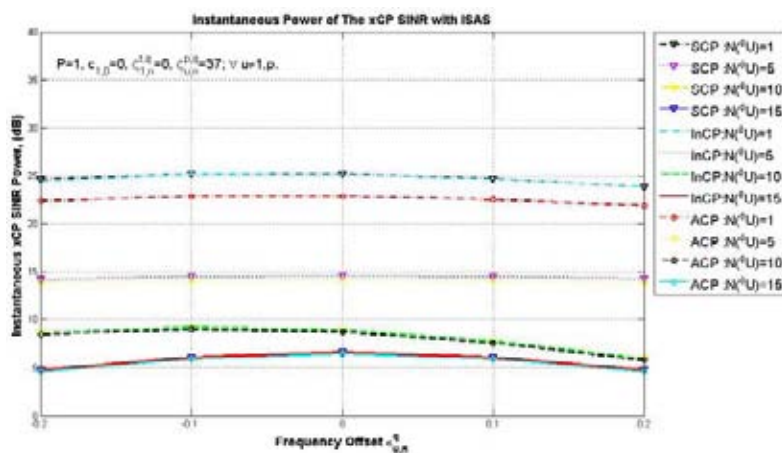


(c)

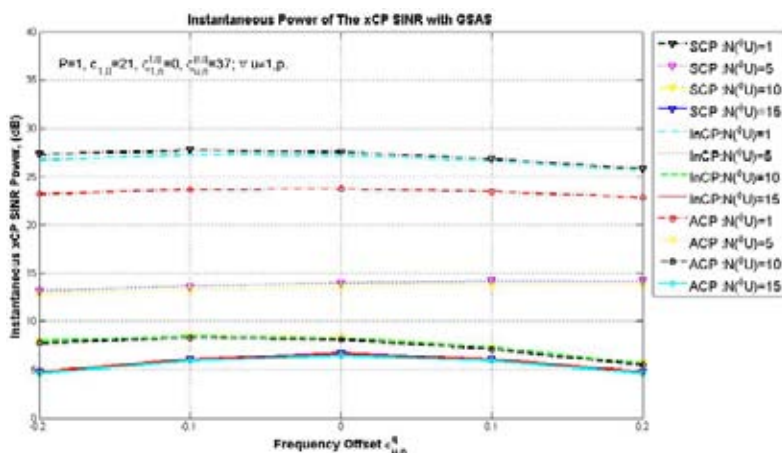
Figure 5.43 Instantaneous {SCP, InCP, ACP} SINR for Various $N^{(\phi, \epsilon)U}$ and $\zeta_{u,n}^{p,q} = 0$ at: (a) $c_{1,0} = 0$ Allocated by BSAS, (b) $c_{1,0} = 0$ Allocated by ISAS, and (c) $c_{1,0} = 21$ Allocated by GSAS for $P=1$



(a)



(b)



(c)

Figure 5.44 Instantaneous {SCP, InCP, ACP} SINR for Various $N(\phi^\varepsilon U)$ and $\zeta_{u,n}^{p,q} = 37$ at: (a) $c_{1,0} = 0$ Allocated by BSAS, (b) $c_{1,0} = 0$ Allocated by ISAS, and (c) $c_{1,0} = 21$ Allocated by GSAS for $P=1$

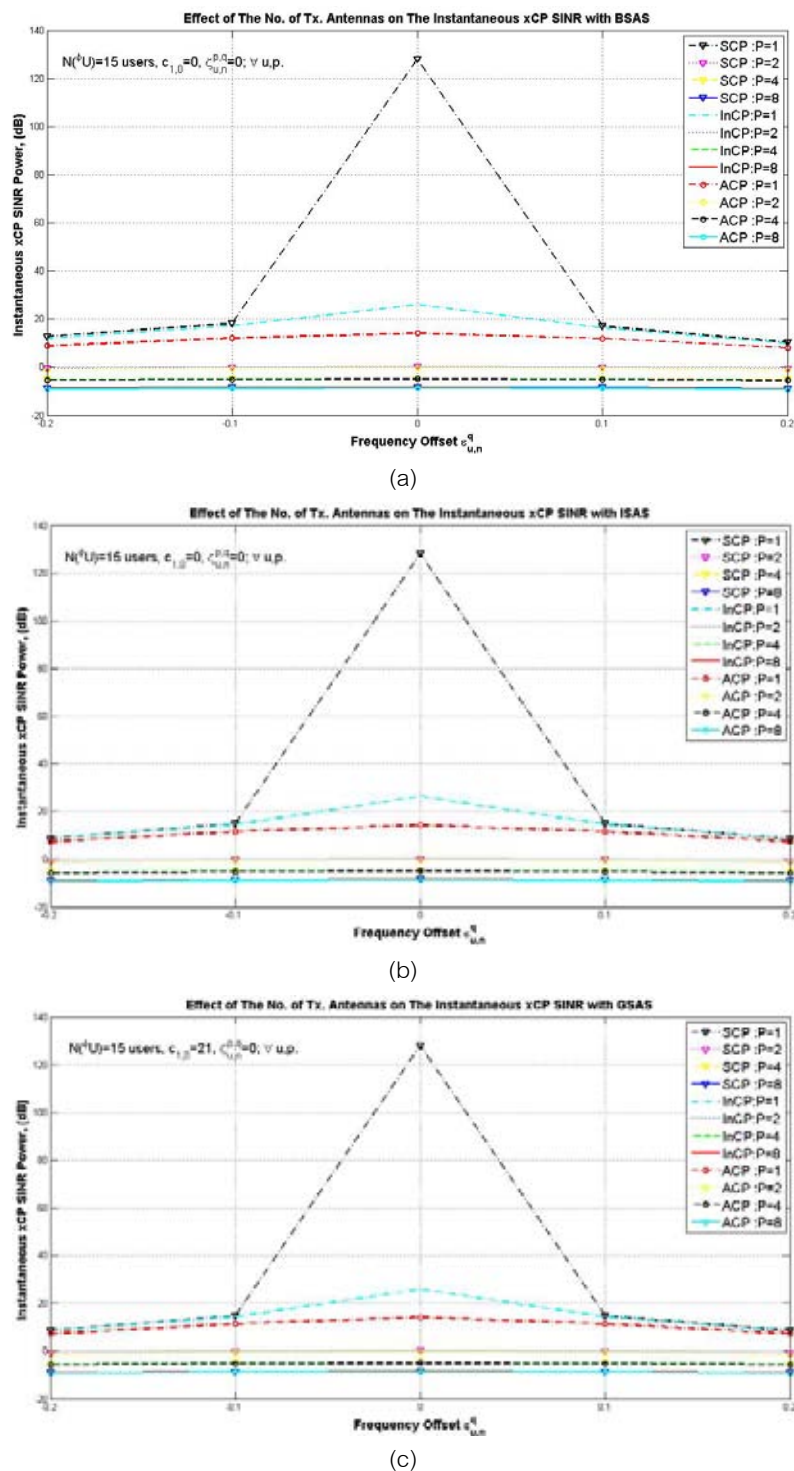
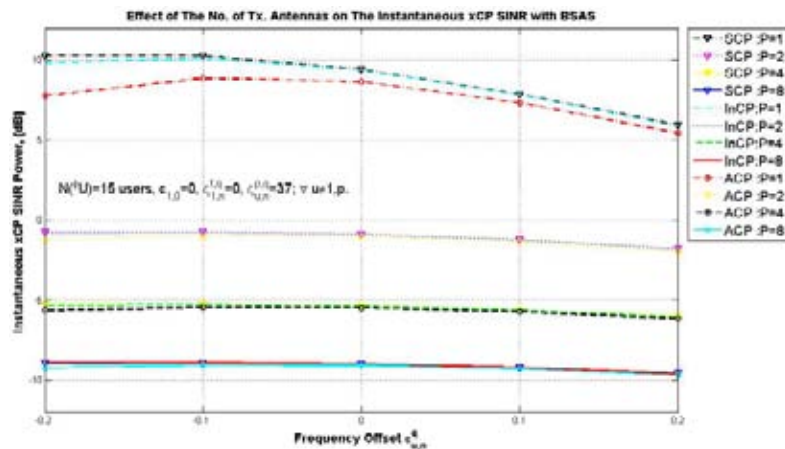
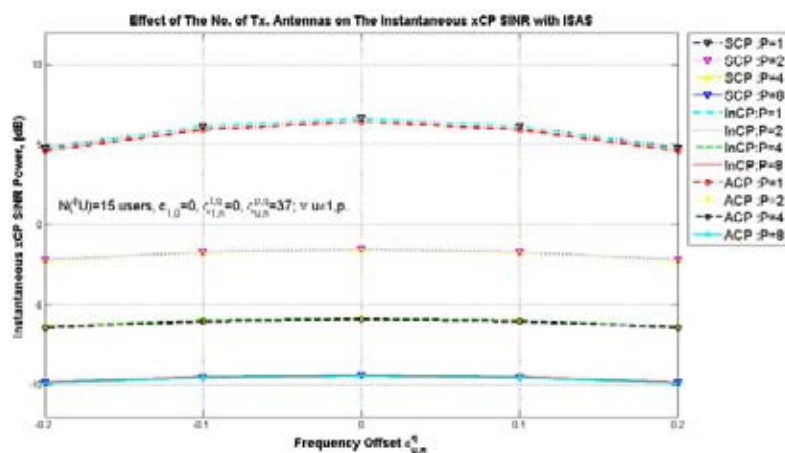


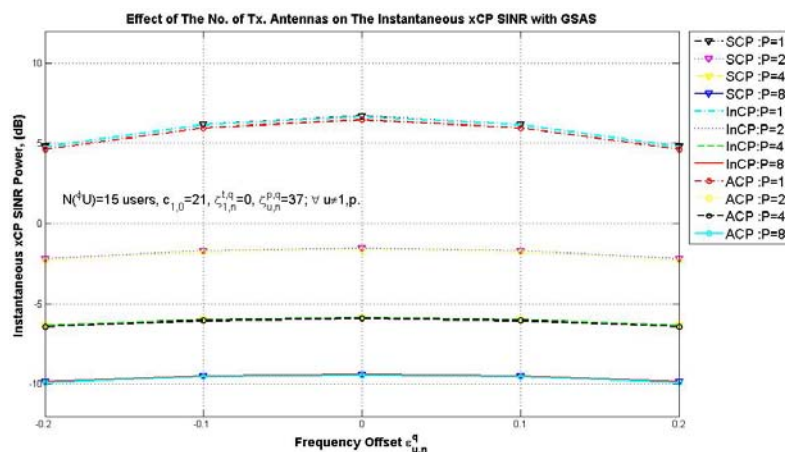
Figure 5.45 Instantaneous {SCP, InCP, ACP} SINR for $P=1, 2, 4,$ and 8 antennas at: (a) $c_{1,0} = 0$ Allocated by BSAS, (b) $c_{1,0} = 0$ Allocated by ISAS, and (c) $c_{1,0} = 21$ Allocated by GSAS for $\zeta_{u,n}^{p,q} = 0$ and $N(\phi, \epsilon) = 15$



(a)

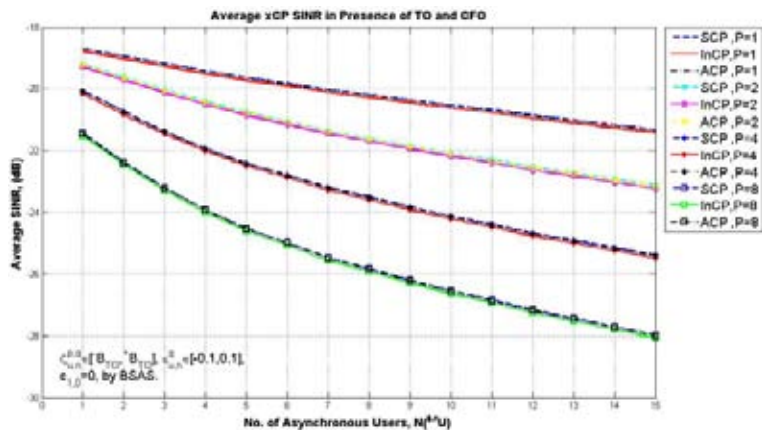


(b)

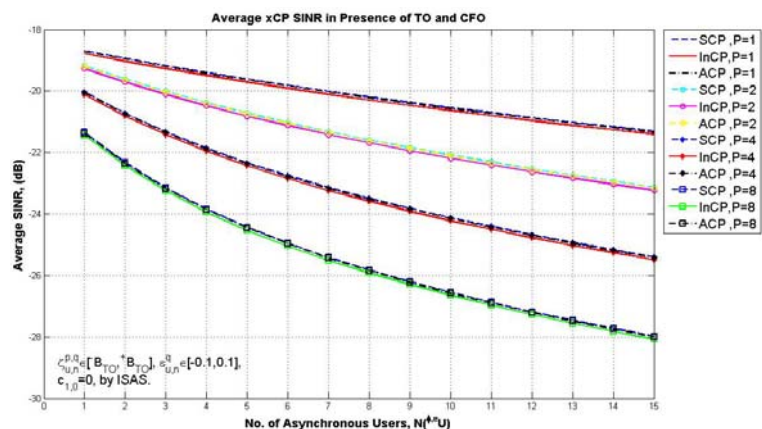


(c)

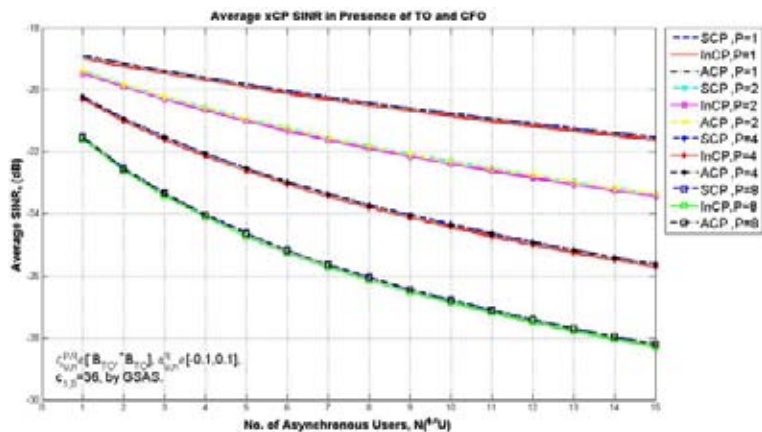
Figure 5.46 Instantaneous {SCP, InCP, ACP} SINR for P=1, 2, 4, and 8 antennas at: (a) $c_{1,0}=0$ Allocated by BSAS, (b) $c_{1,0}=0$ Allocated by ISAS, and (c) $c_{1,0}=21$ Allocated by GSAS for $\zeta_{u,n}^{p,q} = 37$ and $N^{(\phi, \epsilon)}(U)=15$



(a)

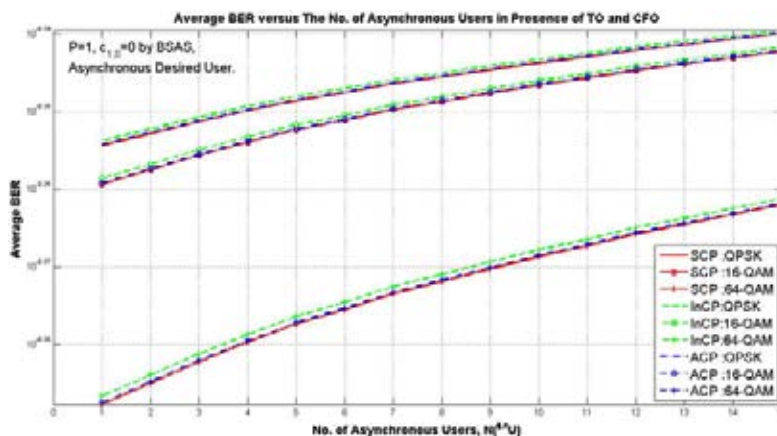


(b)

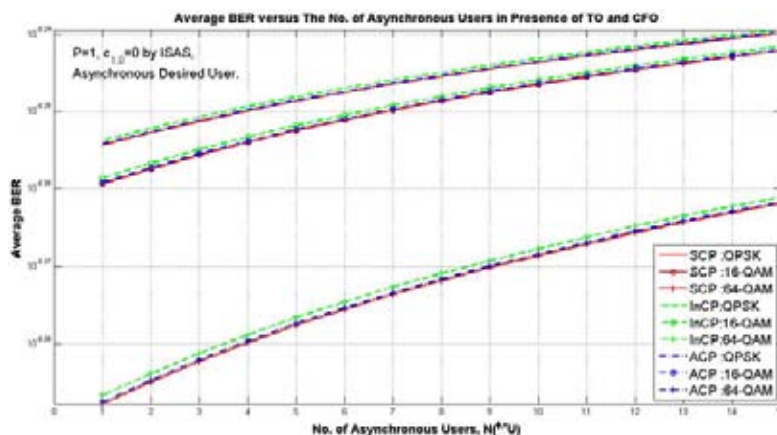


(c)

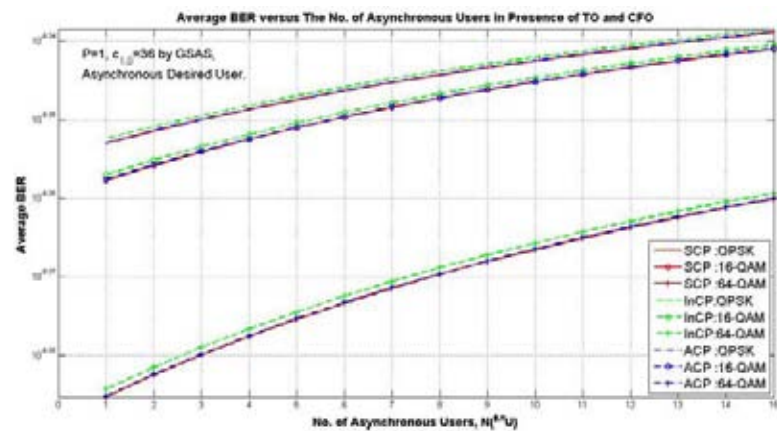
Figure 5.47 Effects of Number of Asynchronous Users $N^A(U)$ and Number of Transmit Antennas, P on the Average {SCP, InCP, and ACP} SINR in Presence of TO and CFO at: (a) $c_{1,0}^a = 0$ Allocated by BSAS, (b) $c_{1,0}^a = 0$ Allocated by ISAS, (c) $c_{1,0}^a = 36$ Allocated by GSAS



(a)

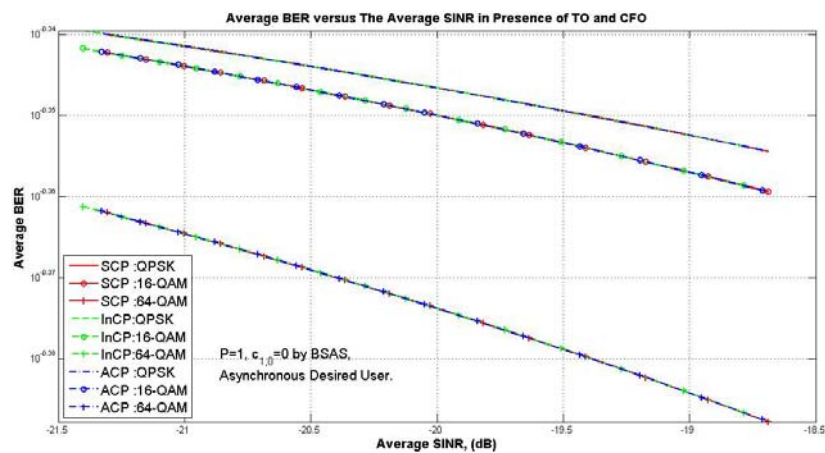


(b)

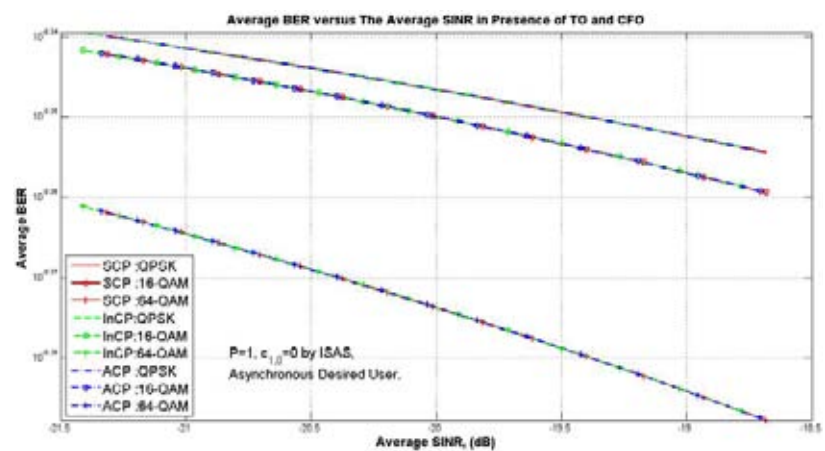


(c)

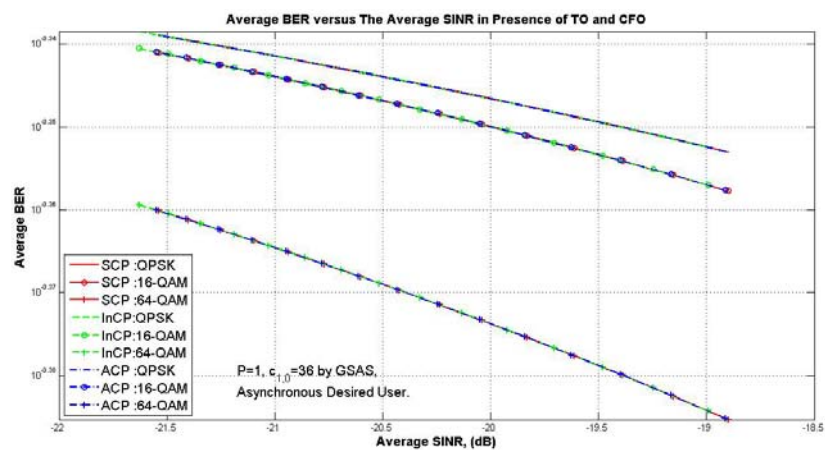
Figure 5.48 Effects of Number of Asynchronous Users $N(\phi, \epsilon, U)$ on the Average {SCP, InCP, and ACP} BER for QPSK, 16-QAM, and 64-QAM at: (a) $c_{1,0}=0$ Allocated by BSAS, (b) $c_{1,0}=0$ Allocated by ISAS, (c) $c_{1,0}=21$ Allocated by GSAS for $P=1$, and Asynchronous Desired User



(a)



(b)



(c)

Figure 5.49 Effects of average SINR on the Average {SCP, InCP, and ACP} BER for QPSK, 16-QAM, and 64-QAM in Presence of TO and CFO at: (a) $c_{1,0}=0$ Allocated by BSAS, (b) $c_{1,0}=0$ Allocated by ISAS, (c) $c_{1,0}=21$ Allocated by GSAS for Asynchronous Desired User

5.5. System Performance In Presence of CFO and SCFO

In this section, the impact of the CFO and SCFO, which is evaluated in section 3.5, is depicted. The derived expression for the received signal in single-transmit antenna single-user system ${}^{\varepsilon, \xi} Y_{u,n}^{p,q}(i)$ in (3.64) and (3.65) for negative and positive SCFO respectively is compared with the conventional expression in (3.62).

5.5.1 The Instantaneous Interference Components and SINR of ${}^{\varepsilon, \xi} Y_{u,n}^{p,q}(i = c_{u,g})$

The instantaneous power of the signal components of ${}^{\varepsilon, \xi} Y_{u,n}^{p,q}(i = c_{u=1,g})$ in (3.64) and (3.65) are depicted in Figures 5.50-5.52 at $c_{u,1}$ allocated by BSAS, ISAS and GSAS respectively, where the instantaneous SINR based on these signal components is depicted in Figure 5.53.

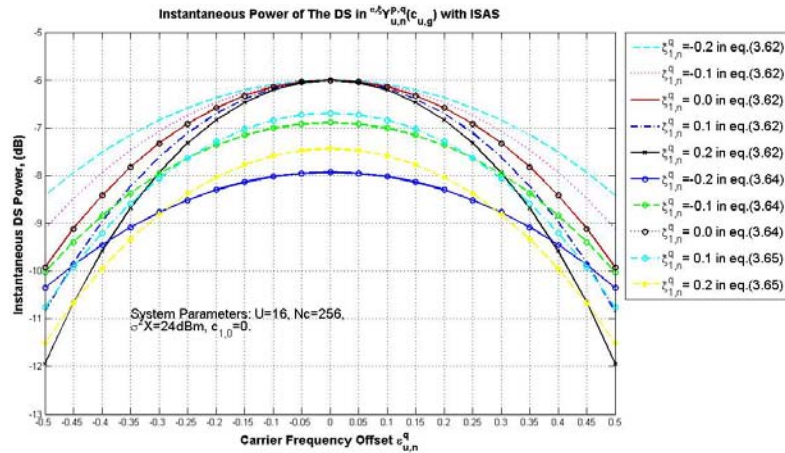
The DS in ${}^{\varepsilon, \xi} Y_{u,n}^{p,q}(i = c_{u=1,g})$ decreases as the CFO and SCFO increases as in Figure 3.50. For example, with ideal CFO, the DS is -6dB, -6.69dB, -6.89dB, -7.44dB, and -7.93dB for $\xi_{u,n}^q = 0, 0.1, -0.1, 0.2,$ and -0.2 respectively at $c_{u,1} = 0$ allocated by BSAS and ISAS when equation (3.64) and (3.65) are applied as in Figure 5.50.

From equations (3.64) and (3.65), it can be noticed that for $\varepsilon_{u,n}^q = 0$, the asynchronous DS with the SCFO is totally depends on the value of the allocated subcarrier i , and the summation sequence which is governed by the $\xi_{u,n}^q$. Therefore, the produced DS by BSAS and ISAS varies with $\xi_{u,n}^q$ particularly with small value of the subcarriers, where the DS by GSAS does not. This is because of the randomness in allocating the subcarriers. Furthermore, with the presence of the CFO, the DS is additionally decreased as the CFO and SCFO increased.

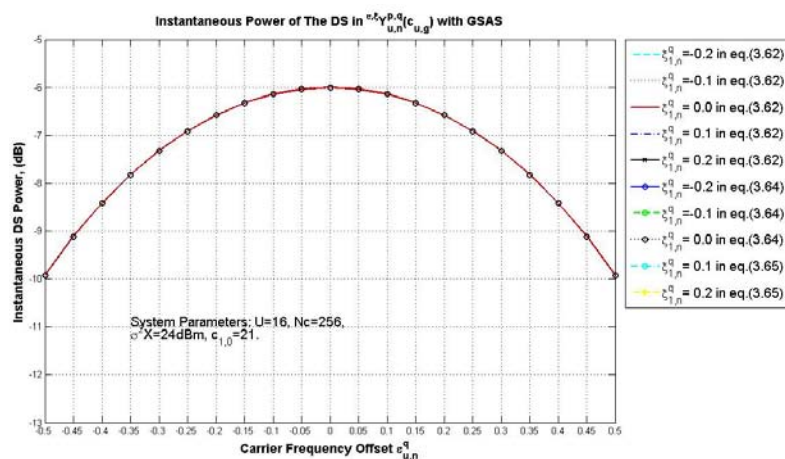
The produced ICI and ISI due to CFO and/or SCFO is crucially affected by the exploited SAS, where the BSAS produces higher ICI than the ISAS and GSAS as can be grasped from Figures 5.44 and 5.45. This can be grasped also from the second and last terms in equations (3.64) and (3.65).



(a)

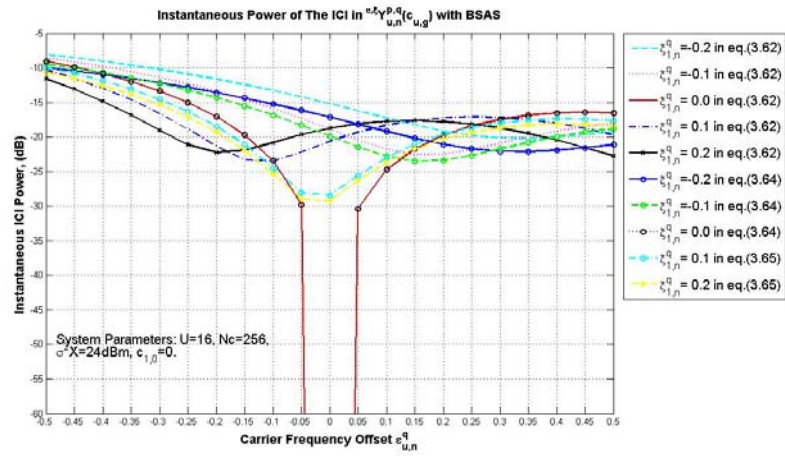


(b)

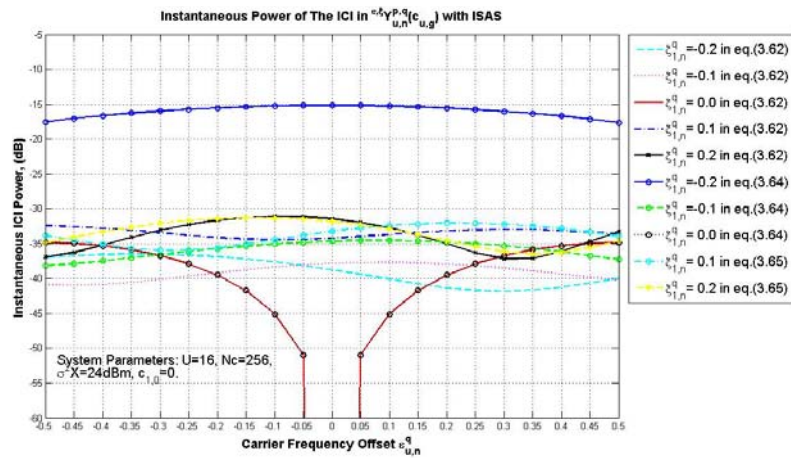


(c)

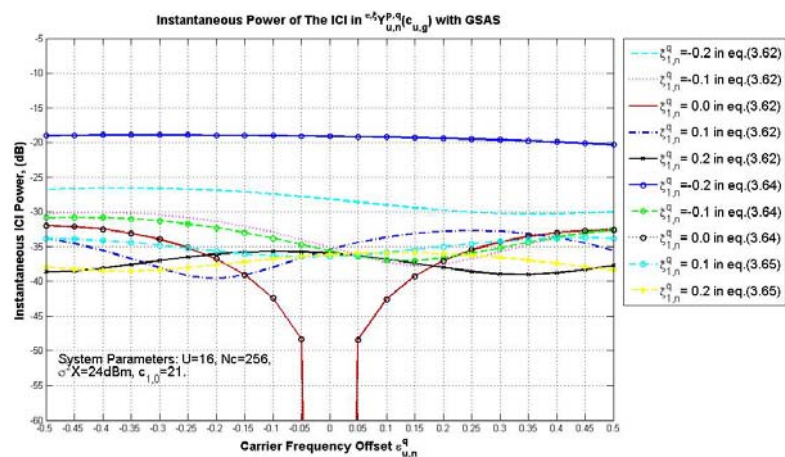
Figure 5.50 Instantaneous Powers of the DS in $\epsilon_{u,n}^{\xi} Y_{u,n}^{p,q}(i=c_{u,g})$ at: (a) $c_{1,0} = 0$ Allocated by BSAS, (b) $c_{1,0} = 0$ Allocated by ISAS, (c) $c_{1,0} = 21$ Allocated by GSAS



(a)

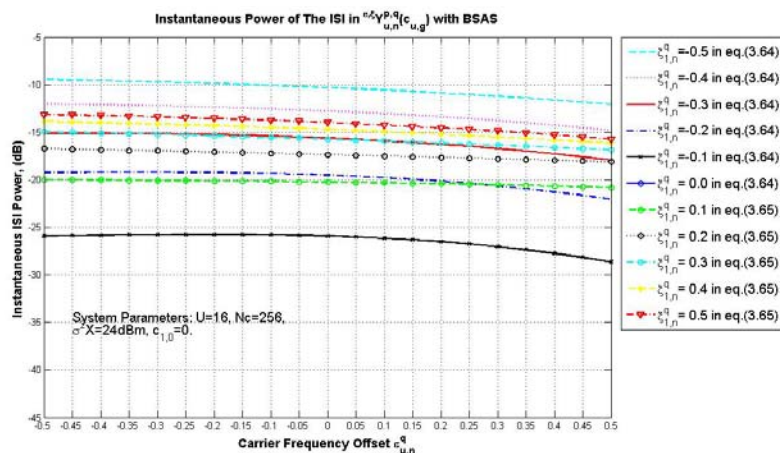


(b)

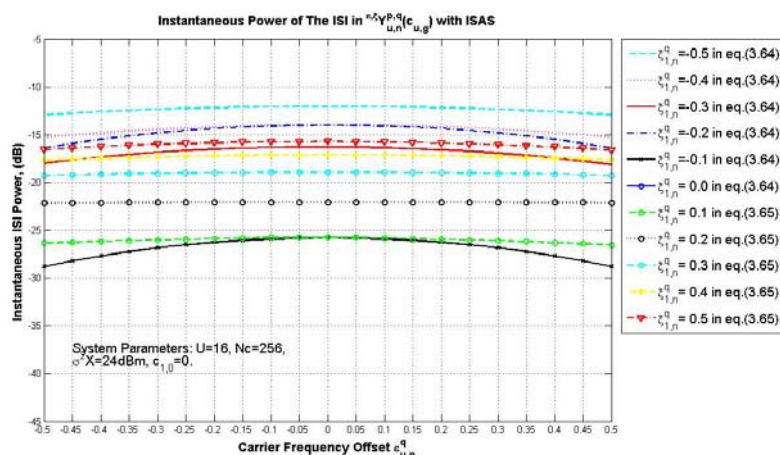


(c)

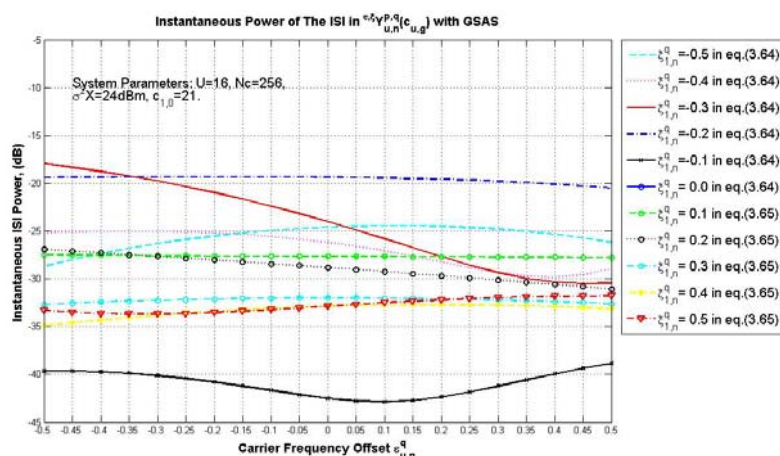
Figure 5.51 Instantaneous Powers of the ICI in $\varepsilon_{u,n}^q Y_{u,n}^{p,q}(i=c_{u,g})$ at: (a) $c_{1,0} = 0$ Allocated by BSAS, (b) $c_{1,0} = 0$ Allocated by ISAS, (c) $c_{1,0} = 21$ Allocated by GSAS



(a)

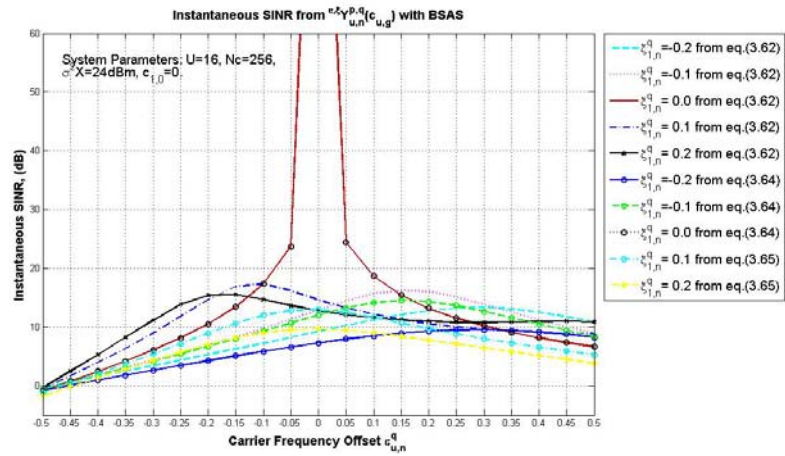


(b)

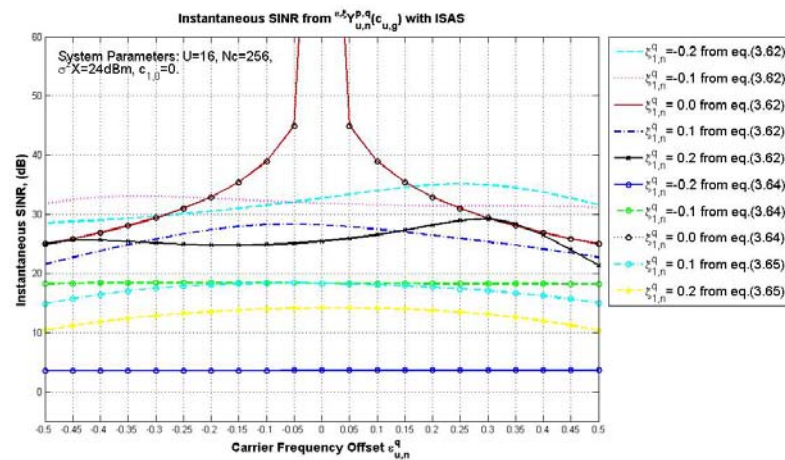


(c)

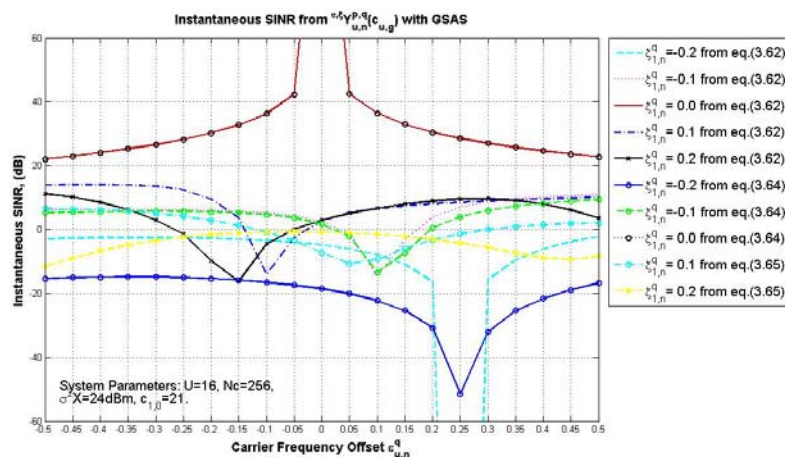
Figure 5.52 Instantaneous Powers of the ISI in $\varepsilon_{u,n}^q Y_{u,n}^{p,q}(i=c_{u,g})$ at: (a) $c_{1,0} = 0$ Allocated by BSAS, (b) $c_{1,0} = 0$ Allocated by ISAS, (c) $c_{1,0} = 21$ Allocated by GSAS



(a)



(b)



(c)

Figure 5.53 Instantaneous SINR from $\epsilon_{u,n}^{\xi} \gamma_{u,n}^{p,q}(i=c_{u,g})$ at: (a) $c_{1,0} = 0$ Allocated by BSAS, (b) $c_{1,0} = 0$ Allocated by ISAS, (c) $c_{1,0} = 21$ Allocated by GSAS

5.5.2 The Instantaneous Interference and SINR for MIMO-OFDMA Uplink Systems

The induced instantaneous power of interferences and the corresponding SINR is presented in this subsection in presence of CFO and SCFO.

A. Instantaneous CAs-SI in Presence of CFO and SCFO

Figure 5.54 shows the induced CAs-SI when the desired user experiences CFO and/or SCFO. The Figure shows that the CAs-Si increases as the transmit-antennas increases. Consider $\xi_{k=1,n}^q = 0$, the CAs-SI increases to be -6.0180dB(-6.0206dB), -1.2468dB(-1.2498dB), and 2.4330dB(2.4304dB) for P=2, 4, and 8 transmit-antennas when $\epsilon_{k=1,n}^q = -0.05(0.05)$ at $c_{k=1,n} = 0$ allocated by BSAS. Table 5.9 and Figure 5.54 present the effect of the exploited SAS on the asynchronous CAs-SI. More specifically, and with $\xi_{k=1,n}^q \neq 0$, the GSAS produces the lowest CAs-SI.

B. Instantaneous MUI in Presence of CFO and SCFO

Figures 5.55 and 5.56 evaluate the instantaneous asynchronous MUI with CFO and SCFO for $N(\epsilon, \xi U) \neq \emptyset$. The properties of the increasable trend of the instantaneous MUI are subject to the value of the CFO and SCFO.

Consider $\epsilon_{u,n}^q = 0$ and P=1, the instantaneous MUI improves from -39.0579dB (-37.2400dB) with $N(\epsilon, \xi U) = 1$ to -30.8011dB (-23.1914dB), -16.1732dB (-12.0075dB), and -15.6256dB (-11.8097dB) with $N(\epsilon, \xi U) = 5, 10, \text{ and } 15$ respectively for $\xi_{1,n}^q = -0.5(0.5)$ at $c_{1,0} = 0$ allocated by BSAS as in Figure 5.55. In $\epsilon_{u,n}^q \neq 0$, an additional instantaneous MUI induces where more ICI is incurred.

However, Figures 5.55 and 5.56 represent that the BSAS is performs better than the ISAS and GSAS in alleviating the instantaneous MUI. For example, the instantaneous MUI with $\epsilon_{u,n}^q = \xi_{u,n}^q = -0.5(0.5)$, is -15.6256dB (-7.6440dB), -8.2664dB (-7.3359dB), and -6.0469dB (-5.0518dB) for $N(\epsilon, \xi U) = 15$ and P=1. The instantaneous MUI increases as the number of transmit-antennas increases where the trend of the MUI with CFO and SCFO is conserved as depicted in Figure 5.57.

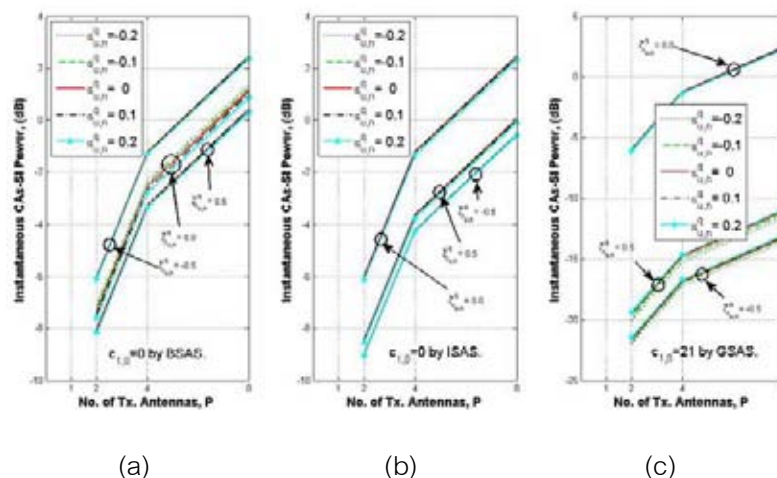


Figure 5.54 Instantaneous Power of the CAs-SI versus the Number of Transmit Antennas at: (a) $c_{1,0}=0$ Allocated by BSAS, (b) $c_{1,0}=0$ Allocated by ISAS, (c) $c_{1,0}=-21$ Allocated by GSAS for $\epsilon_{1,n}^q \in [-0.5, -0.1, 0, 0.1, 0.5]$ and $\xi_{1,n}^q = -0.5, 0$ and 0.5 .

Table 5.9 The Instantaneous asynchronous CAs-SI with CFO and SCFO for different SAS and $P=2$

CAs-SI (dB)	$\epsilon_{1,n}^q = -0.1$		$\epsilon_{1,n}^q = 0.0$		$\epsilon_{1,n}^q = 0.1$	
	$\xi_{1,n}^q = -0.1$	$\xi_{1,n}^q = 0.1$	$\xi_{1,n}^q = -0.1$	$\xi_{1,n}^q = 0.1$	$\xi_{1,n}^q = -0.1$	$\xi_{1,n}^q = 0.1$
BSAS	-6.5119	-6.2351	-6.6102	-6.0995	-6.8275	-6.1636
ISAS	-6.9183	-6.3589	-6.8006	-6.2051	-6.9175	-6.3574
GSAS	-26.6229	-25.4349	-28.9614	-27.2901	-29.7956	-26.7815

C. Instantaneous SINR in Presence of CFO and SCFO

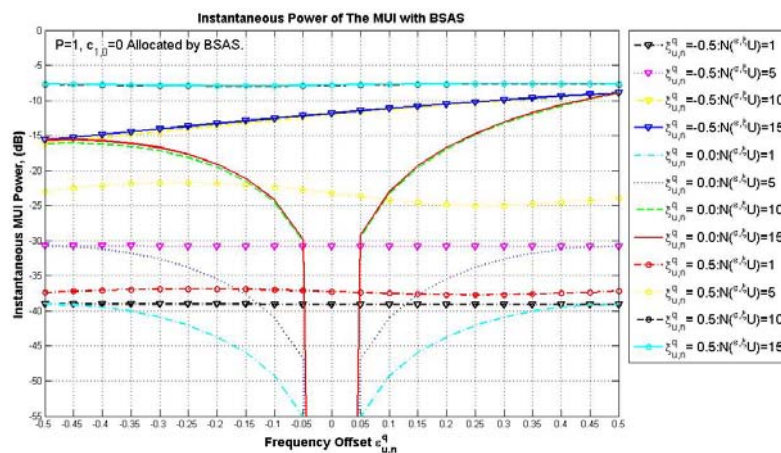
The properties of the instantaneous SINR in presence of the CFO and/or SCFO are reflection of the studied trends of the interference sources in the preceding subsection. Figures 5.58 and 5.59 shows the effect of the synchronization offsets and the number of asynchronous users on the instantaneous SINR.

In the ideal synchronization offset scenario, the instantaneous SINR is very large i.e., >120 dB, which it declines dramatically when CFO and/or SCFO incurs. For example,

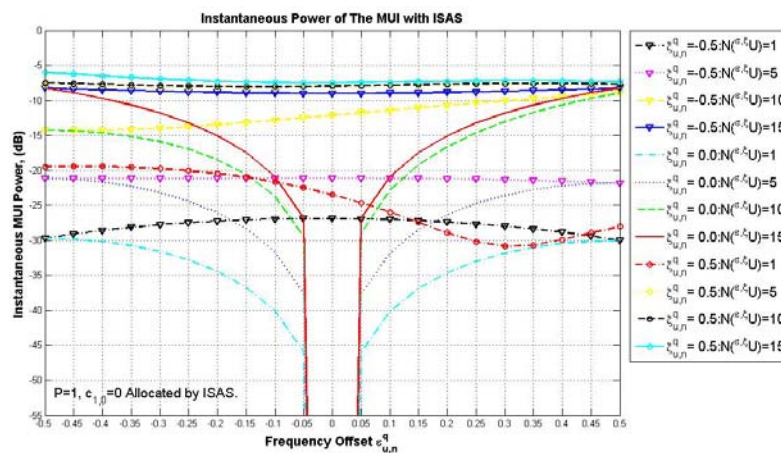
with $\xi_{u,n}^a = 0$, $N(\varepsilon, \xi U) = 1$ and $P=1$, the instantaneous SINR reduces from 137.0309dB with $\varepsilon_{u,n}^a = 0$ to 33.2836dB (33.2766dB) with $\varepsilon_{u,n}^a = -0.1(0.1)$ as in Figures 5.58 and 5.59.

Alternatively, consider $\varepsilon_{u,n}^a = 0$, $N(\varepsilon, \xi U) = 1$ and $P=1$, the instantaneous SINR reduces from 137.0309dB with $\xi_{u,n}^a = 0$ to -3.0580dB (-9.8964dB) with $\xi_{u,n}^a = -0.1(0.1)$. Therefore, it can be concluded that the SCFO is more severe than the CFO to the system performance. This also can be recognized from the interference coefficient in equations (3.64) and (3.65).

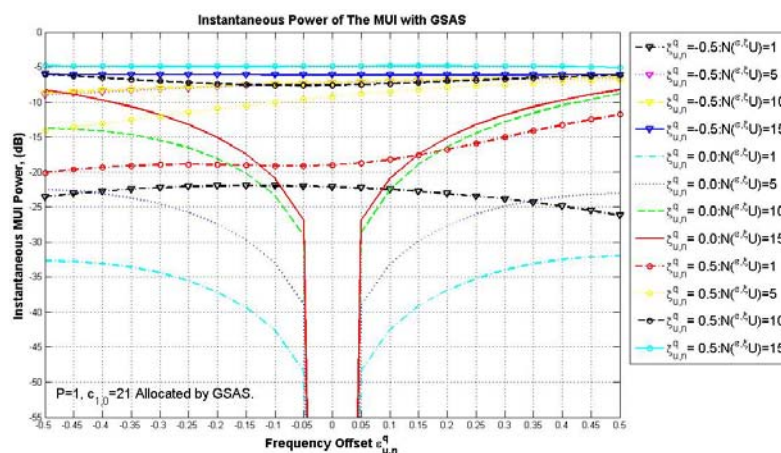
However, in asynchronous desired user mode, the ISAS performs the BSAS and GSAS where high performance is obtained. For example, with $\varepsilon_{u,n}^a = \xi_{u,n}^a = -0.5(0.5)$, $N(\varepsilon, \xi U) = 1$ and $P=1$, the instantaneous SINR is 8.6290dB (8.5114dB), 14.4379dB (9.6972dB), and 1.1399dB (-9.8964dB) at $c_{u,0}$ allocated by BSAS, ISAS and GSAS respectively. Due to exploit the same subcarriers by each simultaneous transmit antennas in the MIMO-OFDAM uplink system, increase the number of transmit-antennas, degrades the instantaneous SINR at the DFT output as depicted in Figure 5.60.



(a)

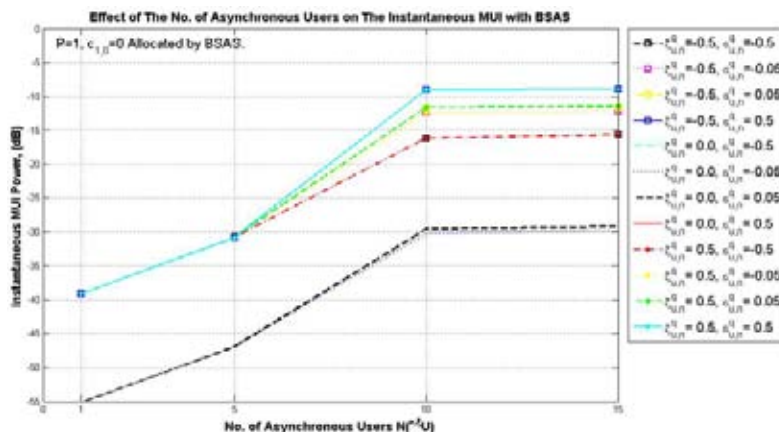


(b)

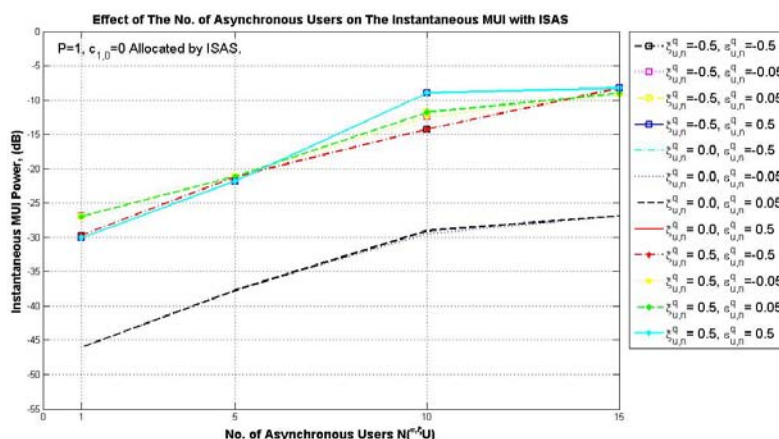


(c)

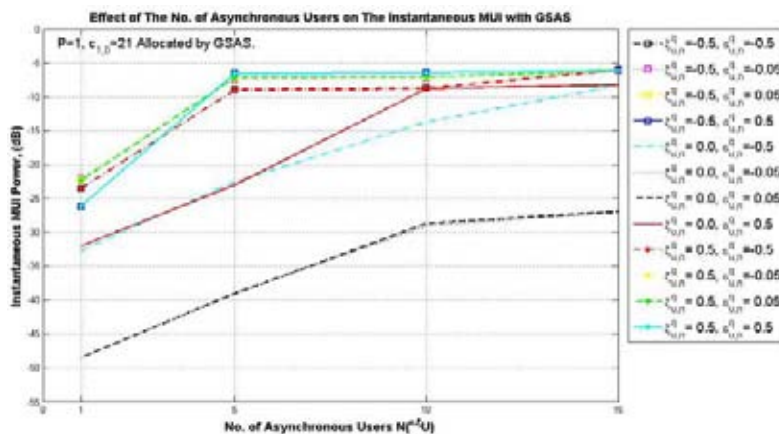
Figure 5.55 Instantaneous MUI for $N(\epsilon_{u,n}^q) \neq \emptyset$, $\xi_{u,n}^q = \{-0.5, 0, 0.5\}$ and $\epsilon_{u,n}^q \in [-0.5, 0.5]$ at: (a) $c_{1,0} = 0$ Allocated by BSAS, (b) $c_{1,0} = 0$ Allocated by ISAS, and (c) $c_{1,0} = 21$ Allocated by GSAS for $P=1$



(a)

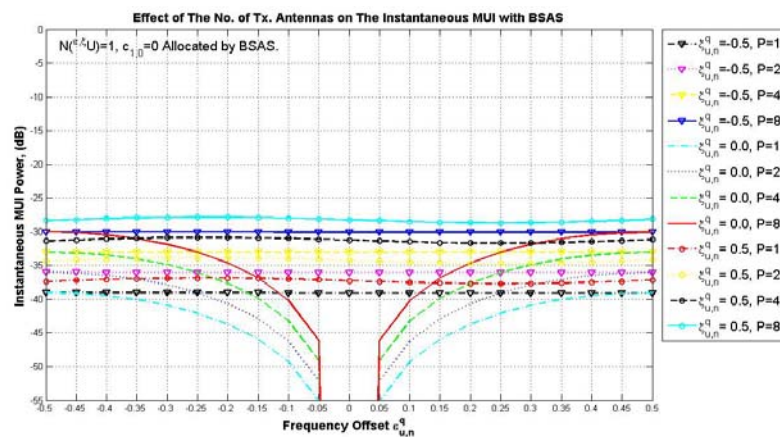


(b)

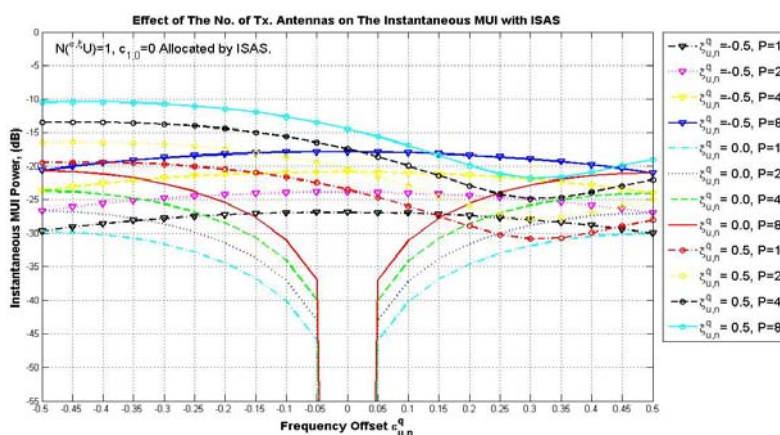


(c)

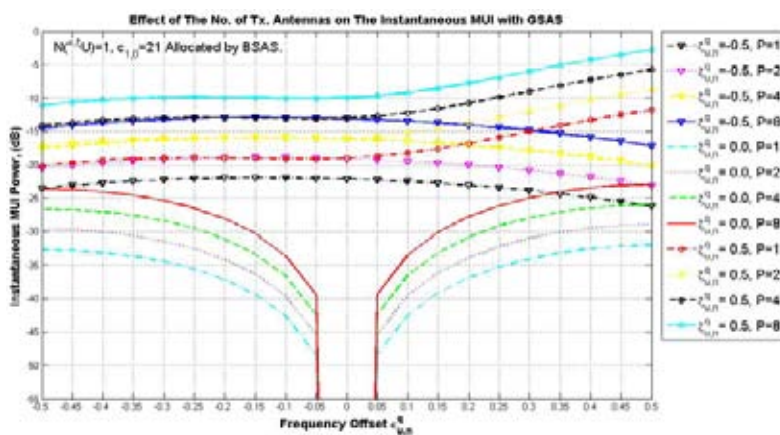
Figure 5.56 Effects of Number of Asynchronous Users $N(\epsilon, \xi)U$ on the instantaneous MUI at: (a) $c_{1,0}=0$ Allocated by BSAS, (b) $c_{1,0}=0$ Allocated by ISAS, (c) $c_{1,0}=21$ Allocated by GSAS for $\mathcal{E}_{u,n}^q = \{-0.5, -0.05, 0.05, 0.5\}$, $\mathcal{X}_{u,n}^q = \{-0.5, 0.0, 0.5\}$ and $P=1$.



(a)

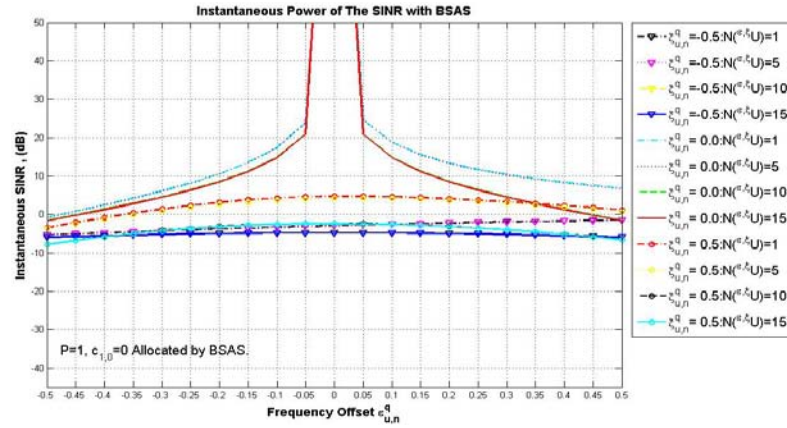


(b)

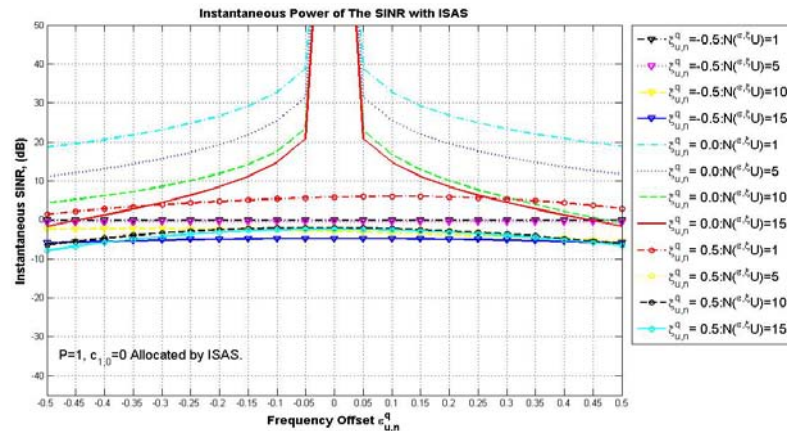


(c)

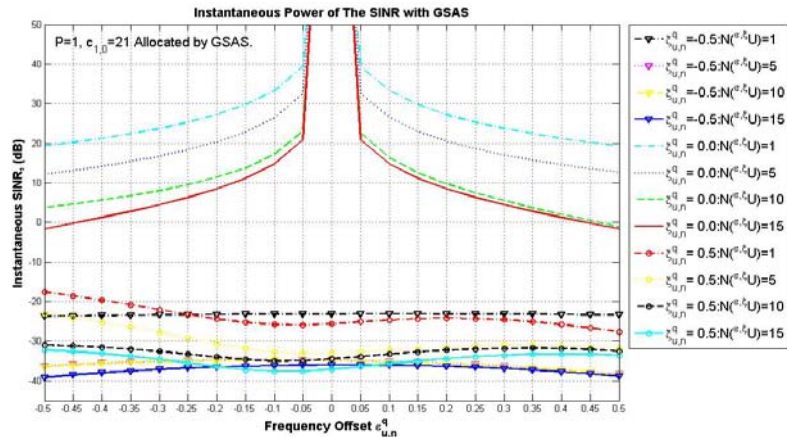
Figure 5.57 Effects of Number of Transmit-Antennas on the Instantaneous Asynchronous MUI at: (a) $c_{1,0}=0$ Allocated by BSAS, (b) $c_{1,0}=0$ Allocated by ISAS, (c) $c_{1,0}=21$ Allocated by GSAS for $N^{\epsilon, \xi} U=1$, $\epsilon_{u,n}^q \in [-0.5, 0.5]$, and $\xi_{u,n}^q = \{-0.5, 0.0, 0.5\}$



(a)

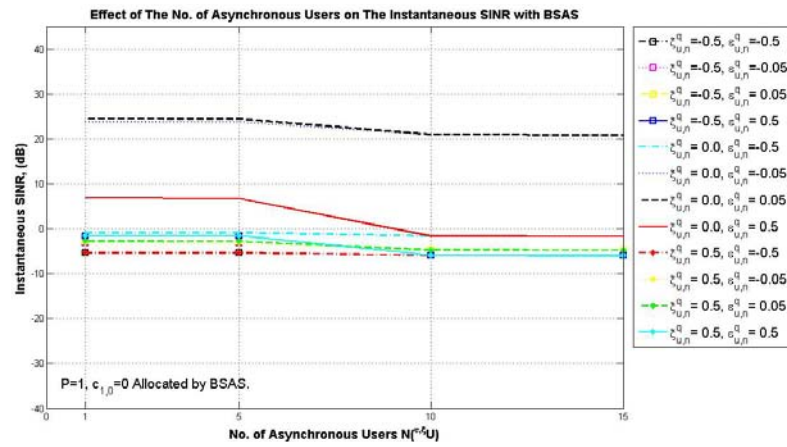


(b)

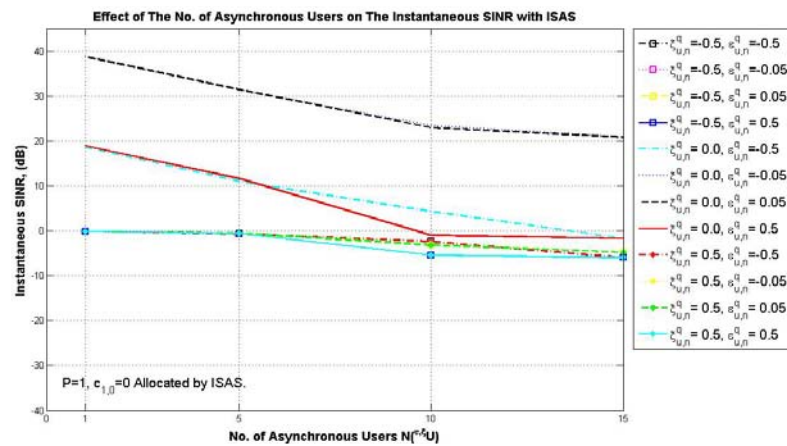


(c)

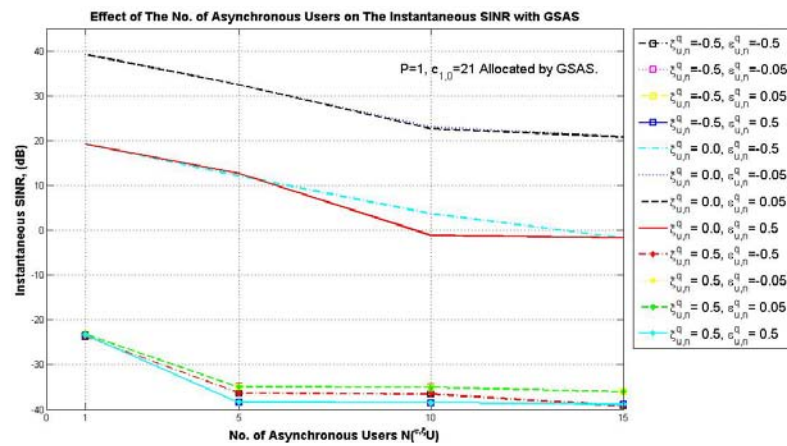
Figure 5.58 Instantaneous SINR for $N(\epsilon_{u,n}^q) \neq \emptyset$, $\xi_{u,n}^q = \{-0.5, 0, 0.5\}$ and $\epsilon_{u,n}^q \in [-0.5, 0.5]$ at: (a) $c_{1,0} = 0$ Allocated by BSAS, (b) $c_{1,0} = 0$ Allocated by ISAS, and (c) $c_{1,0} = 21$ Allocated by GSAS for $P=1$



(a)

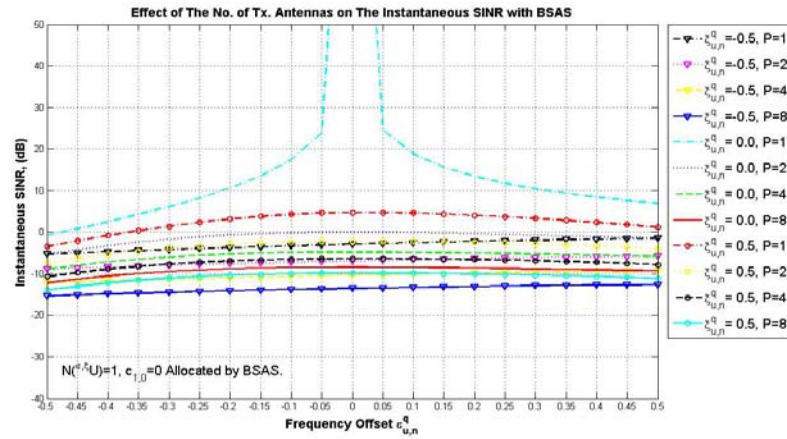


(b)

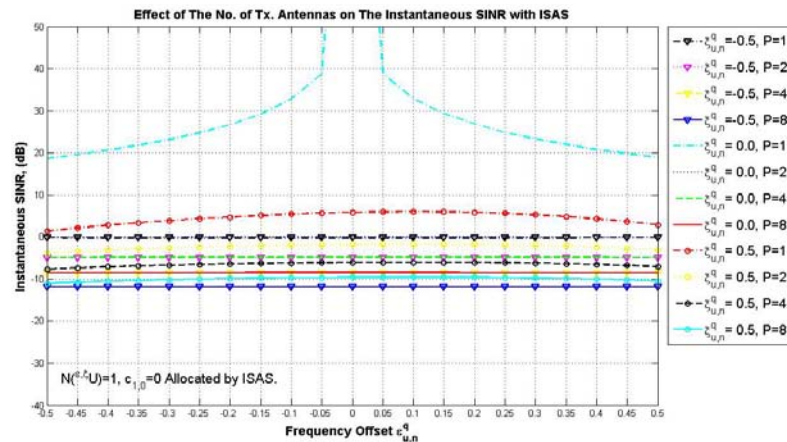


(c)

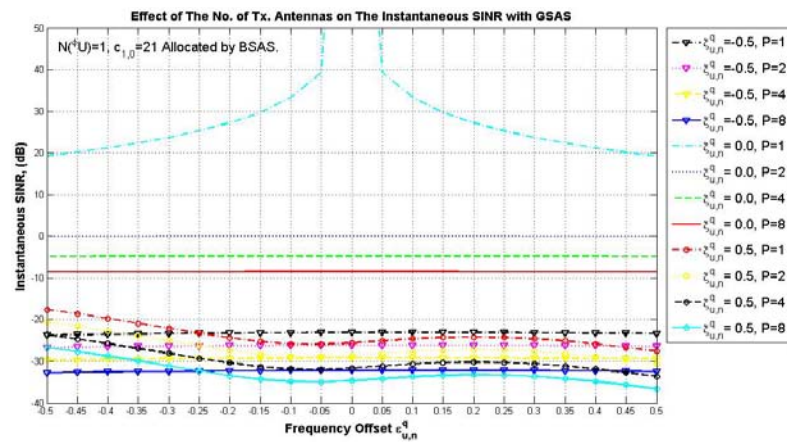
Figure 5.59 Effects of Number of Asynchronous Users $N^{(\epsilon, \xi)U}$ on the Instantaneous SINR at: (a) $c_{1,0}=0$ Allocated by BSAS, (b) $c_{1,0}=0$ Allocated by ISAS, (c) $c_{1,0}=21$ Allocated by GSAS for $\mathcal{E}_{u,n}^q = \{-0.5, -0.05, 0.05, 0.5\}$, $\mathcal{X}_{u,n}^q = \{-0.5, 0.0, 0.5\}$ and $P=1$



(a)



(b)



(c)

Figure 5.60 Effects of Number of Transmit-Antennas on the Instantaneous Asynchronous SINR at: (a) $c_{1,0} = 0$ Allocated by BSAS, (b) $c_{1,0} = 0$ Allocated by ISAS, (c) $c_{1,0} = 21$ Allocated by GSAS for $N(\xi, \xi U) = 1$, $\xi_{u,n}^q \in [-0.5, 0.5]$, and $\xi_{u,n}^q = \{-0.5, 0.0, 0.5\}$

CHAPTER VI

CONCLUSIONS AND RECOMMENDATIONS

6.1. Introduction

In this chapter, a brief summary for the conducted research and the obtained results are presented. Some recommendations and suggestions for extending the research are also introduced.

6.2. Research Overview and Conclusions

This thesis investigates the impact of synchronization offsets on the performance of the uplink MIMO-OFDMA systems over multipath fading channel in terms of SINR at the DFT output of the receiver. A general equivalent model for asynchronous single-user with single-transmit antenna is derived first, for uplink scenario. With this model, expressions for the desired signal (DS), ISI and ICI at the DFT output of the BS's receive antenna. More specifically, and with TO, an extra wide range of the time offset is proposed to comprehensively analyze the incurred interferences. A generalization to asynchronous multiuser MIMO-OFDMA system, where the interferences caused by the multiuser and the multiple antenna, have been achieved. The derived signal expressions are based on the contents of the DFT window along the channel paths. In addition, the instantaneous and average SINR is evaluated whereas the signal components are defined. Moreover, the obtained SINR is exploited to derive the BER/SER at the DFT output.

The system performance evaluation is carried out for arbitrary Subcarrier Allocation Schemes (SASs), and MIMO systems properties as well as various CP conditions, where there is no prior assumption on the interferences' statistical properties.

From the obtained results, the following conclusions can be drawn:

- i. Exploiting sufficient CP in OFDMA symbol eliminates and alleviates the potential of the interference generated by the synchronization offsets especially the TO towards the CP.

- ii. Using sufficient CP and synchronization offset mitigation/alleviation techniques such as ranging and estimation algorithms, which guarantee that the TO lies within the effective CP duration, is important in order to obtain a feasible system performance.
- iii. The BSAS is shown to be more robust to the synchronization offsets than the ISAS and GSAS respectively, for synchronous desired user mode. In asynchronous desired user mode, the ISAS is robust to the synchronization than the GSAS and BSAS respectively.
- iv. Coexistence of more than one type of synchronization offset adds additional degradation to the system performance.
- v. The synchronization offset that produces ISI and ICI are more severe to the system performance than the one that produce only ICI, therefore the TO and SCFO are more severe than the CFO.
- vi. The average incurred interference power decreases as the asynchronous region shortens.

The comprehensive analysis of the trend of the synchronization offsets and its impact on the MIMO-OFDMA uplink system performance, provide a useful reference or test bed in designing suitable synchronization algorithms as well as performance evaluation for related applications.

6.3. Recommendation for Future Work

To complete uncovered area in this research, the following works are proposed for future:

- i. To fully investigate the impact of the synchronization offsets, the Doppler's effect may be included in the derivation and simulation, which is one of the causes of the carrier frequency offset.
- ii. The other scenarios of the CP such as zero padding and known signal prefix, may need to be investigated also, and compared with the addressed CP scenarios in this thesis in presence of synchronization offsets.

- iii. The impact of the other types of the channel such as Rician and m-Nakagami fading channel on the synchronization offsets can be explored in combining with the mobility effects such as Doppler's effect.
- iv. The achieved analysis of the SCFO using the contents of the DFT window may need to be compared with the analysis that considers it as a phase noise.
- v. The coexistence of the TO, CFO and SCFO is not addressed in this thesis, where the coexistence of the TO and SCFO need to be handled carefully because of the produced ISI in both offsets.
- vi. According to the achieved performance measurement, and the comprehensive studies on the impacts of the synchronization offsets, a suitable joint estimation algorithm can be designed.

LIST OF REFERENCES

- 3GPP TR 25.814. Physical Layer Aspects for Evolved UTRA. Release 7, June 2005.
- 3GPP TR 29.913. Requirements for Evolved UTRA and Evolved UTRAN. Release 7, June 2005.
- 802.16a. Amendment to IEEE Standard for Local and Metropolitan Area Networks - Part 16: Air Interface for Fixed Broadband Wireless Access Systems - Medium Access Control Modifications and Additional Physical Layer Specifications for 2-11 GHz, 2003.
- Armstrong, J. Analysis of New and Existing Methods of Reducing Inter-carrier Interference Due to Carrier Frequency Offset In OFDM. IEEE Transaction on Communications, 47, 3 (March 1999): 365-369.
- Athaudage, C. R. N. BER Sensitivity of OFDM Systems to Time Synchronization Error. Proceedings of the 8th IEEE International Conference on Communication Systems (ICCS'02), 25-28 November 2002, 1, pp. 42- 46. : IEEE, 2002.
- Athaudage, C. R. N., and Sathananthan, K. Probability of Error of Space-Time Coded OFDM Systems with Frequency Offset in Frequency-Selective Rayleigh Fading Channels. Proceedings of IEEE International Conference on Communications (ICC05), 16-20 May 2005, 4, pp. 2593- 2599. : IEEE, 2005.
- Baoguo, Y., Letaief, K. B., Cheng, R. S., and Zhigang, C. Timing Recovery For OFDM Transmission. IEEE Journal on Selected Areas in Communications 18, 11 (November 2000): 2278– 2291.
- Barbarossa, S., Pompili, M., and Giannakis, G. B. Channel-Independent Synchronization of Orthogonal Frequency Division Multiple Access Systems. IEEE Journal on Selected Areas in Communications 20, 2 (February 2002): 474– 486.
- Bliss, D.W. and Parker, P. A. Temporal Synchronization of MIMO Wireless Communication in the Presence of Interference. IEEE Transaction on Signal Processing 58, 3 (March 2010): 1794- 1806.

- Cao, Z., Tureli, U., and Yao, Y. Deterministic Multiuser Carrier-Frequency Offset Estimation for Interleaved OFDMA Uplink. IEEE Transactions on Communications 52, 9 (September 2004): 1585 - 1594.
- Cao, Z., Turelli, U., and Yao, Y. D. Efficient Structure-Based Carrier Frequency Offset Estimation for Interleaved OFDMA Uplink. Proceedings of IEEE International Conference on Communications (ICC03), 11-15 May 2003, 5, pp. 3361– 3365. : IEEE, 2003.
- Chen, J., Wu, Y., Ma, S., and Ng, T. Joint CFO and Channel Estimation for Multiuser MIMO-OFDM Systems with Optimal Training Sequences. IEEE Transactions on Signal Processing 56, 8 (August 2008): 4008– 4019.
- Chin, W. –L., and Chen, S. –G. Theoretical Analysis of Joint Synchronization Error Effects For OFDMA Systems. Proceedings of IEEE Conference on Vehicular Technology (VTC), 11-14 May 2008, pp. 1930– 1934, 2008.
- Choi, K. Error Probability of Q-ary Symbol Consisting of Multiple Channel Symbols under Rayleigh Fading. IEEE Communications Letters 8, 1(January 2004): 48-50.
- Ciblat, P. and Vandendorpe, L. On the Maximum-Likelihood Based Data-Aided Joint Frequency Offset and Channel Estimation. Proceedings of European Signal Processing Conference (EUSIPCO), September 2002, pp. 627–630. Toulouse, France, 2002.
- Ciblat, P., Loubaton, P., Serpedin, E., and Giannakis, G. B. Performance of Blind Carrier-Offset Estimation for Non-Circular Transmissions through Frequency-Selective Channels. IEEE Transaction on Signal Processing 50, 1 (January 2002): 130– 140.
- Czylwik, A. Synchronization for Systems with Antenna Diversity. Proceedings of the 50th IEEE Vehicular Technology Conference (VTC), September-Fall 1999, 2, pp. 728-732. : IEEE, 1999.
- Dwight, H. B. Tables of Integrals and other Mathematical Data. 3rd Edition, New York: The Macmillan Company, 1957.

- El-Tanany, M., S., Wu, Y., and Hazy, L. OFDM Uplink for Interactive Broadband Wireless: Analysis and Simulation In The Presence of Carrier, Clock and Timing Errors. IEEE Transaction on Broadcasting 47, 1 (March 2001): 3– 19.
- Engels, M. Wireless OFDM Systems- How to Make Them Work?. New York: Kluwer Academic Publishers, May 2002.
- Fantacci, R., Marabissi, D., and Papini, S. Multiuser Interference Cancellation Receivers For OFDMA Uplink Communications With Carrier Frequency Offset. Proceedings of IEEE Global Telecommunications Conference (GLOBECOM '04), 29 November-3 December 2004, 5, pp. 2808 – 2812. : IEEE, 2004.
- Fazel, K., and Kaizer, S. Multi-Carrier and Spread Spectrum Systems: From OFDM and MC-CDMA to LTE and WiMax. 2nd Edition. London: John Wiley and Sons Inc., 2008.
- Fazel, K., and Kaizer, S. Multi-Carrier and Spread Spectrum Systems. London: John Wiley and Sons Inc., 2003.
- Foschini, G. J., and Gans, M.J. On Limits of Wireless Communications in a Fading Environment when Using Multiple Antennas. Wireless Personal Communications 6 (1998): 311- 335.
- Fuchs, J. Multipath Time-Delay Detection and Estimation. IEEE Transaction on Signal Processing 47, 1 (January 1999): 237– 243.
- Gallardo, A.M., Woodward, M.E., and Rodriguez-Tellez, J. Performance of DVB-T OFDM Based Single Frequency Networks: Effects of Frame Synchronization, Carrier Frequency Offset and Non-Synchronized Sampling Errors. Proceedings of the 54th IEEE Vehicular Technology Conference (VTC2001), October-Fall 2001, 2, pp. 962-966. : IEEE, 2001.
- Gao, J., Zhu, X., Wu, Y., and Nandi, A. K. Adaptive Frequency-Domain Channel Estimation Based on Kalman Smoothing for Uplink MIMO-OFDMA Systems. Proceedings of the 4th IEEE International Conference on Computers and Devices for Communication (CODEC), 14-16 December 2009, pp. 1– 4. : IEEE, 2009.

- Gesbert, D., Shafi, M., Shiu, D., Smith, P. J., and Naguib, A. From Theory to Practice: An Overview of MIMO Space-Time Coded Wireless Systems. IEEE Journal on Selected Areas in Communications 21, 3 (April 2003): 281– 302.
- Hamdi, K. A. Precise Interference Analysis of OFDMA Time-Asynchronous Wireless Ad-hoc Networks. IEEE Transactions on Wireless Communications 9, 1 (January 2010): 134-144.
- Hanzo, L., Münster, M., Choi, B. J., and Keller, T. OFDM and MC-CDMA for Broadband Multi-User Communications, WLAN's and Broadcasting. New York: Wiley, 2003.
- Hara, S., and Prasad, R. Overview of Multicarrier CDMA. Proceedings of IEEE Communications Magazine, 35, 12 (December 1997): 126– 133.
- Holma, H., and Toskala, A. WCDMA for UMTS. John Wiley and Sons Ltd., 2000.
- Horlin, F., De Rore, S., Lopez-Estraviz, E., Naessens, F., and Van der Perre, L. Impact of Frequency Offsets and IQ Imbalance on MC-CDMA Reception Based on Channel Tracking. IEEE Journal on Selected Areas in Communications 24, 6 (June 2006): 1179- 1188.
- Huang, D., Letaief, K. B. An interference-cancellation scheme for carrier frequency offsets correction in OFDMA systems. IEEE Transactions on Communications 53, 7 (July 2005): 1155 – 1165.
- Huang, W., Li, C., and Li, H. An Investigation into the Noise Variance and the SNR Estimators in Imperfectly-Synchronized OFDM Systems. IEEE Transaction on Wireless Communications 9, 3 (March 2010): 1159– 1167.
- Ibars, C., and Bar-Ness, Y. Comparing the Performance of Coded Multiuser OFDM and Coded MC-CDMA over Fading Channels. Proceedings of IEEE Global Telecommunications Conference (GLOBECOM '01), November 2001, 2, pp. 881– 885. : IEEE, 2001.
- Il-Gu, L., Eunyoung, C., Sok-Kyu, L., and Taehyun, J. High Accuracy and Low Complexity Timing Offset Estimation for MIMO-OFDM Receivers. Proceedings of IEEE Wireless Communications and Networking Conference (WCNC06), 3-6 April 2006, 3, pp. 1439– 1443. : IEEE, 2006.

- ITU-R M.1225. Guideline for Evaluation of Radio Transmission Technologies for IMT-2000. 1997.
- Jeffrey, A., Dai, H.-H. Handbook of Mathematical Formulas and Integrals. 4th Edition. Academic Press, 2008
- Jiang, Z., Li, Z., Zhang, X., and Yang, D. Joint Frequency Offset and Channel Estimation Using Rao-Blackwellized Particle Filter for Uplink MIMO-OFDMA Systems. Proceedings of IEEE International Conference on Communications (ICC'08), 19-23 May 2008, pp. 698– 702. : IEEE, 2008.
- Jiang, Z., Zhang, Y., and Zhang, X. Carrier Frequency Offset Estimation Using Likelihood Particle Filter for Uplink MIMO-OFDMA Systems. Proceedings of IEEE Conference on Vehicular Technology (VTC'08), 11-14 May 2008, pp. 1281– 1285. ; IEEE, 2008.
- Jung, H., Zoltowski, M.D. Timing and Frequency Offset Estimation in Asynchronous Multi-User OFDM Systems. Proceedings of IEEE Military Communications Conference (MILCOM 2004), October-November 2004, 3, pp. 1491-1495. : IEEE, 2004.
- Juntti, M., Vehkaperä, M., Leinonen, J., Li, Z., Tujkovic, D., Tsumura, S., and Hara, S. MIMO MC-CDMA Communications for Future Cellular Systems. Proceedings of IEEE Communications Magazine 43, 2 (February 2005): 118– 124.
- Kaiser, S., and Fazel, K. A Spread-Spectrum Multicarrier Multiple-Access System for Mobile Communications. Proceedings of the 1st IEEE International Workshop on Multicarrier Spread Spectrum, April 1997, pp. 49–56. : IEEE, 1997.
- Kim, K. J., Pun, M., and Iltis, R. A. Joint Carrier Frequency Offset and Channel Estimation for Uplink MIMO-OFDMA Systems Using Parallel Schmidt Rao-Blackwellized Particle Filters. IEEE Transactions on Communications 58, 9 (September 2010): 2697- 2708.
- Koivisto, T., and Koivunen, V. Impact of Time and Frequency Offsets on Cooperative Multi-User MIMO-OFDM Systems. Proceedings of the 20th IEEE International

- Symposium on Personal Indoor and Mobile Communications, 13-16 September 2009, pp. 3119- 3123. : IEEE, 2009.
- Kotzsch, V., and Fettweis, G. Interference Analysis in Time and Frequency Asynchronous Network MIMO OFDM Systems. Proceedings of IEEE Wireless Communications and Networking Conference (WCNC), 18-21 April 2010, pp.1-6. : IEEE, 2010.
- Kotzsch, V., Rave, W., and Fettweis, G. ISI Analysis in Network MIMO OFDM Systems with Insufficient Cyclic Prefix Length. Proceedings of the 7th IEEE International Symposium on Wireless Communication Systems (ISWCS), 19-22 September 2010, pp: 189- 193. : IEEE, 2010.
- Langowski, A. Carrier and Sampling Frequency Offset Estimation and Tracking In OFDM Systems. Proceedings of the 16th IEEE International Conference on Software, Telecommunications and Computer Networks (SoftCOM'08), 25-27 September 2001, pp. 319-323. : IEEE, 2001.
- Laourine, A., Stephenne, A., and Affes, S. Blind Sampling Clock Offset Estimation in OFDM Systems Based on Second Order Statistics. Proceedings of the 40th IEEE Conference on Signals, Systems and Computers (ACSSC '06), 29 October-1 November 2006, pp. 1782– 1785. : IEEE, 2006.
- Lashkarian, N., and Kiaei, S. Globally Optimum ML Estimation of Timing and Frequency Offset in OFDM Systems. Proceedings of IEEE International Conference on Communications, June 2000, 2, pp. 1044- 1048. : IEEE, 2000.
- Lee, I.-G., Choi, E., Lee, S.-K., Jeon, T. High Accuracy And Low Complexity Timing Offset Estimation for MIMO-OFDM Receivers. Proceedings of IEEE Wireless Communications and Networking Conference (WCNC2006), 3-6 April 2006, 3, pp. 1439 – 1443. : IEEE, 2006.
- Lee, J., Lou, H. L., Toumpakaris, D., and Cioffi, J. M. Effect of Carrier Frequency Offset on OFDM Systems for Multipath Fading Channels. Proceedings of IEEE Global Telecommunications Conference (GLOBECOM'04), 29 November-3 December 2004, 6, pp. 3721- 3725. : IEEE, 2004.

- Lee, Y., and Park, H. Low-Complexity Detections for Downlink MIMO-MC-CDMA Systems. Proceedings of the 17th IEEE International Symposium on Personal, Indoor and Mobile Radio Communications, 11-14 September 2006, pp. 1- 5. : IEEE, 2006.
- Lin, J. M., Ma, H. P., and Ting, P. A Baseband Transceiver for IEEE 802.16e-2005 MIMO-OFDMA Uplink Communications. Proceedings of IEEE Global Telecommunications Conference (GLOBECOM '07), 26-30 November 2007, pp. 4291– 4295. : IEEE, 2007.
- Lin, J.-M., Ma, H.-P. A High Performance Baseband Transceiver for SISO-/MIMO-OFDA Uplink Communications. IEEE Transactions on Wireless Communications 8, 7, (July 2009): 3330-3334.
- Lin, J.-M., Yu, H.-Y., Wu, Y.-J., and Ma, H.-P. A Power Efficient Baseband Engine for Multiuser Mobile MIMO-OFDMA Communications. IEEE Transactions on Circuits and Systems 57, 7 (July 2010): 1779-1792.
- Lindner, J., Nold, M., Teich, W., and Shreiner, M. MC-CDMA and OFDMA for Indoor Communications: The Influence of Multiple Receiving Antennas. Proceedings of the 5th IEEE International Symposium on Spread Spectrum Techniques and Applications (ISSSTA) 2-4 September, 1, pp. 189– 194. : IEEE, 1998.
- Liu, H., and Tureli, U. A High Efficiency Carrier Estimator for OFDM Communications. IEEE Communication Letters 2, 4 (April 1998): 104- 106.
- Liu, Y., Peng, D., Peng, L., and Chen, C. The Spatial Diversity Algorithm of Sampling Clock Synchronization in MIMO-OFDM Systems. Proceedings of the 4th IEEE International Conference on Wireless Communications Networking and Mobile Computing (WiCOM-08), 12-14 October 2008, pp. 1- 4. : IEEE, 2008.
- Lo, E. S., Chan, P. W. C., Lau, V. K. N., Cheng, R. S. , Letaief, K. B., Murch, R. D., and Mow, W. Ho. Adaptive Resource Allocation and Capacity Comparison of Downlink Multiuser MIMO-MC-CDMA and MIMO-OFDMA. IEEE Transactions on Wireless Communications 6, 3 (March 2007): 1083– 1093.

- Lv, T., and Chen, J. ML Estimation Of Timing And Frequency Offset Using Multiple OFDM Symbols In OFDM Systems. Proceedings of IEEE Global Telecommunications Conference (GLOBECOM03), 1-5 December 2003, 4, pp. 2280– 2284. : IEEE, 2003.
- Mahmoud, H. A. Advanced Transceiver Algorithms for OFDM(A) Systems. Doctoral Dissertation, Department Of Electrical Engineering, College of Engineering, University of South Florida, March 2009.
- Manohar, S., Sreedhar, D., Tikiya, V., and Chockalingam, A. Cancellation of Multiuser Interference Due to Carrier Frequency Offsets in Uplink OFDMA. IEEE Transactions on Wireless Communications 6, 7 (July 2007): 2560 – 2571.
- Mody, A. N., and Stuber, G. L. Synchronization for MIMO-OFDM Systems. Proceedings of IEEE Global Communications Conference, November 2001, 1, pp. 509- 513. : IEEE, 2001.
- Moose, P. H. A Technique for Orthogonal Frequency Division Multiplexing Frequency Offset Correction. IEEE Transaction on Communications 42, 10 (October 1994): 2908- 2914.
- Morelli, M. and Mengali, U. Carrier-Frequency Estimation for Transmissions over Selective Channels. IEEE Transaction on Communications 48, 9 (September 2000): 1580- 1589.
- Morelli, M. Timing and frequency Synchronization for the Uplink of an OFDMA System. IEEE Transaction on Communications 52, 2 (February 2004): 296- 306.
- Morelli, M., Moretti, M. Fine Carrier and Sampling Frequency Synchronization In OFDM Systems. IEEE Transactions on Wireless Communications 9, 4 (April 2010): 1514-1524.
- Mostofi, Y., and Cox, D. C. Mathematical Analysis of the Impact of Timing Synchronization Errors on the Performance of an OFDM System. IEEE Transaction on Communications 54, 2 (February 2006): 226- 230.

- Nguyen-Le, H., Le-Ngoc, T., and Ko, C.C. RLS-Based Joint Estimation and Tracking of Channel Response, Sampling, and Carrier Frequency Offsets for OFDM. IEEE Transactions on Broadcasting. 55, 1 (March 2009): 84-94.
- Nishookar, H., and Prasad, R. On the Sensitivity of Multicarrier Transmission over Multipath Channels to Phase Noise and Frequency Offset. Proceedings of IEEE Personal Indoor Mobile Radio Communications Conference, 15-18 October 1996, 1, pp. 68- 72. : IEEE, 1996.
- Papoulis, A. Probability, Random Variable and Stochastic Processes. New York: McGraw-Hill, Inc., 1965.
- Park, M., Ko, K., Park, B., and Hong, D. Effects of Asynchronous MAI on Average SEP Performance of OFDMA Uplink Systems Over Frequency-Selective Rayleigh Fading Channels. IEEE Transactions on Communications 58, 2 (February 2010): 586- 599.
- Park, M., Ko, K., Yoo, H., and Kong, D. Performance Analysis of OFDMA Uplink Systems With Symbol Timing Misalignment. IEEE Communication Letters 7, 8 (August 2003): 376- 378.
- Peng, Z., Ming, J., Chunming Z., and Wei, X. Error Probability of OFDM Systems Impaired by Carrier Frequency Offset in Frequency Selective Rayleigh Fading Channels. Proceedings of IEEE International Conference on Communications (ICC '07), 24-28 June 2007, pp. 1065– 1070. : IEEE, 2007.
- Phasouliotis, A., and So., D. K.C. A Novel OSSMIC Receiver for Downlink MIMO MC-CDMA Systems. Proceedings of IEEE Vehicular Technology Conference (VTC), 11-14 May 2008, pp. 1271- 1275. : IEEE, 2008.
- Phasouliotis, A., and So., D. K.C. Performance Analysis and Comparison of Downlink MIMO MC-CDMA and MIMO OFDMA Systems. Proceedings of the 69th IEEE Vehicular Technology Conference (VTC), 26-29 April 2009, pp. 1- 6. : IEEE, 2009.

- Pollet, T., Bladel, M. V., and Moeneclaey, M. BER Sensitivity of OFDM Systems to Carrier Frequency Offset and Wiener Phase Noise. IEEE Transaction on Communications 43, 234 (February 1995): 191- 193.
- Pollet, T., Spruyt, P., and Moeneclaey, M. The BER Performance of OFDM Systems Using Non-Synchronized Sampling. Proceedings of IEEE Global Telecommunications Conference (GLOBECOM '94), 28 November-2 December 1994, 1, pp. 253-257. : IEEE, 1994.
- Prema, G., and Ananthi, P. Joint Timing, Carrier Frequency and Sampling Clock Offset Estimation for MIMO OFDM WLAN Systems. Proceedings of IEEE International Conference on Process Automation, Control and Computing (PACC), 20-22 July 2011, pp. 1-6, 2011.
- Proakis, J. G. Digital Communications. 4th Edition. McGraw-Hill Series in Electrical and Computer Engineering, 2001.
- Proakis, J. G., and Salehi, M. Digital Communications. 5th Edition. Singapore: McGraw-Hill Companies, Inc., 2008.
- Pun, M. O., Morelli, M., and Kuo, C. C. J. Maximum-Likelihood Synchronization and Channel Estimation for OFDMA Uplink Transmissions. IEEE Transaction on Communications 54, 4 (April 2006): 726- 736.
- Raghunath, K. and Chockalingam, A. BER Analysis of Uplink OFDMA in the Presence of Carrier Frequency and Timing Offsets on Rician Fading Channels. Proceedings of IEEE International Conference on Communications (ICC10), 23-27 May 2010, pp.1- 5. : IEEE, 2010.
- Raghunath, K., and Chockalingam, A. SIR Analysis and Interference Cancellation in Uplink OFDMA with Large Carrier Frequency and Timing Offsets. IEEE Transaction on Wireless Communication 8, 5 (May 2009): 2202- 2208.
- Rugini, L., and Banelli, P. BER of OFDM systems Impaired by Carrier Frequency Offset in Multipath Fading Channels. IEEE Transaction on Wireless Communications 4, 5 (September 2005): 2279- 2288.

- Saemi, A., Cances, J. P., and Meghdadi, V. Synchronization Algorithms for MIMO OFDMA Systems. IEEE Transaction on Wireless Communications 6, 12 (December 2007): 4441- 4451.
- Santella, G. Frequency and Symbol Synchronization System of OFDM Signals: Architecture and Simulation Results. IEEE Transaction on Vehicular Technology 49, 1 (January 2000): 254- 275.
- Sathananthan, K., and Tellambura, C. Probability of Error Calculation of OFDM Systems with Frequency Offset. IEEE Transaction on Communications 49, 11 (November 2001):1884- 1888.
- Schenk, C. W., and Van Zelst, A. Frequency Synchronization for MIMO OFDM Wireless LAN Systems Time. Proceedings of the 58th IEEE Vehicular Technology Conference (VTC), 6-9 October 2003, 2, pp. 781- 785. : IEEE, 2003.
- Schmidl, T. M., and Cox, D. C. Robust Frequency and Timing Synchronization for OFDM. IEEE Transaction on Communications 45, 12 (December 1997): 1613- 1621.
- Sezginer, S., and Bianchi P. Asymptotically Efficient Reduced Complexity Frequency Offset and Channel Estimators for Uplink MIMO-OFDMA Systems. IEEE Transactions on Signal Processing 56, 3 (March 2008): 964- 979.
- Sezginer, S., and Bianchi, P. Cramér-Rao Bound and Training Sequence Selection for MIMO-OFDMA Transmissions Impaired By Frequency Offsets. Proceedings of IEEE International Conference on Acoustics, Speech and Signal Processing (ICASSP), 14-19 May 2006, 4, pp. 1- 4. : IEEE, 2006.
- Sezginer, S., Bianchi, P., and Hachem, W. Asymptotic Cramér–Rao Bounds and Training Design for Uplink MIMO-OFDMA Systems with Frequency Offsets. IEEE Transactions on Signal Processing 55, 7 (July 2007): 3606- 3622.
- Shaodan, M., Ngai, W., and Tung-Sang, N. Signal Detection for MIMO-OFDM Systems with Time Offsets. Proceedings of IEEE Global Telecommunications Conference (GLOBECOM '06), 27 November-1 December 2006, pp. 1- 5. : IEEE, 2006.

- Simon, E. P., Hijazi, H., and Ros, L. Joint Carrier Frequency Offset and Fast Time-Varying Channel Estimation for MIMO-OFDM Systems. Proceedings of the 7th IEEE International Symposium on Communication Systems Networks and Digital Signal Processing (CSNDSP), 21-23 July 2010, pp. 167– 172. : IEEE, 2010.
- Sliskovic, M. Carrier and Sampling Frequency Offset Estimation and Correction In Multicarrier Systems. Proceedings of IEEE Global Telecommunications Conference (GLOBECOM'01), November 2001, 1, pp. 285-289. : IEEE, 2001.
- Speth, M., Fechtel, S. A., Fock, G., and Meyr, H. Optimum Receiver Design for Wireless Broad-Band Systems Using OFDM- Part I. IEEE Transactions on Communications 47,11 (November 1999): 1668- 1677.
- Stuber, G. L., Barry, J. R., McLaughlin, S. W., Ye, L., Ingram, M. A., and Pratt, T. G. Broadband MIMO-OFDM Wireless Communications. Proceedings of the IEEE 92, 2 (February 2004): 271–294.
- Tomba, L. On the Effect of Wiener Phase Noise in OFDM Systems. IEEE Transactions on Communications 46, 5 (May 1998): 580- 583.
- Tonello, A. M., Laurenti, N., and Pupolin, S. Analysis of the Uplink of An Asynchronous Multi-User DMT OFDMA System Impaired By Time Offsets, Frequency Offsets, and Multi-Path Fading. Proceedings of the 52nd IEEE Vehicular Technology Conference (VTC 2000), September-Fall 2000, 3, pp. 1094– 1099. : IEEE, 2000.
- Tourtier, P. J., Monnier, R. and Lopez, P. Multicarrier Modem for Digital HDTV Terrestrial Broadcasting. Signal Processing: Image Communication 5, 5-6 (December 1993): 379–403.
- Tureli, U., Kivanc, D., and Liu, H. Experimental and Analytical Studies on a High Resolution OFDM Carrier Frequency Offset Estimator. IEEE Transactions on Vehicular Technology 50, 2 (March 2001): 629– 643.
- Tureli, U., Kivanc, D., and Liu, H. Multicarrier Synchronization with Diversity. Proceedings of the 54th IEEE Vehicular Technology Conference (VTC), October-Fall 2001, 2, pp. 952- 956. : IEEE, 2001.

- Van de Beek, J. -J, Sandell, M., and Borjesson, P. O. ML Estimation of Time and Frequency Offset in OFDM Systems. IEEE Transaction on Signal Processing 45, 7 (July 1997): 1800- 1805.
- Van de Beek, J.-J., Borjesson, P. O., Boucheret, M. L., Landstram, D., Arenas, J. M., Odling, P., Ostberg, C., Wahlqvist, M., and Wilson, K. S. A time and frequency synchronization scheme for multiuser OFDM. IEEE Journal on Selected Areas in Communications 17, 11 (November 1999): 1900– 1914.
- Vehkaperä, M., Tujkovic, D., Li, Z., and Juntti, M. Receiver Design For Spatially Layered Downlink MC-CDMA System. IEEE Transaction on Vehicular Technology 54, 3 (May 2005): 1042- 1055.
- Voltz, P. J., Teng, H. -Y., Lu, I.-T.; Yang, Y., and Olesen, R.L. Frequency Domain Re-Sampler for Clock Sampling Offset in MIMO OFDM Systems. Proceedings of the 64th IEEE Vehicular Technology Conference (VTC-06), 25-28 September 2006, pp. 1- 5. : IEEE, 2006.
- Wang, M., Goodwin, G. C., and Meng, D. E. EM-Based Receiver Design for Uplink MIMO-OFDMA Systems. Proceedings of IEEE International Conference on Communications (ICC'08), 19-23 May 2008, pp. 4516– 4520. : IEEE, 2008.
- Wang, X., Tjhung, T. T., Wu, Y., and Caron, B. SER Performance Evaluation And Optimization Of OFDM System With Residual Frequency and Timing Offsets From Imperfect Synchronization. IEEE Transaction on Broadcasting 49, 2 (June 2003): 170- 177.
- Wang, Y., Ciblat, P., Serpedin, E., and Loubaton, P. Performance Analysis of a Class of Non-Data Aided Carrier Frequency Offset and Symbol Timing Delay Estimators for Flat-Fading Channels. IEEE Transaction on Signal Processing 50, 9 (September 2002): 2295– 2305.
- Wang, Z., and Xin, Y. Carrier-Frequency Offset Estimation for MIMO-OFDMA Uplink Transmission. Proceedings of IEEE Vehicular Technology Conference (VTC08), 11-14 May 2008, pp. 1712– 1716. : IEEE, 2008.

- Wei, L., and Schlegel, C. Synchronization Requirements for Multi-User OFDM on Satellite Mobile and Two-Path Rayleigh-Fading Channels. IEEE Transaction on Communications 43, 234 (February/March/April 1995): 887– 895.
- Wei, Z., and Lindner, J. SINR Analysis for OFDMA Systems with Carrier Frequency Offset. Proceedings of the 18th IEEE International Symposium on Personal, Indoor and Mobile Radio Communications (PIMRC 2007), 3-7 September 2007, pp. 1- 5. : IEEE, 2007.
- Wen-Long, C., and Chen, S. Theoretical Analysis of Joint Synchronization Error Effects For OFDMA Systems. Proceedings of IEEE Conference on Vehicular Technology (VTC), 11-14 May, pp: 1930– 1934. : IEEE, 2008.
- Xu, Y., Dong, L., and Zhang, C. Sampling Clock Offset Estimation Algorithm Based on IEEE 802.11n. Proceedings of IEEE International Conference on Networking, Sensing and Control (ICNSC 2008), 6-8 April 2008, pp. 523– 527. : IEEE, 2008.
- Yang, B., Cao, Z., and Letaief, K. B. Analysis of Low-Complexity Windowed DFT-Based MMSE Channel Estimator for OFDM Systems. IEEE Transaction on Communications 49, 11 (November 2001): 1977– 1987.
- Yang, B., Letaief, K.B., Cheng, R.S., and Zhigang, C. Timing Recovery for OFDM Transmission. IEEE Journal on Selected Areas in Communications 18, 11 (November 2000): 2278-2291.
- Yao, Y., and Giannakis, G. B. Blind Carrier Frequency Offset Estimation in SISO, MIMO, and Multiuser OFDM Systems. IEEE Transaction Communications 53, 1 (January 2005): 173– 183.
- Yu, J., Yang, L., Shao, S., and Zhu, H. A Novel Space-Frequency Receiver for Multi-rate MIMO MC-CDMA Systems. Proceedings of the 4th IEEE International Conference on Wireless Communications, Networking and Mobile Computing (WiCOM'08), 12-14 October 2008, pp. 1– 4. : IEEE, 2008.
- Yuanxin, X., Ling, D., and Cheng, Z. Sampling Clock Offset Estimation Algorithm Based on IEEE 802.11n. Proceedings of IEEE International Conference on Networking, Sensing and Control (ICNSC 2008), 6-8 April 2008, pp. 523– 527. : IEEE, 2008.

- Zeng, J., and Minn, H. Diversity Exploiting MIMO-OFDMA Ranging. Proceedings of the 6th IEEE International Conference on Information, Communications and Signal Processing, 10-13 December 2007, pp. 1- 5. : IEEE, 2007.
- Zhang, P., Tao, X., Zhang, J. Wang, Y., Li, L. and Wang, Y. A Vision from the Future Beyond 3G TDD. IEEE Communication Magazine 43, 1, (January 2005): 38– 44.
- Zhang, W., and Lindner, J. SINR Analysis for OFDMA Systems with Carrier Frequency Offset. Proceedings of the 18th IEEE International Symposium on Personal, Indoor and Mobile Radio Communications (PIMRC 2007), 3-7 September 2007, pp. 1-5. : IEEE, 2007.
- Zhang, Z., and Tellambura, C. The Effect of Imperfect Carrier Frequency Offset Estimation on OFDMA Uplink Transmission. Proceedings of IEEE International Conference on Communications (ICC '07), 24-28 June 2007, pp. 6281– 6286. : IEEE, 2007.
- Zhang, Z., Zhang, W., and Tellambura, C. Robust OFDMA Uplink Synchronization by Exploiting the Variance of Carrier Frequency Offsets. IEEE Transactions on Vehicular Technology 57, 5 (September 2008): 3028- 3039.
- Zhangyong, M., Chunming, Z., and Xiaohu, Y. A Novel OFDM Time and Frequency Synchronization Algorithm. Proceedings of IEEE International Conference on Communication Technology (ICCT 03), 9-11 April 2003, 2, pp. 1114– 1118. : IEEE, 2003.
- Zhao, P., Kuang, L., and Lu, J. Carrier Frequency Offset Estimation Using Extended Kalman Filter in Uplink OFDMA Systems. Proceedings of IEEE International Conference on Communications (ICC'2006), 11-15 June 2006, 6, pp. 2870- 2874. : IEEE, 2006.
- Zhongding, L., Xiaoming, P., and Francois, C. V-BLAST Receivers for Downlink MC-CDMA Systems. Proceedings of the 58th IEEE Vehicular Technology Conference (VTC), 6-9 October 2003, 2, pp. 866- 870. : IEEE, 2003.

- Zhou, E., Zhang, X., Zhao, H., and Wang, W. Synchronization Algorithms for MIMO OFDM Systems. Proceedings of IEEE Wireless Communications and Networking Conference (WCNC), 13-17 March 2005, 1, pp. 18– 22. : IEEE, 2005.
- Zhou, P., Jiang, M., Zhao, C., and Xu, W. Error Probability of OFDM Systems Impaired By Carrier Frequency Offset In Frequency Selective Rayleigh Fading Channels. Proceedings of IEEE International Conference on Communications (ICC'07), 24-28 June 2007, pp. 1065-170. : IEEE, 2007.
- Zhou, P., Zhao, C., Yang, Y., and He, X. Error Probability of MPSK OFDM Impaired By Carrier Frequency Offset in AWGN Channels. IEEE Communications Letter 10, 12 (December 2006): 801- 803.
- Zhou, P., Zhao, C., Yang, Y., and Shi, Z. Performance Analysis of PCC-OFDM Systems Impaired by Carrier Frequency Offset. Proceedings of IEEE Global Telecommunications Conference (GLOBECOM 06), 27 November-1 December 2006, pp.1- 6. : IEEE, 2006.
- Ziskind, I., and Wax, M. Maximum Likelihood Localization of Multiple Sources by Alternating Projection. IEEE Transaction on Acoustic Speech, Signal Processing 36, 10 (October 1998): 1553- 1560.

APPENDICES

APPENDIX A

DETAILED DERIVATION OF AVERAGE INTERFERENCE COEFFICIENT WITH
RESPECT TO TIME OFFSET

This appendix presents a detailed derivation of the average interference coefficient in (3.39) and (3.40) with respect of the TO and its ranges.

Equation (3.39) can be rewritten as:

$$\mathbb{E} \left[\left| \frac{(\phi_{2,DS} - \phi_{1,DS} + 1)}{N_c} \right|^2 \right] = \frac{\sum_{\zeta_{k,n}^{t,q} = B_{TO}^-}^{B_{TO}^+} (\phi_{2,DS} - \phi_{1,DS} + 1)^2}{N_c^2 (-B_{TO}^+)} = \frac{\sum_{\phi \in \Phi} \sum_{\zeta_{k,n}^{t,q} = \zeta_1^\phi}^{\zeta_2^\phi} (\alpha_{DS}^\phi \pm \zeta_{k,n}^{t,q})^2}{N_c^2 (B_{TO}^+ - B_{TO}^-)} \quad (\text{A.1})$$

where ζ_1^ϕ , and ζ_2^ϕ are the limits of TO's range ϕ , and α_{DS}^ϕ is a constant with $(\alpha_{DS}^\phi \pm \zeta_{k,n}^{t,q}) \equiv (\phi_{2,DS} - \phi_{1,DS} + 1)$. Note that $N_c^2 (B_{TO}^+ - B_{TO}^-)$ is constant, then the numerator of (A.1) can be represented by:

$$\begin{aligned} \sum_{\phi \in \Phi} \sum_{\zeta_{k,n}^{t,q} = \zeta_1^\phi}^{\zeta_2^\phi} (\alpha_{DS}^\phi \pm \zeta_{k,n}^{t,q})^2 &= \sum_{\phi \in \Phi} \sum_{\zeta_{k,n}^{t,q} = \zeta_1^\phi}^{\zeta_2^\phi} \left((\alpha_{DS}^\phi)^2 \pm 2\alpha_{DS}^\phi \zeta_{k,n}^{t,q} + (\zeta_{k,n}^{t,q})^2 \right) \\ &= \sum_{\phi \in \Phi} \sum_{\zeta_{k,n}^{t,q} = \zeta_1^\phi}^{\zeta_2^\phi} (\alpha_{DS}^\phi)^2 \pm 2\alpha_{DS}^\phi \sum_{\zeta_{k,n}^{t,q} = \zeta_1^\phi}^{\zeta_2^\phi} \zeta_{k,n}^{t,q} + \sum_{\zeta_{k,n}^{t,q} = \zeta_1^\phi}^{\zeta_2^\phi} (\zeta_{k,n}^{t,q})^2 \end{aligned} \quad (\text{A.2})$$

Let $n^\phi = (\zeta_2^\phi - \zeta_1^\phi + 1)$, and utilize the classical summing results:

$$\sum_{\zeta_{k,n}^{t,q} = \zeta_1^\phi}^{\zeta_2^\phi} \zeta_{k,n}^{t,q} = n^\phi (\zeta_1^\phi + \zeta_2^\phi) / 2 \quad \text{and} \quad \sum_{\zeta_{k,n}^{t,q} = 1}^{(n^\phi - 1)} (\zeta_{k,n}^{t,q})^2 = n^\phi (n^\phi - 1) (2n^\phi - 1) / 6, \quad \text{then}$$

equation (A.2) can be given by:

$$\begin{aligned} \sum_{\phi \in \Phi} \sum_{\zeta_{k,n}^{t,q} = \zeta_1^\phi}^{\zeta_2^\phi} (\alpha_{DS}^\phi \pm \zeta_{k,n}^{t,q})^2 &= \sum_{\phi \in \Phi} \left[n^\phi (\alpha_{DS}^\phi)^2 \pm n^\phi \alpha_{DS}^\phi (\zeta_1^\phi + \zeta_2^\phi) + n^\phi (\zeta_1^\phi)^2 \right. \\ &\quad \left. + n^\phi (n^\phi - 1) \zeta_1^\phi + n^\phi (n^\phi - 1) (2n^\phi - 1) / 6 \right] \end{aligned} \quad (\text{A.3})$$

where the $\sum_{\zeta_{k,n}^{t,q} = \zeta_1^\phi}^{\zeta_2^\phi} (\zeta_{k,n}^{t,q})^2$ is evaluated through simple manipulation of the arithmetic progression. By substituting (A.3) into (A.1), the average interference coefficient of the DS can be given by:

$$\mathbb{E} \left[\left| \frac{(\phi_{2,DS} - \phi_{1,DS} + 1)}{N_c} \right|^2 \right] = \frac{1}{N_c^2 (B_{TO}^+ - B_{TO}^-)} \sum_{\phi \in \Phi} \left[n^\phi (\alpha_{DS}^\phi)^2 \pm n^\phi \alpha_{DS}^\phi (\zeta_1^\phi + \zeta_2^\phi) + n^\phi (\zeta_1^\phi)^2 \right. \\ \left. + n^\phi (n^\phi - 1) \zeta_1^\phi + n^\phi (n^\phi - 1)(2n^\phi - 1)/6 \right] \quad (\text{A.4})$$

By analogy, equation (3.40) can be reordered as:

$$\mathbb{E} \left[\left| \sum_{z=\phi_{1,\{ICI,ISI\}}}^{\phi_{2,\{ICI,ISI\}}} \frac{e^{j2\pi z(c_{u,g} - i)/N_c}}{N_c} \right|^2 \right] = \frac{\sum_{\zeta_{u,n}^{r,a} = \theta_{TO}^-}^{B_{TO}^+} \sin^2 \left[\pi \left(\frac{c_{u,g} - i}{N_c} \right) (\phi_{2,\{ICI,ISI\}} - \phi_{1,\{ICI,ISI\}} + 1) \right]}{N_c^2 (B_{TO}^+ - B_{TO}^-) \sin^2 \left[\pi \left(\frac{c_{u,g} - i}{N_c} \right) \right]} \quad (\text{A.5})$$

The numerator of (A.5), where $\sin^2 \left[\pi (c_{u,g} - i)/N_c \right]$ is independent of $(\phi_{2,\{ICI,ISI\}} - \phi_{1,\{ICI,ISI\}} + 1)$, can be expressed as:

$$\sum_{\zeta_{u,n}^{r,a} = -B_{TO}^-}^{+B_{TO}^+} \sin^2 \left[\pi \left(\frac{c_{u,g} - i}{N_c} \right) (\phi_{2,\{ICI,ISI\}} - \phi_{1,\{ICI,ISI\}} + 1) \right] = \sum_{\phi \in \Phi} \sum_{\zeta_{k,n}^{r,a} = \zeta_1^\phi}^{\zeta_2^\phi} \sin^2 \left[\theta (\alpha_{\{ICI,ISI\}}^\phi \pm \zeta_{k,n}^{r,a}) \right] \quad (\text{A.6})$$

where $\theta = \pi (c_{u,g} - i)/N_c$, and $\alpha_{\{ICI,ISI\}}^\phi$ is a constant with $(\alpha_{\{ICI,ISI\}}^\phi \pm \zeta_{k,n}^{r,a}) \equiv (\phi_{2,\{ICI,ISI\}} - \phi_{1,\{ICI,ISI\}} + 1)$. Then,

$$\sum_{\phi \in \Phi} \sum_{\zeta_{k,n}^{r,a} = \zeta_1^\phi}^{\zeta_2^\phi} \sin^2 \left[\theta (\alpha_{\{ICI,ISI\}}^\phi \pm \zeta_{k,n}^{r,a}) \right] = \sum_{\phi \in \Phi} \sum_{\zeta_{k,n}^{r,a} = \zeta_1^\phi}^{\zeta_2^\phi} \left(\frac{e^{j\theta (\alpha_{\{ICI,ISI\}}^\phi \pm \zeta_{k,n}^{r,a})} - e^{-j\theta (\alpha_{\{ICI,ISI\}}^\phi \pm \zeta_{k,n}^{r,a})}}{2j} \right)^2 \\ = -\frac{1}{4} \sum_{\phi \in \Phi} \sum_{\zeta_{k,n}^{r,a} = \zeta_1^\phi}^{\zeta_2^\phi} \left(e^{j2\theta (\alpha_{\{ICI,ISI\}}^\phi \pm \zeta_{k,n}^{r,a})} + e^{-j2\theta (\alpha_{\{ICI,ISI\}}^\phi \pm \zeta_{k,n}^{r,a})} - 2 \right) \\ = -\frac{1}{4} \sum_{\phi \in \Phi} \left[e^{j2\theta (\alpha_{\{ICI,ISI\}}^\phi \pm \zeta_1^\phi)} + e^{-j2\theta (\alpha_{\{ICI,ISI\}}^\phi \pm \zeta_1^\phi)} - 2 + e^{j2\theta (\alpha_{\{ICI,ISI\}}^\phi \pm \zeta_1^\phi + 1)} + e^{-j2\theta (\alpha_{\{ICI,ISI\}}^\phi \pm \zeta_1^\phi + 1)} - 2 \right. \\ \left. + e^{j2\theta (\alpha_{\{ICI,ISI\}}^\phi \pm \zeta_1^\phi + 2)} + e^{-j2\theta (\alpha_{\{ICI,ISI\}}^\phi \pm \zeta_1^\phi + 2)} - 2 + \dots + e^{j2\theta (\alpha_{\{ICI,ISI\}}^\phi \pm \zeta_1^\phi + n^\phi - 1)} + e^{-j2\theta (\alpha_{\{ICI,ISI\}}^\phi \pm \zeta_1^\phi + n^\phi - 1)} - 2 \right] \\ = -\frac{1}{4} \sum_{\phi \in \Phi} \left[e^{j2\theta (\alpha_{\{ICI,ISI\}}^\phi \pm \zeta_1^\phi)} \left(1 + e^{j2\theta} + e^{j2\theta(2)} + \dots + e^{j2\theta(n^\phi - 1)} \right) \right. \\ \left. + e^{-j2\theta (\alpha_{\{ICI,ISI\}}^\phi \pm \zeta_1^\phi)} \left(1 + e^{-j2\theta} + e^{-j2\theta(2)} + \dots + e^{-j2\theta(n^\phi - 1)} \right) - 2n^\phi \right]$$

$$= -\frac{1}{4} \sum_{\phi \in \Phi} \left[e^{j2\theta(\alpha_{\{ICI,ISI\}}^\phi \pm \zeta_1^\phi)} \left(\frac{1 - e^{j2\theta n^\phi}}{1 - e^{j2\theta}} \right) + e^{-j2\theta(\alpha_{\{ICI,ISI\}}^\phi \pm \zeta_1^\phi)} \left(\frac{1 - e^{-j2\theta n^\phi}}{1 - e^{-j2\theta}} \right) - 2n^\phi \right] \quad (\text{A.7})$$

where $\sum_{x=0}^{n^\phi-1} e^{j2\theta x} = \frac{1 - e^{j2\theta n^\phi}}{1 - e^{j2\theta}}$.

By substituting (A.7) into the numerator of (A.5), the average interference coefficient of ICI and ISI can be concluded as follow:

$$\begin{aligned} \mathbb{E} \left[\left| \sum_{z=\phi_1, \{ICI, ISI\}}^{\phi_2, \{ICI, ISI\}} \frac{e^{j2z\theta}}{N_c} \right|^2 \right] &= -\frac{1}{4N_c^2 (B_{TO}^+ - B_{TO}^-) \sin^2 \theta} \\ &\times \sum_{\phi \in \Phi} \left[e^{j2\theta(\alpha_{\{ICI,ISI\}}^\phi \pm \zeta_1^\phi)} \left(\frac{1 - e^{j2\theta n^\phi}}{1 - e^{j2\theta}} \right) + e^{-j2\theta(\alpha_{\{ICI,ISI\}}^\phi \pm \zeta_1^\phi)} \left(\frac{1 - e^{-j2\theta n^\phi}}{1 - e^{-j2\theta}} \right) - 2n^\phi \right] \end{aligned} \quad (\text{A.8})$$

$$\begin{aligned} \mathbb{E} \left[\left| \sum_{z=\phi_1, \{ICI, ISI\}}^{\phi_2, \{ICI, ISI\}} \frac{e^{j2z\theta}}{N_c} \right|^2 \right] &= -\frac{1}{4N_c^2 (B_{TO}^+ - B_{TO}^-) \sin^2 \pi (c_{u,g} - i) / N_c} \\ &\times \sum_{\phi \in \Phi} \left[e^{j2\pi(c_{u,g} - i) / N_c (\alpha_{\{ICI,ISI\}}^\phi \pm \zeta_1^\phi)} \left(\frac{1 - e^{j2\pi n^\phi (c_{u,g} - i) / N_c}}{1 - e^{j2\pi (c_{u,g} - i) / N_c}} \right) + e^{-j2\pi(c_{u,g} - i) / N_c (\alpha_{\{ICI,ISI\}}^\phi \pm \zeta_1^\phi)} \left(\frac{1 - e^{-j2\pi n^\phi (c_{u,g} - i) / N_c}}{1 - e^{-j2\pi (c_{u,g} - i) / N_c}} \right) - 2n^\phi \right] \end{aligned} \quad (\text{A.9})$$

APPENDIX B

DETAILED DERIVATION OF AVERAGE INTERFERENCE COEFFICIENT WITH
RESPECT TO TIME AND CARRIER FREQUENCY OFFSETS

This appendix presents a detailed derivation of the average interference coefficient in (3.39) with respect of the TO and CFO and their ranges.

Equation (3.60) can be rewritten as:

$$\mathbb{E} \left[\left| \sum_{z=\phi_{1,sgl}}^{\phi_{2,sgl}} \frac{e^{\frac{j2\pi z(c_{u,g} + \varepsilon_u^q - i)}{N_c}}}{N_c} \right|^2 \right] = \sum_{\phi \in \Phi} \sum_{\zeta_{u,n}^{\phi} = \zeta_1^{\phi}}^{\zeta_2^{\phi}} \int_{-\varepsilon}^{\varepsilon} \frac{\sin^2 \left[\pi (\alpha_{sgl}^{\phi} \pm \zeta_{u,n}^{p,q}) (c_{u,g} + \varepsilon_u^q - i) / N_c \right]}{N_c^2 (B_{TO}^+ - B_{TO}^-) (2\varepsilon) \sin^2 \left[\pi (c_{u,g} + \varepsilon_u^q - i) / N_c \right]} d\varepsilon_u^q \quad (B.1)$$

where ζ_1^{ϕ} , and ζ_2^{ϕ} are the limits of TO range ϕ , and $(\alpha_{sgl}^{\phi} \pm \zeta_{u,n}^{p,q}) = (\phi_{2,sgl} - \phi_{1,sgl} + 1)$ where α_{sgl}^{ϕ} is constant. The inner integration in (B.1) can be evaluated as:

$$I_1 = \int_{-\varepsilon}^{\varepsilon} \frac{\sin^2 \left[\pi (\alpha_{sgl}^{\phi} \pm \zeta_{u,n}^{p,q}) (c_{u,g} + \varepsilon_u^q - i) / N_c \right]}{\sin^2 \left[\pi (c_{u,g} + \varepsilon_u^q - i) / N_c \right]} d\varepsilon_u^q$$

$$I_1 = \frac{1}{2} \int_{-\varepsilon}^{\varepsilon} \frac{1 - \cos \left[2\pi (\alpha_{sgl}^{\phi} \pm \zeta_{u,n}^{p,q}) (c_{u,g} + \varepsilon_u^q - i) / N_c \right]}{\sin^2 \left[\pi (c_{u,g} + \varepsilon_u^q - i) / N_c \right]} d\varepsilon_u^q$$

where $\sin^2(x) = [1 - \cos(2x)]/2$, then

$$I_1 = \frac{1}{2} \int_{-\varepsilon}^{\varepsilon} \frac{1}{\sin^2 \left[\pi (c_{u,g} + \varepsilon_u^q - i) / N_c \right]} d\varepsilon_u^q - \frac{1}{2} \int_{-\varepsilon}^{\varepsilon} \frac{\cos \left[2\pi (\alpha_{sgl}^{\phi} \pm \zeta_{u,n}^{p,q}) (c_{u,g} + \varepsilon_u^q - i) / N_c \right]}{\sin^2 \left[\pi (c_{u,g} + \varepsilon_u^q - i) / N_c \right]} d\varepsilon_u^q$$

$$I_1 = -\frac{N_c}{2\pi} \left[\cot \left(\pi (c_{u,g} + \varepsilon_u^q - i) / N_c \right) \right]_{-\varepsilon}^{\varepsilon} - \frac{1}{2} \int_{-\varepsilon}^{\varepsilon} \frac{\cos \left[2\pi (\alpha_{sgl}^{\phi} \pm \zeta_{u,n}^{p,q}) (c_{u,g} + \varepsilon_u^q - i) / N_c \right]}{\sin^2 \left[\pi (c_{u,g} + \varepsilon_u^q - i) / N_c \right]} d\varepsilon_u^q \quad (B.2)$$

The integration in the second term of the right hand side of (B.2), I_2 , can be evaluated using the recursive formula as follow:

$$\begin{aligned}
I_2 &= -\frac{1}{2} \int_{-\varepsilon}^{\varepsilon} \frac{\cos \left[2\pi(\alpha_{\text{sgl}}^{\phi} \pm \zeta_{u,n}^{p,q})(c_{u,g} + \varepsilon_u^q - i)/N_c \right]}{\sin^2 \left[\pi(c_{u,g} + \varepsilon_u^q - i)/N_c \right]} d\varepsilon_u^q \\
I_2 &= -\frac{2N_c}{\pi} \int_{-\varepsilon}^{\varepsilon} \frac{\sin \left[(2(\alpha_{\text{sgl}}^{\phi} \pm \zeta_{u,n}^{p,q}) - 1)\pi(c_{u,g} + \varepsilon_u^q - i)/N_c \right]}{\sin \left[\pi(c_{u,g} + \varepsilon_u^q - i)/N_c \right]} d\varepsilon_u^q \\
&\quad + \frac{N_c}{\pi} \int_{-\varepsilon}^{\varepsilon} \frac{\cos \left[(2(\alpha_{\text{sgl}}^{\phi} \pm \zeta_{u,n}^{p,q}) - 2)(c_{u,g} + \varepsilon_u^q - i)/N_c \right]}{\sin^2 \left[\pi(c_{u,g} + \varepsilon_u^q - i)/N_c \right]} d\varepsilon_u^q \\
I_2 &= \frac{2N_c}{\pi \left[2(\alpha_{\text{sgl}}^{\phi} \pm \zeta_{u,n}^{p,q}) - 2 \right]} \sin \left[(2(\alpha_{\text{sgl}}^{\phi} \pm \zeta_{u,n}^{p,q}) - 2)\pi(c_{u,g} + \varepsilon_u^q - i)/N_c \right] \Big|_{-\varepsilon}^{\varepsilon} \\
&\quad + \frac{N_c}{\pi} \int_{-\varepsilon}^{\varepsilon} \frac{\sin \left[(2(\alpha_{\text{sgl}}^{\phi} \pm \zeta_{u,n}^{p,q}) - 3)\pi(c_{u,g} + \varepsilon_u^q - i)/N_c \right]}{\sin \left[\pi(c_{u,g} + \varepsilon_u^q - i)/N_c \right]} d\varepsilon_u^q \tag{B.3} \\
&\quad - \frac{N_c}{2\pi} \int_{-\varepsilon}^{\varepsilon} \frac{\cos \left[(2(\alpha_{\text{sgl}}^{\phi} \pm \zeta_{u,n}^{p,q}) - 2)\pi(c_{u,g} + \varepsilon_u^q - i)/N_c \right]}{\sin^2 \left[\pi(c_{u,g} + \varepsilon_u^q - i)/N_c \right]} d\varepsilon_u^q
\end{aligned}$$

where $\int \frac{\cos[mx]}{\sin^n[x]} dx = -2 \int \frac{\sin[(m-1)x]}{\sin^{n-1}[x]} dx + \int \frac{\cos[(m-2)x]}{\sin^n[x]} dx$ and $\int \frac{\sin[mx]}{\sin^n[x]} dx = 2 \int \frac{\cos[(m-1)x]}{\sin^{n-1}[x]} dx + \int \frac{\sin[(m-2)x]}{\sin^n[x]} dx$ (Bois, 1961 pages 135 and 120 respectively). By substituting (B.3) in (B.2), I_1 can be given by:

$$\begin{aligned}
I_1 &= -\frac{N_c}{2\pi} \cot \left(\pi(c_{u,g} + \varepsilon_u^q - i)/N_c \right) \Big|_{-\varepsilon}^{\varepsilon} \\
&\quad + \frac{2N_c}{\pi \left[2(\alpha_{\text{sgl}}^{\phi} \pm \zeta_{u,n}^{p,q}) - 2 \right]} \sin \left[(2(\alpha_{\text{sgl}}^{\phi} \pm \zeta_{u,n}^{p,q}) - 2)\pi(c_{u,g} + \varepsilon_u^q - i)/N_c \right] \Big|_{-\varepsilon}^{\varepsilon} \\
&\quad + \frac{N_c}{\pi} \int_{-\varepsilon}^{\varepsilon} \frac{\sin \left[(2(\alpha_{\text{sgl}}^{\phi} \pm \zeta_{u,n}^{p,q}) - 3)\pi(c_{u,g} + \varepsilon_u^q - i)/N_c \right]}{\sin \left[\pi(c_{u,g} + \varepsilon_u^q - i)/N_c \right]} d\varepsilon_u^q \tag{B.4} \\
&\quad - \frac{N_c}{2\pi} \int_{-\varepsilon}^{\varepsilon} \frac{\cos \left[(2(\alpha_{\text{sgl}}^{\phi} \pm \zeta_{u,n}^{p,q}) - 2)\pi(c_{u,g} + \varepsilon_u^q - i)/N_c \right]}{\sin^2 \left[\pi(c_{u,g} + \varepsilon_u^q - i)/N_c \right]} d\varepsilon_u^q
\end{aligned}$$

Therefore, $E \left[\left| \left(1/N_c \right) \sum_{z=\phi_{1,sgl}}^{\phi_{2,sgl}} e^{j2\pi z(c_{u,g} + e_u^q - i)} / N_c \right|^2 \right]$ can be obtained when (B.4) is substituted in (B.1). Note that $\int \frac{\sin[2x]}{\sin[x]} dx = 2\sin[x]$ and $\int \frac{\cos[x]}{\sin^2[x]} dx = -\operatorname{cosec}[x]$ (Bois, 1961 pages 119 and 129 respectively)

APPENDIX C

DETAILED DERIVATION OF AVERAGE INTERFERENCE COEFFICIENT WITH
RESPECT TO CARRIER FREQUENCY AND SAMPLING CLOCK FREQUENCY
OFFSETS

This appendix presents a detailed derivation of the average interference coefficient in (3.64-3.65) with respect of the CFO and SCFO.

The entire interference coefficient in (3.64-3.65) can be rewritten in a general expression as:

$$\mathbb{E} \left[\left| \left(\frac{1}{N_c} \right) \sum_{z \in \mathbb{S}_{G_1}} e^{j2\pi\theta} \right|^2 \right] = \int_{-\xi}^{\xi} \int_{-\xi}^{\xi} \frac{\sin^2 \left(\pi \left[(1 + \xi_{u,n}^q) c_{u,g} + (1 + \xi_{u,n}^q) \varepsilon_{u,n}^q - i \right] \delta / N_c \right)}{(2\xi)(2\xi) \sin^2 \left(\pi \left[(1 + \xi_{u,n}^q) c_{u,g} + (1 + \xi_{u,n}^q) \varepsilon_{u,n}^q - i \right] / N_c \right)} d\xi_{u,n}^q d\varepsilon_{u,n}^q \quad (\text{C.1})$$

where the constant δ represents the summation depth. Since $\sin^2(x) = [1 - \cos(2x)]/2$, then inner integration in (C.1), I_1 can be given by:

$$\begin{aligned} I_1 &= \int_{-\xi}^{\xi} \frac{\sin^2 \left(\pi \left[(1 + \xi_{u,n}^q) c_{u,g} + (1 + \xi_{u,n}^q) \varepsilon_{u,n}^q - i \right] \delta / N_c \right)}{\sin^2 \left(\pi \left[(1 + \xi_{u,n}^q) c_{u,g} + (1 + \xi_{u,n}^q) \varepsilon_{u,n}^q - i \right] / N_c \right)} d\xi_{u,n}^q \\ &= \frac{1}{2} \int_{-\xi}^{\xi} \frac{1}{\sin^2 \left(\pi \left[(1 + \xi_{u,n}^q) c_{u,g} + (1 + \xi_{u,n}^q) \varepsilon_{u,n}^q - i \right] / N_c \right)} d\xi_{u,n}^q \\ &\quad - \frac{1}{2} \int_{-\xi}^{\xi} \frac{\cos \left(2\pi \left[(1 + \xi_{u,n}^q) c_{u,g} + (1 + \xi_{u,n}^q) \varepsilon_{u,n}^q - i \right] \delta / N_c \right)}{\sin^2 \left(\pi \left[(1 + \xi_{u,n}^q) c_{u,g} + (1 + \xi_{u,n}^q) \varepsilon_{u,n}^q - i \right] / N_c \right)} d\xi_{u,n}^q \end{aligned} \quad (\text{C.2})$$

$$\text{Let } \theta = \pi \left[(1 + \xi_{u,n}^q) c_{u,g} + (1 + \xi_{u,n}^q) \varepsilon_{u,n}^q - i \right] / N_c \rightarrow \frac{d\theta}{d\xi_{u,n}^q} = \pi \left[c_{u,g} + \varepsilon_{u,n}^q \right] / N_c,$$

$$\theta_1 = \pi \left[(1 - \xi) c_{u,g} + (1 - \xi) \varepsilon_{u,n}^q - i \right] / N_c \text{ and } \theta_2 = \pi \left[(1 + \xi) c_{u,g} + (1 + \xi) \varepsilon_{u,n}^q - i \right] / N_c,$$

Therefore, the first integration of I_1 , can be evaluated as:

$$I_2 = - \frac{N_c}{2\pi(c_{u,g} + \varepsilon_{u,n}^q)} \left[\cot \left(\pi \left[(1 + \xi_{u,n}^q) c_{u,g} + (1 + \xi_{u,n}^q) \varepsilon_{u,n}^q - i \right] / N_c \right) \right]_{\theta_1}^{\theta_2} \quad (\text{C.3})$$

$$\text{where } \int \frac{1}{\sin^2 \theta} d\theta = -\cot \theta.$$

Moreover,

$$\int_{-\varepsilon}^{\varepsilon} I_2 d\varepsilon_{u,n}^q = -\frac{N_c}{2\pi(c_{u,g} + \varepsilon_{u,n}^q)} \int_{-\varepsilon}^{\varepsilon} \left[\cot\left(\pi\left[\frac{(1+\xi_{u,n}^q)c_{u,g} + (1+\xi_{u,n}^q)\varepsilon_{u,n}^q - i}{N_c}\right]\right) \right]_{\theta_1}^{\theta_2} d\varepsilon_{u,n}^q \quad (C.4)$$

$$\begin{aligned} \int_{-\varepsilon}^{\varepsilon} I_2 d\varepsilon_{u,n}^q &= -\frac{N_c}{2\pi} \int_{-\varepsilon}^{\varepsilon} \frac{\cot\left(\pi\left[\frac{(1+\xi)(c_{u,g} + \varepsilon_{u,n}^q) - i}{N_c}\right]\right)}{(c_{u,g} + \varepsilon_{u,n}^q)} d\varepsilon_{u,n}^q \\ &+ \frac{N_c}{2\pi} \int_{-\varepsilon}^{\varepsilon} \frac{\cot\left(\pi\left[\frac{(1-\xi)(c_{u,g} + \varepsilon_{u,n}^q) - i}{N_c}\right]\right)}{(c_{u,g} + \varepsilon_{u,n}^q)} d\varepsilon_{u,n}^q \end{aligned} \quad (C.5)$$

Use:

$$\begin{aligned} \cot\left(\pi\left[\frac{ax-i}{N_c}\right]\right) &= \frac{1}{\pi\left[\frac{ax-i}{N_c}\right]} - \frac{\pi\left[\frac{ax-i}{N_c}\right]}{3} + \frac{\left(\pi\left[\frac{ax-i}{N_c}\right]\right)^3}{45} - \frac{2\left(\pi\left[\frac{ax-i}{N_c}\right]\right)^5}{945} + \dots \\ &\frac{2^{2n} B_n \left(\pi\left[\frac{ax-i}{N_c}\right]\right)^{2n-1}}{(2n)!} - \dots \end{aligned} \quad (C.6)$$

where B_n is the Bernoulli's Number (Dwight, 1957, eq.(415.04, and 45) , page. 82 and 10 respectively), then

$$\begin{aligned} \int_{-\varepsilon}^{\varepsilon} I_2 d\varepsilon_{u,n}^q &= -\frac{N_c}{2\pi} \int_{c_{u,g}-\varepsilon}^{c_{u,g}+\varepsilon} \frac{1}{(c_{u,g} + \varepsilon_{u,n}^q) \pi\left[\frac{(1+\xi)(c_{u,g} + \varepsilon_{u,n}^q) - i}{N_c}\right]} + \frac{N_c}{2\pi(3)} \int_{c_{u,g}-\varepsilon}^{c_{u,g}+\varepsilon} \frac{\pi\left[\frac{(1+\xi)(c_{u,g} + \varepsilon_{u,n}^q) - i}{N_c}\right]}{(c_{u,g} + \varepsilon_{u,n}^q)} \\ &+ \frac{N_c}{2\pi(45)} \int_{c_{u,g}-\varepsilon}^{c_{u,g}+\varepsilon} \frac{\left(\pi\left[\frac{(1+\xi)(c_{u,g} + \varepsilon_{u,n}^q) - i}{N_c}\right]\right)^3}{(c_{u,g} + \varepsilon_{u,n}^q)} + \frac{N_c}{2\pi(945)} \int_{c_{u,g}-\varepsilon}^{c_{u,g}+\varepsilon} \frac{2\left(\pi\left[\frac{(1+\xi)(c_{u,g} + \varepsilon_{u,n}^q) - i}{N_c}\right]\right)^5}{(c_{u,g} + \varepsilon_{u,n}^q)} + \dots \\ &- \frac{N_c}{2\pi} \int_{c_{u,g}-\varepsilon}^{c_{u,g}+\varepsilon} \frac{1}{(c_{u,g} + \varepsilon_{u,n}^q) \pi\left[\frac{(1-\xi)(c_{u,g} + \varepsilon_{u,n}^q) - i}{N_c}\right]} - \frac{N_c}{2\pi(3)} \int_{c_{u,g}-\varepsilon}^{c_{u,g}+\varepsilon} \frac{\pi\left[\frac{(1-\xi)(c_{u,g} + \varepsilon_{u,n}^q) - i}{N_c}\right]}{(c_{u,g} + \varepsilon_{u,n}^q)} \\ &- \frac{N_c}{2\pi(45)} \int_{c_{u,g}-\varepsilon}^{c_{u,g}+\varepsilon} \frac{\left(\pi\left[\frac{(1-\xi)(c_{u,g} + \varepsilon_{u,n}^q) - i}{N_c}\right]\right)^3}{(c_{u,g} + \varepsilon_{u,n}^q)} - \frac{N_c}{2\pi(945)} \int_{c_{u,g}-\varepsilon}^{c_{u,g}+\varepsilon} \frac{2\left(\pi\left[\frac{(1-\xi)(c_{u,g} + \varepsilon_{u,n}^q) - i}{N_c}\right]\right)^5}{(c_{u,g} + \varepsilon_{u,n}^q)} - \dots \end{aligned} \quad (C.7)$$

Thus, the integration can be performed as follow:

$$\begin{aligned}
\int_{-\varepsilon}^{\varepsilon} I_2 d\varepsilon_{u,n}^q &= -\frac{1}{2} \left(\frac{N_c}{\pi} \right)^2 \left[\frac{1}{i} \ln \left(\frac{[(1+\xi)(c_{u,g} + \varepsilon_{u,n}^q) - i]}{(c_{u,g} + \varepsilon_{u,n}^q)} \right) \right]_{c_{u,g}-\varepsilon}^{c_{u,g}+\varepsilon} + \frac{1}{6} [(c_{u,g} + \varepsilon_{u,n}^q)]_{c_{u,g}-\varepsilon}^{c_{u,g}+\varepsilon} - \frac{1}{6} (i) [\ln(c_{u,g} - \varepsilon)]_{c_{u,g}-\varepsilon}^{c_{u,g}+\varepsilon} \\
&+ \frac{1}{90} \left(\frac{\pi}{N_c} \right)^2 (1+\xi)^3 \left[\frac{(c_{u,g} + \varepsilon_{u,n}^q)}{3} \right]_{c_{u,g}-\varepsilon}^{c_{u,g}+\varepsilon} + \frac{3i}{90} \left(\frac{\pi}{N_c} \right)^2 (1+\xi)^2 \left[\frac{(c_{u,g} + \varepsilon_{u,n}^q)}{2} \right]_{c_{u,g}-\varepsilon}^{c_{u,g}+\varepsilon} \\
&+ \frac{3i}{90} \left(\frac{\pi}{N_c} \right)^2 (1+\xi)^2 [(c_{u,g} + \varepsilon_{u,n}^q)]_{c_{u,g}-\varepsilon}^{c_{u,g}+\varepsilon} + \frac{3i^3}{90} \left(\frac{\pi}{N_c} \right)^2 (1+\xi)^2 [(c_{u,g} + \varepsilon_{u,n}^q)]_{c_{u,g}-\varepsilon}^{c_{u,g}+\varepsilon} \\
&- \frac{3i^3}{90} \left(\frac{\pi}{N_c} \right)^2 [\ln(c_{u,g} + \varepsilon_{u,n}^q)]_{c_{u,g}-\varepsilon}^{c_{u,g}+\varepsilon} + \dots + \frac{1}{2} \left(\frac{N_c}{\pi} \right)^2 \left[\frac{1}{i} \ln \left(\frac{[(1-\xi)(c_{u,g} + \varepsilon_{u,n}^q) - i]}{(c_{u,g} + \varepsilon_{u,n}^q)} \right) \right]_{c_{u,g}-\varepsilon}^{c_{u,g}+\varepsilon} \\
&- \frac{1}{6} [(c_{u,g} + \varepsilon_{u,n}^q)]_{c_{u,g}-\varepsilon}^{c_{u,g}+\varepsilon} + \frac{1}{6} (i) [\ln(c_{u,g} - \varepsilon)]_{c_{u,g}-\varepsilon}^{c_{u,g}+\varepsilon} - \frac{1}{90} \left(\frac{\pi}{N_c} \right)^2 (1-\xi)^3 \left[\frac{(c_{u,g} + \varepsilon_{u,n}^q)}{3} \right]_{c_{u,g}-\varepsilon}^{c_{u,g}+\varepsilon} \\
&- \frac{3i}{90} \left(\frac{\pi}{N_c} \right)^2 (1-\xi)^2 \left[\frac{(c_{u,g} + \varepsilon_{u,n}^q)}{2} \right]_{c_{u,g}-\varepsilon}^{c_{u,g}+\varepsilon} - \frac{3i}{90} \left(\frac{\pi}{N_c} \right)^2 (1-\xi)^2 [(c_{u,g} + \varepsilon_{u,n}^q)]_{c_{u,g}-\varepsilon}^{c_{u,g}+\varepsilon} \\
&- \frac{3i^3}{90} \left(\frac{\pi}{N_c} \right)^2 (1-\xi)^2 [(c_{u,g} + \varepsilon_{u,n}^q)]_{c_{u,g}-\varepsilon}^{c_{u,g}+\varepsilon} + \frac{3i^3}{90} \left(\frac{\pi}{N_c} \right)^2 [\ln(c_{u,g} + \varepsilon_{u,n}^q)]_{c_{u,g}-\varepsilon}^{c_{u,g}+\varepsilon} - \dots
\end{aligned} \tag{C.8}$$

Note that there is a special case where $i=0$, can be determine as follow:

$$\begin{aligned}
\int_{-\varepsilon}^{\varepsilon} I_2 d\varepsilon_{u,n}^q &= -\frac{N_c}{2\pi} \left[\frac{1}{\pi(1+\xi)(c_{u,g} + \varepsilon_{u,n}^q)/N_c} - \frac{\pi(1+\xi)(c_{u,g} + \varepsilon_{u,n}^q)/N_c}{3} \right. \\
&\quad \left. \frac{[\pi(1+\xi)(c_{u,g} + \varepsilon_{u,n}^q)/N_c]^3}{135} - \dots \right]_{\pi(1+\xi)(c_{u,g}-\varepsilon)/N_c}^{\pi(1+\xi)(c_{u,g}+\varepsilon)/N_c} \\
&+ \frac{N_c}{2\pi} \left[\frac{1}{\pi(1+\xi)(c_{u,g} + \varepsilon_{u,n}^q)/N_c} - \frac{\pi(1+\xi)(c_{u,g} + \varepsilon_{u,n}^q)/N_c}{3} \right. \\
&\quad \left. \frac{[\pi(1+\xi)(c_{u,g} + \varepsilon_{u,n}^q)/N_c]^3}{135} - \dots \right]_{\pi(1-\xi)(c_{u,g}-\varepsilon)/N_c}^{\pi(1-\xi)(c_{u,g}+\varepsilon)/N_c}
\end{aligned} \tag{C.9}$$

On the other hand,

$$I_2 = -\frac{1}{2} \int_{-\xi}^{\xi} \frac{\cos\left(2\pi\left[(1+\xi_{u,n}^q)c_{u,g} + (1+\xi_{u,n}^q)\varepsilon_{u,n}^q - i\right]\delta/N_c\right)}{\sin^2\left(\pi\left[(1+\xi_{u,n}^q)c_{u,g} + (1+\xi_{u,n}^q)\varepsilon_{u,n}^q - i\right]/N_c\right)} d\xi_{u,n}^q \quad (\text{C.10})$$

Note that $\int \frac{\cos[mx]}{\sin^n[x]} dx = -2 \int \frac{\sin[(m-1)x]}{\sin^{n-1}[x]} dx + \int \frac{\cos[(m-2)x]}{\sin^n[x]} dx$ (Bois, 1961 page 135), then

$$\begin{aligned} I_2 = & -\frac{1}{2} \left[2 \int_{-\xi}^{\xi} \frac{\sin\left(\pi\left[(1+\xi_{u,n}^q)c_{u,g} + (1+\xi_{u,n}^q)\varepsilon_{u,n}^q - i\right](2\delta-1)/N_c\right)}{\sin\left(\pi\left[(1+\xi_{u,n}^q)c_{u,g} + (1+\xi_{u,n}^q)\varepsilon_{u,n}^q - i\right]/N_c\right)} d\xi_{u,n}^q \right. \\ & - 2 \int_{-\xi}^{\xi} \frac{\sin\left(\pi\left[(1+\xi_{u,n}^q)c_{u,g} + (1+\xi_{u,n}^q)\varepsilon_{u,n}^q - i\right](2\delta-3)/N_c\right)}{\sin\left(\pi\left[(1+\xi_{u,n}^q)c_{u,g} + (1+\xi_{u,n}^q)\varepsilon_{u,n}^q - i\right]/N_c\right)} d\xi_{u,n}^q \\ & - 2 \int_{-\xi}^{\xi} \frac{\sin\left(\pi\left[(1+\xi_{u,n}^q)c_{u,g} + (1+\xi_{u,n}^q)\varepsilon_{u,n}^q - i\right](2\delta-5)/N_c\right)}{\sin\left(\pi\left[(1+\xi_{u,n}^q)c_{u,g} + (1+\xi_{u,n}^q)\varepsilon_{u,n}^q - i\right]/N_c\right)} d\xi_{u,n}^q - \dots \\ & \left. - \int_{-\xi}^{\xi} \frac{1}{\sin\left(\pi\left[(1+\xi_{u,n}^q)c_{u,g} + (1+\xi_{u,n}^q)\varepsilon_{u,n}^q - i\right]/N_c\right)} d\xi_{u,n}^q \right] \quad (\text{C.11}) \end{aligned}$$

Each integral term in (C.11), except the last term, can be determined as follow,

where $\int \frac{\sin[mx]}{\sin^n[x]} dx = 2 \int \frac{\cos[(m-1)x]}{\sin^{n-1}[x]} dx + \int \frac{\sin[(m-2)x]}{\sin^n[x]} dx$ (Bois, 1961 page 120):

$$I_3 = \int_{-\xi}^{\xi} \frac{\sin\left(\pi\left[(1+\xi_{u,n}^q)c_{u,g} + (1+\xi_{u,n}^q)\varepsilon_{u,n}^q - i\right](2\delta-1)/N_c\right)}{\sin\left(\pi\left[(1+\xi_{u,n}^q)c_{u,g} + (1+\xi_{u,n}^q)\varepsilon_{u,n}^q - i\right]/N_c\right)} d\xi_{u,n}^q \quad (\text{C.12})$$

Let $\theta = \pi\left[(1+\xi_{u,n}^q)c_{u,g} + (1+\xi_{u,n}^q)\varepsilon_{u,n}^q - i\right]/N_c \rightarrow \frac{d\theta}{d\xi_{u,n}^q} = \pi\left[c_{u,g} + \varepsilon_{u,n}^q\right]/N_c$,

$\theta_1 = \pi\left[(1-\xi_{u,n}^q)c_{u,g} + (1-\xi_{u,n}^q)\varepsilon_{u,n}^q - i\right]/N_c$ and $\theta_2 = \pi\left[(1+\xi_{u,n}^q)c_{u,g} + (1+\xi_{u,n}^q)\varepsilon_{u,n}^q - i\right]/N_c$,

then,

$$\begin{aligned}
I_3 &= \frac{N_c}{\pi(c_{u,g} + \epsilon_{u,n}^q)} \int_{\theta_1}^{\theta_2} \frac{\sin(\theta(2\delta-1))}{\sin(\theta)} d\theta \\
&= \frac{N_c}{\pi(c_{u,g} + \epsilon_{u,n}^q)} \left[2 \int_{\theta_1}^{\theta_2} \cos(\theta(2\delta-2)) d\theta + 2 \int_{\theta_1}^{\theta_2} \cos(\theta(2\delta-4)) d\theta \right. \\
&\quad \left. + 2 \int_{\theta_1}^{\theta_2} \cos(\theta(2\delta-6)) d\theta + \dots + \theta \right]_{\theta_1}^{\theta_2}
\end{aligned} \tag{C.13}$$

$$I_3 = \frac{N_c}{\pi(c_{u,g} + \epsilon_{u,n}^q)} \left[\frac{\sin(\theta(2\delta-2))}{(2\delta-2)} + \frac{\sin(\theta(2\delta-4))}{(2\delta-4)} + \dots + \frac{\sin(2\theta)}{2} + \frac{\theta}{2} \right]_{\theta_1}^{\theta_2} \tag{C.14}$$

$$\begin{aligned}
I_3 &= \frac{N_c}{\pi(c_{u,g} + \epsilon_{u,n}^q)} \left[\frac{\sin(\theta_2(2\delta-2))}{(2\delta-2)} + \frac{\sin(\theta_2(2\delta-4))}{(2\delta-4)} + \dots + \frac{\sin(2\theta_2)}{2} + \frac{\theta_2}{2} \right] \\
&\quad - \frac{N_c}{\pi(c_{u,g} + \epsilon_{u,n}^q)} \left[\frac{\sin(\theta_1(2\delta-2))}{(2\delta-2)} + \frac{\sin(\theta_1(2\delta-4))}{(2\delta-4)} + \dots + \frac{\sin(2\theta_1)}{2} + \frac{\theta_1}{2} \right]
\end{aligned} \tag{C.15}$$

Moreover,

$$\begin{aligned}
\int_{-\epsilon}^{\epsilon} I_3 d\epsilon_{u,n}^q &= \frac{N_c}{\pi} \left[\int_{-\epsilon}^{\epsilon} \frac{\sin(\theta_2(2\delta-2))}{(2\delta-2)(c_{u,g} + \epsilon_{u,n}^q)} d\epsilon_{u,n}^q + \int_{-\epsilon}^{\epsilon} \frac{\sin(\theta_2(2\delta-4))}{(2\delta-4)(c_{u,g} + \epsilon_{u,n}^q)} d\epsilon_{u,n}^q + \dots + \int_{-\epsilon}^{\epsilon} \frac{\theta_2}{2(c_{u,g} + \epsilon_{u,n}^q)} d\epsilon_{u,n}^q \right] \\
&\quad - \frac{N_c}{\pi} \left[\int_{-\epsilon}^{\epsilon} \frac{\sin(\theta_1(2\delta-2))}{(2\delta-2)(c_{u,g} + \epsilon_{u,n}^q)} d\epsilon_{u,n}^q + \int_{-\epsilon}^{\epsilon} \frac{\sin(\theta_1(2\delta-4))}{(2\delta-4)(c_{u,g} + \epsilon_{u,n}^q)} d\epsilon_{u,n}^q + \dots + \int_{-\epsilon}^{\epsilon} \frac{\theta_1}{2(c_{u,g} + \epsilon_{u,n}^q)} d\epsilon_{u,n}^q \right]
\end{aligned} \tag{C.16}$$

Note that in (C.16), the term $\int_{-\epsilon}^{\epsilon} \frac{\sin(\theta_2(2\delta-2))}{(2\delta-2)(c_{u,g} + \epsilon_{u,n}^q)} d\epsilon_{u,n}^q$ can be evaluated as follow:

Using the trigonometric identity: $\sin(a-b) = \sin(a)\cos(b) - \cos(a)\sin(b)$, we can have

$$\begin{aligned}
\int_{-\epsilon}^{\epsilon} \frac{\sin(\theta_2(2\delta-2))}{(2\delta-2)(c_{u,g} + \epsilon_{u,n}^q)} d\epsilon_{u,n}^q &= \cos\left(\frac{\pi[i(2\delta-2)]/N_c}\right) \int_{-\epsilon}^{\epsilon} \frac{\sin\left(\frac{\pi[(1+\xi_{u,n}^q)(c_{u,g} + \epsilon_{u,n}^q)(2\delta-2)]/N_c}{(c_{u,g} + \epsilon_{u,n}^q)}\right)}{(c_{u,g} + \epsilon_{u,n}^q)} d\epsilon_{u,n}^q \\
&\quad - \sin\left(\frac{\pi[i(2\delta-2)]/N_c}\right) \int_{-\epsilon}^{\epsilon} \frac{\cos\left(\frac{\pi[(1+\xi_{u,n}^q)(c_{u,g} + \epsilon_{u,n}^q)(2\delta-2)]/N_c}{(c_{u,g} + \epsilon_{u,n}^q)}\right)}{(c_{u,g} + \epsilon_{u,n}^q)} d\epsilon_{u,n}^q
\end{aligned} \tag{C.17}$$

$$\begin{aligned}
& \int_{-\varepsilon}^{\varepsilon} \frac{\sin(\theta_2(2\delta-2))}{(2\delta-2)(c_{u,g} + \varepsilon_{u,n}^q)} d\varepsilon_{u,n}^q = \cos\left(\frac{\pi[i(2\delta-2)]}{N_c}\right) \left[\ln\left(\frac{\pi[(1+\xi_{u,n}^q)(c_{u,g} + \varepsilon_{u,n}^q)(2\delta-2)]}{N_c}\right) \right. \\
& \left. - \frac{\left(\frac{\pi[(1+\xi_{u,n}^q)(c_{u,g} + \varepsilon_{u,n}^q)(2\delta-2)]}{N_c}\right)^2}{2 \times 2!} + \frac{\left(\frac{\pi[(1+\xi_{u,n}^q)(c_{u,g} + \varepsilon_{u,n}^q)(2\delta-2)]}{N_c}\right)^4}{4 \times 4!} - \dots \right]_{-\varepsilon}^{\varepsilon} \quad (C.18) \\
& - \sin\left(\frac{\pi[i(2\delta-2)]}{N_c}\right) \left[\frac{\left(\frac{\pi[(1+\xi_{u,n}^q)(c_{u,g} + \varepsilon_{u,n}^q)(2\delta-2)]}{N_c}\right)^3}{3 \times 3!} + \frac{\left(\frac{\pi[(1+\xi_{u,n}^q)(c_{u,g} + \varepsilon_{u,n}^q)(2\delta-2)]}{N_c}\right)^5}{5 \times 5!} - \dots \right]_{-\varepsilon}^{\varepsilon}
\end{aligned}$$

$$\begin{aligned}
& \int_{-\varepsilon}^{\varepsilon} \frac{\sin(\theta_2(2\delta-2))}{(2\delta-2)(c_{u,g} + \varepsilon_{u,n}^q)} d\varepsilon_{u,n}^q = \cos\left(\frac{\pi[i(2\delta-2)]}{N_c}\right) \left[\ln\left(\frac{\pi[(1+\xi)(c_{u,g} + \varepsilon)(2\delta-2)]}{N_c}\right) \right. \\
& \left. - \frac{\left(\frac{\pi[(1+\xi)(c_{u,g} + \varepsilon)(2\delta-2)]}{N_c}\right)^2}{2 \times 2!} + \frac{\left(\frac{\pi[(1+\xi)(c_{u,g} + \varepsilon)(2\delta-2)]}{N_c}\right)^4}{4 \times 4!} - \dots \right] \\
& - \cos\left(\frac{\pi[i(2\delta-2)]}{N_c}\right) \left[\ln\left(\frac{\pi[(1+\xi)(c_{u,g} - \varepsilon)(2\delta-2)]}{N_c}\right) \right. \\
& \left. - \frac{\left(\frac{\pi[(1+\xi)(c_{u,g} - \varepsilon)(2\delta-2)]}{N_c}\right)^2}{2 \times 2!} + \frac{\left(\frac{\pi[(1+\xi)(c_{u,g} - \varepsilon)(2\delta-2)]}{N_c}\right)^4}{4 \times 4!} - \dots \right] \\
& - \sin\left(\frac{\pi[i(2\delta-2)]}{N_c}\right) \left[\frac{\left(\frac{\pi[(1+\xi)(c_{u,g} + \varepsilon)(2\delta-2)]}{N_c}\right)^3}{3 \times 3!} + \frac{\left(\frac{\pi[(1+\xi)(c_{u,g} + \varepsilon)(2\delta-2)]}{N_c}\right)^5}{5 \times 5!} - \dots \right] \\
& + \sin\left(\frac{\pi[i(2\delta-2)]}{N_c}\right) \left[\frac{\left(\frac{\pi[(1+\xi)(c_{u,g} - \varepsilon)(2\delta-2)]}{N_c}\right)^3}{3 \times 3!} + \frac{\left(\frac{\pi[(1+\xi)(c_{u,g} - \varepsilon)(2\delta-2)]}{N_c}\right)^5}{5 \times 5!} - \dots \right]
\end{aligned} \quad (C.19)$$

APPENDIX D

DETAILED DERIVATION OF AVERAGE SYMBOL ERROR RATE (SER) WITH

RESPECT TO ASYNCHRONOUS SINR WHEN $M_{\text{xCP}}^{\Delta}(i, y) = e^{-\frac{y}{E[\text{SINR}_{k, \text{xCP}}^{q, \Delta}(i)]}}$

With the aid of equation (4.5), equation (4.10) can be represented as:

$$P_{s, \text{xCP}}^{\Delta} = \left(1 - \frac{1}{M}\right) - 2 \left(1 - \frac{1}{\sqrt{M}}\right) \int_0^{\infty} \frac{1}{\sqrt{\pi y}} e^{-y \left(1 + \frac{1}{E[\text{SINR}_{k, \text{xCP}}^{q, \Delta}(i)]}\right)} dy \quad (\text{D.1})$$

$$+ 2 \left(1 - \frac{1}{\sqrt{M}}\right)^2 \int_0^{\infty} \frac{1}{\sqrt{\pi y}} \text{erfc}(\sqrt{y}) e^{-\frac{y}{E[\text{SINR}_{k, \text{xCP}}^{q, \Delta}(i)]}} dy$$

In the right hand side of equation (D.1), the integration in the second term can be solved as follow:

$$\text{Let } I_1 = \int_0^{\infty} \frac{1}{\sqrt{\pi y}} e^{-y \left(1 + \frac{1}{E[\text{SINR}_{k, \text{xCP}}^{q, \Delta}(i)]}\right)} dy, \text{ and } y \left(1 + \frac{1}{E[\text{SINR}_{k, \text{xCP}}^{q, \Delta}(i)]}\right) = x. \text{ Then, we have}$$

$$dy = \frac{dx}{\left(1 + \frac{1}{E[\text{SINR}_{k, \text{xCP}}^{q, \Delta}(i)]}\right)}, \text{ therefore}$$

$$I_1 = \sqrt{\frac{E[\text{SINR}_{k, \text{xCP}}^{q, \Delta}(i)]}{E[\text{SINR}_{k, \text{xCP}}^{q, \Delta}(i)] + 1}} \int_0^{\infty} \frac{1}{\sqrt{\pi x}} e^{-x} dx = \sqrt{\frac{E[\text{SINR}_{k, \text{xCP}}^{q, \Delta}(i)]}{E[\text{SINR}_{k, \text{xCP}}^{q, \Delta}(i)] + 1}} \quad (\text{D.2})$$

where $\int_0^{\infty} \left(\frac{e^{-x}}{\sqrt{x}}\right) dx = \sqrt{\pi}$ (Stanley, 1977, eq. 56, pp. A-54).

In addition, the integration in the last term of (D.1) can be solved as follow:

$$\text{Let } I_2 = \int_0^{\infty} \frac{1}{\sqrt{\pi y}} \text{erfc}(\sqrt{y}) e^{-\frac{y}{E[\text{SINR}_{k, \text{xCP}}^{q, \Delta}(i)]}} dy, \text{ and } \sqrt{y} = x \Rightarrow dy = 2\sqrt{y} dx.$$

Utilizing the equality: $\text{erfc}(x) = 1 - \text{erf}(x)$, where $\text{erf}(x) = \left(\frac{2}{\sqrt{\pi}}\right) \int_x^{\infty} e^{-t^2} dt$ is the error function, we can get:

$$I_2 = \frac{2}{\sqrt{\pi}} \int_0^{\infty} e^{-x^2 \left(1 + \frac{1}{E[\text{SINR}_{k,\text{XCP}}^{q,\Delta}(i)]}\right)} dx - \frac{2}{\sqrt{\pi}} \int_0^{\infty} \text{erf}(x) e^{-x^2 \left(1 + \frac{1}{E[\text{SINR}_{k,\text{XCP}}^{q,\Delta}(i)]}\right)} dx \quad (\text{D.3})$$

$$I_2 = \sqrt{\frac{E[\text{SINR}_{k,\text{XCP}}^{q,\Delta}(i)]}{E[\text{SINR}_{k,\text{XCP}}^{q,\Delta}(i)]+1}} - \frac{2}{\pi} \sqrt{\frac{E[\text{SINR}_{k,\text{XCP}}^{q,\Delta}(i)]}{E[\text{SINR}_{k,\text{XCP}}^{q,\Delta}(i)]+1}} \tan^{-1} \left(\sqrt{\frac{E[\text{SINR}_{k,\text{XCP}}^{q,\Delta}(i)]}{E[\text{SINR}_{k,\text{XCP}}^{q,\Delta}(i)]+1}} \right) \quad (\text{D.4})$$

where $\int_0^{\infty} e^{-a^2 x^2} dx = \frac{\sqrt{\pi}}{2a}; a > 0$ (Dwight, 1957, eq. 861.3) and

$$\int_0^{\infty} e^{-\alpha^2 x^2} \text{erf}(\beta x) dx = \frac{\tan^{-1}(\beta/\alpha)}{\alpha\sqrt{\pi}}.$$

By substituting (1) and (4) into (1),

$$\begin{aligned} P_{s,\text{XCP}}^{\Delta} &= \left(1 - \frac{1}{M}\right) - 2 \left(1 - \frac{1}{\sqrt{M}}\right) \sqrt{\frac{E[\text{SINR}_{k,\text{XCP}}^{q,\Delta}(i)]}{E[\text{SINR}_{k,\text{XCP}}^{q,\Delta}(i)]+1}} + 2 \left(1 - \frac{1}{\sqrt{M}}\right)^2 \sqrt{\frac{E[\text{SINR}_{k,\text{XCP}}^{q,\Delta}(i)]}{E[\text{SINR}_{k,\text{XCP}}^{q,\Delta}(i)]+1}} \\ &\quad - \frac{4}{\pi} \left(1 - \frac{1}{\sqrt{M}}\right)^2 \sqrt{\frac{E[\text{SINR}_{k,\text{XCP}}^{q,\Delta}(i)]}{E[\text{SINR}_{k,\text{XCP}}^{q,\Delta}(i)]+1}} \tan^{-1} \left(\sqrt{\frac{E[\text{SINR}_{k,\text{XCP}}^{q,\Delta}(i)]}{E[\text{SINR}_{k,\text{XCP}}^{q,\Delta}(i)]+1}} \right) \end{aligned}$$

(D.5)

BIOGRAPHY

MR. OMER ABDEL RAZAG SHARIF ABUBAKER¹ was born in Omdurman, Sudan on June 30, 1978. He received B. Eng. (First class, Honours) and M. Eng. degrees from Sudan University of Science and Technology (SUST), Sudan in July 2003, and Universiti Teknologi Malaysia (UTM), Malaysia in December 2006, respectively.

He has been pursuing the Ph.D. degree in Electrical Engineering at Chulalongkorn University, Thailand since June 2009. Since January 2004 he has been with the Industrial Research and Consultancy Centre (IRCC), Sudan, where he is a researcher.

His current research interests include wireless communications, OFDM systems, metrological radar analysis, and statistical signal processing

¹ E-mail: moshakis111@hotmail.com